METALLIC PHOSPHATES IN BIOMEDICAL APPLICATIONS - DEVELOPMENT, CHEMISTRY AND STRUCTURE

Maria Cristina de Castro Ribeiro

Dissertação elaborada para a obtenção do Grau de Doutor em Engenharia Metalúrgica e de Materiais pela Faculdade de Engenharia da Universidade do Porto

FEUP, 2005

THIS THESIS WAS SUPERVISED BY:

Professor Mário Adolfo Barbosa

Faculdade de Engenharia da Universidade do Porto

THE HOST INSTITUTION OF THIS THESIS WAS:

Laboratório de Biomateriais, INEB - Instituto de Engenharia Biomédica

Universidade do Porto, Portugal

…to my parents, Eduardo and Francisca

This thesis was based on the following publications:

CC Ribeiro, ML Castro Reis, MA Barbosa. Formation of titanium phosphate compounds as a consequence of the interaction of titanium ions with hydroxyapatite. Submitted for publication in Acta Materialia.

CC Ribeiro, IR Gibson, MA Barbosa. The uptake of titanium ions by hydroxyapatite particles- structural changes and possible mechanisms. Submitted for publication in Biomaterials.

CC Ribeiro, MA Barbosa. Affinity of Hydroxyapatite to Metal Cations – a Study on the Composition and Structure of Phosphates Formed in the Presence of Titanium and Aluminium. Key Engineering Materials 2002; 345-349: 87-91.

CC Ribeiro, CC Barrias, MA Barbosa. Calcium-Titanium-Phosphate; properties of an alternative biomaterial. Submitted for publication in Acta Materialia.

CC Ribeiro, CC Barrias, MA Barbosa. Calcium phosphate- alginate microspheres as enzyme delivery matrices. Biomaterials 2004; 25: 4363-4373.

CC Ribeiro, CC Barrias, MA Barbosa. Preparation and characterisation of calcium-phosphate porous microspheres with a uniform size for biomedical applications. Accepted for publication in the Journal of Materials Science: Materials in Medicine.

Related papers to which the author has contributed (see annex):

CC Barrias, CC Ribeiro, MA Barbosa. Adhesion and proliferation of human osteoblastic cells seeded on injectable hydroxyapatite microspheres. Key Engineering Materials 2004; 254-256: 877-880.

CC Barrias, CC Ribeiro, Meriem L, MC Sá Miranda, MA Barbosa. Proliferation, activity and osteogenic differentiation of bone marrow stromal cells cultured on calcium titanium phosphate microspheres. Journal of Biomedical Materials Research A 2005; 72 A: 57-66.

CC Barrias, CC Ribeiro, D Rodrigues, MC Sá Miranda, MA Barbosa. Effect of calcium phosphate addition to alginate microspheres: modulation of enzyme release kinetics and improvement of cell adhesion. Key Engineering Materials 2005; 284-286: 689-692.

Contributions of other authors to the included papers

The author of the present thesis carried out all the experimental work described in this document although in some experiments she had the collaboration of some of the co-authors.

The XRD studies described in **chapter 2 and 3** were assisted respectively by Eng. Maria de Lurdes Reis (Instituto Geológico e Mineiro) and Doctor Iain Gibson (Institute of Medical Sciences, University of Aberdeen) who also contributed to the interpretation of the results.

In **chapter 4** the cell culture studies were assisted by Cristina C Barrias.

Chapter 5 and 6: The work described in these two chapters is the result of a strong collaboration between Cristina C Ribeiro (first author) and Cristina C Barrias (second author). This partnership has arisen from the interest of the first author in finding a new application for calcium titanium phosphate, namely as an injectable bone-filler material, and the interest of the second author in finding alternative ceramic materials for enzyme immobilisation. In **chapter 5**, Cristina C Barrias assisted Cristina C Ribeiro in the preparation and morphological characterisation of the microspheres and in the enzyme immobilisation and release studies. In **chapter 6**, Cristina C Barrias assisted Cristina C Ribeiro in the preparation and morphological characterisation of the microspheres. Cristina C Barrias also participated in the writing of the two manuscripts.

ACKNOWLEDGMENTS

There are a lot of persons to whom I would like to express my sincere gratitude since without them, this thesis would not have been possible. I am afraid not to be able to put into words how grateful I am to those people, but I will try…

First I would like to thank Professor Mário Barbosa, my supervisor, for his support, encouragement, patience, friendship and opportunities he gave me all over the years I have been working with him. His integrity as a person and rigour in everything he does will always be present in my mind as an example to follow.

I would also like to thank Professor Fernando Jorge Monteiro, an excellent teacher I had in the Faculty and who became a good friend.

I had the previlege of working in a renowned institution, INEB, where I found not only excellent researchers to share experiences and learn with, but also good friends that I will keep for life. I had the opportunity of working together with two old friends from my childhood, Ana Paula Filipe and Cristina Martins and is good to see that our friendship is still solid as a rock! Thank you both for being always there whenever I needed. I would also like to thank two other long time friends, Susana Sousa and Pedro Granja, whose friendship goes beyond laboratory relationship and who have also provided me with a considerable enriching of knowledge of my work do to their excellent competence. Special thanks also to Cristina Barrias who rapidly changed from an exceptional bench work to an exceptional friend. Our relationship became more intense due to a cooperation work involving the preparation of microspheres. Due to those small particles, our friendship grew through time. That's why I will always love microspheres!

Thank you very much also to Ana Paula Pêgo, Ana Queiroz, Anabela Dias, Ascensão Lopes, Isabel Amaral, Januário Lima, Judite Barbosa, Manuela Brás, Maria Pia Ferraz and Meriem Lamghari, for their support and friendship. To my other friends and colleagues at INEB (some of them are no longer working there), António

Pedro Fonseca, Cândida Manuel, Carlos Fonseca, Conrado Aparício, Cristina Matos, Daniel Duarte, Dulce Carqueijó, Eugénia Leitão, Fátima Pina, Gabriela Afonso, Hélder Machado, Inês Castro, João Lopes, José Cavalheiro, José Domingos Santos, José Paulo Pereira, Lino Ferreira, Luís Rocha, Marcelo Prado da Silva, Maria José Schuller, Marta Lima, Olga Paiva, Paula Luísa Braga, Pedro Sá, Rui Silva, Sandra Teixeira, Serafim Oliveira, Sofia Teixeira, Susana Carrilho, Vírginia Fonseca, that have in anyway contributed to this work, thank you so much…

I would also like to aknowledge the collaboration of several persons, from different institutions, in the experimental work described in this thesis:

- Eng. Maria de Lurdes Reis (IGM - Instituto Geológico e Mineiro). I am deeply indebted to her not only for the valuable help in the XRD studies but also for her friendship. She is a great woman and a great scientist.

- Doctor Iain Gibson (IRC - Interdisciplinary Research Centre in Biomedical Materials, Queen Mary and Westfield College, University of London), for the assistance in the XRD analysis and for the helpful discussions we had.

- Doctor Carlos Sá (CEMUP- Centro de Materiais da Universidade do Porto) for his availability and help in the XPS studies.

- Dr. Daniela Silva (CEMUP- Centro de Materiais da Universidade do Porto) for her assistance in the SEM analysis.

- Eng. Alexandra Lemos (Departamento de Engenharia Cerâmica e Vidro da Universidade de Aveiro), for the assistance in the Zeta Potential determinations.

- Eng. Paula Marques (Departamento de Engenharia Cerâmica e Vidro da Universidade de Aveiro), for the assistance in the granulometry and surface analysis.

I want also to express my sincere gratitude to my colleagues and friends from Instituto Superior de Engenharia do Porto, especially to Natércia Lima and Drª. Fernanda Freixinho who were always available to help me with the work at the Institute during my PhD training.

Many thanks to all my other friends for their support, particularly in the most difficult times. No one is forgotten even if it is not mentioned! I would especially like to show my gratitude to Nina Maio for her care and true friendship. She is like a guardian angel, always trying to help…

There are no words to express how much I am grateful to my wonderful family for the invaluable support, unconditional love and encouragement. Special thanks to my parents that I adore, for everything they do for me. I am very proud for being their daughter and to take part in their lives. Special thanks also to my sister and brothers, who I love so much…

My last thanks go to Eduardo, my husband and my best friend, and Francisca, my daughter and my precious treasure. Thank you very much Eduardo for your infinite patience, for being always unconditionally present when I needed you most, for trusting and encouraging me, for giving me the willpower to carry on my work, for supporting my choices and for loving me as much as I love you…

Thank you dear "Pimpim" for your patience and comprehension every weekends and holidays (and there were many…) I said I had to work in my thesis instead of being available to be with you. You are unique and I love you more than you can imagine!

ABSTRACT

The degradation of metallic prostheses and implants used in orthopaedic surgery and dental restoration, results in the release of metal ions, which can either accumulate in adjacent tissues surrounding the implant or enter the bloodstream. The biological consequences of the material released into the body are a subject of much concern and investigation. Significant accumulation of a given metal in bone mineral can be expected to alter its characteristics. Studies have been reported concerning the effects of different metal ions, namely aluminium, cadmium and lead in osseous pathologies. Hydroxyapatite (HAp) coatings have been applied onto metals in order to improve osseointegration of metallic orthopaedic implants and it is expected that the ceramic will act as a barrier to elemental transfers from underlying substrates. However, the release of metal ions may compromise the integrity of the metal-coating interface and influence the dissolution behaviour of the coating. Although titanium and its alloys are widely used in the biomedical field, the effects of its metal ions on the molecular structure of HAp (as a coating and as a bone mineral constituent) is not clearly understood. In the present work the influence of different concentrations of titanium ions in the HAp structure was investigated and the characterisation of the products obtained was carried out. It was observed that HAp undergoes structural changes in the presence of titanium ions and, depending on the concentration, the metal ion is either incorporated in the lattice or leads to the formation of a titanium phosphate compound as a result of a dissolution-precipitation process. Since Ti-6Al-4V alloy is the titanium alloy most widely used in the biomedical field, the possibility of existence of a synergistic effect between titanium and aluminium ions was also studied. The results obtained suggest that aluminium and titanium jointly inhibit HAp dissolution and/or lead to formation of a calcium-containing compound.

Another objective of the present work consisted in investigating the applicability of calcium-titanium phosphate (CTP) in orthopaedic surgery. The synthesis of CTP was optimised and the material was chemically and structurally characterised using

different techniques. The ability of CTP to mineralise was investigated in simulated body fluids (SBF). It was observed that CTP induces the formation of an apatitic carbonate layer on its surface when immersed in SBF. The *in vitro* biocompatibility of CTP was evaluated in cultured MG63 cells, in terms of cytoxicity and cell adhesion. It was demonstrated that CTP is cytocompatible and promotes adhesion of MG63 cells. The results obtained showed that this material can be envisaged as an alternative to traditional calcium phosphates.

In the past few years, increasing efforts have been devoted to the development of injectable materials, as an alternative for the treatment of bone defects with less patient discomfort, since they can be applied through minimally invasive surgical procedures. An additional objective of the present study was to develop novel injectable biomaterials in the form of CTP-alginate and HAp-alginate microspheres. The preparation and characterisation of the microspheres, which are intended to be used as protein delivery matrices as well as bone regeneration templates, was carried out. Moreover, studies on the adsorption and release of glucocerebrosidase, an enzyme used in the treatment of Gaucher disease, to which are associated severe bone pathologies, were also performed. It was demonstrated that the proposed methodology enabled the preparation of homogeneous microspheres, which can combine biocompatibility, as well as to act as protein delivery systems. In the present work, porous ceramic injectable microspheres with an interconnected porous network were also prepared based on the sintering of the CTP-alginate and HAp-alginate microspheres previously described. The high and uniform porosity of the microspheres obtained suggests their application as drug delivery matrices with high drug-loading efficiencies, as well as bone tissue engineering scaffolds.

RÉSUMÉ

La dégradation des prothèses métalliques et des implants utilisés dans la chirurgie orthopédique et la restauration dentaire, a pour conséquence la libération des ions métalliques. Ceux ci peuvent s'accumuler dans les tissus adjacents autour de l'implant ou s'infiltrer dans la circulation sanguine. Les effets biologiques, du matériel libéré dans le corps sont un sujet de recherche qui suscite beaucoup d'intérêt. Plusieurs études ont rapporté les effets des différents ions métalliques notamment l'aluminium, le cadmium et la plombe en pathologies osseuses. Des revêtements d'hydroxyapatite (HAp) ont été appliqués sur des métaux afin d'améliorer l'ostéointegration des implants orthopédiques métalliques. Il est espéré que la céramique serve de barrière à la libération des ions à partir du substrat. Cependant la libération de ces ions peut interférer dans l'intégrité de l'interface metale-revêtement et influencer la dissolution du revêtement.

Bien que le titane et ses alliages soient des matières extensivement employées dans le domaine biomédical, les effets des ions métalliques sur la structure moléculaire de l'hydroxyapatite (comme revêtement et comme constituant minéral d'os) ne sont pas clairement compris. Dans ce travail l'influence de différentes concentrations des ions titaniques dans la structure de l'hydroxyapatite a été étudiée ainsi que la caractérisation des produits obtenus. Il a été observé que l'hydroxyapatite subit des changements au niveau de sa structure en présence du titane dans les milieux d'incubation. Selon la concentration utilisée, le titane est incorporé dans la structure moléculaire de l'hydroxyapatite ou conduit à la formation de phosphate de titanium en résultat d'un processus de dissolution-précipitation. Comme l'alliage de Ti-6Al-4V est l'un des alliages du titanium le plus utilisée, il a été également étudié la possibilité de l'existence d'un effet synergique entre les ions du titanium et l'aluminium au niveau de la structure de l'hydroxyapatite. Les résultats obtenus suggèrent que l'aluminium et le titanium inhibent la dissolution de l'hydroxyapatite et/ou conduisent à la formation d'un composé contenant du calcium.

Un autre objectif de ce travail a été également d'étudier l'application d'un phosphate de calcium-titanium (CTP) en chirurgie orthopédique. La synthèse de CTP a été optimisée. La caractérisation du matériel, chimiquement et structurellement, en utilisant différentes techniques a été également réalisé. La capacité de CTP de minéraliser a été étudiée dans des solutions simulant le milieu physiologique (SBF). Il a été observé que le CTP induit la formation d'une couche apatitique de carbonate au niveau de sa surface une fois immergé dans le SBF. La biocompatibilité, *in vitro*, du CTP a été évalué en utilisant les cellules ostéoblastiques MG63. Des tests de cytotoxicité et d'adhésion cellulaire ont été réalisé. Il a été démontré que le CTP est non cytotoxique et favorise l'adhésion des cellules MG63. Ces résultats montrent que ce matérial peut être utilisé comme une alternative aux phosphates de calcium traditionnellement employés en médecine régénérative.

Des efforts croissants ont été consacré au développement des matériaux injectables, comme alternative pour le traitement des défauts osseux une fois que ces matériaux peuvent être utilisés en chirurgie mini invasive avec un minimum de traumatisme provoqué chez le patient. Dans ce travail, des matériaux injectables sous forme de microsphères de CTP-alginate et d'hydroxyapatite-alginate ont été développé. La préparation et la caractérisation des microsphères destinées à être utilisées à la fois en tant que matrices de relargage de protéines et matériaux de régénération osseuse a été realisé. Des études d'adsorption et de relargage de glucocerebrosidase, une enzyme utilisée dans le traitement de la maladie de Gaucher auquel sont associées différentes pathologies osseuses, ont été également effectué. Il a été démontré que la méthodologie proposée a permis la préparation des microsphères homogènes, qui peuvent associer la biocompatibilité, aussi bien que la possibilité d'agir en tant que système de relargage de protéines. Dans ce travail, des microsphères injectables poreuses en céramique, obtenues a partir de la sintérisation des microsphères de CTP-alginate et HAp-alginate ont été préparé et caractérisé. La porosité élevée et l'uniformité des microsphères obtenues suggèrent leur application en tant que matrices de relargage de molécules actives avec une efficacité élevée en tant que support pour l'usage dans la technologie de tissu d'os.

RESUMO

A degradação de próteses metálicas e implantes usados em cirurgia ortopédica e restauração dentária, resulta na libertação de iões metálicos que se podem acumular nos tecidos adjacentes que circundam o implante ou alternativamente entrar na corrente sanguínea. As consequências biológicas dessa libertação constituem um tópico de grande interesse e preocupação para a comunidade científica. Existem vários estudos descritos na bibliografia da área relativos aos efeitos de diferentes iões metálicos, nomeadamente alumínio, cádmio e chumbo em patologias ósseas. Os revestimentos de hidroxiapatite têm vindo a ser aplicados em implantes metálicos ortopédicos por forma a melhorar a osseointegração dos mesmos. Espera-se igualmente que o cerâmico funcione como uma barreira à libertação de iões do substrato. No entanto a libertação desses mesmos iões pode comprometer a integridade da interface metal-revestimento e influenciar a dissolução do revestimento.

Se bem que o titânio e as suas ligas sejam materiais muito usados na área biomédica, o efeito dos seus iões na estrutura molecular da hidroxiapatite (como revestimento e como constituinte mineral ósseo) não está claramente entendido. No presente trabalho foi investigada a influência de diferentes concentrações de iões titânio na estrutura da hidroxiapatite e foi feita a caracterização dos produtos obtidos. Foi observado que a hydroxiapatite sofre alterações estruturais na presença de titânio no meio de incubação e dependendo da concentração, o ião metálico é incorporado na rede de hidroxiapatite ou conduz à formação de um fosfato de titânio como resultado de um processo de dissolução-precipitação. Uma vez que a liga Ti-6Al-4V é a liga de titânio mais usada em implantologia, foi também estudada a possibilidade de existência de um efeito sinérgico entre os iões titânio e alumínio na estrutura da hidroxiapatite. Os resultados obtidos sugerem que o alumínio e o titânio inibem conjuntamente a dissolução da hidroxiapatite e/ou levam à formação de um composto contendo cálcio.

Um outro objectivo do presente trabalho consistiu em investigar a aplicabilidade de um fosfato de cálcio e titânio (CTP) em cirurgia ortopédica. A síntese do composto

foi optimizada e o material foi química e estruturalmente caracterizado usando diferentes técnicas analíticas. Foi também investigada a capacidade do material mineralisar quando imerso em fluídos simuladores de meio fisiológico (SBF) tendo sido observado que o CTP induz a formação de um filme de apatite carbonatada à sua superfície. Foram efectuados estudos de biocompatibilidade *in vitro* usando culturas de células do tipo MG63 com o objectivo de avaliar a citotoxicidade do material e estudar a adesão celular no mesmo. Foi demonstrado que o CTP é citocompatível e promove a adesão de células MG63 em elevado número. Os resultados obtidos mostram que este materials pode ser visto como uma alternativa promissora aos tradicionais fosfatos de cálcio usados em medicina regeneradora.

Nos últimos anos tem havido um grande interesse no desenvolvimento de materiais injectáveis como uma alternativa para o tratamento de defeitos ósseos, conduzindo a um menor desconforto para o paciente, uma vez que os mesmos podem ser aplicados através de procedimentos de cirurgia minimamente invasiva. Um objectivo adicional do presente estudo foi o de desenvolver novos biomateriais injectáveis na forma de microesferas constituídas por CTP-alginato e HAp-alginato. Foi efectuada a preparação e caracterização das microsferas cuja aplicação se pretende seja a de matrizes libertadoras de proteínas e sistemas regeneradores ósseos. Complementarmente foram também realizados estudos de adsorção e libertação de glucocerebrosidase, uma enzima usada no tratamento da doença de Gaucher, à qual estão associadas diferentes patologias ósseas. Foi demonstrado que a metodologia proposta conduz à preparação de microesferas homogéneas, que permitem combinar aspectos como biocompatibilidade e actuarem como sistemas libertadores de proteínas. Procedeu-se ainda à preparação e caracterização de microsferas cerâmicas injectáveis e porosas, obtidas a partir da sinterização das esferas de CTP-alginato e HAp-alginato. A elevada e uniforme porosidade das microsferas produzidas sugerem que as mesmas poderão ser aplicadas como matrizes libertadoras de fármacos, com elevada capacidade de carga, bem como serem utilizadas como substrato para engenharia de tecidos.

TABLE OF CONTENTS

LIST OF FIGURES AND TABLES

Chapter 1

Chapter 2

Chapter 3

Chapter 4

Chapter 5

Chapter 6

Chapter 7

LIST OF ABBREVIATIONS

AAS -	Atomic absorption spectroscopy
ACP -	Amorphous calcium phosphate
ATR-FTIR -	Attenuated total reflectance Fourier transform infrared
BET -	Brunauer Emmel and Teller
BMP -	Bone morphogenetic protein
BSA -	Bovine serum albumin
CTP -	Calcium-titanium-phosphate
CZP -	Calcium-zirconium-phosphate
DCPD -	Dicalcium phosphate dihydrate
DMSO -	Dimethylsulfoxide
DTA -	Differential thermal analysis
EDS -	Energy dispersive spectroscopy
EDTA -	Ethylenediaminetetra acetic acid
FCS -	Foetal calf serum
FT-IR -	Fourier transform infrared spectroscopy
FT-Raman -	Fourier transform Raman
GCR -	Glucocerebrosidase
HAp -	Hydroxyapatite
HSA -	Human serum albumin
HPLC -	High performance liquid chromatography
HP-SEC -	High performance size exclusion chromatography
JCPDS- ICDD -	Joint Committee on Powder Diffraction Standards- International Centre for Diffraction Data
α-MEM -	α- minimal essential medium
MTT -	Mitochondrial tetrazolium test
NMR -	Nuclear magnetic resonance
OCP -	Octacalcium phosphate
PBS -	Phosphate-buffered saline
PGA -	Polyglycolic acid
PIXE -	Particle induced X-ray emission
PLA -	Polylactic acid
PMMA -	Poly(methyl methacrylate)
RALLS -	Right angle laser light scattering
SBF -	Simulated body fluid
SEM -	Scanning electron microscopy
α-TCP -	α- tricalcium phosphate
β-TCP -	β- tricalcium phosphate
TCPS -	Tissue-culture polystyrene
Tof-SIMS -	Time of flight- secondary ion mass spectrometry
TTCP -	Tetracalcium phosphate
XPS -	X-ray photoelectron spectroscopy
XRD -	X-ray diffraction
ZP -	Zeta potential

AIM AND STRUCTURE OF THE THESIS

One of the main purposes of this thesis was to study the effect of titanium ions on the molecular structure of hydroxyapatite (HAp). Another objective was to investigate the applicability of calcium titanium phosphate (CTP), a material that could act in specific situations as an alternative to traditional calcium phosphates, in orthopaedic surgery. In order to use CTP in an injectable form, two different types of ceramic-based microspheres were developed, namely ceramic-alginate microspheres and porous ceramic microspheres.

The first chapter of this thesis consists in a brief overview of calcium phosphate materials to be used in bone regeneration, giving emphasis to HAp and CTP. Aspects like the cationic and anionic substitutions in the HAp lattice are discussed. The potential advantages of using injectable ceramic-based microspheres in bone tissue regeneration are also addressed.

Chapters 2 to 7 describe the experimental work in the form of a compilation of papers already published or submitted for publication in international refereed journals.

In chapters 2 and 3 the investigation concerning the interaction of titanium ions with HAp is described and the possible mechanisms of titanium uptake are proposed. The identification and characterisation of the titanium phosphate formed for high concentrations of metal ion in solution are reported in chapter 2. The possible synergistic effect between aluminium and titanium ions was also investigated and the results are reported in chapter 4.

Chapter 5 describes the physical and chemical characterisation of CTP and the studies performed to investigate its applicability as a biomaterial for bone tissue regeneration purposes. The capacity of the material to mineralise was studied, as well as its cytotoxicity and cell adhesion.

In chapter 6, the preparation and characterisation of injectable CTP-alginate and HAp-alginate microspheres to be used as bone delivery matrices and for bone regeneration is described. Studies on the immobilisation and release of the therapeutic enzyme glucocerebrosidase (GCR), employed in the treatment of Gaucher disease, were also performed. The advantages of using CTP over HAp to immobilise GCR are discussed.

The preparation and characterisation of porous injectable CTP and HAp microspheres are described in chapter 7. The potential benefits of using these microspheres as bone defect fillers and scaffolds for bone tissue regeneration are also addressed.

The thesis concludes with a general discussion (chapter 8) and future work perspectives (chapter 9).

An Annex containing a compilation of three papers in which the author of this thesis has participated as second author is included. The intention is to provide the reader with other key results of further work that support and complement the applicability of the microspheres described in this thesis.

Chapter 1

INTRODUCTION

Biomaterials historical outline

A biomaterial is defined as a material intended to interface with biological systems to evaluate, treat, augment or replace any tissue, organ or function of the body [1].

The use of certain materials as constituents of surgical implants is not new. Substitutions of bone parts for repairing seriously damaged portions of the human body have been reported since the pre-Christian era. The historical pathway of biomaterials science has known profound changes through time and has evolved from one of clinical trial and error to a scientific discipline based upon the design and control of the interface between tissues and materials. It is generally accepted that biomaterials are now in their third generation of existence [2].

The first generation of biomaterials appeared during the 1960s and 1970s and the implanted prostheses were based on materials selected from engineering practice. The goal of this generation of materials was to "achieve a suitable combination of physical properties to match those of the replaced tissue with a minimal toxic response in the host" [3], a common feature of most of the materials used being their biological inertness [2]. Implantable devices were produced with inert materials (e.g. alumina, metals and polymers) that could satisfied mechanical demands and be biologically safe, but which could not be integrated into the body [4]. While providing an effective immediate solution for many patients, the outcome of these materials was often time-limited [5] and the development of biomaterials with extended lifetime in-patients was needed.

As a consequence of the limitations of the first generation of biomaterials, research was carried out in order to develop materials more closely resembling the biological template [5]. By the mid-1970s the field of biomaterials began to shift in emphasis from achieving exclusively a bioinert tissue response to producing instead bioactive components that could elicit a controlled interaction with the living organism [6]. Different types of bioactive materials, namely glasses, ceramics, glass ceramics and composites reached clinical use in several orthopaedic and dental applications [7-24]. Hench *et al* developed the first man-made material that was found to bind to living bone, consisting of a glass (Bioglass®) of the system Na_2O-CaO-SiO_2-P_2O_5 [7]. Another important innovation of this second generation of biomaterials was the utilisation of synthetic hydroxyapatite $Ca_{10}(PO_4)_6(OH)_2$ in bone regeneration in the form of powders, porous implants and coatings on metallic prostheses. Also, hydroxyapatite-polymer composites began to be used as bone grafts. This application was pioneered by Bonfield *et al* who developed hydroxyapatite-reinforced polyethylene composites [8], tailor made to provide matching deformation characteristics and superior fracture toughness to cortical bone, so as to produce bone apposition rather than bone resorption at an implant surface [4]. Other advances observed in this period of biomaterials history were the development of controlled drug delivery systems [25-27] and the use of resorbable materials which are replaced by the regenerating tissues [15, 17-19, 28, 29]. In this latter group are included not only ceramics, such as β-TCP (β-tricalcium phosphate), but also polymers, as for instance polylactic (PLA) and polyglicolic (PGA) acids.

Although progress was achieved with the second generation of biomaterials, revision surgery is still needed in many cases and failure rates are not satisfactory. Nowadays, a third-generation of biomaterials is being designed to stimulate specific cellular responses at the molecular level and the separate concepts of bioactive and resorbable materials have converged [2]. Research on two different alternative routes of repair, based on tailored biomaterials, is currently being pursued, namely [2]:

-*Tissue Engineering*: is a process whereby functional biological prostheses are created by seeding progenitor cells onto synthetic biodegradable substrates that act as scaffolds, and allow diffusion of nutrients to the cells and the cell-to-cell contact that leads to the formation

of new tissue [30]. The tissue-engineered constructs are then implanted into the patients to replace diseased or damaged tissues [2]. Different tissues are being engineered using this route of repair, including fabricated artery, bladder, skin, cartilage, bone, ligament and tendon [31].

-*In situ tissue regeneration*: this approach involves the use of bioactive materials in the form of gels, solutions, powders, granules, or microparticles to stimulate local tissue repair [2]. The biomaterials used can be loaded with different chemicals or growth factors as bone morphogenetic proteins (BMP) in order to stimulate cells and favour tissue regeneration.

The bone model

General aspects

Bone is a composite material of organic and inorganic components. The mineral phase of bone comprises approximately 60 to 70% of the total dry bone weight while the remaining organic fraction is composed largely (85% to 90%) of the fibrous protein collagen [32]. It is the combination of mineral and protein fractions that yields the mechanical strength required for the skeletal support role which bone performs as a structural component of the body [32]. Bone mineral is involved in both biomechanical and metabolic functions of osseous tissue [32, 33]. Besides giving structural stability to the skeleton, it provides the body fluids with inorganic ions to maintain the biologically required levels. It also acts as detoxifying depository to store ions unwanted in the organism (e.g. lead, strontium, etc). Bone mineral composition varies depending on species, strain, type of bone, diet, etc [34]. However, according to Legros *et al* [35], its chemical composition can be represented approximately by a single chemical formula:

$$Ca_{8.3}\square_{.7}(PO_4)_{4.3}\ (HPO_4 \text{ and } CO_3)_{1.7}\ (2OH \text{ and } CO_3)_{0.15}\ \square_{1.7}$$

in which □ represents a vacancy. The amount of HPO_4^{2-} and CO_3^{2-} may vary considerably, however the sum of divalent ions is quite constant in most bone tissues [34]. Other ions are present in smaller quantities, such as Mg^{2+}, Fe^{2+} (in the blood), F^- and Cl^-. Due to cellular

turnover, very small amounts of Na^+, K^+, ascorbic acid, citric acid, polysaccharides, among other substances, are also present [36]. Some specific heavy atoms may occasionally be found, such as Ba^{2+}, Sr^{2+}, Pb^{2+}, which show a preference for fixation precisely in bone tissues. The amount of vacancies in cationic sites and in monovalent anionic sites is always very high and close to the maximum attainable for an apatitic structure. Although bone mineral is often described as an "hydroxyapatite" ($Ca_{10}(PO_4)_6OH_2$), it can be seen from the above formula that it contains very few OH^- [34].

Bone seems lifeless but it is made up of a very alive, porous framework that is constantly being remodelled. The cells found in bone are of different types: osteoblasts, osteocytes, bone lining cells and osteoclasts, with the first three cell types being derived from mesenchymal-type cells called osteoprogenitor cells [33]. Bone tissue replaces itself through the action of osteoclasts that produce acids to dissolve (resorb) apatite and enzymes to break down collagen [36]. The resulting release of calcium and protein prompts other cells (osteoblasts), to lay down a new matrix that mineralises, forming apatite and collagen [36]. In normal conditions bone density is maintained due to the dynamic equilibrium between the functions of osteoclasts and osteoblasts. If there is a change in this equilibrium, the resultant amount of bone formed is reduced and bone disorders, such as osteoporosis, arise. In order to control bone remodelling, either increasing or decreasing it, bone cells produce growth factors such as morphogenetic proteins.

The initial stage of formation of bone mineral is extremely difficult to study, due to the tiny size of the crystals and their very high reactivity. The detailed chemical composition and microstructure of freshly deposited bone mineral, and how these properties change with bone maturation, have been studied intensively and still remain controversial. A key problem is whether the calcium phosphate phase, particularly in young bone, consists wholly of a poorly crystalline hydroxyapatite, or contains residual amounts of a initial precursor. Several hypotheses involving the existence of mineral precursors, such as amorphous calcium phosphate (ACP), dicalcium phosphate dihydrate or brushite (DCPD) and octacalcium phosphate (OCP) have been proposed, based on the study of calcium phosphate formation, *in vitro* [37-41]. However, despite isolated studies claiming the formation of one or the other of these phases, none of them has been reproducibly detected [34]. By the use of

spectroscopic techniques, namely Fourier transform infrared (FT-IR) spectroscopy, and phosphorous-31 (^{31}P) solid-state nuclear magnetic resonance (NMR) spectroscopy, it was possible to obtain information about the short-range order and crystal environment of specific ions in bone [42-50]. The existence of "non-apatitic" environments, different from those existing in pure well-crystallised apatites that are specific to bone mineral crystals and freshly precipitated apatites in physiological conditions, were observed. Moreover, in early stages of bone formation, features such as a low carbonate and a high HPO_4^{2-} content are also characteristic [35]. During ageing, however, the amount of non-apatitic environments and that of HPO_4^{2-} ions decrease, whereas the proportion of carbonate increases, and bone mineral evolves towards a regular carbonated apatite with a better crystallinity (maturation) [34].

Metal ions and bone

Metallic devices have been widely used in orthopaedic surgery for stabilisation of fractures and for total joint replacement as well as in dental restoration. In general, metallic implants are well accepted by the body. However, degradation of metallic prostheses occurs *in vivo* and ionic species resulting from the electrochemical dissolution of the implants are released into the surrounding tissues [51-68], including bone.

The release of metal ions may have an effect not only in the skeleton cells and/or extracellular matrix but also in the bone mineral where a heteroionic exchange and/or adsorption process may occur [69]. Significant accumulation of a given metal in the mineral phase of bone can be expected to alter its characteristics. If, in addition, the metal interacts with bone cells, their metabolism may be affected, e.g. osteoblast and osteoclast function [69]. After being incorporated in bone, the return of a metal into the circulation will depend on when the bone mineral will be resorbed.

Titanium and its alloys are frequently used in orthopaedic and dental procedures due to their adequate mechanical properties, corrosion resistance and biological tolerance. Although a protective oxide is naturally formed on their surfaces, studies described in the literature indicate that metal ions are released due to the degradation of these materials [12, 51-54, 59-

68]. Merrit and Brown [68], in fretting corrosion tests, have shown that the body receives not only particulate but also ionic titanium during the function of the devices. Works of several authors indicate that titanium ions interact with bone [63, 65-67]. For instance, a study of the tissue response associated with dental titanium implants, using SEM, TEM and electron diffraction techniques, revealed the presence of titanium in the implant-bone interface and in the bone tissue [65]. Another study [66] on the titanium-bone interaction, where a titanium implant/bone interface formed after 6 months was examined using Tof-SIMS, showed that titanium diffuses into the bone, and the diffusion area noted during the follow up period was 100 μm thick.

Ti-6Al-4V is the most commonly used titanium alloy in biomedical procedures and aluminium takes part of its composition for metallurgical reasons. The aluminium ion has been associated with several bone disorders [70-79]. Interest in the interaction between aluminium and bone resulted from the observation that patients submitted to long term dialysis accumulated substantial amounts of aluminium in their skeleton, leading to bone disease characterised by impaired mineralisation and diminished bone cell activity [70]. Nevertheless, the presence of aluminium in bone was also observed as the result of degradation of Ti-6Al-4V alloy [63, 80]. The biopsis of maxillary bone of patients with screws of this alloy revealed that newly formed lamellar bone had marked aluminium accumulation, both near the screw surfaces and at a distance greater than 1-2 mm [80]. In that study, titanium was only detected in soft tissues and not in lamellar bone, even though its content in the alloy is higher than that of aluminium. In another investigation using microbeam-PIXE (PIXE= particle induced X-ray emission) [63], titanium and aluminium were detected in bone cortex, bone marrow and soft tissues surrounding implants of Ti-6Al-4V.

Although there are several papers concerning the release of metal ions into the body, their effects in the biology of bone still needs extensive exploration.

Calcium phosphates for medical applications

In the last two decades, the biomedical applications of calcium phosphates have increased significantly due to their biological properties. Different types of calcium

phosphates are used in the biomedical field, namely resorbable and non-resorbable ceramics, cements, prosthetic coatings, and composites. They are suited for several applications, including bone defect filling, bone reconstruction (especially in maxilla-facial applications), bone replacement (especially small bones and middle ear bones), drug carrier (antibiotics, anticancerous drugs, growth factors), coatings of metal prostheses (hip and knee joints), and even nerve guides [34].

In the ternary system $Ca(OH)_2$-H_3PO_4-H_2O, there are several known calcium-phosphates, with calcium-to-phosphate (Ca/P) molar ratios varying from 0.5 to 2 [81] but only the ones indicated in Table 1 are used as biomaterials.

Table 1- Ca-P compounds used as biomaterials (adapted from reference [34]).

Name and formula	**Type of application**	**Occurrence**
Stoichiometric Hydroxyapatite $Ca_{10}(PO_4)_6(OH)_2$	Plasma spraying coatings Drug carrier composites	Close to enamel tissue
Non-stoichiometric apatites* $Ca_{10-x}(HPO_4)_x(PO_4)_{6-x}(OH)_{2-x}.nH_2O$; $0 < x < 1$, n = 0-2.5	Low temperature coating Composites Drug carrier	Bone tissue Ectopic calcification end-term of Ca-P cements
α- or β- Tricalcium Phosphate $Ca_3(PO_4)_2$	Bulk ceramics, Composites, Cements, Plasma spraying coatings, Drug carriers	High temperature phase Impurities in plasma spraying coatings
Dicalcium Phosphate Dihydrate $CaHPO_4.2H_2O$	Cements	Forms also during Ca-P cement setting
Anhydrous Dicalcium Phosphate $CaHPO_4$	Cements	
Octacalcium Phosphate $Ca_8(PO_4)_4(HPO_4)_2.5H_2O$	Cements	Forms also during Ca-P cement setting
Tetracalcium Phosphate $Ca_4(PO_4)_2O$	Cements	Impurity in plasma spraying coatings
Amorphous calcium phosphate*	Cements, Drug carrier, Low temperature coating	Biomineralisations Plasma spraying coatings

*Several chemical formulae have been proposed

The most produced and less expensive industrial calcium phosphate biomaterial, remains hydroxyapatite (HAp). Tricalcium phosphate is also available on an industrial scale and is probably the most used bioresorbable material [34]. It exists under two crystallographic forms: β-tricalcium phosphate (β-TCP) and α-tricalcium phosphate (α-TCP). The α-form is

unstable at low temperature and is obtained by heating the β-form above approximately 1125ºC [34, 82, 83], the precise transformation temperature remaining unclear. The β-form cannot be obtained by direct precipitation. It results from the calcining to 700-800ºC of Ca-deficient apatite, with the loss of water, according to the equation [82]:

$$Ca_9(HPO_4)(PO_4)_5(OH) \rightarrow 3Ca_3(PO_4)_2 + H_2O$$

β-TCP is stabilised by the presence of small amounts of ionic impurities, such as Mg^{2+} ions, frequently associated with calcium salts [34, 84]. It should not be confused with whitlockite, a natural iso-structural compound that contains Mg^{2+} ions substituted for Ca^{2+} and HPO_4^{2-} ions substituted for PO_4^{3-} [34].

Hydroxyapatite

Preparation methods

Several methods of preparation of HAp have been reported in the literature, including precipitation, conversion of other calcium salts, solid state reactions, and sol-gel crystallisation [85-95]. The two main ways of producing HAp are however the wet methods and solid state reactions. Depending upon the technique used, some variability may appear in the final product in terms of morphology, stoichiometry and crystallinity [96]. Apatites prepared from nonaqueous systems are considerably larger in size than those prepared from aqueous systems. Solid state reactions usually give a stoichiometric and well-crystallised product but they require relatively high temperatures and long heat treatment times [97]. Moreover, sinterability of such powders is usually low. In the case of precipitation methods, temperature does not exceed 100ºC and nanometric size crystals can be prepared. The crystallinity and Ca/P ratio of the product obtained depend strongly on the preparation conditions and are in many cases lower than for well-crystallised stoichiometric hydroxyapatite. Chemically precipitated hydroxyapatites are often non-stoichiometric (usually calcium- and hydroxyl deficient). Generally, they have a high specific surface area (between 50 and 90 m^2/g) that may adsorb many ions or constituents, which can be incorporated into

the lattice during growth or maturation of the crystals [34]. A general formula is suggested for non-stoichiometric (carbonate free) hydroxyapatites [94]:

$Ca_{10-x}(HPO_4)_x(PO_4)_{6-x}(OH)_{2-x}.nH_2O$; $0 < x < 1$, n = 0-2.5

Calcium deficient hydroxyapatites are less thermally stable than stoichiometric hydroxyapatites and when heated to about 600ºC calcium pyrophosphate is formed [32, 98]. Further heating until c.a. 800ºC, a temperature that does not affect stoichiometric hydroxyapatite, results in the Ca-deficient hydroxyapatite dehydration to form β-TCP plus some residual apatite [32, 98]. If the Ca/P ratio is equal to 1.5, no hydroxyapatite will exist after pyrolysis.

Another aspect related to wet methods of preparation of HAp is the incorporation of carbonate ions and/or other impurities, such as sodium or potassium in the lattice of the crystallised HAp, since these cations are frequently introduced in the precipitation system with the reactants. Carbonate is so readily incorporated in HAp that the preparation of a CO_3-free material requires the use of solutions free of carbonate and nitrogen purging during the experiment. In laboratory preparations with no precautions taken, one obtains a precipitated HAp with about 1% CO_3 by weight [32]. Biological apatites precipitated from body fluids are about 4% in CO_3 content [32].

Structure of HAp

The stoichiometric form of HAp is monoclinic with space group $P2_1/b$ [99-101]. This structure is characterised by ordering within OH^- ion columns to form a sequence OH^- OH^- OH^- OH^-, with an ordered arrangement of these columns, so that the b-axis is doubled giving lattice parameters a=9.421(8), b=2a, c=6.8814(7) Å, γ=120º [99]. Although many preparations of HAp have been described, only in few studies the HAp produced is reported to be monoclinic [85, 101]. This can be justified by the difficulty that exists in controlling the stoichiometry, because the simple precipitation route yields a basic calcium phosphate of variable composition. The calcium phosphate formed can have a Ca/P molar ratio in the range 9/6 to 10/6 (possibly beyond these limits) and contain variable amounts of water and hydrogen phosphate, yet retain the apatite structure [101]. Normally, only those preparations

having a final high-temperature stage (e.g. hydrothermal or heating in steam at 900ºC) have the possibility of yielding monoclinic HAp [99]. Other preparations are normally hexagonal, presumably because sufficient OH^- ions are missing, replaced by H_2O or impurity ions, so that the ordering is disturbed [102]. Slightly non-stoichiometric HAp has a hexagonal space group $P6_3/m$ with a=9.421 and c=6.884 Å [100].

Substitutions in the HAp lattice

There has been considerable interest in the ion-exchange properties of hydroxyapatites, in part as a consequence of their relevance in biological systems and as a result of potential applications for the removal of environmentally undesirable elements from both solids and liquids [102-107].

The apatite structure is capable of accommodating various substituents (e.g. Sr^{2+} for Ca^{2+}, F^- for OH^-, CO_3^{2-} for PO_4^{3-}) and still maintain its structure. "Apatite" is a general term for crystalline minerals with a composition of $M_{10}(ZO_4)_6X_2$. The name was taken from the Greek word "apato" which means deceive, by Werner, a mineralogist in 1790 [108, 109] and its choice is justified because of the difficulties involved in the identification of apatites due to their non-stoichiometric existence.

All ionic sites of the apatitic structure accept substituents [34, 95, 109, 110]. The substitutions in the HAp are isoionic (ions from a solution phase exchange with identical ions of a solid phase in contact with it), or heteroionic (an ion of a solid phase is displaced by a different ion from a solution in contact with it, thereby altering the composition of both phases). The criteria for the substitution are the similarity of charge and proximity of sizes of the ions concerned [109, 110].

In what concerns HAp applicability in the biomedical field, the capacity of its lattice to act as a host for different chemical species has been explored. The most common example is the preparation of carbonate-substituted HAp [111, 112] and fluoride-substituted HAp [113, 114]. Another potential method for improving the biological activity of HAp is the incorporation of silicon (or silicate groups) into its lattice [115].

Chemical and physical properties of apatites affected by the substitutions in the lattice

The HAp properties that are affected by substitutions in the lattice are: lattice parameters (a- and c-axis dimensions), crystal size and shape, crystal strain, "crystallinity" from X-ray diffraction patterns, infrared absorption spectral properties, dissolution properties, thermal stability [109]. In some cases more than one substitution occurs simultaneously in the HAp lattice and the presence of the substituents may have additive, synergistic or opposite effects on the properties of the apatite crystallites [109]. For instance, the combined effects of $Mg^{2+}$and CO_3^{2-} on reducing crystallinity are greater than the addition of their individual effects [116]. The simultaneous presence of CO_3^{2-} and F^- gives an additive effect on the contraction of the a-axis dimension [112]. As a consequence of the substitution, the lattice parameters can be expanded or contracted depending on the size and amount of the substituent [94, 109, 110, 117, 118]. Usually, if the substituent is larger than the ion substituted for (e.g. Sr^{2+} for Ca^{2+}; Cl^- for OH^-), the effect is to expand one or both of the lattice parameters. In some cases of substitutions, both a and c axes are affected either in the same or opposite directions. In other cases, only the a-axis dimensions are either increased or decreased, while the c-axis dimensions are not significantly different from the unsubstituted OH-apatite [109, 117]. Some substitutions are coupled with others to maintain charge balance or neutrality in the apatite, e.g. CO_3^{2-} for PO_4^{3-} coupled with Na^+ for Ca^{2+}. The type of substituent also affects the crystallinity of the apatites. For instance, an increase in crystallinity is observed in apatite as a consequence of F^- incorporation, while a decrease is observed due to CO_3^{2-} incorporation [99, 109]. Moreover, the characteristics of the substituent influence the dissolution properties of apatite. Fluoride, carbonate and magnesium have specific effects on the solubility of HAp. Fluoride decreases the solubility of HAp [109, 119, 120] whether carbonate and magnesium increases it [109, 121, 122].

Substituents for Ca^{2+}

The substitution of divalent ions for calcium in hydroxyapatite is well known for both aqueous and non-aqueous systems. Such substitutions are accompanied by changes in the apatite lattice parameters and these changes are generally related to the size of the ionic radii of the cation compared to that of Ca^{2+} (0.99 Å) [109, 117, 118]. For instance, the

contraction in lattice parameters due to the partial substitution of Cd^{2+} (0.97 Å) or Mn^{2+} (0.80 Å) for Ca^{2+} is due to the fact that these cations have smaller ionic radii than Ca^{2+}. Contrarily, Sr^{2+} (1.12 Å) , Ba^{2+} (1.34 Å) , and Pb^{2+} (1.20 Å) are ions larger than Ca^{2+} and they cause expansion in both the a- and c-axis dimensions when they substitute in the apatite lattice. The incorporation of these ions also causes changes in the infrared absorption spectra [85, 109, 123] namely on the PO_4^{3-} absorption bands and the disappearance or masking of the OH^- absorption bands ascribed to its librational vibration mode [109]. Their effects on the crystallinity of apatites are not clear. Strontium-substituted apatites were reported to be more soluble than strontium-free apatites [124]. The unit cell lattice parameters were found to vary linearly with the Sr content in different Sr-HAp solid solutions [125]. The substitution of Ca^{2+} by Sr^{2+} ions in the apatite lattice is a very important heteroionic substitution since it is known to interfere with the calcification mechanism [124, 126]. There have been reports indicating that non-toxic amounts of Sr^{2+} may be beneficial in osteoporosis [127, 128]. High Sr^{2+} intake seems however to result in poor bone formation and mineralisation, since the metabolism of Ca is depressed [69].

Magnesium is a metal ion whose presence in the body has important biological implications. The incorporation of Mg^{2+} in the HAp structure is very limited [99, 109, 129] with no perceptible effect on the lattice parameters in spite of the smaller atomic radius of Mg^{2+} compared to that of Ca^{2+} [109]. Several works described in the literature indicate that the presence of Mg^{2+} in the solution in which the apatite forms, causes a reduction in apatite crystallite size, favours the formation of Mg substituted- TCP, and promotes the formation and stabilisation of ACP at 37ºC [130-133]. Posner *et al* suggested that magnesium ions delay the ACP to HAp conversion and the direct HAp precipitation reactions by substituting for Ca^{2+} in forming embryonic clusters of HAp [134]. This results in a distortion and subsequent destabilisation of these prenuclei due to the smaller size of magnesium relative to calcium ions, decreasing the probability of the initial formation of HAp crystals [75]. Webster *et al* prepared HAp with 2 mol% substituted Mg^{2+} and found that osteoblasts adhesion was significantly greater on these substrates than on undoped HAp [135, 136].

Other divalent cations which can also substitute Ca^{2+} in the HAp lattice are Zn^{2+}, Cd^{2+} and Pb^{2+}. Zn^{2+} is reported to substitute Ca^{2+} up to 25 atom% when present in the

supersaturated solution [137]. However, bone HAp studies with labelled ^{65}Zn have shown 100% substituted of Ca^{2+} by Zn^{2+} ions [138]. The substitutions of Cd^{2+} and Pb^{2+} for Ca^{2+} are associated with bone disorders. Cadmium ions interact directly with bone cells diminishing their ability to mineralise [139]. Moreover, their presence accelerates bone turnover, particularly bone resorption, a result of the induced calcium deficiency [140]. The interference of Cd^{2+} with mineralisation can certainly be explained by its inhibitory effect on HAp nucleation and growth in addition to any cellular involvement [141]. Cd^{2+} incorporation into the HAp lattice results in a decreasing of c-axis spacing and a corresponding crystal size decrease in that direction [141]. In what concerns Pb^{2+}, inorganic lead enters the body through inhalation, ingestion, or adsorbed through skin and is distributed in the organism in the blood, soft tissues and bone. The skeleton represents an accumulating reservoir containing approximately 95% of the body burden of lead in adults [142]. The mean residence time in cortical bone is 30 years [143]. Lead stored in bone may be released in states where demineralisation may occur, such as pregnancy, lactation, immobilisation, etc, resulting in endogenous exposure. The mechanism involved in lead fixation in bone is attributed to isomorphous substitution of Ca^{2+} by Pb^{2+}, resulting in the formation of solid solutions of HAp and lead hydroxyapatite [110].

The incorporation of monovalent ions in HAp lattice such as Na^+, Li^+ and K^+ is also possible but it has to be coupled with another substitution to maintain charge neutrality [41, 109]. The coupled substitution of Na^+ for Ca^{2+} with CO_3^{2-} for PO_4^{3-} is an example [144].

Trivalent ions are also known to substitute for Ca^{2+}. For instance Ergun *et al* synthesised yttrium substituted HAp and has shown that the doped ceramic had improved cytocompatibility properties for osteoblast adhesion [135, 136]. In what concerns Al^{3+}, some authors indicate that it substitutes calcium in the HAp structure [109, 118, 145] while others consider that the uptake of this metal ion is due to adsorption processes [77]. Apatites obtained from solutions containing Al^{3+} showed expanded a- and c- axis dimensions when compared to the lattice parameters of pure HAp, supporting the possibility of substitution [118]. The adsorption theory is based on the fact that metal ions with ionic radii significantly different from the one of Ca^{2+} tend to adsorb rather than enter the HAp lattice [145]. As previously mentioned in the "Metal ions and bone" section, aluminium is associated with

several bone disorders. It accumulates in the skeleton, inhibits mineralisation and acts on bone cells [69, 70-78]. Aluminium appears to enter skeletal tissue along with calcium, competing with it [71]. Although the mechanism by which aluminium disrupts bone calcification and leads to osteomalacia is not completely understood, it is suggested that aluminium ions block the calcification sites [74].

The cationic sites of hydroxyapatite can also accept vacancies: up to a maximum of 2 sites out of the 10 existing in stoichiometric apatites [34].

Substituents for PO_4^{3-}

Phosphate ions in the HAp can be substituted by other trivalent ions such as vanadate VO_4^{3-} or arsenate AsO_4^{3-}, and also by bivalent or tetravalent ions like carbonate CO_3^{2-}, hydrogenophosphate HPO_4^{2-}, or silicate SiO_4^{4-} [34, 94, 109, 115]. The trivalent anionic phosphate sites cannot accept vacancies, probably because the trivalent anions are quite large and vacancies would destabilise the lattice [34].

The substitution of HPO_4^{2-} for PO_4^{3-} occurs in hydroxyapatites prepared using aqueous methods where the concentration of HPO_4^{2-} is high and this substitution can be detected by the changes that occur in the a-axis dimension which becomes larger [109]. The presence of HPO_4^{2-} can be indirectly determined by the formation of $P_2O_7^{4-}$ upon ignition [32, 98], as mentioned before in the "Preparation methods" section. This type of substitution occurs to a limited extent and causes a slight increase in the crystallinity of the apatite [109].

The substitution of CO_3^{2-} for PO_4^{3-} has been established in HAp and fluorapatites [99, 109, 111, 112]. Carbonate ions exists on two distinct lattice sites of HAp, designated A and B [44, 47, 90, 111, 112]. Type A carbonated hydroxyapatite results from the replacement of two OH^- groups by CO_3^{2-}, whether type B corresponds to the substitution of PO_4^{3-} by CO_3^{2-} and is observed in apatites prepared by precipitation or hydrolysis methods. Compared to the carbonate free HAp, the type B carbonated apatites show smaller a- and larger c- axis dimensions [109, 110, 112]. Also, the morphology of the crystals change from needle or pencil shape to rod-shaped or equi-axed crystals [109, 146]. The crystallinity of the substituted apatites decreases contrarily to the extent of dissolution that increases as a

function of carbonate contents [109, 112]. The extent of carbonate incorporation is influenced by the presence of other ions in the solution from which the apatite forms. The presence of Na^+, NH_4^+ or Sr^{2+} limits the amount of CO_3^{2-} incorporated into the apatite [109].

The substitution of a phosphate group (PO_4^{3-}) for a silicate group (SiO_4^{4-}) in HAp crystal structure would be feasible provided there is charge balance to account for the more negative silicate group [115]. Silicon substituted HAp results in a decrease in the a- axis and an increase in the c- axis of the unit cell of HAp although the unit cell volume remains almost unchanged [115]. Recent studies show a more rapid remodelling of bone surrounding silicon substituted HAp when compared to pure HAp [147].

Substituents for OH^-

In calcium phosphate apatites the monovalent anionic site substitution of OH^- by F^-, Cl^-, or Br^- is possible to occur [113, 114, 148]. Apatites without any ions in these lattice positions have never been described [109]. These sites may also be occupied by carbonate ions, as already mentioned, resulting in a type A carbonated HAp [44, 47, 90, 111, 112].

Substitution of CO_3^{2-} for OH^- has been observed in apatites from non-aqueous systems prepared at 1000ºC. The effect of such substitution on the lattice parameters is opposite to the CO_3^{2-} for PO_4^{3-} substitution, namely the former causes an expansion of the a- and a contraction of the c-axis [111, 112]. The frequencies of the CO_3^{2-} infrared absorption bands are also different in these two types of carbonate substitution. The extent of CO_3^{2-} for OH^- substitution is 100 mol% ($Ca_{10}(PO_4)_6CO_3$).

In what concerns the substitution of Cl^- for OH^-, it differs in extent for apatites obtained from aqueous and those from nonaqueous systems (40 and 100% respectively) [109]. This substitution is accompanied by expansion in the a-with the contraction in the c-axis dimensions, changes in the characteristics of the absorption bands of the OH groups in the case of partially substituted (Cl, OH)- apatites and decrease in thermal stability [114, 148]. However, it is predicted from the atomic arrangements of OH, F and Cl- apatites that structural stability is in the decreasing order: F-Ap > OH-Ap > Cl-Ap [99]. The substitution of F^- for OH^- predominates in mineral apatites. In both aqueous and nonaqueous systems, F^-

for OH^- substitution can be partial or full, $Ca_{10}(PO_4)_6(F, OH)_2$ or $Ca_{10}(PO_4)_6F_2$, respectively. The incorporation of F^- in the apatite is accompanied by a decrease in the a-axis without any significant change in the c-axis, an increase in crystallinity, and decrease in dissolution rates and solubility in acid buffers [99, 113, 114].

Calcium-Titanium-Phosphate

Calcium-Titanium-Phosphate (CTP), $CaTi_4(PO_4)_6$, belongs to a family of compounds called NZP because the prototype of that broad family is the $NaZ_2(PO_4)_3$ compound [149]. The most important fact in this family of compounds is the stability and flexibility of its three dimensional skeleton in its generalised form $[A_{2n}(XO_4)_{3n}]^{m-}$, which allows the existence of several hundreds of compositions, the possibility of chemical absorption, exchange reactions, redox reactions and intercalation processes [149]. These reactions may take place at low temperature in suspensions, at medium temperature in fused salts or at high temperature in the solid state. The skeleton $[Ti_4(PO_4)_6]^{2-}$ is build up by two chemical groups: the octahedral TiO_6 units and the tetrahedral PO_4 units that share corners only through strong bonds like Ti-O-P. The $[Ti_4(PO_4)_6]^{2-}$ groups repeat along the threefold axis and the so-formed columns connect together in a hexagonal array (Figure 1).

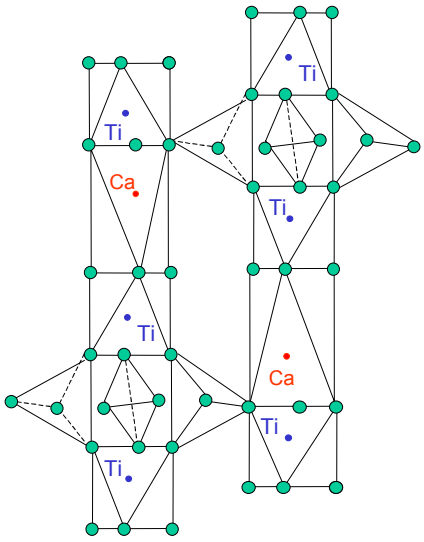

Figure 1 - The crystal structure of CTP consisting of three-dimensional hexagonal skeletal network of PO_4 tetrahedra sharing corners with TiO_6 octahedra. The oxygen atoms are represented in green. For simplicity, P atoms, which position is in the centre of the tetrahedra, are not assigned in the cell.

Szmukler-Moncler *et al* [150] first provided some preliminary results about the biocompatibility of Calcium-Zirconium-Phosphate (CZP), which is a compound iso-structural with calcium-titanium-phosphate. The *in vitro* biocompatibility of this compound was studied using L929 fibroblasts. The preliminary *in vivo* biocompatibility was assessed into dogs in osseous and non-osseous sites. The material did not indicate any adverse reaction. The extensive remodelling activity at the direct contact of the CZP after 9 months of implantation indicated an excellent bioactivity.

Metallic phosphates, namely calcium-titanium-phosphates, may be good candidates as coating materials, in particular if they show chemical affinity to the implant surface, leading to a higher adhesion and bone-binding properties. An attempt was made by Lugscheider *et al* [151] to produce plasma-spraying coatings of CTP and the results obtained suggested that functional coatings of CTP could be produced although it was observed that the crystallinity of the coatings decreased during the spray deposition. A two step process (plasma spraying - thermal post treatment of the surface) is expected to improve the coating crystallinity. Also, decomposition of the calcium-titanium-phosphate into other phases was observed for some of the grain sizes used. Cell culture studies to modulate osteogenesis *in vitro* by calcium titanium and calcium titanium zirconium phosphate coatings on titanium substrata, showed that these materials facilitated the osteoblastic phenotype at least as much as the titanium surface [152].

Gross *et al* [153] investigated the biological behaviour of ceramic cylinders, whose main phase was calcium-titanium-phosphate with small amounts of calcium pyrophosphate, implanted into the distal femur epiphysis of female Chinchilla rabbits, 7, 28 and 84 days postoperatively. The findings regarding the tissue response of the new implant material were considered very favourable. The histological assessment displayed bone bonding to the material and therefore favourable bioactivity comparable to HAp. The macrophage reaction was minimal and there were no obvious signs of leaching of particle release from the material surface in soft tissue interfaces.

Calcium Titanium Phosphate has also interesting properties as a support for immobilisation of several enzymes. Enzymes are immobilised onto a wide range of porous

supports, either particulate or membranous. Inorganic support materials are very attractive because they are usually resistant to sterilisation. Hosono *et al* [154] developed a porous glass ceramic with a skeleton of $CaTi_4(PO_4)_6$ and β-$Ca_3(PO_4)_2$ glass ceramic. Suzuki and co-workers [155] investigated the characteristics of this porous ceramic as an immobilising carrier for various enzymes, namely invertase, β-galactosidase, and alkalophilic proteinase. They have shown that the microporous ceramic is a more suitable material than the conventional silica glass carriers to serve as an efficient and stable enzyme reactor for long term operations.

Bone tissue regeneration

Bone grafts

Bone tissue has the capacity to self-regenerate after injuries. However, when the injury is too severe the mechanical functionality of the bone is not completely restored due to loss of volume and formation of fibrous tissue and consequently bone grafts are needed [159-160]. The ideal bone graft is biocompatible, able to induce bone formation (osteoinductive), able to support bone formation (osteoconductive), mechanically compatible with bone, and able to support angiogenesis [156]. Biological and synthetic bone grafts have been utilised for bone repair. Biological grafts include autografts (usually taken from iliac crest of the patient), allografts (donated by individuals or procured from cadavers), and xenografts (obtained from other species). Histo-incompatibility and the possibility of transferring infectious diseases limit the use of allografts and xenografts. Since autografts provide no risks of immune rejection or disease transfer, they are clinically preferred. However, they are limited in supply, and since their properties and shape do not match exactly those of the bone to be replaced, multiple surgical operations are needed [156-157]. Intensive investigation is being carried out to produce synthetic bone grafts in order to overcome these problems.

Injectable ceramic-based graft materials for bone regeneration

General aspects

In the past few years, increasing efforts have been devoted to the development of improved injectable materials aimed at providing an alternative for the filling of bone defects. The use of injectable materials in bone regeneration presents several advantages over the usual implantation surgical procedures. These materials can be applied through minimally invasive surgical procedures and consequently reduce cost and patient discomfort. Since they are introduced in the bone defect with a needle, they allow filling cavities of any shape and the injured area is significantly reduced, as well as the access to infectious agents, when compared to what happens in a traditional surgical intervention. Moreover, injectable materials can be used as delivery systems of different agents namely antibiotics, other drugs and cells.

The injectable ceramic-based materials consist essentially of pastes and micro or nanoparticles suspended in either autologous blood or other appropriate vehicle prior to injection. Different ceramic phases have been used, HAp and TCP being the most common [3-7, 156], as well as several polymeric matrices both from synthetic [158-162] or natural origin, the latter including collagen, chitosan, gelatine, and alginate, among others [163-168].

Microspheres as bone defect fillers and vehicles for bioactive molecules and cells

Several forms of particulate products are used as bone fillers including irregular multifaceted particles and rounded smooth granules with solid or porous structures. In a ceramic-based bone graft material, the shape of the particles has a direct influence on bone formation. Irregularly or densely packed granules have been described in the literature as being the cause of inflammatory reactions and slower bone formation [169]. Contrarily, uniformly packed spherical particles would lead to a regular inter-particle porosity, thus contributing to easier migration of bone cells and helping in faster bone ingrowth. Furthermore, spherical particles are more suitable for implantation than non-homogeneous granules since they conform better to irregular implant sites and present unique packing characteristics with uniform pores between particles. Moreover, their flowing properties

during injection will be more predictable since their shape and size are more regular [169]. In certain applications, the effectiveness of the microspheres can be highly improved if they can act simultaneously as carriers for biologically active molecules or cells. Microspheres can be loaded with different agents (proteins as for instance growth factors, enzymes, antibiotics) in order to stimulate the regeneration of bone tissue [170-172] or even be seeded with cells prior to implantation [173-175]. Consequently, the advantages presented by injectable systems for bone regeneration based on microspheres stimulates further research in this area.

Two different types of ceramic-based microspheres are used as bone defect fillers, namely ceramic-polymer composites or pure ceramic particles. Several methodologies are described in the literature concerning the preparation of spherical particles [170-172, 176-182]. For instance, Paul *et al* and Sunny *et al* [170, 176] produced HAp/chitosan microspheres by the dispersion of HAp/chitosan slurry in liquid paraffin, with the addition of gluteraldehyde to harden the spheres, followed by sintering. Sivakumar *et al* [171, 172] developed a method to produce coralline HAp/chitosan and coralline HAp/gelatin composite microspheres using a PMMA dispersion solution containing toluene as a crosslinking agent. Krylova *et al* [177] developed a technique to prepare hydroxyapatite/polysaccharide microgranules based on the formation of hydroxyapatite by co-precipitation from sodium alginate and sodium carboxymethylcellulose aqueous solutions with the use of diphasic calcium phosphate dihydrate and calcium hydroxide. Qiu *et al* [178] developed hollow ceramic microspheres with a composition of 58-72% SiO_2, 28-42% Al_2O_3 (wt%) coated with hydroxyapatite particulate sol, to be used as microcarriers for 3-D bone tissue formation in rotating bioreactors. The same authors [179] also produced composite microspheres to be used as bone grafts using PLA (polylactic acid) as the matrix and two different fillers, hydroxyapatite and modified bioactive glass. The method used by Komlev *et al* [180] to produce microspheres was based on the liquids immiscibility effect. A suspension of HAp powder in aqueous solution of gelatin and oil as a dispersion media were used. The stirring of the mixture results in the beads formation due to the surface tension forces. After washing, the beads were heated to burn-off gelatin followed by sintering. Most of the methodologies described above present the disadvantage of needing fastidious washing processes to eliminate the reactants used in the preparation of the microspheres.

References

[1] Williams DF. The Williams Dictionary of Biomaterials. Liverpool, UK: Liverpool University Press, 1999.

[2] Hench LL, Polak JM. Third-generation biomedical materials. Science 2002; 298: 917-1180.

[3] Hench LL. Biomaterials. Science 1980; 208: 826-831.

[4] Williams DF. Titanium for medical applications. In: Brunette DM, Tengvall P, Textor M, Thomsen P, editors. Titanium in Medicine- Materials Science, Surface Science, Engineering, Biological Responses and Medical Applications. Berlin, Germany: Springer Verlag, 2001. p.14-23.

[5] Bonfield W. Biomaterials Research and Development. In: European White Book on Fundamental Research in Materials Science, Max-Planck Institut Fur Metallforschung Stuttgart, 2001.

[6] Hench LL, Wilson J. Surface-active biomaterials. Science 1984; 226: 630-636.

[7] Hench LL, Splinter RJ, Allen WC, Greenlee TK. Bonding mechanism at the interface of ceramic prosthetic materials. J Biomed Mater Res 1971; 2: 117-141.

[8] Bonfield W, Grynpas MD, Tully AE, Bauman J, Abram J. Hydroxyapatite reinforced polyethylene - a mechanically compatible implant material for bone replacement. Biomaterials 1981; 2: 185-186.

[9] Bonfield W, Behiri JC, Doyle C, Bowman S, Abram J. Hydroxyapatite reinforced polyethylene composites for bone replacement. In: Ducheyne P, van der Perre G, Aubert AE editors. Biomaterials and Biomechanics. Amsterdam, Holland: Elsevier Science, 1984. p.421-426.

[10] Greenlee TK, Beckham CA, Crebo AR, Malmborg JC. Glass-ceramic bone implants. J Biomed Mater Res 1972; 6: 235-244.

[11] Cameron HU, MacNeb I, Pilliar RM. Evaluation of a bidegradable ceramic. J Biomed Mater Res 1977; 11: 179-186.

[12] Jarcho M. Calcium phosphate ceramics as hard tissue prosthetics. Clin Orthop and Rel Res 1981; 157: 259-278.

[13] Kato K, Aoki H, Tabota T, Ogiso M. Biocompatibility of apatite ceramics in mandibles. Biomed Med Dev Art Org 1979; 7: 291-297.

[14] Ogino M, Ochuchi F, Hench LL. Compositional dependence of the formation of calcium phosphate films on bioglass. J Biomed Mater Res 1980; 14: 55-59.

[15] Groot de K. Degradable ceramics. In: Williams DF, editor. Biocompatibility of Clinical Implant Materials, Vol I. Boca Raton, USA: CRC-Press, 1981. p.199-224.

[16] Grote JJ, Kuypes W, de Groot K. Use of sintered hydroxylapatite in middle ear surgery. ORI 1981; 43: 248-254.

[17] Bhaskar SN, Brady JM, Getter L, Growen MP, Driskell T. Biodegradable ceramic implants in bone. Oral Surg 1971; 32: 334-346.

[18] Mors WA, Kaminsk EJ. Osteogenic replacement of tricalcium phosphate ceramic implants in the dog palate. Arch Oral Biol 1975; 20: 365-368.

[19] Rejda BV, Peelen JGJ, de Groot K. Tricalcium phosphate as a bone substitute. J Bioeng 1977; 1: 93-97.

[20] Ferraro JW. Experimental evaluation of ceramic calcium-phosphate as a substitute for bone grafts. Plast Reconstruct Surg 1979; 63: 634-640.

[21] Hench LL. Ceramics, glasses and composites in medicine. Med Instrum 1973; 7: 136-144.

[22] Groot de K, Geesink RGT, Serekian P, Klein CPAT. Plasma sprayed coatings of hydroxylapatite. J Biomed Mater Res 1987; 21: 1375-1381.

[23] Ducheyne P, van Raemdonck W, Heughebaert JC, Heughebaert M. Structural analysis of hydroxyapatite coatings on titanium. Biomaterials 1986; 7: 97-103.

[24] Geesink RGT, de Groot K, Klein CPAT. Chemical implant fixation using hydroxylapatite coatings. Clin Orthop 1987; 225: 147-170.

[25] Wood DA. Biodegradable drug delivery systems. Int J Pharma 1980; 7: 1-18.

[26] Rhine W, Hsieh DS, Langer R. Polymers for sustained macromolecule release: procedures to fabricate reproducible delivery systems and control release kinetics. J Pharm Sc 1980; 69: 265-270.

[27] Wahlig H, Dingeldein E. Antibiotics and bone cements. Experimental and clinical long-term observations. Act Orthop Scand 1980; 51: 49-56.

[28] Kulkarni RK, Moore EG, Hegyeli AF, Leonard F. Biodegradable poly(lactic acid) polymers. J Biomed Mater Res 1971; 5: 169-181.

[29] Gilding DK, Reed AM. Biodegradable polymers for use in surgery: polyglycolic acid/ poly(lactic acid) homo- and copolymers. Polymer 1979; 20: 1459-1464.

[30] Ferber D. Tissue engineering: lab-grown organ began to take shape. Science 1999; 284: 422-425.

[31] Lee KY, Mooney DJ. Hydrogels for Tissue Engineering. Chem Rev 2001; 101: 1869-1879.

[32] Posner AS. The mineral of bone. Clinical Orthopaedics 1985; 200: 87-99.

[33] Larsson C, Esposito M, Liao H, Thomsen P. The titanium-bone interface *in vivo*. In: Brunette DM, Tengvall P, Textor M, Thomsen P, editors. Titanium in Medicine-Materials Science, Surface Science, Engineering, Biological Responses and Medical Applications. Berlin, Germany: Springer Verlag, 2001. p.587-648.

[34] Rey C. Calcium Phosphates for Medical Applications. In: Zahid Amjad, editor. Calcium Phosphates in Biological and Industrial Systems. Boston, USA: Kluwer Academic Publishers, 1998. p.217-251.

[35] Legros R, Balmain N, Bonel G. Age related changes in mineral of rat and bovine cortical bone. Calcif Tissue Int 1987; 41: 137-144.

[36] Jain AK, Panchagnula R. Review- Skeletal drug delivery systems. Int J Pharm 2000; 206: 1-12.

[37] Termine JD, Posner AS. Amorphous/crystalline interrelationships in bone mineral. Calcif Tissue Res 1967; 1: 8-23.

[38] Eanes ED, Termine JD, Posner AS. Amorphous calcium phosphate in skeletal tissues. Clin Orthoped 1967; 53: 223-235.

[39] Siew C, Gruninger SE, Chow LC, Brown WE. Procedure for the study of acidic calcium and phosphate precursor phases in enamel mineral formation. Calcif Tissue Int 1992; 50: 144-148.

[40] Brown WE, Smith JP, Lehr JR, Frasier AW. Crystallographic and chemical relations between octacalcium phosphate and hydroxyapatite. Nature 1962; 196: 1050-1055.

[41] Termine JD, Posner AS. Infrared analysis of rat bone: age dependency of amorphous and crystalline mineral fractions. Science 1966; 153: 1523-1525.

[42] Boskey AL, Camacho NP, Mendelsohn R, Doty SB, Binderman I. FT-IR microscopic mappings of early mineralization in chick limb bud mesenchymal cell cultures. Calcif Tissue Int 1992; 51: 443-448.

[43] Boskey AL, Pleshko N, Doty SB, Mendelsohn R. Applications of Fourier transform infrared (FT-IR) microscopy to the study of the mineralization in bone and cartilage. Cells and Materials 1992; 2: 209-220.

[44] Rey C, Collins B, Goehl T, Dickson IR, Glimcher MJ. The carbonate environment in bone mineral: a resolution-enhanced Fourier transform infrared spectroscopy study. Calcif Tissue Int 1989; 45: 157-164.

[45] Rey C, Shimizu M, Collins B, Glimcher MJ. Resolution enhanced Fourier transform infrared spectroscopy study of the environment of phosphate ion in the early deposits of a solid phase calcium phosphate in bone and enamel and their evolution with age: investigations in the $\nu_3 PO_4^{3-}$ domain. Calcif Tissue Int 1991; 49: 383-388.

[46] Rey C, Shimizu M, Collins B, Glimcher MJ. Resolution enhanced Fourier transform infrared spectroscopy study of the environment of phosphate ion in the early deposits of a solid phase calcium phosphate in bone and enamel and their evolution with age: investigations in the $\nu_4 PO_4^{3-}$ domain. Calcif Tissue Int 1990; 46: 384-394.

[47] Rey C, Renugopalakrishnan V, Collins B, Glimcher MJ. Fourier Transform infrared spectroscopic study of the carbonate ions in bone mineral during aging. Calcif Tissue Int 1991; 49: 251-258.

[48] Herzfeld J, Berger SE. Sideband intensities in NMR spectra of samples spinning at the magic angle. J Chem Phys 1980; 73: 6021-6030.

[49] Aue WP, Roufosse AH, Glimcher MJ, Griffin RG. Solid-state phosphorous-31 nuclear magnetic resonance studies of synthetic solid phases of calcium phosphate: potential models of bone mineral. Biochemistry 1984; 23: 6110-6114.

[50] Wu Y, Glimcher MJ, Rey C, Ackerman JL. A Unique protonated phosphate group in bone mineral not present in synthetic calcium phosphates - Identification by phosphorous-31 solid state NMR spectroscopy. J Mol Biol 1994; 244: 423-435.

[51] Bauer TW, Stulberg BN, Ming J, Geesink RGT. Uncemented acetabular components: histologic analysis of retrieved hydroxyapatite-coated and porous implants. J Arthroplasty 1993; 8: 167-177.

[52] Porter AE, Taak P, Hobbs LW, Coathup MJ, Blunn GW, Spector M. Bone bonding to hydroxyapatite and titanium surfaces on femoral stems retrieved from human subjects at autopsy. Biomaterials 2004; 25: 5199-5208.

[53] MacDonald DE, Betts F, Stranick M, Doty S, Boskey AL. Physicochemical study of plasma-sprayed hydroxyapatite-coated implants in humans. J Biomed Mater Res 2001; 54: 480-490.

[54] Michel R. Trace element analysis in biocompatibility testing. CRC Crit Rev Biocomp; 1987. p.235-317.

[55] Lewandowska-Szumielm M, Komender J. Aluminium release as a new factor in the estimation of alumina bioceramic implants. Clin Mater 1990; 5: 167-175.

[56] Jones LC, Hungerford DS. Urinary metal ion levels in patients implanted with porous coated total hip prostheses. Trans Orthop Res Soc 1987; 32: 317.

[57] Black J. Does corrosion matter? J Bone Joint Surg 1988; 70 B: 517-520.

[58] Sunderman FW Jr., Hopfer SM, Swift T, Rezuke WN, Ziebka L, Highman P, Edwards B, Folcik M, Gossling HR. Cobalt, chromium and nickel concentrations in body fluids of patients with porous-coated knee or hip prostheses. J Orthop Res 1989; 7: 307-315.

[59] Woodman JL, Jacobs JJ, Galante JO, Urban RM. Metal ion release from titanium-based prosthetic segmental replacements of long bones in baboons: a long term study. J Orthop Res 1984; 1: 421-430.

[60] Ducheyne P, Healy K, Black J, Cuckler J. The effect of hydroxyapatite coatings on the metal ion release from porous titanium and cobalt chromium alloys. Trans Orthop Res Soc 1987; 12: 315.

[61] Black J, Skipor A, Jacobs J, Urban RM, Galante JO. Release of metal ions from titanium-base alloy total hip replacement prostheses. Trans Orthop Res Soc 1989; 14: 501.

[62] Ektessabi AM, Otsuka T, Tsuboi Y, Yokoyama K, Albrektsson T, Sennerby L, Johansson CB. Quantitative measurement of metal-ion release from biomedical implants- application of microbeam PIXE to detection of titanium ion release from dental and orthopaedic implants. Int J PIXE 4 1994; 2/3: 81-91.

[63] Ektessabi AM, Otsuka T, Tsuboi Y, Horino Y, Mokuno Y, Fujii K, Albrektsson T, Sennerby L, Johansson C. Preliminary experimental results on mapping of the elemental distribution of the organic tissues surrounding titanium-alloy implants. Nuc Inst Meth Phys Res B 1996; 109/110: 278-283.

[64] Niki Y, Matsumoto H, Otani T, Suda Y, Toyama Y. Metal ion concentrations in the joint fluid immediately after total knee arthroplasty. Mod Reum 2001; 11: 192-196.

[65] Tanaka N, Ichinose S, Kimijima Y, Mimura M. Investigation of titanium leak to bone tissue surrounding dental titanium implant: electron microscopic findings and analysis by electron diffraction. Med Elec Mic 2000; 33: 96-101.

[66] Lijian Z, Ti-Sheng C, Wei W, Lei C. Study of commercially pure titanium implants bone integration mechanisms. Eur J Plas Surg 2000; 23: 301-304.

[67] Bianco PD, Ducheyne P, Cuckler JM. Local accumulation of titanium released from a titanium implant in the absence of wear. J Biomed Mater Res 1996; 31: 227-234.

[68] Merritt K, Margevicius, Brown SA. Storage and elimination of titanium, aluminium, and vanadium salts, *in vivo*. J Biomed Mater Res 1992; 26: 1503-1515.

[69] Bronner F. Metals in bone: aluminium, boron, cadmium, chromium, lead, silicon, and strontium. In: Bilezikian JP, Lawrence GR, Gideon AR, editors. Principles of bone biology. San Diego, USA: Academic Press, 1996. p.295-303.

[70] Goodman WG, Duarte MEL. Aluminum: effects on bone and role in the pathogenesis of renal osteodystrophy. Miner Electrolyte Met 1991; 17: 221-232.

[71] Posner AS, Blumenthal NC. *In vitro* model of aluminium- induced osteomalacia: inhibition of hydroxyapatite formation and growth. J Calcif Tissue Int 1984; 36: 439-441.

[72] Andress DL, Maloney NA, Endres DB, Sherrard DJ. Aluminum-associated bone disease in chronic renal failure: high prevalence in a long-term dialysis population. J Bone Min Res 1986; 1: 391-398.

[73] Andress DL, Maloney NA, Coburn JW, Endres DB, Sherrard DJ. Osteomalacia and aplastic bone disease in aluminum-related osteodystrophy. J Clin End & Metab 1987; 65: 11-16.

[74] Severson AR, Haut CF, Firling CE, Huntley TE. Influence of short-term aluminum exposure on demineralized bone matrix induced bone formation. Arch Toxicol 1992; 66: 706-712.

[75] Posner AS, Blumenthal NC, Boskey AL. Model of aluminum-induced osteomalacia: inhibition of apatite formation and growth. Kidney Int 1986; 29: 17-19.

[76] Christoffersen MR, Christoffersen J. The effect of aluminium on the rate of dissolution of calcium hydroxyapatite: a contribution to the understanding of aluminium- induced bone diseases. Calcif Tissue Int 1985; 37: 673-676.

[77] Christoffersen MR, Thyregod HC, Christoffersen J. Effects of aluminum(III), chromium(III), and iron(III) on the rate of dissolution of calcium hydroxyapatite crystals in the absence and presence of chelating agent desferrixamine. Calcif Tissue Int 1987; 41: 27-30.

[78] O´Brien Aaj, Moore DP, Keogh JAB. Aluminium osteomalacia in chronic renal failure patients neither on dialysis nor taking aluminium containing phosphate binders. Irish J Med Sci 1990; 150: 74-76.

[79] Bordji K, Jouzeau JY, Mainard D, Payan E, Netter P, Rie KT, Stucky T, Hage-Ali M. Cytocompatibility of Ti-6Al-4V and Ti-5Al-2.5Fe alloys according to three surface treatments, using human fibroblasts and osteoblasts. Biomaterials 1996; 17: 929-940.

[80] Zaffe D, Bertoldi C, Consolo U. Accumulation of aluminium in lamellar bone after implantation of titanium plates, Ti-6Al-4V screws, hydroxyapatite granules. Biomaterials 2004; 25: 3837-3844.

[81] Tung SM. Calcium phosphates: structure, composition, solubility and stability. In: Zahid Amjad, editor. Calcium Phosphates in Biological and Industrial Systems. Boston, USA: Kluwer Academic Publishers; 1998. p.1-19.

[82] Gibson IR, Rehman I, Best SM, Bonfield W. Characterization of the transformation from calcium-deficient apatite to β-tricalcium phosphate. J Mater Sci Mater Med 2000; 12: 799-804.

[83] Welcht JH, Gutt W. High temperature studies of the system calcium oxide-phosphorous pentoxide. J Chem Soc 1961; 2: 4442-4444.

[84] Schroeder LW, Dickens B, Brown WE. Crystallographic studies of the role of Mg as a stabilizing impurity in β-$Ca_3(PO_4)_2$ - II. Refinement of Mg-containing β-$Ca_3(PO_4)_2$. J Sol State Chem 1977; 22: 253-262.

[85] Fowler BO. Infrared studies of apatites. II Preparation of normal and isotopically substituted calcium, strontium, and barium hydroxyapatites and spectra-structure-composition correlations. Inorg Chem 1974; 13: 207-214.

[86] LeGeros RZ, Daculsi G, Orly I, Abergas T, Torres W. Solution mediated transformation of octacalcium phosphate (OCP) to apatite. Scann Microsc 1989; 3: 129-138.

[87] Cheng PT. Formation of octacalcium phosphate and subsequent transformation to hydroxyapatite at low supersaturation: a model for cartilage calcification. Calcif Tissue Int 1987; 40: 339-343.

[88] Tanahashi M, Kamiya K, Suzuki T, Nasu H. Fibrous hydroxyapatite grown in the gel system: effects of pH of the solution on the growth rate and morphology. J Mater Sci Mater Med 1992; 3: 48-53.

[89] Takahashi H, Yashima M, Kakihana M, Yoshimura M. Synthesis of stoichiometric hydroxyapatite by a "gel" route from the aqueous solution of citric and phosphonoacetic acids. Eur J Solid State Inorg Chem 1995; 32 :829-835.

[90] Posner AS, Blumenthal N, Betts F. Chemistry and Structure of Precipitated Hydroxyapatites. In: Nriagu JO, Moore PB, editors. Phosphate Minerals. New York, USA: Springer Verlag, 1984. p.330-347.

[91] Bonel G, Heughebaert JC, Heughebaert M, Lacout JL, Lebugle A. Apatitic calcium orthophosphates and related compounds for biomaterials preparations. In: Ducheyne P, Lemons J, editors. Bioceramics: Material characteristics versus *in vivo* behavior, Vol.253. New York, USA: Ann New York Acad Sci, 1988. p.115-130

[92] Roy DM, Linnehan SA. Hydroxyapatite formed from coral skeleton carbonate by hydrothermic exchange. Nature 1974; 247: 220-227.

[93] Brendel T, Engel A, Ruessel C. Hydroxyapatite coatings by a polimeric route. J Mater Sci: Mater in Med 1992; 3: 175-178.

[94] Yamashita K, Kanazawa T. Hydroxyapatite. In: Kanazawa T, editor. Inorganic Phosphate Materials. Tokyo, Japan: Kodansha, 1989. p.15-54.

[95] Koutsopoulos S. Synthesis and characterization of hydroxyapatite crystals: a review study on the analytical methods. Biomaterials 2002; 62: 600-612.

[96] Young RA, Holcomb DW. Variability of hydroxyapatite preparations. Calcif Tissue Inter 1082; 34: 517-532.

[97] Suchanek W, Yoshimura M. Processing and properties of hydroxyapatite-based biomaterials for use as hard tissue replacement implants. J Mat Res 1998; 13: 94-117.

[98] Elliot JC. PhD Thesis 1964, University of London, London, England.

[99] Elliot JC. In: Elliot JC, editor. Structure and chemistry of the apatites and other calcium orthophosphates. Amsterdam, Holland: Elsevier, 1994.

[100] Elliot JC, Mackie PE, Young RA. Monoclinic hydroxyapatite. Science 1973; 180: 1055-1057.

[101] Morgan H, Wilson RM, Elliot JC, Dowker SEP, Anderson P. Preparation and characterisation of monoclinic hydroxyapatite and its precipitated carbonate apatite intermediate. Biomaterials 2000; 21: 617-627.

[102] Watanabe T, Makitsuru K, Nakazawa H, Hara S, Suehiro T, Yamamoto A, Hiraide T, Ogawa T. Separation of double strand DNA fragments by high-performance liquid chromatography using a ceramic hydroxyapatite column. Anal Chim Acta, 1999; 386: 69-75.

[103] LeGeros RZ. Biological and synthetic apatites. In: Brown PW, Constanz B, editors. Hydroxyapatites and Related Materials, Boca Raton, USA: CRC Press, 1994. p.3-28.

[104] Bett JAS, Christner LG, Hall WK. Studies of the hydrogen held by solids. XII. J Am Chem Soc 1967; 89: 5535-5541.

[105] Matsumara Y, Kanai H, Moffat JB. Catalytic oxidation of carbon monoxide over stoichiometric and non-stoichiometric hydroxyapatites. J Chem Soc, Faraday Trans, 1997; 93: 4383-4387.

[106] Takeuchi Y, Arai H. Removal of coexisting Pb^{2+}, Cu^{2+} and Cd^{2+} ions from water by addition of hydroxyapatite powder. J Chem Eng of Japan 1990; 23: 75-80.

[107] Suzuki T, Hastushika T, Miyake M. Synthetic. Hydroxyapatites as inorganic cation exchangers-Part 2. J Chem Soc, Faraday Trans I, 1981; 78: 3605-3611.

[108] Aoki H. In: Aoki H, editor. Science and Medical Applications of Hydroxyapatite. Tokyo, Japan: Takayama Press System Center, 1991.

[109] LeGeros RZ. Ultrastructural Properties of Human Enamel Apatite. In: Lazzari EP editor. Handbook of Experimental Aspects of Oral Biochemistry. Florida, USA: CRC Press, 1983. p.159-179.

[110] Narasaraju TSB, Phebe DE. Review: Some physico-chemical aspects of hydroxyapatite. J Mat Sci 1996; 31: 1-21.

[111] Bonel G, Montel G. Sur une nouvelle apatite carbonatée synthétique. Compt Rend 1964; 258: 923-926.

[112] LeGeros RZ, Trautz OR., LeGeros JP, Klein E. Carbonate substitution in the apatite structure (1). Extrait du bulletin de la societé chimique de France 1968; special number: 1712-1718.

[113] LeGeros RZ, Singer L, Ophaug RH, Quirolgico G, Thein A, LeGeros J P. The effect of fluoride on the stability of synthetic and biological (bone) mineral apatites. In: Menczel J, Robin GC, Makin M, Steinbeg R, editors. Osteoporosis. New York, USA: Wiley & Sons, 1982. p. 327-341.

[114] Kreidler ER, Hummel FA. The crystal chemistry of apatite: structure fields of fluor and chloroapatite. The American Mineralogist 1970; 55: 171-184.

[115] Gibson IR, Best SM, Bonfield W. Chemical characterisation of silicon-substituted hydroxyapatite. J Biomed Mater Res 1999; 44: 422-428.

[116] LeGeros RZ, Shirra WP, Miravite M, LeGeros JP. Amorphous calcium phosphates: synthetic and biological. Physico-chimie et cristallographie des apatites d'interet biologique 1975; CNRS N°230: 105-115.

[117] LeGeros RZ, Miravite MA, Quirolgico GB, Curzon MEJ. The effect of some trace elements on the lattice parameters of human and synthetic apatites. Calc Tiss Res 1977; 22: 362-367.

[118] LeGeros RZ, Taheri MH, Quirolgico GB, LeGeros JP. Formation and stability of apatites: effects of some cationic substituents. In: Proceedings of 2nd International Congress on Phosphorous Compounds. Boston, USA, 1980. p.89-103.

[119] Sudarsanan K, Markie PE, Young RA. Comparison of synthetic and mineral fluorapatite $Ca_5(PO_4)_3F$, in crystallographic detail. Mat Res Bull 1972; 7: 1331-1338.

[120] Moreno EC, Kresak M, Zahradnik RT. Fluoridated hydroxyapatite solubility and caries formation. Nature 1974; 247: 64-65.

[121] LeGeros RZ, Trautz OR, LeGeros JP, Shirra WP. Apatite crystallites: effects of carbonate on morphology. Science 1967; 155: 1409-1411.

[122] Dickens B, Brown WE. The crystal structure of $Ca_7Mg_9(Ca, Mg)_2(PO_4)_{12}$. Tmpm 1971; 16: 79-104.

[123] Trombe JC, Montel G. Process for treating apatites applicable to other minerals. CR Acad Sci Ser C 1974; 278: 1227-1230.

[124] Christoffersen J, Christoffersen MR, Kolthoff N, Barenholdt O. Effects of strontium ions on growth and dissolution of hydroxyapatite and on bone mineral detection. Bone 1997; 20: 47-54.

[125] Koutsoukos PG, Nancollas GH. Influence of strontium ion on the crystallization of hydroxyapatite from aqueous solutions. J Phys Chem 1981; 85: 2403-2408.

[126] Neuman WF, Bjornerstedt B, Mulryan BJ. Synthetic hydroxyapatite crystals II. Aging and strontium incorporation. Arch Biochem Biophys 1963; 101: 215-224.

[127] Morohashi T, Sane T, Yamada S. Effects of strontium on calcium metabolism in rats. I. A distinction between the pharmacological and toxic doses. Japn J Pharmacol 1994; 64: 155-162.

[128] Brandi UL. New treatment strategies: Ipiflavone, strontium, vitamin D metabolites and analogs. Am J Med 1993; 95: 695-745.

[129] Ben Abdelkader S, Khattech I, Rey C, Jemal M. Synthése, caractérisation et thermochimie d'apatites calco magnésiennes hydroxylées et fluorées. Thermochimica Acta 2001; 376: 25-36.

[130] LeGeros RZ. Phosphate minerals in human tissues. In: Nriagu JO, Moore PB, editors. Phosphate Minerals. Berlin, Germany: Springer Verlag, 1984. p.351-385.

[131] LeGeros RZ. Variations in the crystalline components of human dental calculus. I. Crystallographic and spectroscopic analysis. J Dent 1974; 53: 45-50.

[132] LeGeros RZ, Contiguglia SR, Alfrey AC. Pathological calcifications associated with uremia: two types of calcium phosphates deposits. Calcif Tissue Res 1973; 13: 173-179.

[133] Boskey AL, Posner AS. Mg stabilization of amorphous calcium phosphates: a kinetic study. Mater Res Bull 1974; 9: 907-916.

[134] Posner AS, Betts F. Molecular control of tissue mineralization. In: Veis A, editor. The chemistry and biology of mineralized connective tissue. New York, USA: Elsevier-North Holland, 1981. p.257.

[135] Ergun C, Webster TJ, Bizios R, Doremus RH. Hydroxylapatite with substituted magnesium, zinc, cadmium, and yttrium. I. Structure and microstructure. J Biomed Mater Res 2002; 59: 305-311.

[136] Webster TJ, Ergun C, Doremus RH, Bizios R. Hydroxylapatite with substituted magnesium, zinc, cadmium, and yttrium. II. Mechanisms of osteoblast adhesion. J Biomed Mater Res 2002; 59: 312-317.

[137] Bigi A, Foresti E, Gandolfi M, Gazzano M, Roveri N. Inhibiting effect of zinc on hydroxylapatite crystallisation. J Inorg Biochem 1995; 58: 49-58.

[138] Samachon J, Dennis H, Fowler R, Schmitz A. The reaction of ^{65}Zn with the surfaces of bone and bone mineral. Biochim Biophys Acta 1967; 148: 767-773.

[139] Miyahara T, Yomada H, Takeuchi M, Kozuka H, Kato T, Sudo H. Inhibitory effects of cadmium on *in vitro* calcification of a clonal osteogenic cell, Mc3T3-E1. Toxicol Appl Pharmacol 1988; 96: 52-59.

[140] Chang LW, Reuhl KR, Wade PR. Pathological effects of cadmium poisoning. In: Nriagu JO, editor. Cadmium in the environment, Part II: Health effects. New York, USA: Wiley, 1981. p.784-839.

[141] Blumenthal NC, Cosma V, Skyler D, LeGeros J, Walters M. The effect of cadmium on the formation and properties of hydroxyapatite *in vitro* and its relation to cadmium toxicity in the skeletal system. Calcif Tissue Int 1995; 56: 316-322.

[142] Barry PS. A comparison of concentrations of lead in human tissues. Br J Ind Med 1975; 32: 119-139.

[143] Levin SM, Goldberg M. Clinical evaluation and management of lead-exposed construction workers. Am J Ind Med 2000; 37: 23-43.

[144] El Feki H, Savariault JM, Ben Salah A. Structure refinements by Rietveld method of partially substituted hydroxyapatite: $Ca_9Na_{0.5}(PO_4)_{4.5}(CO_3)_{1.5}(OH)_2$. J Alloys Compounds 1999; 287: 114-120.

[145] Koutsoukos PG. Influence of metal ions on the crystal growth of calcium phosphates. In: Zahid Amjad, editors. Calcium Phosphates in Biological and Industrial Systems. Boston, USA: Kluwer Academic Publishers, 1998. p.143-171.

[146] Blumenthal NC, Betts F, Posner AS. Effect of carbonate and biological macromolecules on formation and properties of HAp. Calcif Tiss Res 1975; 18: 81-90.

[147] Porter AE, Patel N, Skepper JN, Best SM, Bonfield W. Effect of sintered silicate-substituted hydroxyapatite on remodelling processes at the bone-implant interface. Biomaterials 2004; 37: 34-39.

[148] LeGeros RZ. The unit-cell dimensions of human enamel apatite: effect of chloride incorporation. Archs Oral Biol 1974; 20: 63-71.

[149] Alamo J. Chemistry and properties of solids with NZP skeleton. Solid State Ionics 1993; 63-65: 547-561.

[150] Szmukler-Moncler S, Daculsi G, Delécrin J, Passuti N, Deudon C. Calcium-Metallic-Phosphates: a new coating biomaterial? In: Doherty PJ *et al*, editor. Biomaterial-Tissue Interfaces. Advances in Biomaterials, vol.10. Elsevier Science Publishers BV, 1992. p.377-383.

[151] Lugsheider E, Berger G, Knepper M, Sicking R, Nyland A. Plasma sprayed coatings of calcium titanium phosphate: a new generation of bioactive coatings. In: Wilson J *et al*, editors. Bioceramics, vol. 8. Pergamon/Elsevier Science Ltd, 1995. p.317-322.

[152] Knabe C, Berger G, Gildenhaar R, Klar F, Zreiqat H. The modulation of osteogenesis *in vitro* by calcium titanium phosphate coatings. Biomaterials 2004; 25: 4911-4919.

[153] Gross U, Muller Mai C, Voigt C, Mesgaran M, Berger G, Ploska U. Tissue response in the femur of rabbits after implantation of a new calcium titanium phosphate composition. Key Eng Mat 2001; 192-195: 383-386.

[154] Hosono H, Abe Y. Porous glass-ceramics composed of a titanium phosphate crystal skeleton: a review. J of Non-Cryst Solids 1995; 190: 185-197.

[155] Suzuki T, Toriyama M, Hosono H, Abe Y. Application of a microporous glass-ceramic with a skeleton of $CaTi_4(PO_4)_6$ to carriers for immobilization of enzymes. J Ferment Bioeng 1991; 72: 384-391.

[156] Laurencin CT, Lu HH. Polymer-ceramic composites for bone tissue engineering. In: Davies JE, editor. Bone engineering. Toronto, Canada: EM Squared Inc, 2000. p.463-472.

[157] Schnettler R, Stahl JP, Alt V, Pavlidis T, Dingeldein E. Calcium phosphate-based bone substitutes. Eur J Trauma 2004; 4: 219-229.

[158] Sims CD, Butler PEM, Casanova R, Lee BT, Randolph MA, Lee WPA, Vacant CA, Yamremchuk MJ. Injectable cartilage using polyethylene oxide polymer substrates. Plast Reconstr Surg 1996; 98: 843-850.

[159] Suggs LJ, Shive MS, Garcia CA, Anderson JM, Mikos AG. *In vitro* cytotoxicity and *in vivo* biocompatibility of poly (propylene fumarate-co-ethylene glycol) hydrogels. J Biomed Mater Res 1999; 46: 22-32.

[160] Suggs LJ, Krishnan RS, Garcia CA, Peter SJ, Anderson JM, Mikos AG. *In vitro* and *in vivo* degradation of poly(propylene fumarate-co-ethylene glycol) hydrogels. J Biomed Mater Res 1998; 42: 312-320.

[161] Frazier DD, Lathi VK, Gerhart TN, Hayes WC. Ex vivo degradation of a poly (propylene glycol-fumarate) biodegradable particulate bone cement. J Biomed Mater Res 1997; 35: 383-389.

[162] Kharas GB, Kamanetsky M, Simantirakis J, Beinlich KC, Rizzo A-MT, Caywood GA, Watson K. Synthesis and characterization of fumarate-based polyesters for use in bioresorbable bone cement composites. J Appl Polym Sci 1997; 66: 1123-1137.

[163] Paige KT, Cima LG, Yaremchuck MJ, Vacant JP, Vacant CA. Injectable cartilage. Plast Reconstr Surg 1995; 96: 1390-1400.

[164] Paige KT, Cima LG, Yaremchuck MJ, Vacant JP, Vacant CA. De novo cartilage generation using calcium-alginate-chondrocyte constructs. Plast Reconstr Surg 1996; 97: 168-180.

[165] Kulseng B, Skjak-Braek G, Ryan L, Andersson A, King A, Faxvaag A, Espevik T. Transplantation of alginate microcapsules. Transplantation 1999; 67: 978-984.

[166] Martinetti R, Dolcini L, Ravaglioli A, Krajewski A, Mangano C. Experimental study on hydroxyapatite/N-carboxymethyl chitosan fillers. In: Sedel L, Rey C, editors. Bioceramics, vol. 10. Oxford, UK: Elsevier, 1997. p.503-506.

[167] Maruyama M, Ito M. *In vitro* properties of a chitosan-bonded self-hardening paste with hydroxyapatite granules. J Biomed Mater Res 1996; 32: 527-532.

[168] Dupraz A, Nguyen TP, Richard M, Daculsi G, Passuti N. Influence of a cellulosic ether carrier on the structure of biphasic calcium phosphate ceramic particles in an injectable composite material. Biomaterials 1999; 20: 663-673.

[169] Misiek DJ, Kent JN, Carr RT. Soft tissue responses to hydroxylapatite particles of different shapes. J Oral Maxilllofac Surg 1984; 42: 150-160.

[170] Paul W, Sharma CP. Development of porous spherical hydroxyapatite granules: application towards protein delivery. J Mater Sci: Mater Med 1999; 10: 383-388.

[171] Sivakumar M, Manjubala I, Rao KP. Preparation, characterisation and in-vitro release of gentamicin from coralline hydroxyapatite-chitosan composite microspheres. Carbohydrate Polymers 2002; 49: 281-288.

[172] Sivakumar M, Rao KP. Preparation, characterization and *in vitro* release of gentamicin from coralline hydroxyapatite-gelatin composite microspheres. Biomaterials 2002; 23: 3175-3181.

[173] Hsu FY, Chueh SC, Wang Y. Microspheres of hydroxyapatite reconstituted collagen as supports for osteoblast cell growth. Biomaterials 1999; 20: 1931-1936.

[174] Wu TJ, Huang H-H, Lan C-H,Lin C-H, Hsu F-Y, Wang Y-J. Studies on the microspheres comprised of reconstituted collagen and hydroxyapatite. Biomaterials 2004; 25: 651-658.

[175] Senuma Y, Franceschin S, Hilborn JG, Tissières P, Bisson I, Frey P. Bioresorbable microspheres by spinning disk atomization as injectable cell carrier: from preparation to *in vitro* evaluation. Biomaterials 2000; 21: 1135-1144.

[176] Sunny MC, Ramesh P, Varma HK. Microstructured microspheres of hydroxyapatite bioceramic. J Mater Sci: Mater Med 2002; 13: 623-632.

[177] Krylova E, Ivanov A, Orlovski V, El-Registan G, Barinov S. Hydroxyapatite-polysaccharide granules for drug delivery. J Mater Sci: Mater Med 2002; 13: 87-90.

[178] Qiu QQ, Ducheyne P, Ayyaswamy PS. Fabrication, characterization and evaluation of bioceramic hollow microspheres used as microcarriers for 3-D bone tissue formation in rotating bioreactors. Biomaterials 1999; 20: 989-1001.

[179] Qiu QQ, Ducheyne P, Ayyaswamy PS. Bioactive, degradable composite microspheres: effect of filler material on surface reactivity. Ann N Y Acad Sci: 2002; 974: 556-564.

[180] Komlev VS, Barinov SM, Koplik EV. A method to fabricate porous spherical hydroxyapatite granules intended for time-controlled drug release. Biomaterials 2002; 23: 3449-3454.

[181] Qiu QQ, Ducheyne P, Ayyaswamy PS. New bioactive, degradable composite microspheres as tissue engineering substrates. J Biom Mater Res 2000; 52: 66-76.

[182] Borden M, Attawia M, Khan Y, Laurencin CT. Tissue engineered microsphere-based matrices for bone repair: design and evaluation. Biomaterials 2002; 23: 551-559.

Chapter 2

FORMATION OF TITANIUM PHOSPHATE COMPOUNDS AS A CONSEQUENCE OF THE INTERACTION OF TITANIUM IONS WITH HYDROXYAPATITE

Cristina C. Ribeiro[1,2,3], M. Lurdes C. Reis[4] and Mário A. Barbosa[1,2]

1 - INEB - Instituto de Engenharia Biomédica, Laboratório de Biomateriais, Rua do Campo Alegre 823, Porto 4150-180, Portugal
2 - FEUP - Faculdade de Engenharia da Universidade do Porto, Dep. de Eng. Metalúrgica e de Materiais, Porto, Portugal
3 - ISEP - Instituto Superior de Engenharia do Porto, Dep. de Física, Porto, Portugal
4 - IGM - Instituto Geológico e Mineiro, Porto, Portugal.

Abstract

The aim of this study was to contribute to the understanding of the effect of titanium ions on the molecular structure of hydroxyapatite ($Ca_{10}(PO_4)_6(OH)_2$). The effects of hydroxyapatite crystallinity, titanium concentration, incubation media, and time and temperature of incubation were investigated. The solids were analysed by X-ray diffraction and Fourier transform infrared spectroscopy. The results clearly indicate the formation of a titanium protonated phosphate compound with a layered structure ($Ti(HPO_4)_2.nH_2O$ (n=1-3)). The formation of this compound is dependent on the titanium concentration and its crystallinity slightly increases with the time and temperature of incubation.

Keywords: hydroxyapatite, titanium, titanium-phosphate, X-ray diffraction.

Introduction

Hydroxyapatite (HAp) coatings have been applied onto metals in order to improve osseointegration of metallic orthopaedic implants. The long-term behaviour of these implants has to rely on a low rate of dissolution of the hydroxyapatite and on the integrity of the metal/coating interface. In spite of the excellent corrosion resistance of titanium and its alloys to physiological chloride solutions, metallic implants eventually undergo some degradation in the body through a variety of mechanisms including corrosion. High concentrations of titanium have been found in tissues adjacent to titanium implants [1-5] in some cases reaching values of several thousand parts per-million. An investigation of the tissue response associated with dental titanium implants revealed the presence of titanium not only in the implant/bone interface but also in the bone tissue [4]. Metal ions released from the substrate may influence the dissolution behaviour of the hydroxyapatite and affect its adhesion to the metal. Furthermore, if these metal ions are released into the body, they may interfere with the dissolution and formation processes of hydroxyapatite bone crystallites, leading to osseous pathologies. Studies have been reported concerning the effects of aluminium on bone disorder in individuals with chronic renal disease subjected to dialysis [6-8]. Lead and cadmium are also considered to be a risk factor for osteoporosis [9-11]. Little has been reported concerning the chemical interactions of hydroxyapatite with transition elements. In this work, X-ray diffraction (XRD) studies were performed with the aim of contributing to the understanding of the effect of titanium ions on the molecular structure of hydroxyapatite. The influence of HAp crystallinity, titanium concentration, incubation media and time and temperature of incubation on the extent of interaction of hydroxyapatite with titanium ions were investigated.

Materials and Methods

Commercial hydroxyapatite (CAM Implants), in the as-received condition and after heat treatment at 1000°C, were used in the experiments. Dissolution tests were carried using two different solutions as incubation media, namely de-ionised water and a saline physiological solution of 0.9% NaCl, to which the metal cation was added in the form of concentrated salt solution (Titrisol Merck Standard - $TiCl_4$ in 18% HCl). A solid/liquid ratio

of 500 mg of HAp/50 ml of solution was used. The samples were tested in polyethylene flasks, in a warm air cabinet equipped with an orbital shaker. An agitation speed of 250 r.p.m. was used throughout the experiments. HAp powders were incubated in solutions containing different concentrations of titanium ranging from 200 to 2000 ppm. Several testing periods, varying from 10 to 379 days, were used. Two incubation temperatures were employed, namely 37 and 65°C (±0.2°C). After incubation, the solid and liquid phases were separated by centrifuging at 4000 r.p.m and the supernatant liquid was analysed by atomic absorption spectroscopy for titanium ions. All the solid samples were thoroughly washed with de-ionised water to eliminate chloride and sodium ions, and dried in a stove at 60°C for 24 hours.

To elucidate the composition of the reaction products resultant from the interaction of Ti ions with HAp, the solid phases obtained after incubation of HAp for 10 days in solutions with different titanium concentrations, were heated at 100, 250 and 1000°C for 1h, in an attempt to improve their crystallinity.

Since it was impossible to find titanium phosphate in the market, to be used as reference material, an attempt to precipitate the compound was made. A solution of 0.02 M of $Na_2HPO_4.12H_2O$ and 0.01M of $TiCl_4$ was prepared with de-ionised water. Fifty millilitres of this solution were kept at 37°C for different times of incubation. After centrifugation, the solid obtained was washed with de-ionised water. This solid will be identified as "prepared solid" throughout the text.

X-ray powder data were obtained using a Philips diffractometer and a PW 1710 diffractometer control unit with a monochromator in the reflected beam, a $CuK\alpha_{(1+2)}$ radiation with a wavelength of 1.5418 Å and a proportional detector. A Si standard sample was used for calibration of the camera and of the zero shifts of the goniometer. The experimental conditions used are indicated in Table I.

The solids for X-ray diffraction studies were gently ground and mixed with an X-ray transparent solvent to obtain a thin layer of sedimented powder fixed on a glass plate. In order to minimise the heterogeneity effects of the sample a specimen spinner holder was used. When higher sensitivity was required, the technique of film X-ray diffraction was used.

The powders were moulded into cylinders and the analysis was performed using a 114.6 mm diameter Debye-Scherrer camera, and $CuK\alpha_{(1+2)}$ filtered radiation (Ni filter).

Table I - Experimental conditions used in the XRD analysis.

Accelerating voltage	40 kV
Filament current	20 mA
Take-off angle of X-ray tube	4°
Fixed divergence slit	1°
Detector slit	0.1 mm

FT-IR analysis was performed using a Perkin Elmer 2000 FT-IR spectrometer. The samples were prepared as KBr discs and were run at a spectral resolution of 4 cm^{-1}. Two hundred of scans were accumulated in each analysis.

Results

Hydroxyapatite characterisation

Figure 1 shows the X-ray diffraction patterns obtained for the HAp in the as-received condition, and after heat treatment at 1000°C. The two powders showed no extraneous peaks over the range of two theta degrees (2θ) studied, confirming the purity of the ceramic.

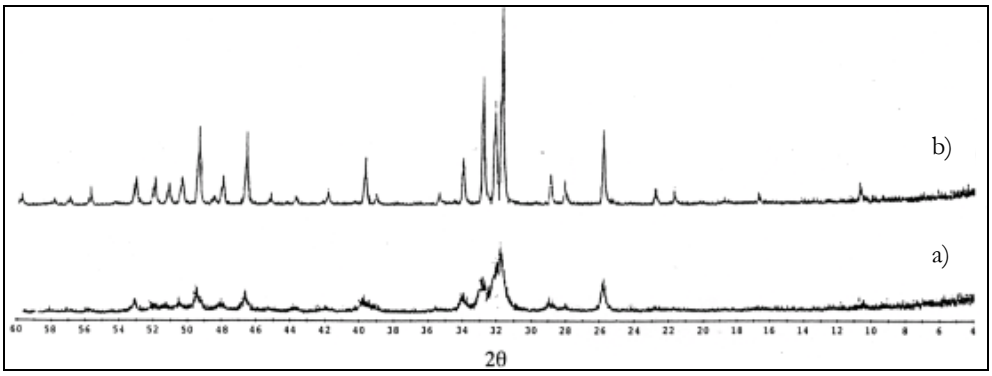

Figure 1 - XRD patterns of HAp powders: a) in the as-received condition; b) after heat treatment at 1000°C.

The d(hkl) spacing and intensity values found in X-ray diffraction analysis matched the standard values for hydroxyapatite (file 9-432 JCPDS). There was a significant narrowing of the peaks after heat treatment of the as-received HAp, indicating an increase in crystallinity. Crystallinity and crystallite size of HAp powders were evaluated using the Scherrer equation. The results obtained are shown in Table II. There is an increase of crystallinity indicated by a decrease of $\Delta 2\theta^o$ and/or increase of crystallite size as a function of temperature.

Table II - Crystallinity and crystallite size dimension of the HAp powders used.

Hydroxyapatite $Ca_{10}(PO_4)_6(OH)_2$	"Crystallinity" $\Delta 2\theta°$	Crystallite size Scherrer equation: $D_{002} = \frac{k\lambda}{b*\cos\theta}$ Å
HAp - as received	0.275º± 0.025º	289 Å
HAp - heat treated	0.150º± 0.025º	520 Å

D_{002} - domain size in Å
k: shape constant = 0.9
$\lambda_{Cuk\alpha}$ = 1.5418 Å
b* = peak broadening in radian

Influence of HAp crystallinity and titanium concentration

X-ray diffraction analysis of powders collected after a 10 days testing period revealed that the addition of Ti to HAp in the as-received condition, in concentrations close to 400 ppm, leads to destruction of the structure of HAp (Figure 2). In the less concentrated samples (Ti concentration < 400 ppm), some of the peaks characteristic of HAp spectrum are still present. For Ti concentrations higher than 400 ppm, the powder diffraction patterns consist of diffuse bands, indicating that a new solid phase appears, mainly as very small crystallites and/or as a disordered state (low crystallinity). The same results were observed when the HAp heat treated at 1000°C was used, indicating that HAp crystallinity is not a factor that determines the interaction of Ti ions with the ceramic. The X-ray spectrum of the "prepared solid" is quite similar to the ones obtained for the more concentrated samples (> 400 ppm), suggesting that the solids are similar in structure. However, they are different in composition, as Energy Dispersive Spectroscopy (EDS) analysis revealed the presence of Ca in the more Ti concentrated samples. Analysis of the solutions after incubation revealed that

Ti was below the detection limit (1.1 ppm) of the used instrumentation (GBC 904-AA spectrometer), indicating that practically all the Ti was incorporated in the solid phase.

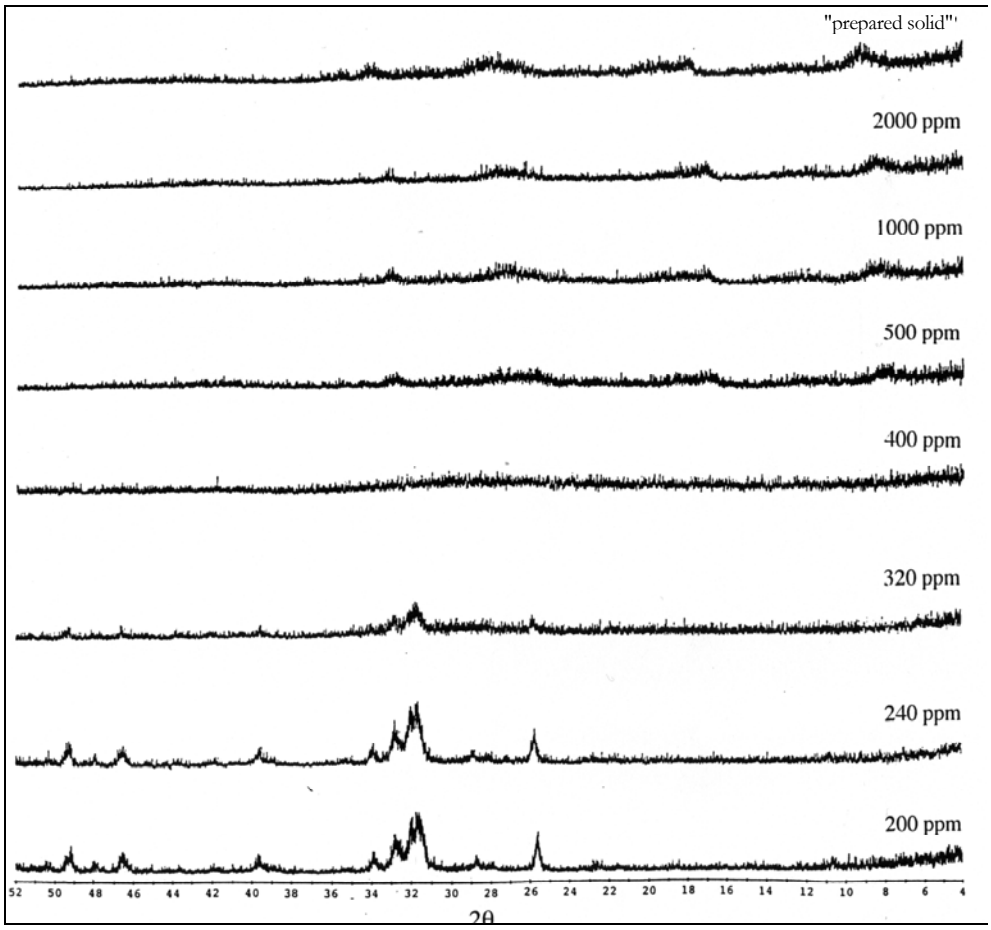

Figure 2 - X-ray diffraction patterns of powders obtained after 10 days' incubation of HAp in 0.9% NaCl solution with different concentrations of Ti and of the "prepared solid" powder, obtained after the same time of incubation.

Influence of incubation solution, time and temperature of incubation

No differences were observed in the X-ray diffraction pattern of the solids obtained after incubation of HAp in the two incubation media (de-ionised water and 0.9% NaCl), suggesting that sodium and chloride ions do not interfere with the process of formation of the solids (results not shown).

An increase in time (Figure 3) or temperature (Figure 4) of incubation slightly increases the crystallinity (and/or quantity) of the solid phase formed, after incubation of HAp in 0.9%

NaCl solution with a concentration of 500 ppm of Ti. Even after 379 days of incubation, the XRD spectrum obtained is not characteristic of a crystalline compound, indicating that the kinetics of formation and/or crystallisation of the solids is very slow.

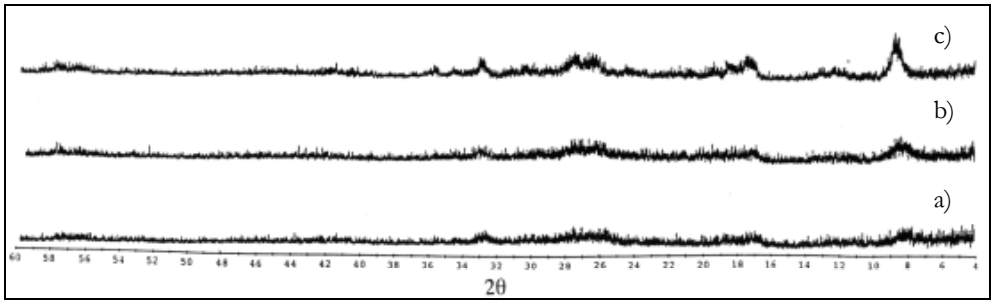

Figure 3 - X-ray diffraction patterns of powders obtained after different times of incubation of HAp in 0.9% NaCl solution with a Ti concentration of 500 ppm: a) 10 days; b) 147 days; c) 379 days.

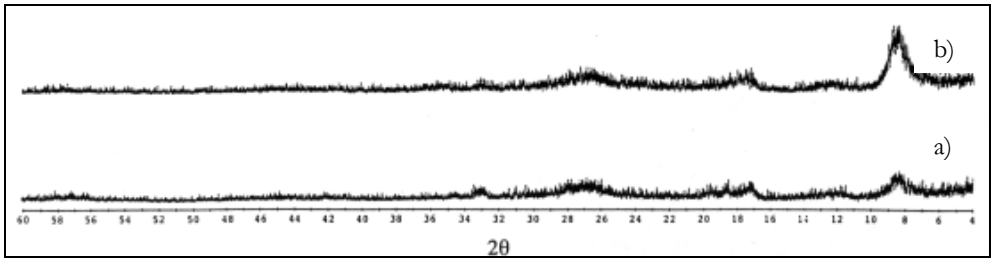

Figure 4 - X-ray diffraction patterns of powders obtained after 10 days' incubation at different temperatures of HAp in 0.9% NaCl solution with a Ti concentration of 500 ppm: a) 37°C; b) 65°C.

Influence of ageing temperature

When the solids obtained after incubation of HAp in 0.9% NaCl solution with a titanium concentration of 500 ppm were heated at 100°C, no significant changes in the XRD pattern of the solid were introduced (Figure 5b)). However, after further heating to 250°C, the X-ray pattern obtained is characterised by the absence of definite peaks (Figure 5c)). Taking together this observation with the results of the thermogravimetric analysis described in a previous work [12] where a weight loss during heating was observed, it may be concluded that the titanium-rich solid phase(s) is hydrated and becomes amorphous when it looses its water of constitution.

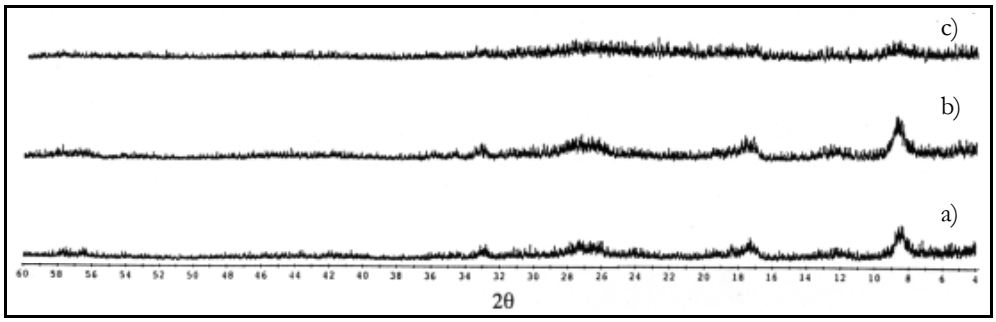

Figure 5 - X-ray diffraction patterns of powders obtained after 379 days' incubation of HAp in 0.9% NaCl solution with a Ti concentration of 500 ppm: a) non heated; b) heated at 100°C for 1h; c) heated at 250°C for 1h.

When the solid phases obtained after incubation of HAp in solutions of 0.9% NaCl with different concentrations of titanium are heated at 1000°C, they undergo thermal decomposition instead of increasing their crystallinity. The same was observed for the "prepared solid" sample. The products obtained were identified by XRD (Table III and Figure 6).

Table III - Crystalline phases identified in the solids heated at 1000°C for 1h.

Sample reference	Identified phases
240 ppm Ti	β-$Ca_3(PO_4)_2$ + HAp
500 ppm Ti	$CaTi_4(PO_4)_6$+$(TiO)_2P_2O_7$ +TiP_2O_7
1000 ppm Ti	$CaTi_4(PO_4)_6$+$(TiO)_2P_2O_7$ +TiP_2O_7
2000 ppm Ti	$CaTi_4(PO_4)_6$+$(TiO)_2P_2O_7$ +TiP_2O_7
"prepared solid"	$(TiO)_2P_2O_7$ +TiP_2O_7

These results indicate that although the XRD spectrum of the "prepared solid" is quite similar to those of the samples with higher titanium concentrations (500, 1000 and 2000 ppm), they differ in composition. A new calcium phase is probably present in the solid phases obtained after incubation of HAp in solutions rich in titanium. However, its presence could not be detected by XRD, which leads to the assumption that it is either amorphous or present in small concentrations (less than 5%). Upon heat treatment this phase becomes crystalline and was identified as being a calcium-titanium-phosphate, $CaTi_4(PO_4)_6$.

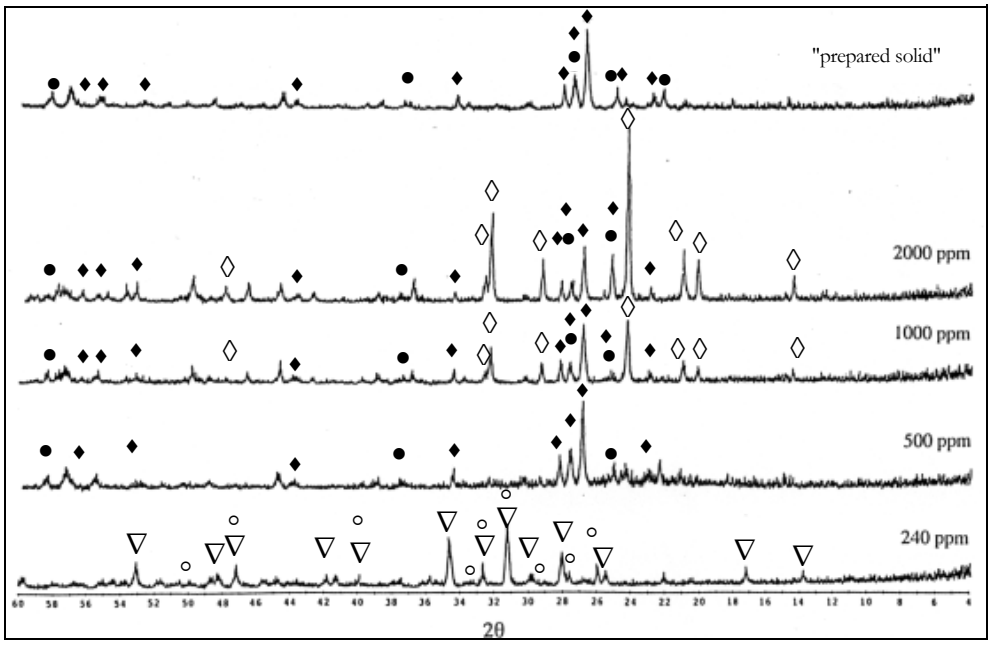

Figure 6 - X-ray diffraction patterns of powders obtained after 10 days' incubation of HAp in 0.9% NaCl solution with different concentrations of Ti and of the "prepared solid", heated at 1000°C for 1h, ♦ - Titanium Oxide Phosphate: $(TiO)_2P_2O_7$, ● - Titanium Pyrophosphate: TiP_2O_7, ◊ - Calcium Titanium Phosphate: $CaTi_4(PO_4)_6$, ∇ - Tricalcium Phosphate: β-$Ca_3(PO_4)_2$, ° - Hydroxyapatite: $Ca_{10}(PO_4)_6(OH)_2$.

Identification of the Ti rich solid phase(s)

The different test conditions used in the experiments (HAp crystallinity, time, temperature of incubation, and ageing temperature) did not improve considerably the quality of the diffraction data, necessary for a correct identification of the phase(s) present in the solids obtained. However, in an attempt to do that identification, powder diffraction data of layered titanium phosphate compounds described in the literature [13] were compared with the Debye Scherrer powder pattern of the solid phases obtained after 230 days incubation of HAp in 0.9% NaCl solution with a Ti concentration of 500, 1000, 2000 ppm and of the "prepared solid" sample. The diffraction patterns were practically identical suggesting similar structural characteristics of all the samples. Two main types of layered titanium phosphates are known, namely the α and γ phases, which are mono- and di- hydrated respectively, both containing two phosphorous atoms per atom of group IV element [14, 15]. The two phases differ not only in hydration state but also in atomic arrangement within the layer. In the α-

TiP phase, all the phosphorous atoms are in the form of HPO_4^{2-} groups and its chemical formula can be represented as $Ti(HPO_4)_2.H_2O$ [13-16]. In the γ-phase, half of the phosphorous atoms exists in the form of $H_2PO_4^-$ and the rest in the form of PO_4^{3-} groups and therefore, the formula for γ-TiP should be written as $Ti(H_2PO_4)PO_4.2H_2O$ [13, 16, 17]. In Table IV the X-ray diffraction data of the reference compounds [13] and the experimental data obtained for the 2000 ppm of Ti sample are presented.

In Table V, the crystal lattice parameters of α- TiP and γ- TiP are presented, including the calculated basal spacing for each of the phases.

If we compare the data in table IV, it becomes apparent that several lines of the two reference patterns are present in the pattern of the solid phase in study, while others do not correspond to the α-TiP or γ-TiP phases. This is indicative that we are not in the presence of a mixture of α-TiP and γ-TiP phases, since mixtures of two or more different substances which exist as separate crystals generate X-ray diffraction patterns that correspond to the superposition of the individual patterns of the constituents. However, all the X-ray diffraction lines of the solid in study are consistent with a structure corresponding to a regular array of scattering atoms of the two layered structural phases (α-TiP and γ-TiP), stacked 1:1 along the c axis in a multitude of parallel spaced atomic planes of approximately 19.2 Å (7.597+11.643) (Table V). Due to the structural similarity of the α-$Ti(HPO_4)_2.H_2O$ and γ-$Ti(H_2PO_4)PO_4.2H_2O$ phases, hydrogen phosphate hydrated compounds may exist in which the individual crystals are composed of elementary layers of the two types. The theoretical basal reflections of the proposed structure for the (002), (003) and (004) planes are presented in Table VI. The values obtained are very similar to the interplanar distances **d** observed for the solid in study (Table IV) that do not match the diffraction patterns of α and γ phases, providing evidence for the interlayering of these phases during titanium phosphate crystallisation.

Table IV - X-ray diffraction data of the reference compounds (α-$Ti(HPO_4)_2.H_2O$ and γ-$Ti(H_2PO_4)PO_4.2H_2O$ [13]) and of the compound in study.

d_{obs} /Å α - TiP	h k l	d_{obs} /Å γ -TiP	h k l	d_{obs} /Å compound in study
-		11.600	001	-
-		-		10.669
-		-		9.054
7.604	002	-		7.557
-		-		6.458
-		5.560	011	5.193
-		-		4.854
-		-		4.530
4.261	110	4.297	$10\bar{2}$	-
4.232	$20\bar{2}$	-		-
4.046	$11\bar{2}$	3.951	$11\bar{1}$	4.077
-		3.854	003	3.705
3.457	112	3.558	$11\bar{2}$	3.579
3.422	$20\bar{4}$	3.450	$10\bar{3}$	3.373
-		3.300	013	-
3.150	210	3.170	020	3.144
3.026	014	3.058	021	2.913
2.876	$30\bar{2}$	-		2.810
-		2.786	$10\bar{4}$	2.710
2.611	114	-		2.651
2.585	$20\bar{6}$	2.590	$20\bar{1}$	2.550
2.533	006	2.552	$11\bar{4}$	-
2.503	020	2.526	200	-
2.494	$31\bar{2}$	2.450	023	2.460
2.390	204	-		-
2.374	$11\bar{6}$	2.336	$12\bar{3}$	-
2.244	023	2.217	$21\bar{3}$	-
2.157	214	2.150	202	2.144
2.022	116	2.080	031	2.054
1.960	222	1.986	032	1.984
1.942	$40\bar{6}$	1.951	130	-
1.875	206	-		-
1.865	$11\bar{8}$	1.846	016	1.839

Table V - Comparison of crystal lattice parameters and other calculated parameters of α and γ titanium hydrogen phosphate hydrates [13].

Parameters	α-$Ti(HPO_4)_2.H_2O$	γ- $Ti(H_2PO_4)PO_4.2H_2O$
a(Å)	8.630	5.181
b(Å)	5.006	6.347
c(Å)	16.189	23.762
β°	110.20	102.59
Basal spacing ($\frac{c}{2} sen\beta$)Å	7.597	11.643
ab $(Å)^2$	43.20	32.88
$V(Å)^3$	657.4	765.67
Z	4	4
d(g/cm3)	2.59	2.38

Table VI - Basal reflections observed for the solid in study (planes (002), (003), (004)).

Basal reflections (Å)	h k l	Intensity
9.06	002	broad strong
6.40	003	very weak and very diffuse
4.80	004	very weak and very diffuse

The most significant difference is observed for the basal reflections of the (002) plane (9.06 instead of 9.6). This could be attributed to the broadness of the diffraction ring difficulting the correct measurement of its thickness.

The FT-IR spectrum of the Ti-rich solid phase confirmed the presence of an hydrated phosphate compound (Figure 7). The bands at 3406 and 1630 cm^{-1} are assigned to lattice water. In general, lattice water (i.e., water held in a crystal lattice by hydrogen bonds to anions, or by weak co-ordinate bonds to the metal, or by both), absorbs in the region 3550-3200 cm^{-1} (antisymmetric ν_3 and ν_1 modes and symmetric OH stretching) and at 1630-1600 cm^{-1} (HOH bending ν_2 mode) [18]. There are also intense absorption bands at 999 and 1123 cm^{-1} that belong to the stretching modes of P-O bonds in the HPO_4^{2-} group. HPO_4^{2-} ion can be considered as a distorted PO_4^{3-} tetrahedron, which consequently exhibits bands in PO_4^{3-} domains. The free ion has C_{3v} symmetry, leading to eight normal modes of vibration [19].

The symmetric ν_2 A mode and the doubly degenerate ν_6 E P-O stretch appear in the 900-1200 cm^{-1} region. When this ion is incorporated into a crystal lattice, the ν_2 mode appears as a doublet [20], which, in the compound in study, may correspond to the band at 999 cm^{-1} and to the small shoulder at approximately 1025 cm^{-1}. The ν_6 mode appears in the spectrum at 1123 cm^{-1}. In what concerns the low wavenumber region, the bands at 572, 546 and 467 cm^{-1} may also arise from the HPO_4^{2-} or PO_4^{3-} groups [19, 21, 22]. The weak bands in the 2000-2360 cm^{-1} interval correspond to P-O-H stretching vibration [19].

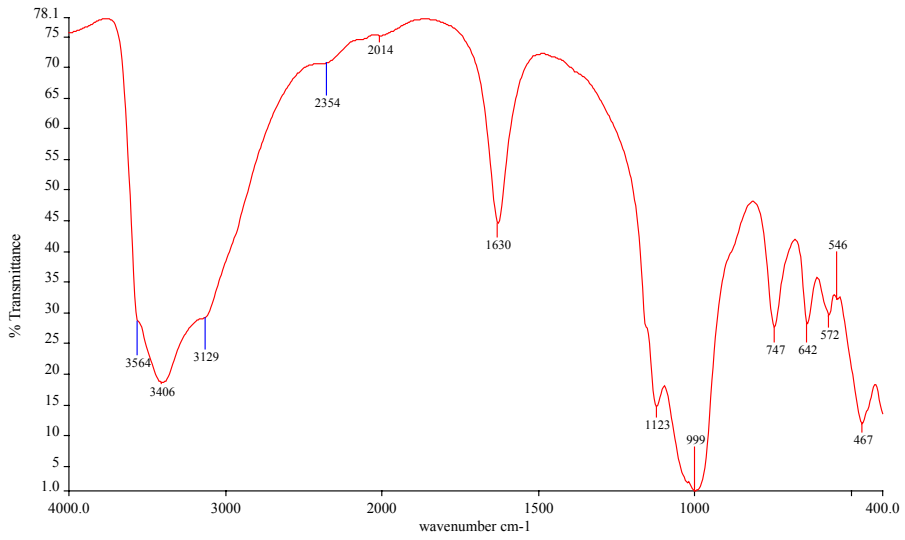

Figure 7 - FT-IR spectrum of the solid phase obtained after 230 days' incubation of HAp in 0.9% NaCl solution with a Ti concentration of 2000 ppm.

Discussion and Conclusions

The results obtained in this study have shown that the hydroxyapatite structure is disturbed by the presence of Ti ions. In concentrations smaller than 400 ppm Ti ions are probably uptaken by hydroxyapatite without provoking significant changes in its X-ray diffraction pattern. The chemical analysis of the supernatant liquid obtained after HAp incubation revealed that Ti was not present in solution, supporting the idea that the metal ion has been incorporated in the solid or adsorbed on its surface. This affinity of hydroxyapatite for titanium cations was also observed in other works of the authors where different analytical techniques were used [12, 23]. Many trace elements (cations) can be incorporated

into the apatites and therefore affect their physical and chemical properties [24]. The replacement of ions in the HAp lattice may play a major role in the biochemistry of bone. Certain metals such as aluminium, iron, cadmium and lead are known to cause bone pathologies in humans and animals [6-11]. Further investigation should be performed in order to better clarify the mechanism of interaction of Ti with HAp for the mentioned concentrations of titanium (<400 ppm).

For Ti concentrations of approximately 400 ppm, a non-crystalline phase was formed. For higher concentrations of Ti, the results obtained suggest that the non crystalline precursor phase leads to the formation of a titanium protonated phosphate compound ($Ti(HPO_4)_2.nH_2O$ (n=1-3)). The model that we propose to describe the structure of this titanium phosphate is the stratification of two layered structural phases (α-$Ti(HPO_4)_2.H_2O$ and γ-$Ti(H_2PO_4)PO_4.2H_2O$) stacked 1:1 along the c axis with a layer spacing of approximately 19.2 Å. The compound crystallinity slightly increases with time and temperature of incubation and is not influenced by the crystallinity of the HAp used in its preparation.

The presence of $(TiO)_2P_2O_7$ and TiP_2O_7 phases in the Ti-rich powders after being heated till 1000ºC for 1h, can be explained by the following mechanism:

$$4Ti(HPO_4)_2.nH_2O\ (s) \rightarrow (TiO)_2P_2O_7\ (s) + 2TiP_2O_7\ (s) + P_2O_5\ (g) + (n+4)H_2O\ (g)$$

When a solid orthophosphate, containing hydrogen bonds is heated to an appropriate temperature, there is a loss of water accompanied by pyrophosphate formation [25, 26]. The amount of pyrophosphate formed is related to the number of hydrogen bonds present in the system. The $(TiO)_2P_2O_7$ results from the partial decomposition of TiP_2O_7 as follow [27]:

$$2\ TiP_2O_7\ (s) \rightarrow (TiO)_2P_2O_7\ (s) + P_2O_5\ (g)$$

The interest in the synthesis and properties of layered structured titanium phosphates has resulted from the search for compounds with properties suitable to be used as ion exchangers, sorbents, ionic conductors and catalyst supports rather than from the use of the ceramic in the biomedical field [15, 16]. From an engineering perspective, these kinds of

phosphates are very attractive materials due to the capacity of insertion of guest species into their layered structured host lattices. For instance, amorphous zirconium phosphate was used successfully in kidney machines for the removal of NH_3 and NH_4^+ from human blood after catalytic decomposition of urea to NH_3 and CO_2 [28]. Further research should be performed in the future in order to evaluate the applicability of layered titanium phosphates in the biomedical field. It would also be important to investigate the possibility of *in vivo* formation of this type of compounds at the interface of titanium prostheses coated with hydroxyapatite and its implications in the biological system.

References

[1] Pohler OEM. Degradation of metallic orthopedic implants. In: Rubin LR, editor. Biomaterials in Reconstructive Surgery. St Louis, USA. The C. V. Mosby Company; 1983. p.158-228.

[2] Black J. Systemic effects of biomaterials. Biomaterials 1984; 5: 11-18.

[3] Dorr LD, Bloebaum R, Emmanual J, Meldrun R. Histologic, biochemical and ion analysis of tissue and fluids retrieved during total hip arthroplasty. Clin Orthop Rel Res 1990; 261: 82-95.

[4] Tanaka N, Ichinose S, Kimijima Y, Mimura M. Investigation of titanium leak to bone tissue surrounding dental titanium implant: electron microscopic findings and analysis by electron diffraction. Med Elec Mic 2000; 33: 96-101.

[5] Lijian Z, Ti-sheng C, Wei W, Lei C. Study on commercially pure titanium implants bone integration mechanism. Europ J Plastic Surg 2000; 23: 301-304.

[6] Christofferson MR, Christofferson J. The effect of aluminum on the rate of dissolution of calcium hydroxyapatite - a contribution to the understanding of aluminum-induced bone diseases. Calcif Tissue Int 1985; 37: 673-676.

[7] Christofferson MR, Thyregod HC, Christofferson J. Effects of aluminum (III), chromium (III), and iron (III) on the rate of dissolution of calcium hydroxyapatite crystals in the

absence and presence of chelating agent desferrioxamine. J Calcif Tissue Int 1987; 41: 27-30.

[8] Posner AS, Blumenthal NC. *In vitro* model of aluminum-induced osteomalacia: inhibition of hydroxyapatite formation and growth. Calcif Tissue Int 1984; 36: 439-441.

[9] Goyer RA, Epstein S, Bhattacharyya M, Korach KS, Pounds J. Environmental risk factors for osteoporosis on the evaluation of carcinogenic risks to humans. Environ Health Persp 1994; 102: 390-393.

[10] Aoki H. In: Aoki H, editor. Science and Medical Applications of Hydroxyapatite. Tokyo, Japan: Takayama Press System Center; 1991. p.52-54.

[11] Tsuchiya K. Clinical signs, symptoms, and prognosis of cadmium poisoning. In: Nriagu JO, editor. Cadmium in the environment. PartII. Health effects. New York, USA: Wiley, 1981. p.39-68.

[12] Ribeiro CC, Barbosa MA, Machado AASC, Tudor A, Davies MC. Modifications in the molecular structure of hydroxyapatite induced by Ti ions. J Mat Sci: Mat in Med 1995; 6: 829-834.

[13] Christensen AN, Andersen EK, Andersen IGK, Alberti G, Nielsen M, Lehmann MS. The crystal structure of α-$Ti(HPO_4).H_2O$ and a proposed structure for γ-$Ti(H_2PO_4)(PO_4).2H_2O$. Acta Chem Scand 1990; 44: 865-872.

[14] Bortun AI, Bortun L, Clearfield A, Villa-García MA, García JR, Rodriguez J. Synthesis and characterization of a novel layered titanium phosphate. J Mater Res 1996; 11: 2490-2498.

[15] Yamanaka S, Hattori M. Two-dimensional layered phosphates. In: Kanazawa T, editor. Inorganic Phosphate Materials. Tokyo, Japan: Kodansha, 1989. p.131-160.

[16] Alberti G. Other group (IV) acid salts. In: Clearfield A, editor. Inorganic ion exchange materials. Florida, USA: CRC Press Inc, 1982. p.76-90.

[17] Allulli S, Ferragina C, La Ginestra A, Massucci MA, Tomassini N. Preparation and ion-exchange properties of a new phase of the crystalline titanium phosphate, $Ti(HPO_4)_2.2H_2O$. Inorg Nucl Chem 1977, 39: 1043-1048.

[18] Nakamoto K. In: Nakamoto K, editor. Infrared and Raman spectra of inorganic and coordination compounds. New York, USA: John Wiley & Sons Inc, 1978.

[19] Bailey RT, Holt C. Fourier transform infrared spectroscopy and characterisation of biological calcium phosphates. In: Hukins DWL, editor. Calcified Tissues. Basingstoke, Great Britain: Mac Millan Press, 1989. p.93-120.

[20] Berry EE, Baddiel CB. The infrared spectrum of dicalcium phosphate dihydrate (brushite). Spectrochim Acta 1967; 23a: 2089-2097.

[21] Ross SD. Phosphates and other Oxy-anions of group V. In: Farmer VC, editor. The infrared spectra of minerals. London, Great Britain: Adlard & Sons Ltd, 1974. p.383-422.

[22] Socrates L. In: Socrates L, editor. Infrared and Raman Characteristic Group Frequencies - Tables and Charts. Chichester, England: John Wiley & Sons, Ltd, 2001. p.277, 287.

[23] Ribeiro MCC, MSc thesis, Faculdade de Engenharia da Universidade do Porto, Porto, 1995.

[24] LeGeros RZ, Taheri MH, Quirolgico GB, LeGeros JP. Formation and stability of apatites: effects of some cationic substituents. In: Proceedings of 2nd International Congress on Phosphorous Compounds. Boston, USA, 1980. p.89-103.

[25] Elliot JC. PhD Thesis, University of London, London, England, 1964.

[26] Posner AS. The mineral of bone. Clinical Orthopaedics 1985; 200: 87-99.

[27] Bamberger CE, Begun GM. Synthesis and characterisation of titanium phosphates, TiP_2O_7 and $(TiO)_2P_2O_7$. J Less Common Metals 1987; 134: 201-206.

[28] Gordon A, Better OS, Greenbaum MA, Marantz LB, Gral T, Maxwell MH. Clinical maintenance hemodialysis with a sorvent-based, low volume dialysate regeneration system. Trans Am Soc Artif Int Organs 1971; 17: 253-258.

Chapter 3

THE UPTAKE OF TITANIUM IONS BY HYDROXYAPATITE PARTICLES - STRUCTURAL CHANGES AND POSSIBLE MECHANISMS

Cristina C. Ribeiro[1,2,3], Iain R. Gibson[4] and Mário A. Barbosa[1,2]

1 - INEB - Instituto de Engenharia Biomédica, Laboratório de Biomateriais, Rua do Campo Alegre 823, Porto 4150-180, Portugal
2 - FEUP - Faculdade de Engenharia da Universidade do Porto, Dep. de Eng. Metalúrgica e de Materiais, Porto, Portugal
3 - ISEP - Instituto Superior de Engenharia do Porto, Dep. de Física, Porto, Portugal
4 - University of Aberdeen - Institute of Medical Sciences, Dep. of Biomedical Sciences, Foresterhill, Aberdeen, UK

Abstract

In order to understand the effect of titanium ions on the molecular structure of hydroxyapatite (HAp), HAp powders were incubated in solutions with different titanium concentrations. After incubation, the powders obtained were analysed using different techniques, namely X-ray diffraction (XRD), Fourier transform infrared spectroscopy (FT-IR), differential thermal analysis (DTA), X-ray photoelectron spectroscopy (XPS), and energy dispersive spectroscopy (EDS). The results suggest that, depending on the concentration of titanium in solution, two different mechanisms of interaction with HAp occur. For concentrations equal to or smaller than 200 ppm, the titanium uptake by the solid seems to be primarily due to incorporation in the lattice. For higher concentrations, a dissolution-precipitation process seems to occur, leading to formation of a titanium phosphate compound.

Keywords: hydroxyapatite, titanium, titanium phosphate.

Introduction

Due to its crystallographic similarity to various calcified tissues of vertebrates, hydroxyapatite, $Ca_{10}(PO_4)_6(OH)_2$ (HAp), has been extensively used as a substitute material for damaged teeth or bone over the past three decades, and its compatibility with surrounding tissues has been experimentally proven.

Several methods to prepare HAp have been reported in the literature, including precipitation, conversion of other calcium phosphate salts, solid state reactions, and sol gel crystallisation [1-3].

Chemically precipitated HAp differs from the apatites obtained by high temperature, hydrothermal and igneous preparations because of its submicroscopic crystal size, structural distortion and non-stoichiometry, since it is usually calcium and hydroxyl deficient [4]. At present, the following formula is generally suggested [5] for non-stoichiometric (carbonate free) hydroxyapatites:

$$Ca_{10-x}(HPO_4)_x(PO_4)_{6-x}(OH)_{2-x}.nH_2O;\ 0 < x < 1,\ n = 0\text{-}2.5$$

The degree of non-stoichiometry depends on the synthesis method and is usually characterised by the Ca/P ratio. The total electrical charge is assumed to be compensated by the introduction of H^+, giving rise to H_2O molecules replacing OH^- ions.

Bone mineral is a heterogeneous material, which is in constant evolution. Its composition varies, depending on species, type of bone, diet, etc. However, its chemical composition can be represented approximately by a single chemical formula:

$$Ca_{8.3}\square_{0.7}(PO_4)_{4.3}(HPO_4 \text{ and } CO_3)_{1.7}(2OH \text{ and } CO_3)_{0.15}\square_{1.7}$$

in which □ represents a vacancy [6]. With maturation, the bone crystal approaches, but never reaches, the perfect HAp structure.

HAp easily forms solid solutions via chemical reactions with various metal oxides, halides, and carbonates. Apatite is capable of accommodating several substituents, while still

maintaining its basic structure. Ca^{2+} can be substituted to some extent by monovalent (Na^{+}, K^{+}) [7], divalent (Sr^{2+}, Ba^{2+}, Pb^{2+}) [8-10] and trivalent (Y^{3+}) cations [11]. Among the anionic substitutions, the significant ones are replacement of OH^{-} by CO_3^{2-}[12], F^{-} [13, 14], Cl^{-} [14], and PO_4^{3-} by CO_3^{2-} [15], AsO_4^{3-} and VO_4^{3-} [16]. Some substitutions are coupled with others [17-20] to maintain charge balance in the apatite, e.g. CO_3^{2-} for PO_4^{3-} coupled with Na^{+} for Ca^{2+}. The trivalent anionic phosphate sites cannot accept vacancies, probably because the trivalent anions are quite large and vacancies would destabilise the lattice [21]. By contrast, the cationic sites can accept vacancies, up to a maximum of 2 sites out of the 10 existing in stoichiometric apatites [21].

Due to its interesting chemical and physical properties, synthetic HAp finds various applications, not only as a biomaterial, but also as an adsorbent for chromatography to separate proteins and enzymes [22, 23], as a catalyst for dehydrogenation and dehydration of alcohols [24, 25], and as an effective means for removing dissolved divalent cations from solution. For instance, it has been regarded as a possible solid for immobilisation of pollutant metals, particularly Pb^{2+}, from aqueous solutions [26, 27].

In what concerns HAp applicability in the biomedical field, the capacity of its lattice to act as a host for different chemical species has been explored. The most common example is the preparation of carbonate-substituted HAp [12, 15] and fluoride-substituted HAp [13, 14]. Another potential method for improving the biological activity of HAp is the incorporation of silicon (or silicate groups) into its lattice [28].

The properties of HAp that are affected by substituents are: lattice parameters (a and c axis dimensions), crystal size and shape, crystal strain, crystallinity, infrared absorption spectral properties and thermal stability [29]. When the substituents are present simultaneously, they may have additive, synergistic, or opposite effects on the properties of the apatite crystallites [20, 30-32].

The principal constituent of the inorganic part of human and animal bone and teeth is quite similar to HAp. The type and amount of ionic substitutions in the apatite phase of bone vary from the wt% level (e.g. 5 wt% CO_3^{2-}) to the ppm- ppb level (e.g. Sr^{2+} or Ba^{2+}) [8, 9, 15].

Although these levels of substitution are small, the replacement ions play a major role in the biochemistry of hard tissues. Certain metals, such as aluminium, iron, cadmium and lead, are known to cause bone pathologies in humans and animals. Studies have been reported concerning the effects of aluminium in bone disorders in individuals with chronic renal disease subjected to dialysis [33-35]. Lead poisoning [36], also known as "plumbism", is caused by inhalation of lead in the form of dust or its absorption through the skin, the mechanism involved being attributed to isomorphous substitution of Ca^{2+} by Pb^{2+} in bone, leading to formation of solid solutions of HAp and lead HAp. Also, the interaction of cadmium with biological apatites is responsible for an osseous disease with effects similar to osteoporosis [37, 38].

Although titanium is one of the metallic materials more widely used in the biomedical field, its interaction with apatites is not clearly understood. This work aims at contributing to the study of the influence of titanium ions in the structure of hydroxyapatite.

Materials and Methods

Commercial HAp powders (CAM Implants) pre-heated at 1000ºC were incubated in solutions containing different concentrations of titanium, ranging from 50 to 350 ppm. These samples will be identified as HApXTi throughout the text, X being the amount of Ti, in ppm, that was present in the incubation media. All the solutions were prepared with de-ionised water and the chemical reagents were of p.a. grade. The dissolution studies were carried out using a saline solution of 0.9% NaCl to which the metal ions were added in the form of a concentrated salt solution (Titrisol Merck Standard -$TiCl_4$ in 18% HCl). A solid-to-liquid ratio of 500 mg of HAp to 50 ml of solution was used. The samples were tested in polyethylene flasks, maintained at 37ºC (± 0.2ºC) for 10 days in a warm air cabinet equipped with an orbital shaker. An agitation speed of 250 r.p.m. was used throughout the experiments.

After incubation, the solid and liquid phase were separated by centrifuging at 4500 r.p.m. and the supernatant liquid was analysed by atomic absorption spectroscopy (AAS) for Ti ions using a GBC 904-AA spectrometer. The solid samples were thoroughly washed with

de-ionised water to eliminate Cl^- and Na^+ ions and dried in a stove at 60ºC for 24h. The solids were then analysed using X-ray diffraction (XRD), Fourier transform infrared (FT-IR) spectroscopy, energy dispersive spectroscopy (EDS), differential thermal analysis (DTA) and X-ray photoelectron spectroscopy (XPS).

The phase composition of the as-received HAp and of the powders incubated in solutions containing different concentrations of Ti were determined using a Siemens D5000 diffractometer with CuK_α radiation; the X-ray generator operated at 40 kV and 40 mA. A secondary monochromator was used on the diffracted beam side with a scintillation counter detector. Data were collected over the 2θ range with a step size of 0.02º and a count time of 12s. Identification of phases was achieved by comparing the diffraction patterns of the ceramic powders with ICDD (JCPDS) standards. Determination of the structural parameters of HAp and of the powders incubated in solutions containing different concentrations of Ti was made by Rietveld refinement of the X-ray diffraction data collected for the powders. The refinement software GSAS was used and the refinements were based on the structural data of Kay *et al* [39] using the space group $P6_{3/m}$. The following parameters were refined: background parameters, scale factor, zero point, lattice parameters, and atomic positions. The FT-IR spectra were obtained using a Perkin Elmer 2000 FT-IR spectrometer. All the samples were prepared as KBr discs and were run at a spectral resolution of 4 cm^{-1}. Five hundred scans were accumulated in order to obtain a high signal-to-noise level. A nitrogen purge of the sample compartment was performed to minimise artefacts that could arise from residual air bands (CO_2 and H_2O vapour). The derivative and curve fitting algorithms were performed with the software PeakFit from AISN Software. Initial peak positions were obtained from second derivative spectra of the raw data. Second derivative spectra were calculated based on the Stavitzky and Golay method [40], which provides a combined approach to smoothing and derivatisation. The number and position of the peaks obtained were used as initial input parameters in the curve-fitting algorithm. A Lorentzian band-shape was used to fit the contours. The curve-fitting algorithm creates Lorentzian bands that are added to produce a computed spectrum, which is compared with the experimental one. The process is iterated until a satisfactory fit between the computed and experimental bands is obtained by a least

square regression analysis. The calculated area of each subband is reported as a percentage of the computed contour.

Energy dispersive spectroscopy studies were performed with a JEOL JSM-35C scanning electron microscope in conjunction with an energy dispersive spectrometer Tracor-TN 2000. Differential thermal analysis was carried out using a Seteram Labsys DTA/DSC 1600. The temperature was scanned from room temperature to 1200ºC, at a uniform heating rate of 5ºC/min and α-Al_2O_3 powder was used as reference. The values of the transformation temperature were determined with an accuracy of ± 0.2ºC. XPS measurements were carried out on a VG Scientific Escalab 200A (UK) spectrometer using magnesium Kα (1253.6 eV) as a radiation source. The photoelectrons were analysed with a take off angle of 55º. Survey spectra were collected over a range of 0-1150 eV with an analyser pass energy of 50 eV. High-resolution spectra of C1s, O1s, P2p, Ca2p and Ti2p, were collected with an analyser pass energy of 20 eV. All the spectra were fitted using asymmetrical Gaussian-Lorentzian profiles.

Results

The stoichiometric form of HAp is monoclinic with space group $P2_{1/b}$ [41-43], but slightly non-stoichiometric HAp has a hexagonal space group $P6_{3/m}$. This is characterised by ordering within OH^- ion columns to form a sequence OH-OH-OH-OH-, with an ordered arrangement of these columns, so that the b-axis is doubled, giving lattice parameters a=9.421(8), b=2a, c=6.8814(7) Å, and θ=120º [41]. Normally, only those preparations, that have a final high temperature stage (e.g. hydrothermal or heating in steam at 900ºC) have the possibility of yielding monoclinic HAp [41]. Other preparations are usually hexagonal, presumably because sufficient OH^- ions are missing, replaced by H_2O or impurity ions, so that ordering is disturbed [43]. The results presented here are treated assuming a hexagonal symmetry of HAp.

AAS and EDS analysis

The AAS analysis showed that no titanium was found in solution (limit of detection of the instrument: 1.1 ppm). The EDS analysis of the solids showed the presence of Ti, even for the less concentrated samples (50 ppm Ti). The Ca/P ratio obtained by EDS was the one expected for HAp (1.67).

Infrared Spectroscopy

The FT-IR spectrum of the HAp used is represented in Figure 1. It is characterised by OH stretching (3572 cm^{-1}) and librational (632 cm^{-1}) bands, and PO_4 (ν_3 ~1090 cm^{-1} and 1041 cm^{-1}, ν_1 963 cm^{-1}, ν_4 602 and 571 cm^{-1}, ν_2 473 cm^{-1}) bands.

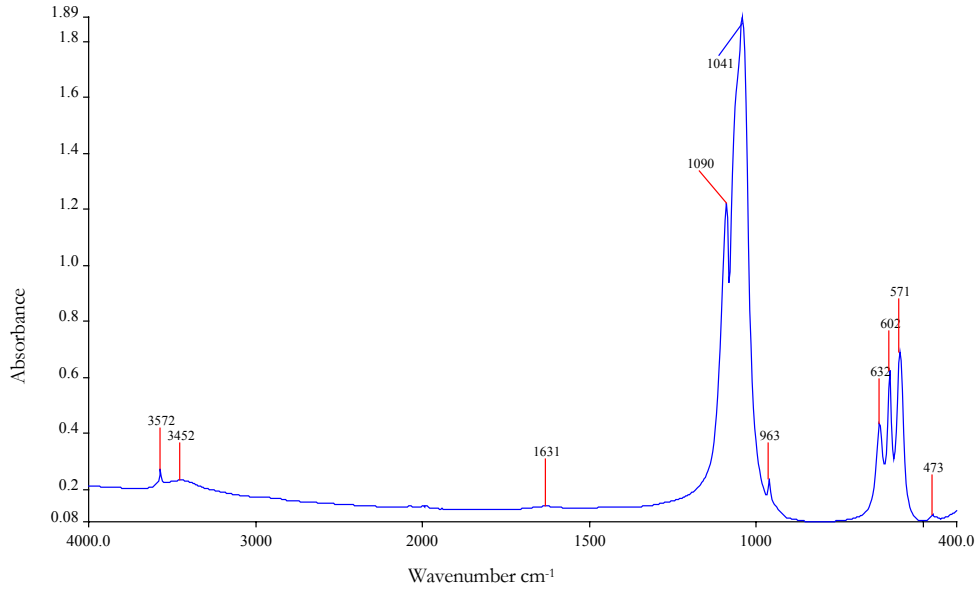

Figure 1 - FT-IR spectrum of hydroxyapatite powder.

There is no evidence of CO_3^{2-} or other impurities in the powder. The bands corresponding to the ν_3 vibration of C-O between 1410 and 1470 cm^{-1} and the ν_2 vibrations between 850 and 890 cm^{-1}, characteristic of the carbonate group [44, 45], are not observed in the FT-IR spectrum of HAp.

The broad and not very intense bands at 3452 and 1631 cm^{-1} in hydroxyapatite are due to the presence of lattice water in the solid [46, 47]. According to Joris *et al* [48], the broadness of the O-H stretching band in the region 3550-3200 cm^{-1} is caused by the H-bonding between the adsorbed H_2O and the OH^- group of the apatite.

The second derivative of the spectrum of hydroxyapatite in the ν_4 and ν_1 and ν_3 domains are shown in Figures 2a) and 2b), respectively.

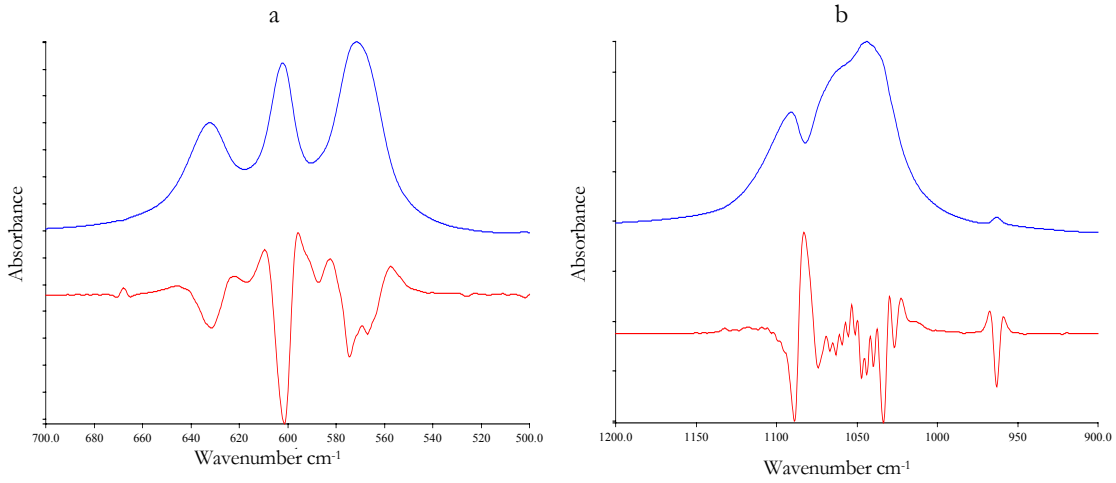

Figure 2 - Second derivative hydroxyapatite spectrum of the ν_4 (a) and ν_1, ν_3 (b) domains.

Table I shows the second derivative peak position of HAp spectrum in the ν_1, ν_3 and ν_4 phosphate region and their assignments from literature values. Derivative spectra are of considerable potential value because of their inherent property of discrimination against broader peaks, a consequence of the fact that the amplitude of the principal peak in the derivative decreases both with increasing width of the original peak and increasing order of derivatisation. This enables the location of peaks that are too closely spaced in the absorption spectrum to be resolved. The bands assigned in the second derivative spectra of HAp can be attributed to molecular vibrations of the phosphate (PO_4^{3-}) moiety in an apatitic/stoichiometric environment of HAp.

Table I - Second derivative peak positions (cm^{-1}) in the ν_1, ν_3 and ν_4 phosphate region and their assignments from literature values.

Position (cm^{-1})	Assignments	References
569	$\nu_4\ PO_4^{3-}$	[49]
574	$\nu_4\ PO_4^{3-}$	[49-52]
588	$\nu_4\ PO_4^{3-}$	[49]
602	$\nu_4\ PO_4^{3-}$	[49-52]
615	$\nu_4\ PO_4^{3-}$	[49, 50]
962	$\nu_1\ PO_4^{3-}$	[51-56]
1017	$\nu_3\ PO_4^{3-}$ from non stoichiometric apatite	[53,55]
1027	$\nu_3\ PO_4^{3-}$	[53,55,57]
1033	$\nu_3\ PO_4^{3-}$	[51,53,55,57]
1040	$\nu_3\ PO_4^{3-}$ (not part of apatitic structure in OCP)	[49,51,52,55]
1045	$\nu_3\ PO_4^{3-}$	[49,51,53,58]
1051	$\nu_3\ PO_4^{3-}$	[49]
1056	$\nu_3\ PO_4^{3-}$	[49,55,56,58]
1061	$\nu_3\ PO_4^{3-}$	[53]
1066	$\nu_3\ PO_4^{3-}$	[49,53]
1073	$\nu_3\ PO_4^{3-}$	[49,51,55-57]
1090	$\nu_3\ PO_4^{3-}$	[49,51-53]
1097	$\nu_3\ PO_4^{3-}$	[55-58]
1100	Occurs in nonstoichiometric apatites containing (HPO_4^{2-}) ions	[53]
1111	Present in newly precipitated apatite	[53]
	Found in mature poorly crystalline HAp (HPO_4^{2-})	[55,58]

The presence of titanium in the incubation media leads to changes in the infrared spectra of the powders. Figure 3 shows the overlay of the FT-IR normalised spectra of the powders obtained for different concentrations of Ti in solution.

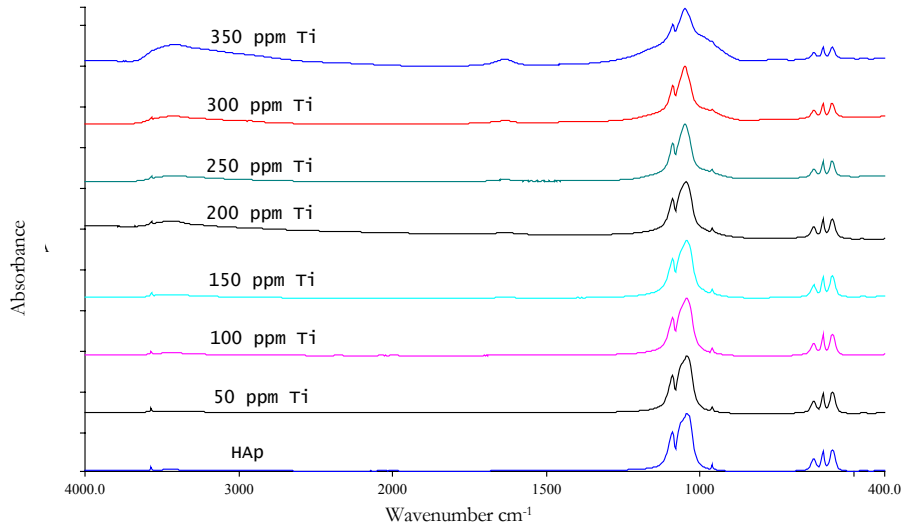

Figure 3 - FT-IR spectra of HAp and of HAp powders obtained after incubation in solutions with different Ti concentrations.

As the Ti concentration increases, the contribution of the area that corresponds to the phosphate bands decreases, while the contribution of the bands that are assigned to the characteristic vibrations of water (3452 cm^{-1} and 1631 cm^{-1}) increase. Figure 4 shows the changes in the relative area of water bands with the increase of Ti concentration.

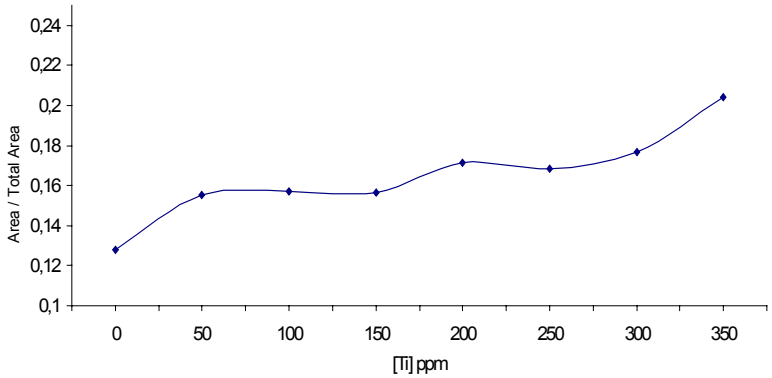

Figure 4 - Normalised area of water bands for HAp (0 ppm of Ti) and for HAp powders obtained after incubation in solutions with different Ti concentrations.

A shift of the band at 1041 cm^{-1} in HAp (ν_3 PO_4) to higher values (1050 for a concentration of 350 ppm of Ti) can also be observed in the spectra represented in Figure 3. The bands at 473 and 963 cm^{-1} progressively disappear with the increase of Ti concentration;

for the concentration of 350 ppm of Ti they are almost absent. Also, the intensity of the OH stretching band of HAp (3572 cm^{-1}) decreases in the presence of increasing concentrations of Ti.

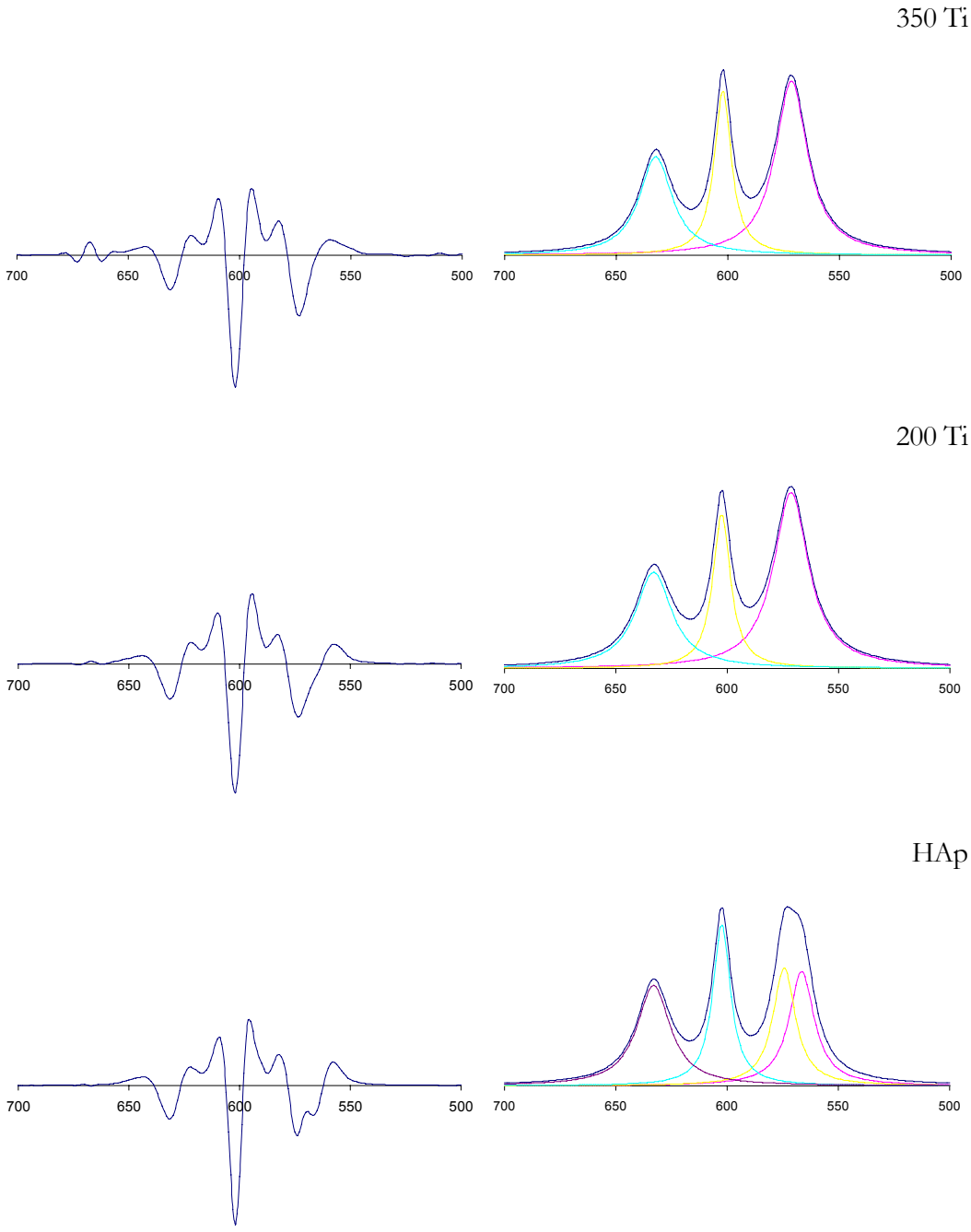

Figure 5 - Second derivative and FT-IR deconvoluted spectra of the ν_4 domain for HAp, HAp200Ti and HAp350Ti samples.

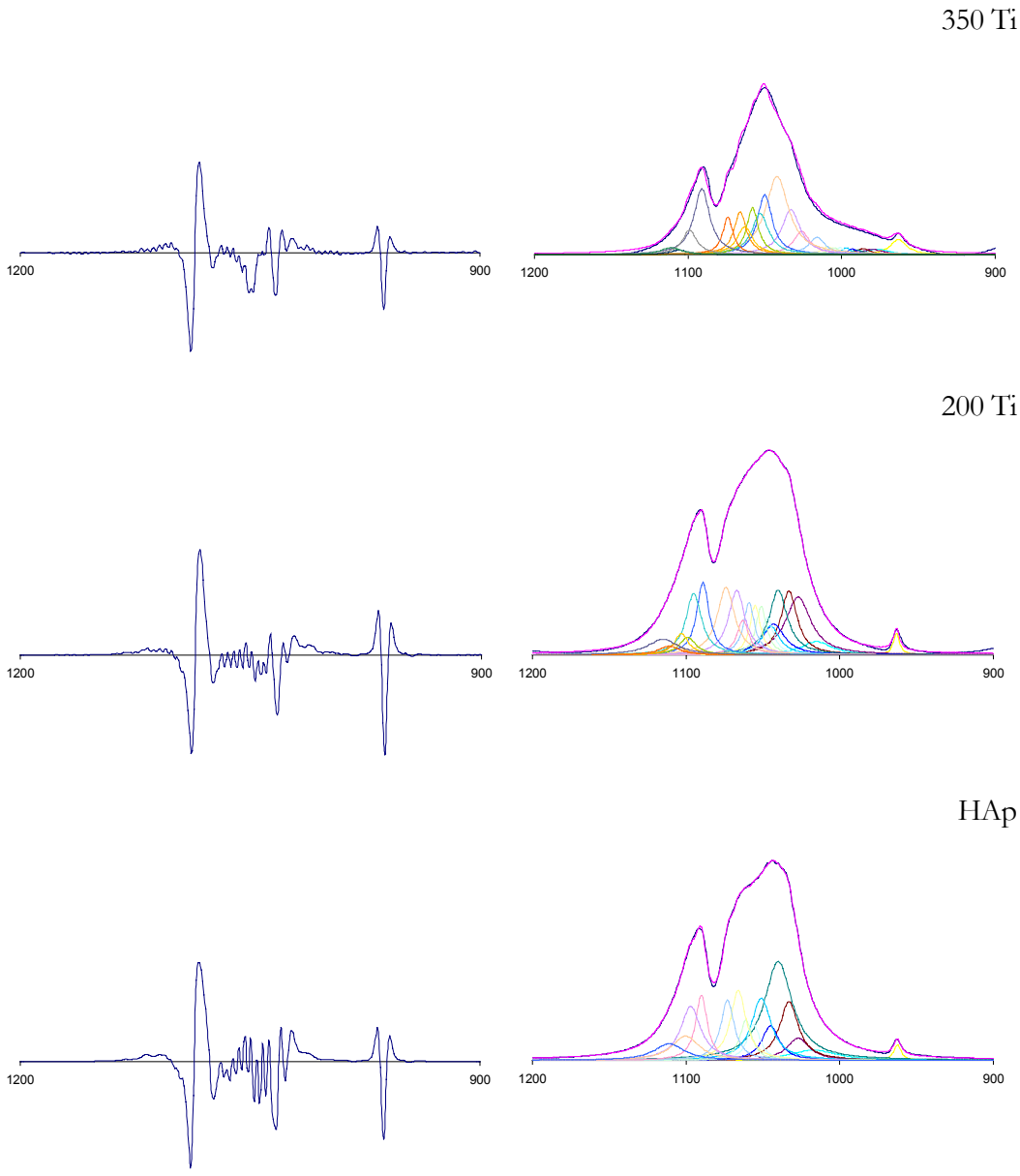

Figure 6 - Second derivative and FT-IR deconvoluted spectra of the ν_1 and ν_3 domains for HAp, HAp200Ti and HAp350Ti samples.

To evaluate the subtle spectral changes occurring as a consequence of the addition of Ti to the dissolution media, the raw spectra in the spectral regions of 500-700 cm^{-1} (ν_4 PO_4 domain) and 900-1200 cm^{-1} (ν_1 and ν_3 PO_4 domains) were analysed by means of second derivatisation and curve fitting (Figures 5 and 6). Only the results obtained for HAp,

HAp200Ti and HAp350Ti samples are shown, which clearly evidentiate the strong changes that occur in the FT-IR spectra of HAp in the presence of Ti.

XRD analysis

X-ray diffraction patterns of HAp and HAp incubated in solutions with different concentrations of titanium were obtained. The HAp powder and the HAp50Ti, HAp100Ti, HAp150Ti and HAp200Ti samples produced reflections that matched the ICDD (JCPDS) standard for HAp, with no additional phases. For higher concentrations of Ti, the higher the concentration the more amorphous the HAp powder became. The lattice parameters were calculated and are represented in Figure 7. The sample HAp350Ti was practically amorphous and consequently the lattice parameters were not determined. a and c parameters decrease with increasing Ti concentration until 150 ppm, suggesting a change in the unit cell of HAp in the presence of Ti. Furthermore, when a single peak for various Ti concentrations is superimposed (e.g. the (102) and (210)), a clear shift in the peak position is observed (Figure 8). This corresponds to a classical description of a change in the unit cell.

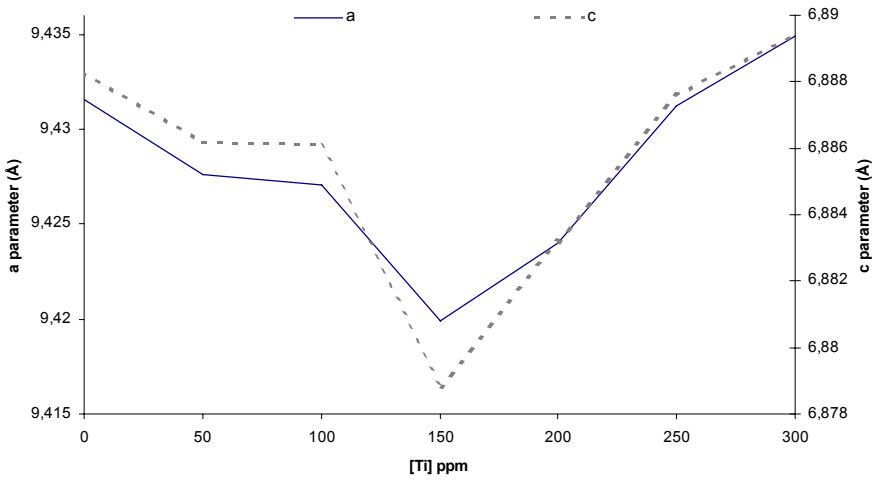

Figure 7 - Lattice parameters (a and c) of HAp powders after incubation in solutions with different Ti concentrations.

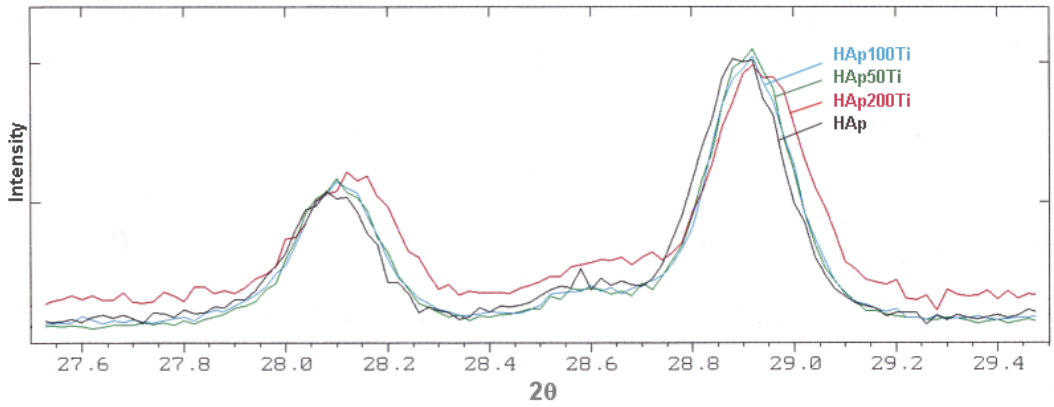

Figure 8 - Overlay of the basal plane (102) and (210) reflection peaks for the HAp, HAp50Ti, HAp100Ti and HAp200Ti samples.

Thermal analysis

In order to evaluate the thermal stability of the HAp powders after being incubated in Ti solutions, differential thermal analysis (DTA) was performed on the following samples: HAp, HAp50Ti, HAp100Ti and HAp200Ti.

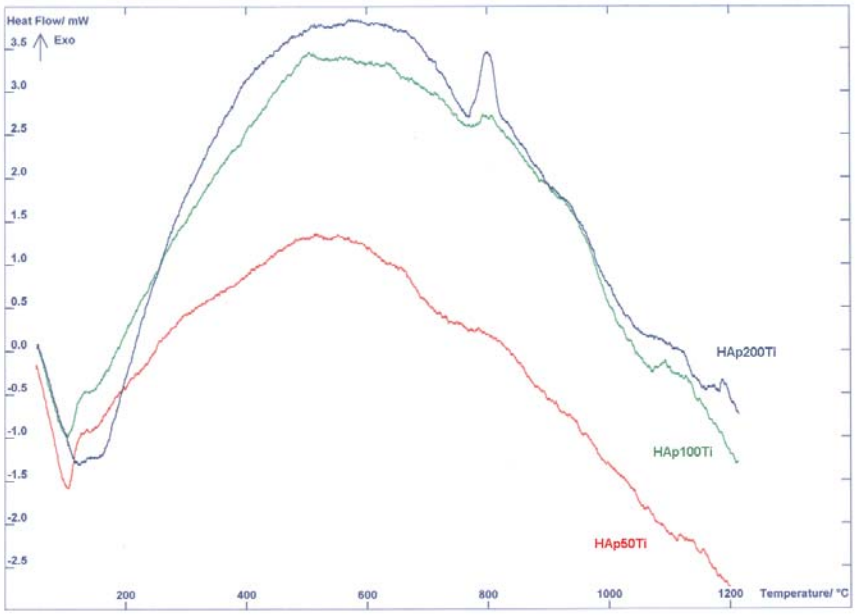

Figure 9 - DTA thermograms of HAp50Ti, HAp100Ti and HAp200Ti samples.

The results showed that in the more concentrated samples analysed (100 and 200 ppm of Ti), an exothermic peak at 794ºC was observed (Figure 9) not present in the thermograms

of HAp and HAp50Ti samples. This is the temperature at which the endothermic reaction that corresponds to the transformation from Ca-deficient apatite to β-TCP occurs [59]. It is also at temperatures of this order that TiP_2O_7 undergoes an exothermic process corresponding to a change in its crystalline structure [60].

After DTA analysis, the powders obtained were analysed by FT-IR spectroscopy (Figure 10).

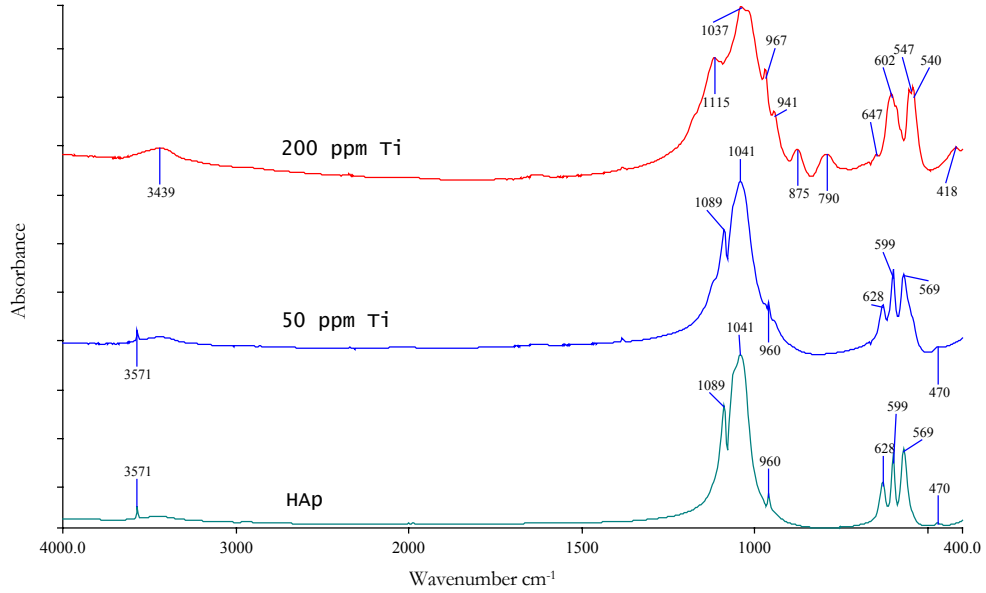

Figure 10 - FT-IR spectra of HAp, HAp50Ti and HAp200Ti samples after DTA analysis.

The FT-IR spectrum of HAp50Ti sample after DTA analysis, when compared with the one of HAp50Ti before DTA analysis, presents some differences, namely the broadening of the band at 1041 cm^{-1}, and also the emergence of shoulders at 1120 cm^{-1} and 546 cm^{-1}, characteristic of the presence of β-TCP. Moreover, the bands at 960 and 628 cm^{-1} decrease their intensity. β-TCP is one of the two crystallographic forms of tricalcium-phosphate whose theoretical transition temperature to α-TCP is 1125ºC, although the precise transformation temperature remains unclear [41]. As the samples were heated at 1200ºC, one could expect the presence of α-TCP instead of β-TCP in the resultant powders. However, the β-form may be stabilised by several ionic impurities as for instance Mg^{2+} ions [61], which are frequently associated with calcium-salts. For samples with higher concentrations of Ti

(200 ppm Ti), the FT-IR analysis shows the presence not only of the already mentioned characteristic bands of β-TCP, but also two new bands at 790 and 875 cm^{-1}, which are possible associated to the presence of titanium in the solid.

XPS analysis

XPS spectra were obtained for HAp powders and for the HAp100Ti, HAp200Ti and HAp250Ti samples. Prior to the XPS analysis, the powders were pressed into very thin pellets in order to obtain more homogeneous surfaces. The XPS survey scans of HAp showed the presence of Mg and Na as contaminants, besides carbon that was present in all the samples analysed. Carbon impurity had atomic percentages varying from 3.3 to 18.9% for the different samples and the source of this contamination was most likely due to the adventitious deposition of hydrocarbon contaminants from the atmosphere. The carbon peak was actually used for binding energy calibration by setting its binding energy to 285 eV to correct for sample charging. XPS core levels of the P2p, Ca2p, Ti2p and O1s orbitals were examined. High-resolution XPS scans were curve-fitted and the peak area intensities of the core levels were normalised to their respective atomic sensitive factors. The precision of the binding energies measurements was ± 0.2 eV.

Table II shows the values of the binding energies determined for the main components of the various samples. In what concerns the Ca2p, P2p and O1s bands, there was no notable variation of their position with the presence of Ti in the incubation media. The titanium band positions ($Ti2p_{1/2}$ and $Ti2p_{3/2}$) and the distance between the peaks (5.7 eV) did not vary with the titanium concentration in solution, corresponding to Ti^{4+}.

Table II - XPS binding energies (eV).

Sample	*P2p*	*Ca2p$_{1/2}$*	*Ca2p$_{3/2}$*	*O1s*	*Ti2p$_{1/2}$*	*Ti2p$_{3/2}$*
HAp	133.2	347.1	350.6	531.2		
HAp100Ti	133.2	347.2	350.6	531.2	458.8	464.5
HAp200 Ti	132.2	347.1	350.6	531.1	458.7	464.4
HAp250 Ti	132.1	347.0	350.5	531.0	458.7	464.4

Table III shows the variation of the chemical composition of the HAp powders after incubation in Ti solutions. In this and in other investigations [62-65] it has been found that XPS Ca/P ratio of HAp is consistently lower than the bulk stoichiometric value (1.67) (the same is observed with other calcium phosphates). An explanation for this observation was given by Chusuei *et al* [63], who pointed out that this might be due to the instability of the compounds and prolonged exposure of the powders to the X-ray source, leading to selective ejection of calcium. The results presented in Table III also show that the Ti/Ca ratio increased as the titanium concentration in the incubation media increased, while the Ca/P ratio decreased. The P/O ratio is relatively constant in all the samples, which indicates that there was little or no loss of phosphate from the surface.

Table III - XPS atomic percentages and elemental ratios.

	P	Ca	O	Ti	$\frac{Ca}{P}$	$\frac{P}{O}$	$\frac{Ti}{Ca}$	$\frac{Ti}{P}$	$\frac{(Ca+Ti)}{P}$
	Atomic %	Atomic %	Atomic %	Atomic %					
HAp	18.70	22.38	58.92	-	1.20	0.32	-	-	1.20
100HApTi	19.27	20.87	57.80	2.05	1.08	0.33	0.10	0.11	1.19
200HApTi	20.29	19.96	56.95	2.80	0.98	0.36	0.14	0.14	1.12
250HApTi	20.14	18.17	58.23	3.47	0.90	0.35	0.19	0.17	1.07

Discussion

A characteristic property of HAp is its ability to undergo isomorphous substitutions, iso or heteroionic, which may be defined as a replacement of one ion by another in a crystal lattice without disrupting its crystal structure. Isoionic substitution is a process by which ions from a solution phase exchange with identical ions of a solid phase in contact with it, the composition of the two phases being unaltered [66]. In heteroionic substitution an ion of a solid phase is displaced by a different ion from a solution in contact with it, thereby altering the composition of both phases [66].

Two general mechanisms have been proposed to explain the ability of apatites, particularly those with relatively high surface areas, to take up metal ions:

1) Adsorption of ions on the ceramic surface, followed by their diffusion into the solid, and the release of cations originally contained within the solid;

2) Dissolution of the ceramic in the aqueous solution containing the donor ions, followed by precipitation or co-precipitation.

For instance, Ma *et al* [67], Xu and Schwartz [68] and Lower *et al* [69] have suggested the dissolution and precipitation mechanism for the immobilisation of aqueous Pb^{2+} with hydroxyapatite. If a similar process would occur with titanium ions, the reactions involved would be:

(1) Dissolution process:

$$Ca_{10}(PO_4)_6(OH)_2\,(solid) + 14H^+\,(aq.) \rightarrow 10Ca^{2+}\,(aq.) + 6H_2PO_4^-\,(aq.) + 2H_2O$$

(2) Precipitation process:

$$5Ti^{4+}\,(aq.) + 6H_2PO_4^-\,(aq.) + 2H_2O \rightarrow Ti_5(PO_4)_6(OH)_2\,(solid) + 14H^+(aq.)$$

The adsorption of Ti ions on the HAp, followed by their diffusion into the solid, and the release of Ca to the incubation solution, could be another possible mechanism for the immobilisation of Ti. In this case, the substitution of Ca by Ti in the HAp lattice would occur according to the reaction:

$$Ca_{10}(PO_4)_6(OH)_2\,(solid) + \frac{n}{2}Ti^{4+} \rightarrow (Ca_{10-n}\,Ti\frac{n}{2})(PO_4)_6(OH)_2 + nCa^{2+} + \frac{n}{2}\square$$

where $\square$ represents a vacancy.

The data in Table III supports this mechanism. From XPS analysis, the Ca/P ratio decreases and the Ti/Ca and Ti/P ratios increase as the amount of Ti (n/2) increases, whereas the P/O ratio remains constant. As the value of n/2 is allowed to increase in the above mechanism, the same trends in these elemental ratios would be observed.

Besides Ca^{2+}, PO_4^{3-} can also be substituted in the HAp lattice. Gibson *et al* [28] have successfully prepared a silicon-substituted hydroxyapatite by a simple aqueous precipitation

method. Their studies were based on the fact that the substitution of a phosphate group (PO_4^{3-}) for a silicate group (SiO_4^{4-}) in a crystal structure would be feasible provided there was electrical charge balance to account for the more negative silicate group. Similarly, a substitution mechanism that would describe the substitution of a phosphate group for a titanate group, with an appropriate mechanism for charge balance, is given by the equation:

$$Ca_{10}(PO_4)_6(OH)_2\,(solid) + xTiO_4^{4-}(aq.) \rightarrow Ca_{10}(PO_4)_{6-x}(TiO_4)_x(OH)_{2-x}\,(aq.) + xPO_4^{3-}\,(aq.) + xOH^-\,(aq.)$$

Another possibility to explain the mechanism of interaction of Ti with HAp would be that a dissolution-precipitation process occurs, leading to formation of a new compound. In a previous work, the authors have found that for concentrations of Ti in solution higher than 350 ppm, an hydrated hydrogen titanium phosphate ($Ti(HPO_4)_2.nH_2O$) was formed [70]. Other authors reported the same mechanism with different ions, namely Fe^{3+}, Al^{3+} and La^{3+} [71, 72]. They have shown that the ion exchange of calcium with these metals in acidic solutions destroys the HAp crystals to form phosphates of these ions.

Finally, we should also consider the possibility that in the experiments where HAp was exposed to Ti in solution, any Ti uptake on the solid was primarily due to adsorption and not to incorporation in the lattice. However, this is the less plausible hypothesis according to the results obtained. In the present study, evidence for the incorporation of Ti into the HAp lattice is given by the X-ray diffraction results. No additional phases were observed for the Ti-HAp samples and the diffraction pattern was identical to that obtained for stoichiometric apatite. The changes in the lattice parameters, and the shift in the peak position that corresponds to a basal plane with increasing Ti concentration, suggest that changes occurred in the HAp lattice. The effect of substituents on the lattice parameters of hydroxyapatite depends on their size and amount. Usually, if the substituent is larger than the ion substituted for (e.g. Sr^{2+} for Ca^{2+} or Cl^- for OH^-), the effect is to expand one or both of the parameters [29]. In some cases of substitution, both a and c axes are affected, either in the same or opposite directions. In other cases, only the a-axis dimensions are either increased or decreased, while the c-axis dimensions are not significantly different from the unsubstituted hydroxyapatite [29]. For instance, the substitution of cadmium and manganese for calcium,

both ions having an ionic radius smaller than calcium, leads to a decrease in both a and c axis of the substituted hydroxyapatite [29]. Since the ionic radius of Ti^{4+}(0,68 Å) is smaller than that of Ca^{2+} (0,99 Å), a Ti for Ca substitution is expected to cause a decrease in either or both of the lattice parameters. A decrease of both parameters with the increase of Ti concentration in solution was observed for concentrations below 200 ppm. It should be noted that the incorporation of Ti into the HAp lattice may be a surface effect i.e. there may be a significant amount of the HAp particles that remain unchanged. The lattice parameters determination resulted in relatively small changes in the a and c axes, but this may be due to the effect being diluted by a high proportion of unchanged HAp, relative to the Ti modified HAp. For Ti concentrations higher than 150 ppm the a, and c parameters increased suggesting another mechanism of interaction of Ti with HAp. Previous results [70] indicate that for those concentrations the formation of a poorly crystalline Ti-P-O phase is favoured, explaining why the material became more amorphous as the amount of Ti increased.

The XPS results concerning the surface composition of the powders are in agreement with the ones obtained for the bulk structure. The analysis showed that although the presence of Ti in solution does not result in a change of the binding energies of Ca, P and O, when compared to the ones of HAp, the changes in the atomic percentages of the elements suggest a possible substitution of Ca by Ti when small concentrations of Ti are in solution (100 ppm). The (Ca+Ti)/P ratio obtained for the HAp100Ti sample is practically the same as the Ca/P ratio of HAp. For higher concentrations of Ti, the XPS results suggest that another mechanism is occurring in parallel with substitution. Formation of a new compound is a plausible explanation.

The infrared absorption spectrum of calcium hydroxyapatite is characterised by the absorption bands reflecting the different vibration modes of the OH^- and PO_4^{3-} groups, as previously mentioned. Since the PO_4^{3-} groups serve as the skeletal framework of the apatite structure, it is expected that any substitution will have a very pronounced effect on the environment of these groups. This effect will be manifested in the frequencies and resolutions of their infrared absorption bands.

Under $P6_{3/m}$ space group symmetry (hexagonal symmetry), the C_s site group (Table IV) defines the effective symmetry of phosphate ion sites. The C_{6h} factor group describes the symmetry of the unit cell [49, 51]. The free PO_4^{3-} ion is tetrahedral and presents four vibrational modes which are an A_1 symmetric stretch (ν_1), an E bend (ν_2), an F_2 antisymmetric stretch (ν_3) and an F_2 bend (ν_4). The ν_3 and ν_4 modes are both infrared and Raman active, whereas the ν_1 and ν_2 modes are normally inactive in infrared spectroscopy when the ion is in the regular tetrahedral symmetry (only two bands due to the ν_3 and ν_4 modes may be observed) [54]. However, in crystalline calcium phosphate compounds, the number of bands that is observed in the absorption domain of the vibrational modes of the free PO_4^{3-} ion (up to 18 for hydroxyapatite [41, 51]), is larger than the theoretically expected. This is due to site symmetry of PO_4^{3-} groups in the crystal and eventually coupling of groups in equivalent crystallographic position (group factor theory) [54].

Table IV - Correlation diagram and spectral activity for the T_2 vibrational mode of phosphate ion in space group $P6_{3/m}$ (adapted from references [49, 51]).

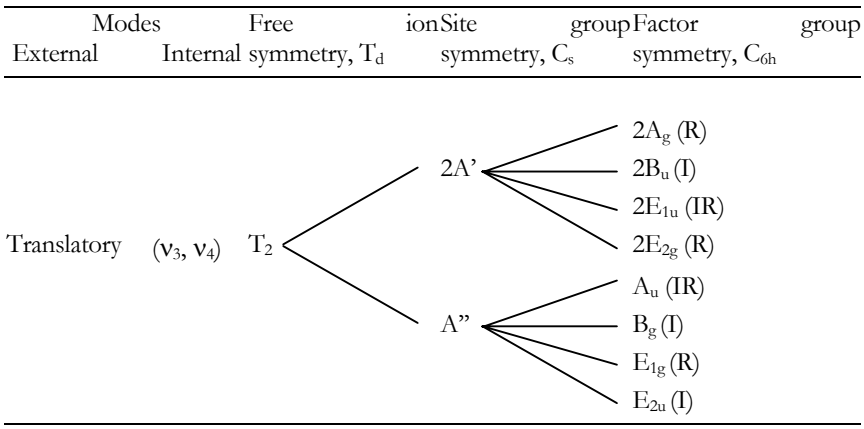

IR: Infrared active; R: Raman active; I: Inactive in both infrared and Raman spectra

Bands located at 963 cm^{-1} (ν_1) and 473 cm^{-1} (ν_2), although infrared forbidden in tetrahedral symmetry [49, 51], have infrared active components in the hydroxyapatite. These modes become active when the phosphate group is slightly distorted to specific symmetries less than T_d [51], giving rise to infrared bands of weak intensity which provide little information on the the mineral environment [49]. Contrarily, the ν_3 (1000-1100 cm^{-1}) and ν_4

(550-620 cm^{-1}) bands are infrared allowed in the theoretical free-ion spectrum and belong to the T_2 symmetry point group [49]. The splitting of these bands is due to the low site symmetry of the mineral matrix and intermolecular vibrational coupling [49]. If HPO_4^{2-} ions or local distortions of the PO_4 environment, due to the presence of vacancies or substitutes, are taken into account, the number of bands could be even greater and further complicate the problem of differentiating all the phosphate moieties by IR [53].

The FT-IR bands obtained for the HAp under study are the ones that should be expected for a stoichiometric HAp according to the literature (see Table I), which is in agreement with the XRD results. No chemical changes did occur during heating after DTA analysis, and the powder obtained still presented the FT-IR characteristic bands of HAp.

Type B carbonate and HPO_4^{2-} containing apatites, which are described as non-stoichiometric apatites, generate spectra quite similar to that of HAp. They are characterised by intense additional bands at 1020 and 1100 cm^{-1} [53]. Rey *et al* [53] also showed that HPO_4^{2-}-containing apatites present a band at 1143 cm^{-1}, which has been assigned to HPO_4^{2-} ions. This is observed in most biological apatites, especially in the early stages of mineral deposition. Also, two low wavenumber bands at 520-530 and 540-550 cm^{-1} are assigned to HPO_4^{2-} and exist in HPO_4^{2-} containing apatite, brushite and octacalcium phosphate. None of these particular bands were assigned in the spectrum of the HAp under investigation. Nevertheless, the second derivative of the spectrum revealed the presence of weak bands at 1017, 1100 and 1111 cm^{-1}, which can be attributed to HPO_4^{2-} or labile phosphate. The deconvolution of the FT-IR spectrum of HAp indicates that the HPO_4^{2-} acid ion must be residual in the HAp powder in study, as the area of its characteristic bands is very small. In what concerns the influence of Ti on the hydroxyapatite structure, several infrared parameters are consistent, showing that there is a change of the orthophosphate ion environment with the presence of Ti. For small concentrations of Ti in solution (up to approximately 100 ppm) the phosphate ions of HAp tend to exhibit the features of phosphate ions in well-crystallised HAp. In the more concentrated samples, the divergences from the regular apatitic environment appear quite evident. From the ν_3 domain in IR deconvoluted spectra (Figure 6) it is clear that the spectrum becomes more complex, as the

Ti concentration in solution increases, as indicated by the higher number of bands that compose it.

The infrared absorption of the OH^- groups also shows interesting changes. The librational mode of the OH^- group (632 cm^{-1}) is especially sensitive to substitutions in the apatite structure [39]. The strength of this peak is well known to correlate with the degree of crystallinity of HAp [1, 30]. In the presence of Ti the area of the OH librational band decreases, suggesting a decrease in HAp crystallinity. In general, a decrease in crystallinity is attributed to a decrease in crystallite size, an increase in lattice imperfections, or a combination of these effects. The OH^- stretching band, which appears in HAp as a symmetrical and narrow peak at 3572 cm^{-1}, decreases with the increase of Ti concentration (for a concentration of 350 ppm of Ti it is almost absent). This band falls into the range indicative of weakly hydrogen-bonded OH^- groups [5]. According to Baddiel *et al* [57], the only atoms in the HAp structure to which such bonding might be considered are the oxygen atoms of the neighbouring OH^- and PO_4^{3-} groups. In HAp, the oxygen atoms of the phosphate groups and the oxygen atoms of the hydroxyl groups are sufficiently close (3.05 Å distance) for a H bond, such as O-H….OPO_3, to occur. Contrarily, the O-O distance between neighbouring OH^- groups is too large (3.44 Å) for a hydrogen bond to be formed [78]. The decrease in intensity of the OH^- stretching band is also indicative of changes in the HAp structure.

FT-IR data show that two broad bands centred at approximately 3400 and 1630 cm^{-1}, which are due to the presence of lattice water, increase in the powder samples as the Ti concentration increases. Water in inorganic salts may be classified as lattice or co-ordinated water. There is, however, no definite borderline between the two. The former term denotes water molecules trapped in the crystalline lattice, either by weak hydrogen bonds to the anion or by weak ionic bonds to the metal, or by both [46]. The latter term refers to water molecules bonded to the metal through partially covalent bonds. In general, lattice water absorbs at 3550-3200 cm^{-1} (antisymmetric ν_3 and symmetric ν_2 OH stretching) and at 1630-1600 cm^{-1} (ν_1 HOH bending). That observation supports the idea of formation of a hydrated compound with the increase in Ti concentration.

The infrared spectra of the powders obtained after DTA analysis showed the existence of β-TCP phase, its presence becoming increasingly evident as the Ti concentration in the incubation solution was augmented. The formation of β-TCP is a sensitive indicator of a composition with Ca/P ratio lower than stoichiometric HAp. After being submitted to heating until 1200ºC, HAp still presented its characteristic infrared spectrum with no unusual bands assigned. The most likely explanation for the existence of β-TCP phase in the heated Ti-HAp powders is that the presence of Ti in the incubation media leads to the formation of a calcium-deficient apatite that has a Ca/P ratio less than 1.67 and contains HPO_4^{2-} groups. Calcium-deficient hydroxyapatites are less thermally stable than stoichiometric hydroxyapatites. For example, the formation of pyrophosphate at about 600ºC occurs only in calcium-deficient apatites and not in perfect apatites. When heated to above 750ºC, a temperature which does not affect stoichiometric hydroxyapatite, calcium-deficient hydroxyapatite dehydrates to form β-$Ca_3(PO_4)_2$ plus some residual apatite (if the Ca/P ratio is equal to 1.5 there is no residual apatite detected after pyrolisis). During thermal treatment the ionic group of HPO_4^{2-} decomposes via pyro-type phosphate $(P_2O_7)^{4-}$ to PO_4^{3-} in non-stoichiometric apatites according to the reactions:

$$HPO_4^{2-} \rightarrow \frac{1}{2} P_2O_7^{4-} + H_2O\ (g) \qquad 600ºC$$

$$P_2O_7^{4-} + 2OH^- \rightarrow 2\ PO_4^{3-} + H_2O\ (g) \qquad 700ºC \text{ a } 800ºC$$

However, for the 200 ppm of Ti samples two other bands (790 and 875 cm^{-1}), that could not be attributed to β-TCP, were also detected by FT-IR analysis. The broad band centred at 790 cm^{-1} seems to be associated to the presence of Ti-O bonds according to several authors although this region of the spectrum is also characteristic of pyrophosphate group vibrations [41, 44]. Vilchez *et al* [74] refers that $[TiO_4]^{4-}$ ion presents ν_1 and ν_3 stretching bands at 761 and 770 cm^{-1}. Bamberger *et al* [75] and El Jazouli *et al* [76] assigned, by Raman spectroscopy, a strong band around 750-800 cm^{-1}, observed in the titanyl orthophosphate ($NaTiOPO_4$: 745 cm^{-1}, $LiTiOPO_4$: 783 cm^{-1}, $Ni_{0.5}TiOPO_4$: 750 cm^{-1}), to the Ti-O vibrations in the -Ti-O-Ti-O- chains. Also, Chernorukov *et al* [77] associated the bands comprised in the

725-800 cm^{-1} interval, observed in the infrared spectra of different titanium compounds, to the stretching vibrations of Ti-O bonds. As already mentioned, the formation of a titanium protonated phosphate ($Ti(HPO_4)_2.nH_2O$) for high concentrations of Ti in the incubation media (>350 ppm of Ti) has been reported by the present authors [70]. This titanium phosphate phase, when heated up to a temperature of 1200ºC, would decompose according to the reaction:

$$4Ti(HPO_4)_2.nH_2O\ (s) \rightarrow (TiO)_2P_2O_7\ (s) + 2Ti\ P_2O_7\ (s) + P_2O_5\ (g) + (n+4)H_2O\ (g)$$

The $(TiO)_2P_2O_7$ phase results from the partial decomposition of TiP_2O_7 [78]. The presence of pyrophosphate ions in the HAp200Ti sample after DTA analysis could be justified if, for that concentration in Ti, the titanium protonated phosphate phase already existed in the non heat-treated sample. However, its presence was not detected by XRD, which leads to the assumption that the phase is either amorphous or exists in very small concentrations. The band at 875 cm^{-1} can be assigned to pyrophosphate group [44] or correspond to the stretching vibration of distorted tetrahedral phosphate [77].

The DTA data for the Ti concentration of 200 ppm show an exhotermic peak at 790ºC. This is the temperature at which the endothermic reaction that corresponds to the transformation from Ca deficient apatite to β-TCP occurs [59]. It is possible that two transformations are occurring at the same temperature (rearrangement of TiP_2O_7 to a cubic three-dimensional structure - exothermic - and formation of β-TCP - endothermic), the thermal balance of both phenomena resulting in an exothermic reaction.

Conclusions

The results obtained with the different techniques used clearly indicate that HAp undergoes structural changes in the presence of Ti in the incubation media.

The mechanism of interaction of Ti ions with HAp seems to be dependent of the ion concentration.

Although, as to the best of our knowledge, the substitution of Ca for Ti has not been reported by other authors, it seems to be the mechanism that better explains the changes that are observed for concentrations in Ti lower than 200 ppm. For higher concentrations, the formation of a titanium phosphate, already reported in a previous study, is observed.

Acknowledgements

Cristina C Ribeiro is grateful to Doctor Serena Best for supporting and enabling her to carry out research in IRC as part of her Ph.D.. The authors would also like to thank Doctor Carlos Sá (CEMUP) for assistance in the XPS investigation.

References

[1] Fowler BO. Infrared studies of apatites. II Preparation of normal and isotopically substituted calcium, strontium, and barium hydroxyapatites and spectra-structure-composition correlations. Inorg Chem 1974; 13: 207-214.

[2] LeGeros RZ, Daculsi G, Orly I, Abergas T, Torres W. Solution mediated transformation of octacalcium phosphate (OCP) to apatite. Scann Microsc 1989; 3: 129-138.

[3] Takahashi H, Yashima M, Kakihana M, Yoshimura M. Synthesis of stoichiometric hydroxyapatite by a "gel" route from the aqueous solution of citric and phosphonoacetic acids. Eur J Solid State Inorg Chem 1995; 32: 829-835.

[4] Posner AS, Blumenthal N, Betts F. Chemistry and Structure of Precipitated Hydroxyapatites. In: Nriagu JO, Moore PB, editors. Phosphate Minerals. New York, USA: Springer Verlag, 1984. p.330-347.

[5] Yamashita K, Kanazawa T. Hydroxyapatite. In: Kanazawa T, editor. Inorganic Phosphate Materials. Tokyo, Japan: Kodansha, 1989. p.15-54.

[6] Legros R, Balmain N, Bonel G. Age related changes in mineral of rat and bovine cortical bone. Calcif Tissue Int 1987; 41: 137-144.

[7] LeGeros RZ, Quirolgico G, LeGeros JP. Trace elements: incorporation of monovalent cations, Na^+, K^+, Li^+. J Dent Res 1981; 60B: 452-458.

[8] Christoffersen J, Christoffersen MR, Kolthoff N, Barenholdt O. Effects of strontium ions on growth and dissolution of hydroxyapatite and on bone mineral detection. Bone 1997; 20: 47-54.

[9] Suzuki T, Hatsushika T, Hayakawa Y. Synthetic hydroxyapatites employed as inorganic cation-exchangers. J Chem Soc, Faraday Trans 1981; 77: 1059-1062.

[10] Miyake M, Ishigaki K, Suzuki T. Structure refinements of Pb^{2+} ion exchanged apatites by X-ray powder pattern-fitting. J Solid State Chem 1986; 61: 230-235.

[11] Ergun C, Webster TJ, Bizios R, Doremus RH. Hydroxylapatite with substituted magnesium, zinc, cadmium, and yttrium. I. Structure and microstructure. J Biomed Mater Res 2002; 59: 305-311.

[12] Bonel G, Montel G. Sur une nouvelle apatite carbonatée synthétique. Compt Rend 1964; 258: 923-926.

[13] LeGeros RZ, Singer L, Ophaug RH, Quirolgico G, Thein A, LeGeros J P. The effect of fluoride on the stability of synthetic and biological (bone) mineral apatites. In: Menczel J, Robin GC, Makin M, Steinbeg R, editors. Osteoporosis. New York, USA: Wiley & Sons; 1982. p.327-341.

[14] Kreidler ER, Hummel FA. The crystal chemistry of apatite: structure fields of fluor and chloroapatite. The American Mineralogist 1970; 55: 171-184.

[15] LeGeros RZ, Trautz OR, LeGeros JP, Klein E. Carbonate substitution in the apatite structure (1). Extrait du bulletin de la societé chimique de France 1968; special number: 1712-1718.

[16] Azimov SY, Ismatov AA, Fedorov NF. Synthetic silicophosphates, silicovanadates, and silicoarsenates with the apatite structure. Inorg Mat 1981; 17: 1384-1387.

[17] Termine JD, Lundy DR. Hydroxide and carbonate in rat bone mineral and its synthetic analogues. Calcif Tissue Res 1973; 13: 73-78.

[18] Lacout JL, Nounah A, Ferhat M. Strontium-cadmium substitution in hydroxy-and fluor-apatites. Ann Chim Sci Mat 1998; 23: 57-60.

[19] El Feki H, Savariault JM, Ben Salah A. Structure refinements by Rietveld method of partially substituted hydroxyapatite: $Ca_9Na_{0.5}(PO_4)_{4.5}(CO_3)_{1.5}(OH)_2$. J Alloys Compounds 1999; 287: 114-120.

[20] LeGeros RZ. Apatites in biological systems. Prog in Crystal Growth Charact 1981; 4: 1-45.

[21] Rey C. Calcium Phosphates for Medical Applications. In: Zahid Amjad, editor. Calcium Phosphates in Biological and Industrial Systems. Boston, USA: Kluwer Academic Publishers, 1998. p.217-251.

[22] Watanabe T, Makitsuru K, Nakazawa H, Hara S, Suehiro T, Yamamoto A, Hiraide T, Ogawa T. Separation of double strand DNA fragments by high-performance liquid chromatography using a ceramic hydroxyapatite column. Anal Chim Acta 1999; 386: 69-75.

[23] LeGeros RZ. Biological and synthetic apatites. In: Brown PW, Constanz B, editors. Hydroxyapatites and Related Materials. Boca Raton, USA: CRC Press, 1994. p.3-28.

[24] Bett JAS, Christner LG, Hall WK. Studies of the hydrogen held by solids. XII. J Am Chem Soc 1967; 89: 5535-5541.

[25] Matsumara Y, Kanai H, Moffat JB. Catalytic oxidation of carbon monoxide over stoichiometric and non-stoichiometric hydroxyapatites. J Chem Soc Faraday Trans 1997; 93: 4383-4387.

[26] Takeuchi Y, Arai H. Removal of coexisting Pb^{2+}, Cu^{2+} and Cd^{2+} ions from water by addition of hydroxyapatite powder. J Chem Eng of Japan 1990; 23: 75-80.

[27] Suzuki T, Hastushika T, Miyake M. Synthetic. Hydroxyapatites as inorganic cation exchangers-Part 2. J Chem Soc, Faraday Trans I, 1981; 78: 3605-3611.

[28] Gibson IR, Best SM, Bonfield W. Chemical characterisation of silicon-substituted hydroxyapatite. J Biomed Mater Res 1999; 44: 422-428.

[29] LeGeros RZ. Ultrastructural Properties of Human Enamel Apatite. In: Lazzari EP, editor. Handbook of Experimental Aspects of Oral Biochemistry. Florida, USA: CRC Press, 1983. p.159-179.

[30] Young RA, Elliott JC. Atomic-scale bases for several properties of apatites. Archs Oral Biol 1966; 11: 699-707.

[31] Elliott JC. The problems of the composition and structure of the mineral components of hard tissues. Clin Orthoped 1973; 93: 313-317.

[32] LeGeros RZ. Phosphate minerals in human tissues. In: Nriagu JO, Moore PB, editors. Phosphate Minerals. New York, USA: Springer Verlag, 1984. p.351-385.

[33] Christofferson MR, Cristofferson J. The effect of aluminum on the rate of dissolution of calcium hydroxyapatite - a contribution to the understanding of aluminum-induced bone diseases. Calcif Tissue Int 1985; 37: 673-676.

[34] Christofferson MR, Thyregod HC, Cristofferson J. Effects of aluminum (III), chromium (III) and iron (III) on the rate of dissolution of calcium hydroxyapatite crystals in the absence and presence of chelating agent desferrioxamine. Calcif Tissue Int 1987; 41: 27-30.

[35] Posner AS, Blumenthal NC. *In vitro* model of aluminum-induced osteomalacia: inhibition of hydroxyapatite formation and growth. Calcif Tissue Int 1984; 36: 439-441.

[36] Levin SM, Goldberg M. Clinical evaluation and management of lead-exposed construction workers. Am J Ind Med 2000; 37: 23-43.

[37] Aoki H. In: Aoki H, editor. Science and Medical Applications of Hydroxyapatite. Tokyo, Japan: Takayama Press System Center, 1991. p.52-54.

[38] Blumenthal NC, Cosma V, Skyler D, LeGeros J, Walters M. The effect of cadmium on the formation and properties of hydroxyapatite *in vitro* and its relation to cadmium toxicity in the skeletal system. Calcif Tissue Int 1995; 56: 316-322.

[39] Kay MI, Young RA, Posner AS. Crystal structure of hydroxyapatite. Nature 1964; 204: 1050-1052.

[40] Stavitzky A, Golay MJE. Smoothing and differentiation of data by simplified least squares procedures. Anal Chem 1964; 36: 1627-1639.

[41] Elliot JC. In: Elliot JC, editor. Structure and chemistry of the apatites and other calcium orthophosphates. Amsterdam, Holland: Elsevier, 1994.

[42] Elliot JC, Mackie PE, Young RA. Monoclinic hydroxyapatite. Science 1973; 180: 1055-1057.

[43] Morgan H, Wilson RM, Elliot JC, Dowker SEP, Anderson P. Preparation and characterisation of monoclinic hydroxyapatite and its precipitated carbonate apatite intermediate. Biomaterials 2000; 21: 617-627.

[44] Socrates L. In: Socrates L, editor. Infrared and Raman Characteristic Group Frequencies - Tables and Charts. Chichester, England: John Wiley & Sons, 2001. p.277.

[45] Rehman I, Bonfield W. Characterization of hydroxyapatite and carbonated apatite by photo acustic FTIR spectroscopy. J Mater Sci: Mater Med 1997; 8: 1-4.

[46] Nakamoto K. In: Nakamoto K, editor. Infrared and Raman spectra of inorganic and coordination compounds. New York, USA: John Wiley & Sons Inc, 1978.

[47] LeGeros RZ, Bonel G, Legros R. Types of "H_2O" in human enamel and in precipitated apatites. Calcif Tissue Res 1978; 26: 111-118.

[48] Joris SJ, Amberg CH. The nature of deficiency in non-stoichiometric hydroxyapatites. II. Spectroscopic studies of calcium and strontium hydroxyapatites. J Phys Chem 1971; 75: 3172-3178.

[49] Leung Y, Walters MA, LeGeros RZ. Second derivative infrared spectra of hydroxyapatite. Spectroc Acta 1990; 46A, 10: 1453-1459.

[50] Miller LM, Vaiaravamurthy V, Chance MR, Mendelshon R, Paschalis EP, Betts F, Boskey AL. In situ analysis of mineral content and crystallinity in bone using infrared micro-spectroscopy of the ν_4 PO_4^{3-} vibration. Biochim et Biophys Acta 2001; 1527: 11-19.

[51] Fowler BO. Infrared studies of apatites I. Vibrational assignments for calcium, strontium and barium hydroxyapatites utilizing isotopic substitutions. Inorg Chem 1974; 13: 194-207.

[52] Fowler BO, Moreno EC, Brown WE. Infra-red spectra of hydroxyapatite, octacalcium phosphate and pyrolised calcium phosphate. Arch Oral Biol 1966; 11: 477-492.

[53] Rey C, Shimizu M, Collins B, Glimcher MJ. Resolution enhanced Fourier transform infrared spectroscopy study of the environment of phosphate ion in the early deposits of a solid phase calcium phosphate in bone and enamel and their evolution with age: investigations in the $\nu_3 PO_4^{3-}$ domain. Calcif Tissue Int 1991; 49: 383-388.

[54] Rey C, Shimizu M, Collins B, Glimcher MJ. Resolution enhanced Fourier transform infrared spectroscopy study of the environment of phosphate ion in the early deposits of a solid phase calcium phosphate in bone and enamel and their evolution with age: investigations in the $\nu_4 PO_4^{3-}$ domain. Calcif Tissue Int 1990; 46: 384-394.

[55] Gadaleta SJ, Paschalis EP, Betts F, Mendelsohn R, Boskey AL. Fourier transform infrared spectroscopy of the solution-mediated conversion of amorphous calcium phosphate to hydroxyapatite: new correlations between X-ray diffraction and infrared data. Calcif Tissue Int 1996; 58: 9-16.

[56] Bailey RT, Holt C. Fourier transform infrared spectroscopy and characterisation of biological calcium phosphates. In: Hukins DWL, editor. Calcified Tissues. Basingstoke, Great Britain: Mac Millan Press, 1989, p.93-120.

[57] Baddiel CB, Berry EE. Spectra structure correlations in hydroxy and fluorapatite. Spectroc Acta 1966; 22: 1407-1416.

[58] Paschalis EP, Di Carlo E, Betts F, Sherman P, Mendelsohn R, Boskey AL. FTIR Microspectroscopic analysis of human osteonal bone. Calcif Tissue Int 1996; 59: 480-487.

[59] Gibson IR, Rehman I, Best SM, Bonfield W. Characterization of the transformation from calcium-deficient apatite to β-tricalcium phosphate. J Mater Sci: Mater Med 2000; 12: 799-804.

[60] Szirtes L, Riess L, Megyeri J. Thermoanalytical investigation of layered titanium salts. J Thermal Anal Calorim 2003; 73: 209-218.

[61] Schroeder LW, Dickens B, Brown WE. Crystallographic studies of the role of Mg as a stabilizing impurity in β-$Ca_3(PO_4)_2$ - II. Refinement of Mg-containing β-$Ca_3(PO_4)_2$. J Sol State Chem 1977; 22: 253-262.

[62] Leadley SR, Davis MC, Ribeiro CC, Barbosa MA, Paul AJ, Watts JF. Investigation of the dissolution of the bioceramic hydroxyapatite in the presence of titanium ions using ToF-SIMS and XPS. Biomaterials 1997; 18: 311-316.

[63] Chusuei CC, Goodman DW, Van Stipdonk MJ, Justes DR, Schweikert EA. Calcium phosphate phase identification using XPS and time-of-flight cluster SIMS. Anal Chem 1999; 71: 149-153.

[64] Lu HB, Campbell CT, Graham DJ, Ratner BD. Surface characterization of hydroxyapatite and related calcium phosphates by XPS and TOF-SIMS. Anal Chem 2000; 72: 2886-2894.

[65] Tanahashi M, Matsuda T. Surface functional group dependence on apatite formation on self-assembled monolayers in a simulated body fluid. J Biomed Mater Res 1997; 34: 305-315.

[66] Narasaraju TSB, Phebe DE. Review: Some physico-chemical aspects of hydroxyapatite. J Mat Sci 1996; 31: 1-21.

[67] Ma QY, Traina SJ, Logan TJ, Ryan JA. *In situ* lead immobilization by apatite. Environ Sci Technol 1993; 27: 1803-1810.

[68] Xu Y, Schwartz FW. Lead immobilization by hydroxyapatite in aqueous solutions. J Contam Hydro 1994; 15: 187-206.

[69] Lower SK, Maurice PA, Traina SJ, Carlson EH. Aqueous Pb sorption by hydroxylapatite: applications of atomic force microscopy to dissolution, nucleation, and growth studies. Amer Min 1998; 83: 147-158.

[70] Ribeiro CC, Barbosa MA, Machado A, Tudor A, Davies MC. Modifications in the molecular structure of hydroxyapatite induced by Ti ions. J Mater Sci: Mater in Med, 1995; 6: 829-834.

[71] Tanizawa Y, Sawamura K, Suzuki T. Reaction characteristics of dental and synthetic apatites with Fe^{2+} and Fe^{3+} ions. J Chem Soc Faraday Trans 1990; 86: 1071-1075.

[72] Tanizawa Y, Sawamura K, Suzuki T. Reaction characteristics of dental and synthetic apatites with Al^{2+} and La^{3+} ions in acidic solutions. J Chem Soc Faraday Trans 1990; 86: 4025-4029.

[73] Gonzalez-Diaz PF, Santos M. On the hydroxyl ions in apatites. J Sol State Chem 1977; 22: 193-199.

[74] Vilchez G F, Griffith WP. Transition-metal tetra-oxo-complexes and their vibrational spectra. J Chem Soc, Dalton, 1972; II: 1416-1421.

[75] Bamberger CE, Begun GM, Cavin OB. Synthesis and characterization of sodium-titanium phosphates, $Na_4(TiO)(PO_4)_2$, $Na(TiO)PO_4$ and $NaTi_2(PO_4)_3$. J Solid State Chem 1988; 73: 317-324.

[76] EL Jazouli A, Krimi S, Manoun B, Chaminade JP, Gravereau P, De Waal D. Preparation and structural characterization of two new titanium phosphates $NaCa_{0.5}Ti(PO_4)_3$ and $Ni_{0.5}TiOPO_4$. Ann Chim Sci Mat 1998; 23: 7-10.

[77] Chernorukov NG, Korshunov IA, Zhuk MI. Hydro-ortho-derivatives of titanium of composition $Ti(OH)PO_4$ and $Ti(OH)AsO_4$. Russ J of Inorg Chem 1982; 27: 1728-1731.

[78] Bamberger CE, Begun GM. Synthesis and characterisation of titanium phosphates, TiP_2O_7 and $(TiO)_2P_2O_7$. J Less Common Metals 1987; 134: 201-206.

Chapter 4

AFFINITY OF HYDROXYAPATITE TO METAL CATIONS – A STUDY ON THE COMPOSITION AND STRUCTURE OF PHOSPHATES FORMED IN THE PRESENCE OF TITANIUM AND ALUMINIUM

Cristina C. Ribeiro[1,2,3] and Mário A. Barbosa[1,2]

1 - INEB - Instituto de Engenharia Biomédica, Laboratório de Biomateriais, Rua do Campo Alegre 823, Porto 4150-180, Portugal
2 - FEUP - Faculdade de Engenharia da Universidade do Porto, Dep. de Eng. Metalúrgica e de Materiais, Porto, Portugal
3 - ISEP - Instituto Superior de Engenharia do Porto, Dep. de Física, Porto, Portugal

Abstract

The purpose of this study was to contribute to the understanding of the effect of titanium, aluminium and titanium/aluminium on the HAp structure and to investigate if a synergistic effect between the two cations exists. The effect of the metal ion concentration was studied. The solids were analysed by X-ray diffraction, Fourier transform infrared spectroscopy, FT-Raman spectroscopy and energy dispersive X-ray analysis.

Keywords: hydroxyapatite, titanium, aluminium, phosphates.

Introduction

At present, much attention is being given to the effects of the incorporation of metal ions in apatites. For instance, the mineral phase of bone, made up essentially of hydroxyapatite (HAp), may take up a variety of metals in the course of bone formation. Uptake by the bone mineral will be a function of the affinity of a given metal for it. Significant accumulation of a metal in the mineral phase of bone can be expected to alter its characteristics. Furthermore, by studying the detailed mechanisms of metal accumulation- ionic exchange and/or deposition- one might contribute to a better understanding of the mineralisation process.

The effects of metallic elements on the stability of HAp as a bone mineral constituent have been associated with several bone pathologies. For instance, the inhibiting action of aluminium on the HAp formation has been associated to hypocalcemia and hyperphosphatemia in patients submitted to hemodialysis for long periods of time [1-4]. Also, *in vitro* results [5,6] indicate the existence of an inhibitory effect of titanium and vanadium ions on the formation of apatite.

This study aims, at contributing to the understanding of the effect that aluminium, titanium and titanium/aluminium ions may have on the degradation of HAp coatings and on HAp as a bone mineral constituent.

Materials and Methods

Commercial HAp powder pre-heated at 1000ºC was incubated in solutions containing different concentrations of aluminium, titanium and a mixture of aluminium and titanium ions. All the solutions were prepared with de-ionised water and the chemical reagents were of p.a. grade. The dissolution studies were carried out using a saline physiological solution of 0.9% NaCl to which the metal ions were added in the form of a concentrated salt solution (Titrisol Merck Standard -$TiCl_4$ in 18% HCl, $AlCl_3$ in water). A solid-to-liquid ratio of 500 mg of HAp to 50 ml of solution was used. The samples were tested in polyethylene flasks, maintained at 37ºC (± 0.2ºC) for 10 days in a warm air cabinet equipped with an orbital shaker. An agitation speed of 250 r.p.m. was used throughout the experiments. Samples with

titanium and aluminium concentrations ranging from 10 to 2000 ppm were prepared. In the experiments with the two cations, the titanium/aluminium concentration ratio was 15 (the ratio that corresponds to the Ti-6Al-4V alloy). The following concentrations were studied: 150ppmTi/10ppmAl, 180ppmTi/12ppmAl, 240ppmTi/16ppmAl, 300ppmTi/20ppmAl, 375ppmTi/25ppmAl, 450ppmTi/30ppmAl. After incubation, the solid and liquid phases were separated by centrifuging at 4500 r.p.m. and the supernatant liquid was analysed by atomic absorption spectroscopy for Ca, Ti and Al ions. The total P in the liquid phase was determined by ultraviolet spectroscopy using the molybdenum blue method. The solid samples were thoroughly washed with de-ionised water to eliminate Cl and Na ions and dried in a stove at 60ºC for 24h. The solids were then analysed using X-ray diffraction techniques, Fourier Transform Infrared (FT-IR) spectroscopy, Fourier Transform Raman (FT-Raman) spectroscopy and energy dispersive spectroscopy (EDS). X-ray diffraction was performed on a Philips PW 1710 diffractometer. When higher sensitivity was required, the Debye-Scherer X-ray diffraction technique was used. The FT-Raman and FT-IR spectra were obtained using a Perkin Elmer 2000 FT-IR/FT-Raman spectrometer. All samples were run at a spectral resolution of 4 cm^{-1}. The operating laser power for the FT-Raman analysis as well as the number of scans varied according to the sample characteristics. For the FT-IR analysis, all the samples were prepared as KBr discs. Energy dispersive spectroscopy studies were performed with a scanning electron microscope JEOL JSM-35C in conjunction with an energy dispersive spectrometer Tracor-TN 2000.

Results and Discussion

The presence of aluminium has a significant effect on the dissolution of HAp. Separate experiments with addition of HCl free of aluminium have shown that the calcium and phosphorous concentration cannot be attributed simply to pH changes. There is a linear relationship between the aluminium concentration and calcium concentration in solution (Figure 1). For the less concentrated samples ([Al] ≤500 ppm), the X-ray diffraction data revealed that the HAp structure is not significantly affected by the presence of the metal cation. For an aluminium concentration of 2000 ppm and a time of incubation of 60 days, the X-ray radiograms indicated the presence of an hydrated aluminium phosphate ($Al_{11}(PO_4)_9(OH)_6.38H_2O$) poorly crystalline.

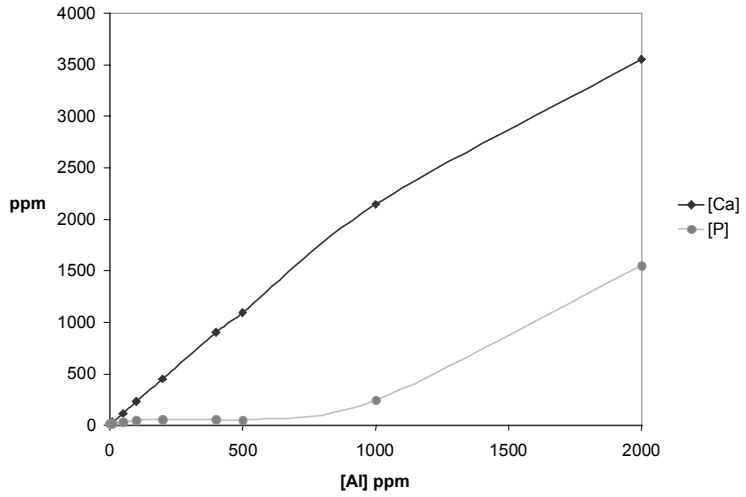

Figure1 - Influence of Al concentration on the dissolution of HAp.

In what concerns the influence of titanium concentration, it was shown in a previous work [7] that depending on the metal concentration in solution, the formation of an amorphous titanium protonated phosphate compound with a layered structure is observed. The formation of this new compound is clearly supported by FTIR spectroscopy. The presence of bands located at approximately 3420 cm^{-1} and 1636 cm^{-1} is indicative of the phosphate being hydrated.

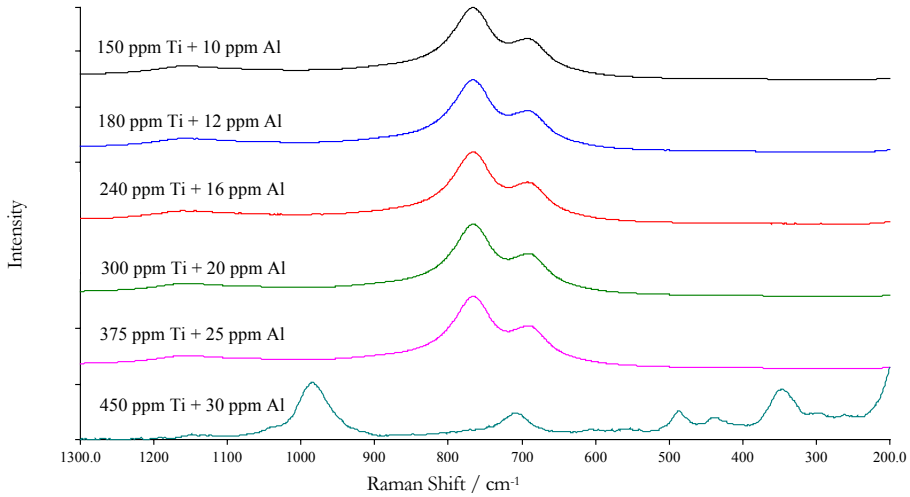

Figure2 - Overlay of FT- Raman spectra of powders obtained after 10 days' incubation of HAp in 0.9% NaCl solution with different concentrations of Ti and Al cations.

When titanium and aluminium are in solution, the FT-Raman data show that for titanium concentrations lower than or equal to 375 ppm, there are no differences between

the spectrum obtained and the one that corresponds to HAp, but for a titanium concentration of 450 ppm of Ti, new bands arise (Figure 2). The spectrum is more complex, with the appearance of bands at 984, 708, 485, 440, 347, 296 and 261 cm^{-1}. The most intense band at 984 and the band at 440 cm^{-1} can be attributed respectively to the phosphate stretching frequency ν_1 and to the bend frequency ν_2, clearly indicating the presence of a phosphate compound. There are no differences between this spectrum and the one obtained for HAp incubated in a solution with a concentration of 450 ppm of titanium in the absence of aluminium.

Nevertheless, if we observe the FT-IR spectra for the same concentrations we can see that changes in the spectrum arise for smaller concentrations in titanium and aluminium (Figure 3). For the 180ppmTi/12ppmAl concentration, bands at 3420 cm^{-1} and 1636 cm^{-1} are present. For higher titanium and aluminium concentrations, the intensity of these bands increases and the OH stretching band, in the form of a narrow peak at 3573 cm^{-1}, disappears.

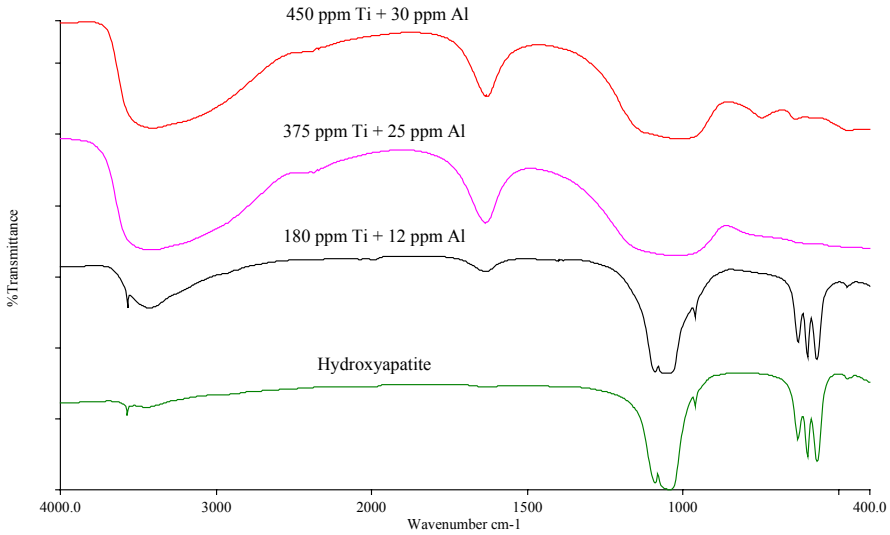

Figure 3 - Overlay of FT-IR spectra of HAp and of powders obtained after 10 days' incubation of HAp in 0.9% NaCl solution with different concentrations of Ti and Al cations.

The FT-IR spectra of the powders of HAp incubated in solutions with titanium and aluminium are practically identical to those of the powders incubated in the absence of aluminium, except for the concentration of 375ppmTi/25ppmAl. For this concentration in

metal cations, changes are observed in the FT-IR spectrum with the absence of bands located at 750, 637 and 464 cm^{-1}.

Another important observation is that when aluminium is present together with titanium in the incubation solution, the calcium concentration in the supernatant liquid is lower than when only titanium is present, although the aluminium is added in the form of an acid solution (Figure 4). This result is in agreement with the energy dispersive data for the powders of HAp incubated in the mentioned solutions (Figure 5). In these experiments, the wt% of calcium in the HAp powders incubated in solutions with aluminium is higher than the wt% of calcium in the powders incubated without aluminium.

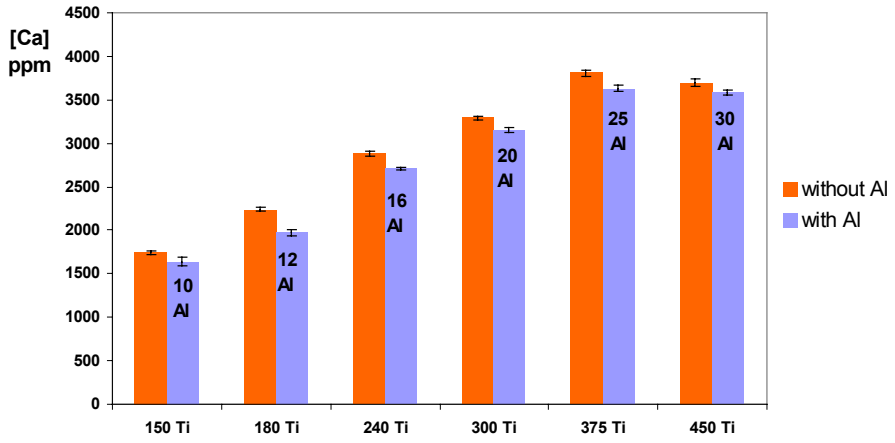

Figure 4 - Effect of the presence of Al in the Ca concentration of the supernatant liquid after incubation.

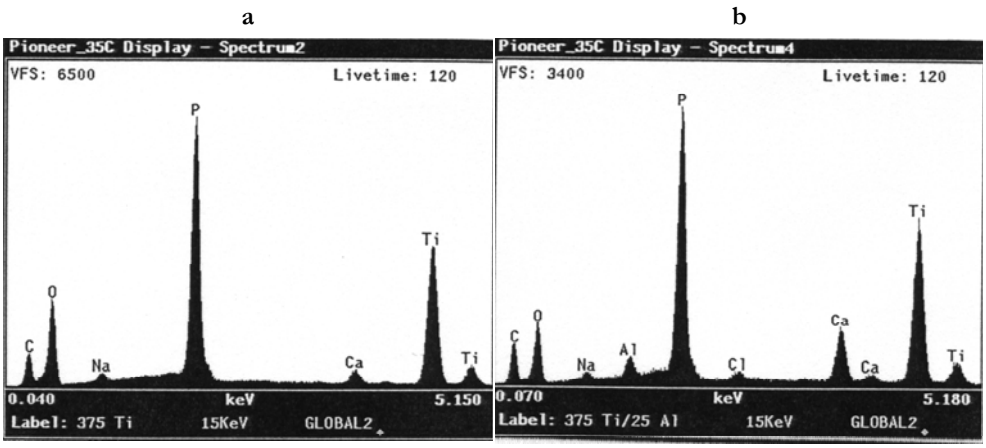

Figure 5 - Spectra from EDS of powders obtained after 10 days' incubation of HAp in: (a) 0.9% NaCl solution with a concentration of 375ppmTi; 0.9% NaCl solution with a concentration of 375ppmTi/25ppmAl.

Conclusions

The results obtained in this study suggest that for most metal ion concentrations titanium has an effect on FT-IR and FT-Raman spectra that masks any possible influence of aluminium. Nevertheless, for the concentration of 375ppmTi/25ppmAl, the formation of an hydrated phosphate compound seems to occur. It appears that this compound is different from the one formed in the presence of the same concentration of titanium and in the absence of aluminium. Also, the fact that the calcium concentration in the supernatant liquid is lower when aluminium is present suggests that aluminium and titanium jointly inhibit HAp dissolution and/or lead to formation of a calcium-containing compound. Although the results obtained may be indicative of a synergistic effect between the two cations, research on this aspect is being pursued.

Acknowledgements

The authors gratefully acknowledge Eng. Maria de Lurdes Reis from IGM for the assistance with the X-ray diffraction work.

References

[1] Andress DL, Maloney NA, Endres DB, Sherrard DJ. Aluminum-associated bone disease in chronic renal failure: high prevalence in a long-term dialysis population. J Bone Min Res 1986; 1: 391-398.

[2] Posner AS, Blumenthal NC, Boskey AL. Model of aluminum-induced osteomalacia: inhibition of apatite formation and growth. Kidney Int 1986; 29: 17-19.

[3] Christoffersen MR, Christoffersen J. The effect of aluminium on the rate of dissolution of calcium hydroxyapatite: a contribution to the understanding of aluminium- induced bone diseases. Calcif Tissue Int 1985; 37: 673-676.

[4] Christoffersen MR, Thyregod HC, Christoffersen J. Effects of aluminum(III), chromium(III), and iron(III) on the rate of dissolution of calcium hydroxyapatite crystals

in the absence and presence of chelating agent desferrixamine. Calcif Tissue Int 1987; 41: 27-30.

[5] Blumenthal NC, Cosma V. Inhibition of apatite formation by titanium and vanadium ions. J Biomed Mater Res 1989; 23: 13-22.

[6] Gerber H, Perren SM. Evaluation of tissue compatibility of in vitro cultures of embryonic bone. In: Winter GD, Leray JL, de Groot K, editors. Evaluation of Biomaterials. New York, USA: Wiley, 1980. p.307-314.

[7] Ribeiro CC, Barbosa MA, Machado AASC, Tudor A, Davies MC. Modifications in the molecular structure of hydroxyapatite induced by Ti ions. J Mat Sci: Mat in Med 1995; 6: 829-834.

Chapter 5

CALCIUM-TITANIUM-PHOSPHATE; PROPERTIES OF AN ALTERNATIVE BIOMATERIAL

Cristina C. Ribeiro[1,2,3], Cristina C. Barrias[1,2] and Mário A. Barbosa[1,2]

1 - INEB - Instituto de Engenharia Biomédica, Laboratório de Biomateriais, Rua do Campo Alegre 823, Porto 4150-180, Portugal
2 - FEUP - Faculdade de Engenharia da Universidade do Porto, Dep. de Eng. Metalúrgica e de Materiais, Porto, Portugal
3 - ISEP - Instituto Superior de Engenharia do Porto, Dep. de Física, Porto, Portugal

Abstract

The present research is aimed at characterising physically and chemically calcium titanium phosphate (CTP- $CaTi_4(PO_4)_6$), and investigating its applicability as a biomaterial for bone tissue regeneration purposes. The CTP synthesis methodology followed in this investigation enabled the preparation of a very pure ceramic phase. The material was studied using different techniques, namely X-ray diffraction (XRD), Fourier transform infrared spectroscopy (FT-IR), Fourier transform Raman (FT-Raman) spectroscopy, energy dispersive spectroscopy (EDS), X-ray photoelectron spectroscopy (XPS) and differential thermal analysis (DTA). Its granulometry and specific surface area were evaluated using laser granulometry and the Brunauer, Emmel and Teller (BET) method respectively. The solubility of CTP in Tris-HCl solution was determined as well as the zeta potential at different pHs. The capacity of the material to mineralise was also investigated. It has been observed that CTP induces the formation of an apatitic carbonate layer on its surface when immersed in a simulated body fluid (SBF). The *in vitro* biocompatibility of CTP was evaluated in culture

MG63 cells, in terms of cytoxicity and cell adhesion. It has been shown that CTP is cytocompatible and promotes adhesion of MG63 cells.

Keywords: calcium-titanium-phosphate, mineralisation, cytoxicity.

Introduction

Calcium Titanium Phosphate (CTP), $CaTi_4(PO_4)_6$, belongs to a family of compounds called NZP, the prototype of which is $NaZ_2(PO_4)_3$ compound [1, 2]. The most important property of this family of compounds is the stability and flexibility of its three dimensional skeleton in its generalised form $[A_{2n}(XO_4)_{3n}]^{m-}$, which allows the existence of several hundreds of compositions, the possibility of chemical absorption, exchange and redox reactions and intercalation processes [1]. These reactions may take place at low temperature in suspensions, at medium temperature in fused salts or at high temperature in the solid state. The skeleton $[Ti_4(PO_4)_6]^{2-}$ is build up by two chemical groups: the octahedral TiO_6 units and the tetrahedral PO_4 units that share corners only through strong bonds like Ti-O-P. The $[Ti_4(PO_4)_6]^{2-}$ groups repeat along the threefold axis and the so-formed columns connect together in a hexagonal array.

Preliminary results about the biocompatibility of Calcium-Zirconium-Phosphate (CZP), which is a compound iso-structural with Calcium-Titanium-Phosphate, were first provided by Szmukler-Moncler *et al* [3]. The *in vitro* biocompatibility of this compound was studied using L929 fibroblasts. The preliminary *in vivo* biocompatibility was assessed in dogs in osseous and non-osseous sites. The material did not indicate any adverse reaction. The extensive remodelling activity at direct contact of the CZP after 9 months of implantation indicated an excellent bioactivity.

More recently, Gross *et al* [4] investigated the biological behaviour of ceramic cylinders, the main phase of which was Calcium-Titanium-Phosphate with small amounts of calcium pyrophosphate, implanted into the distal femur epiphysis of female Chinchilla rabbits, 7, 28 and 84 days postoperatively. The tissue response of the new implant material was considered very favourable. The histological assessment indicated bone bonding to the material and therefore favourable bioactivity comparable to that of HAp. The macrophage reaction was minimal and there were no obvious signs of leaching of particle released from the material surface in soft tissue interfaces.

Calcium-Titanium-Phosphate has also interesting properties as a support for immobilisation of several enzymes. Enzymes are immobilised onto a wide range of porous supports, either particulate or membranous. Inorganic support materials are very attractive because they are usually resistant to sterilisation. Hosono *et al* [5] developed a porous glass ceramic with a skeleton of $CaTi_4(PO_4)_6$. Suzuki and co-workers [6] investigated the characteristics of this porous ceramic as an immobilising carrier for various enzymes, namely invertase, β-galactosidase, and alkalophilic proteinase. They have shown that the microporous ceramic is a more suitable material than the conventional silica glass carriers to serve as an efficient and stable enzyme reactor for long term operations.

In a previous study [7] the authors have shown that CTP can act as a carrier for the enzyme glucocerebrosidase (GCR). This enzyme is used in the treatment of Gaucher disease (type I) which is characterised by a number of severe disabling symptoms, including bone pathologies [8]. GCR is highly unstable in solution under physiological conditions [9] and consequently its immobilisation is being studied in our group as part of a strategy to overcome this problem. Although the results obtained with CTP concerning the immobilisation of this particular enzyme were very promising (CTP adsorbs a much higher amount of enzyme per unit surface area than hydroxyapatite), further aspects should be investigated in order to better characterise this material and evaluate the possibility of using it in bone tissue regeneration applications. In the present study CTP was synthesised and physically and chemically characterised using different techniques namely XRD, DTA, EDS, XPS, FT-IR and FT-Raman spectroscopies. The solubility of CTP in Tris-HCl solution was determined as well as the zeta potential at different pHs. The capacity of the material to mineralise was investigated in simulated body fluid (SBF). Cytotoxicity evaluation of CTP was performed using material extracts. Preliminary studies on cell adhesion were also conducted.

Materials and Methods

Synthesis of Calcium-Titanium-Phosphate compound

CTP was synthesised using $Ca_3(PO_4)_2$ (Merck), $NH_4H_2PO_4$ (Merck) and TiO_2 (Anatase-Goodfellow) in stoichiometric proportions. The reagents were mixed and ground with p.a. acetone and heated in air in alumina containers up to 500ºC. After that, the product obtained was ground again with acetone and heated till 1200ºC for 10h. A heating rate of 5ºC/min was used in both cycles.

Characterisation of the Calcium-Titanium- Phosphate compound

XRD analysis

X-ray powder data was obtained using a Philips diffractometer and a PW 1710 diffractometer control unit with a monochromator in the reflected beam, $CuK_{\alpha(1+2)}$ radiation with a wavelength of 1.5418 Å and a proportional detector. A Si standard sample was used for calibration of the camera and of the zero shifts of the goniometer.

FT-IR and FT-Raman analysis

FT-IR and FT-Raman spectra were obtained using a Perkin-Elmer 2000 system spectrometer. For the FT-IR analysis the samples were prepared as KBr discs whether for the FT-Raman analysis they were used in the form of a compacted powder. A spectral resolution of 4 cm^{-1} was used and two hundred scans were accumulated in order to obtain a high signal to noise level. A 200 mW laser power was used in the FT-Raman analysis.

EDS analysis

EDS studies were performed with a JEOL JSM-6301F scanning electron microscope in conjunction with an energy dispersive spectrometer Tracor-TN 2000.

XPS analysis

XPS measurements were carried out on a VG Scientific Escalab 200A spectrometer using magnesium Kα (1253.6 eV) as a radiation source. The photoelectrons were analysed with a take off angle of 55º. Survey spectra were collected over a range of 0-1150 eV with analyser pass energy of 50 eV. High-resolution spectra of C1s, O1s, P2p, Ca2p and Ti2p, were collected with an analyser pass energy of 20 eV. All the spectra were fitted using asymmetrical Gaussian-Lorentzian profiles.

DTA analysis

Differential thermal analysis (DTA-50 Shimadzu) was used to evaluate the thermal stability of the ceramic. The temperature was scanned from 20ºC to 1100ºC at a uniform heating rate of 5ºC/min using α-Al_2O_3 powder as a reference. After DTA analysis the ceramic was analysed by XRD and FT-IR spectroscopy to evaluate if any changes in the composition of the ceramic were observed.

Zeta potential measurements

The Zeta potential of CTP powders was determined at several initial pH values using a Coulter Delsa 440 instrument. The electrolyte used was a KCl (10^{-3} M) solution, where the powders were dispersed. The initial pH was adjusted using either a HCl (0.1M) or a KOH (0.1M) solution.

Granulometric analysis and evaluation of the specific surface area

Prior to the granulometric analysis and evaluation of specific surface area, the CTP powders were sieved and only the particles with a granulometry comprised between 25 and 32 μm were used. Particle size distribution was determined using a laser scanner particle size analyser (Coulter Electronics Incorporation). Specific surface area of the CTP powder was measured by gas adsorption according to the BET (Brunauer Emmel and Teller) method using a Gemini 2370 V5.00 instrument.

Dissolution tests

The dissolution tests were performed according to the International Standard ISO/FDIS 10993-14 [10]. The simulation test is based on a TRIS-HCl buffer solution of pH 7.4±0.1 that simulates the body's normal pH level. The solution was freshly prepared by dissolving 13.25 g of tris (hydroxymethyl) aminomethane in 500 ml of de-ionised water. The pH was adjusted with an appropriate amount of 1mol/l hydrochloric acid to pH 7.4±0.1 at a temperature of (37±1)ºC. The volume was then made up to 1000 ml with de-ionised water. A solid/solution ratio of 500 mg of ceramic powder (with granulometry comprised between 25 and 32 μm) to 10 ml of solution was used throughout the experiments. The samples were tested in polyethylene screw flasks, maintained for 24 and 120 h at a temperature of 37±0.2ºC in an warm air cabinet equipped with an orbital shaker. An agitation speed of 120 r.p.m. was used throughout the experiments. After incubation, the solid and liquid phases were separated by centrifuging at 4000 r.p.m., and the supernatant was filtered using a 0.2 μm sterilised filter. The liquid phase was analysed by atomic absorption spectroscopy for Ca and Ti ions. The total phosphorous in solution was determined by UV-spectroscopy using the molybdenum blue method.

In vitro mineralisation studies

Discs of CTP were obtained by sintering CTP powder with a granulometry comprised between 25 and 32 μm, at 1100ºC with a uniform heating rate of 5ºC/min and a 1h stage at the maximum temperature. The discs were immersed at 37ºC in SBF solution [11] (pH=7.4) using a material surface to solution volume ratio of c.a. 0.5 cm^{-1}. Polyethylene screw flasks were used. The SBF solution was renewed every 24 hours and kept at 4ºC between renewals. Periods of immersion in SBF ranged from 2 to 15 days. Before further examination, all materials were rinsed with de-ionised water and dried at room temperature.

Surface characterisation

Scanning Electron Microscopy (SEM) and Energy Dispersive Spectroscopy (EDS) analysis were carried out at 15 kV using a JEOL JSM-6301F scanning electron microscope.

Observations were made on sputtered carbon-coated specimens. The calcium phosphate films formed were characterised by Attenuated Total Reflectance Fourier Transform Infrared (ATR-FTIR) spectroscopy with a Perkin Elmer system 2000 FT-IR spectrometer, using the Split Pea accessory (Harrick Scientific Corporation), equipped with a silicon hemispherical crystal. All samples were run at a spectral resolution of 4 cm^{-1}. The number of scans varied according to the sample characteristics. As a control sample, a crystalline commercial hydroxyapatite was used (kindly provided by Cam Implants, Holland).

Biocompatibility testing

Cell culture

MG63 cells were obtained from the European Collection of Cell Cultures (Salisbury, UK). Cells were routinely maintained at 37ºC in a humidified atmosphere of 5% v/v CO_2 in air, in MEM Alpha Medium (α-MEM) supplemented with 10% foetal calf serum (FCS), 2.5 μg/ml fungizone and 50 μg/ml gentamicine (further referred as complete culture medium). The culture medium was renewed every 3 days. For subculture, cells were rinsed with sterile phosphate-buffered saline (PBS) and harvested with trypsin-EDTA, which was inactivated with culture medium after cell detachment. Finally, cells were centrifuged and re-suspended in fresh α-MEM complete culture medium prior to re-culture in 96-well plates.

Cytotoxicity evaluation (MTT assay)

Cytotoxicity evaluation was carried out using extracts from the materials, as follows: CTP powder was sterilised (3h, 180ºC) and incubated in serum-free culture medium (with 2.5 μg/ml fungizone and 50 μg/ml gentamicine) as the extraction vehicle, at a ratio of 0.2 g/ml as recommended by the ISO/DIS 10993-5 standards [12]. Samples were maintained at 37ºC±0.2ºC in an orbital shaker under an agitation speed of 120 rpm, for 120 h. Sterile polypropylene tubes were used as the extraction containers. An aliquot of the extraction medium was incubated under the same conditions to be assayed as a control. At the end of the exposure time, extracts were recovered, supplemented with 10% FCS and sterile-filtered (0.22 μm). Serial dilutions (50%, 10%, 1%) were prepared in fresh complete culture medium

and used immediately. Tests were performed in 96-well plates where cells were seeded at a density of 2×10^4 cells/well and incubated for 4h at 37ºC in a humidified atmosphere with 5% CO_2. After cell attachment (4h), the supernatants were discarded and replaced by the extracts and dilutions thereof. Extracted and fresh culture medium, were used as controls. For each material/dilution, 6 replicates were prepared. The cultures were incubated (37ºC, 5% v/v CO_2), for different periods of time (1, 3 and 5 days), and at the completion of each period cells viability was evaluated using the mitochondrial tetrazolium test (MTT) [13] as follows: 10 µl of 3-(4,5-dymethylthiazol-2-yl)-2,5-diphenyltetrazolium bromide solution (5 mg/ml in PBS) were added to each well, and cells were incubated (37ºC, 5% v/v CO_2) for 4h. At the end, supernatants were discarded and 100 µl of dimethylsulfoxide (DMSO) were added to dissolve the resultant formazan crystals. The intensity of the developed coloration was quantified at 540 nm and 620 nm using a plate-reader spectrophotometer (SLT Spectra).

Adhesion tests

Tests were performed on sterile (3h, 180ºC) CTP discs, prepared as previously described and pre-incubated in complete culture medium over-night. Cells were plated on the surface of the discs at a density of 2×10^4 cells/cm^2, or directly on standard tissue-culture polystyrene (TCPS) as a control. After 24h, discs were transferred to empty wells, rinsed twice in PBS, and fresh complete culture medium was added. The MTT assay was then performed as previously described to estimate the percentage of adherent cells with respect to the control.

Cell morphology was observed after 4 and 24h by SEM: samples were fixed with 1.5% v/v glutaraldehyde in 0.14M sodium cacodylate (pH 7.3), dehydrated in a graded series of ethanol (50-60-70-80-90-100% v/v), transferred gradually from ethanol to hexamethydisilazane (25-50-75-100% v/v) and air-dried. Samples were finally sputter-coated with gold and observed using a JEOL JSM-6301F scanning electron microscope.

Results

Characterisation of Calcium-Titanium-Phosphate compound

XRD analysis

Figure 1 shows the typical X-ray diffraction spectrum of calcium-titanium-phosphate powder obtained with the preparation previously described. The d(hkl) spacing and intensity values found, matched the standard values for $CaTi_4(PO_4)_6$ (file 35-740 JCPDS) indicating that the ceramic is crystalline and very pure. Several batches and granulometries were analysed in order to confirm the reproducibility of the results. Only in a few batches, the presence of TiO_2 (rutile) was observed, but in residual concentration.

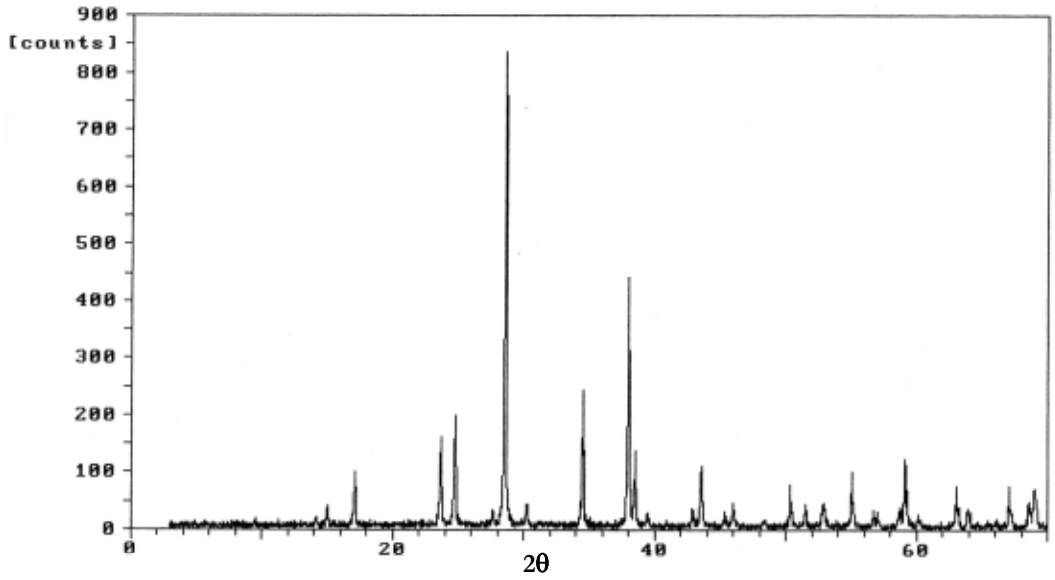

Figure 1 - X-ray diffraction pattern of CTP powder.

FT-IR and FT-Raman analysis

Figure 2 a) and b) show respectively the FT-IR and FT-Raman spectrum of CTP.

The vibrational spectra of CTP compound reflect its characteristic structure of a $[Ti_4(PO_4)_6]^{2-}$ skeleton build up by octahedral TiO_6 units and tetrahedral PO_4 units that share corners only through strong bonds like Ti-O-P [1].

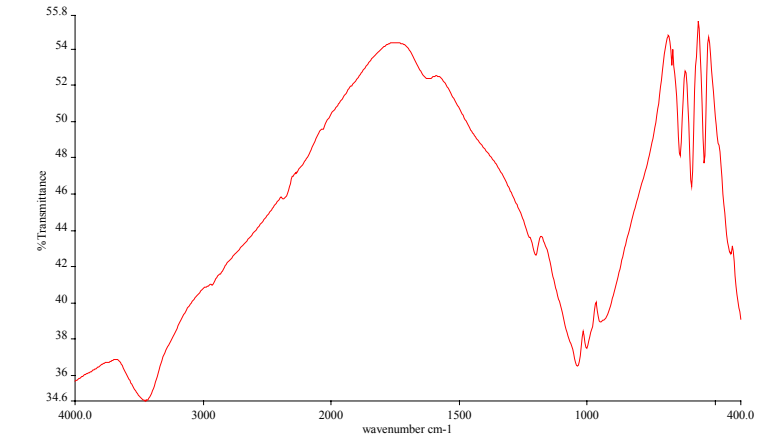

a)

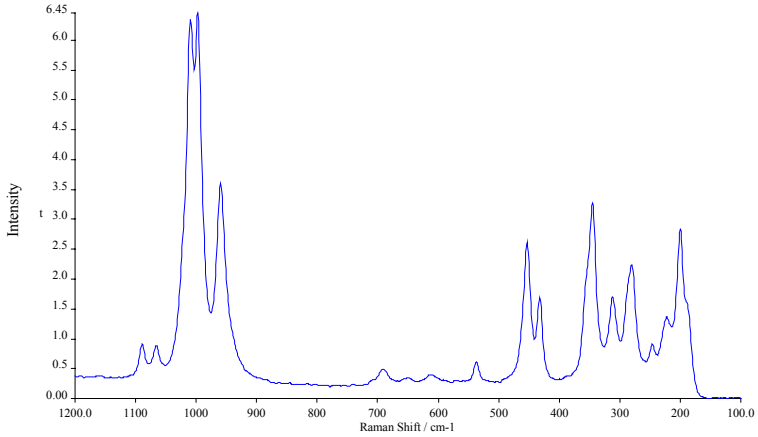

b)

Figure 2 - FT-IR spectrum (a) and FT-Raman (b) of CTP powder

The FT-IR spectrum shows two main areas of absorption in the 400-4000 cm^{-1} range corresponding to the P-O bond, one at 560-660 cm^{-1} (antisymmetric bending of PO_4 units) and another at 950-1200 cm^{-1} (symmetric and antisymmetric stretching of PO_4 units). It is suggested in some vibrational spectroscopy studies concerning glasses and crystals belonging to the Nasicon family, that the band at 1200 cm^{-1} corresponds to pyrophosphate $[P_2O_7]^{4-}$ groups. Although this observation does not seem to be consistent with the chemistry of these compounds, according to Rao *et al* [14] the presence of $[P_2O_7]^{4-}$ groups is possible if there are facile chemical and structural disproportionations of phosphate anions occurring in them. Since in the spectrum of CTP no other bands characteristic of pyrophosphate group are assigned, it is reasonable to assume that the 1200 cm^{-1} band corresponds to the P-O antisymmetric stretching vibration of PO_4 group, common to several other phosphates [15].

The particularly strong infrared absorption at 545 cm^{-1} may be taken as an indication of octahedrally co-ordinated Ti [14]. The band at 640 cm^{-1} is also possibly due to a vibrational mode involving Ti-O bond [15]. The band at 445 cm^{-1} is assigned to the symmetric bending modes of the PO_4 tetrahedra. The two broad bands at 1620 and 3453 cm^{-1} are characteristic of adsorbed water in the ceramic.

In what concerns the FT-Raman spectrum, the bands observed in the high-energy region (959-1089 cm^{-1}) are due to the isolated phosphate groups. They are assigned to symmetric and antisymmetric stretching vibrations ν_1 and ν_3 and are the strongest in CTP compound. The bands observed in the interval 344 and 600 cm^{-1} are due to O-P-O deformation (ν_2 and ν_4 PO_4 modes) and Ti-O vibration [16]. The bands at 312 cm^{-1} and below are possibly attributed to lattice vibrations [16, 17].

EDS analysis

The $\frac{Ti}{Ca}$, $\frac{Ti}{P}$ and $\frac{Ti}{O}$ atomic ratios obtained by EDS (Table I) were the ones expected according to the stoichiometry of the compound, confirming its purity.

Table I - EDS atomic ratios for CTP.

Atomic Ratio	$\frac{Ti}{Ca}$	$\frac{Ti}{P}$	$\frac{Ti}{O}$
Theoretical Values	4.00	0.67	0.17
Experimental Values	4.05 ± 0.12	0.64 ± 0.03	0.16 ± 0.02

XPS analysis

Prior to the XPS analysis, CTP powders were pressed into very thin pellets in order to obtain more homogeneous surfaces. The XPS survey scans of CTP showed the presence of carbon due to the adventitious deposition of hydrocarbon contaminants from the atmosphere. This peak does not affect the interpretation of the results and was actually used for binding energy calibration, by setting its binding energy to 285.0 eV to correct for sample

charging. XPS core levels of the P2p, Ca2p, Ti2p and O1s orbitals were examined. High-resolution XPS scans were curve-fitted and the peak area intensities of the core levels were normalised to their respective atomic sensitive factors. The precision of the binding measurements was ±0.2 eV.

Table II - XPS binding energies (eV).

Sample	*P2p*	*Ca2p$_{1/2}$*	*Ca2p$_{3/2}$*	*O1s*	*Ti2p$_{1/2}$*	*Ti2p$_{3/2}$*
CTP	133.4	347.7	351.3	531.2	459.5	465.4

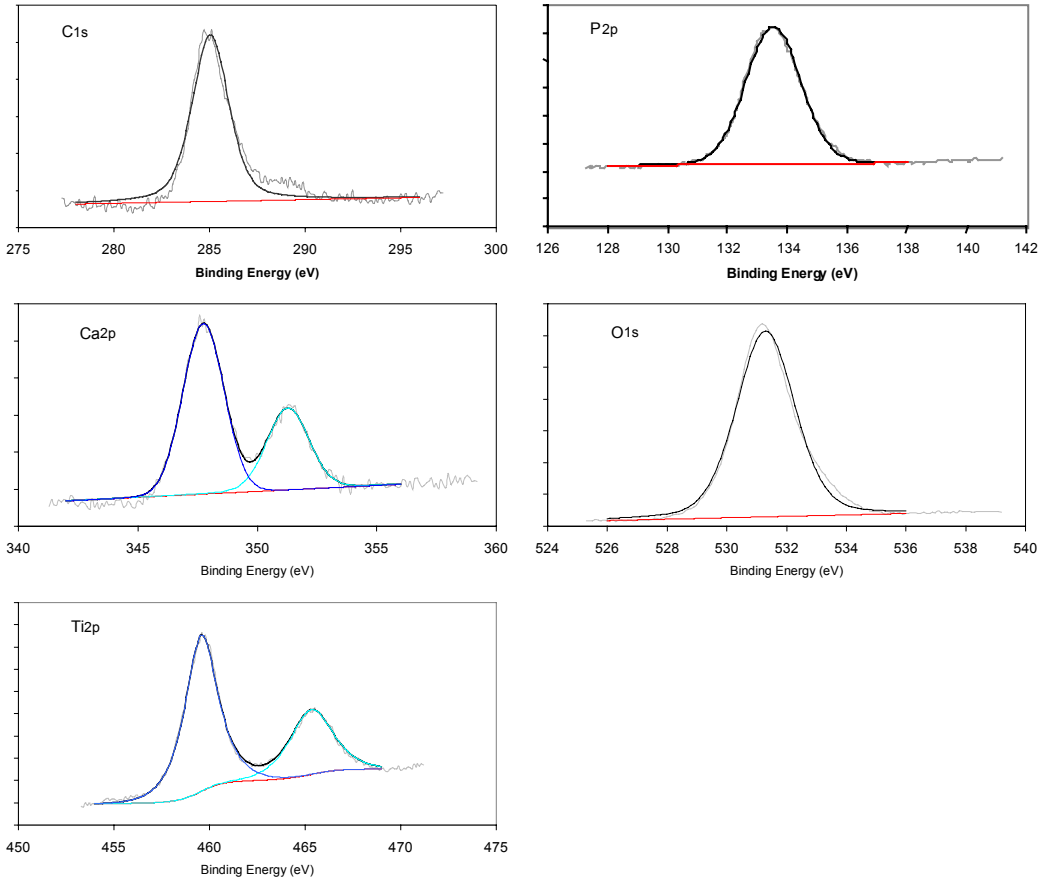

Figure 3 - XPS C1s, P2p, Ca2p, O1s and Ti2p high-resolution spectra of CTP surface.

The binding energies determined for the main components of the samples are presented in Table II. The high resolution Ti2p spectrum (Figure 3) identified the presence

of two major peaks at 459.5 and 465.4 eV that are attributed to $Ti^{4+}2p_{3/2}$ and $Ti^{4+}2p_{1/2}$ respectively. The deconvolution of the $Ca2p_{3/2}$ revealed the presence of calcium in the Ca^{2+} form. Comparing the P2p peak positions to published spectra of different phosphate compounds [18-22] it is observed that PO_4^{3-} containing species have similar peak positions. The CTP showed a clear O1s peak at 531.2 eV, which agreed well with the P-O bond of PO_4 groups. The PO_4 tetrahedra in CTP are nearly regular which implies that the P-O distances are comparable to those in usual phosphates [23]. The same position of O1s peak is observed for instance for hydroxyapatite [18, 19]. The fact that high-resolution O1s spectra delineated a symmetrical peak suggests that all oxygens are chemically equivalent and that no more than one oxygen specie was present on the surface.

DTA analysis

No endo or exothermic reactions were observed in the thermogram of CTP powder (Figure 4) indicating that the compound does not undergo any transformation within the temperature range used in the analysis. This observation is supported by the XRD and FT-IR results, which showed that after DTA analysis no changes in the ceramic phase were observed.

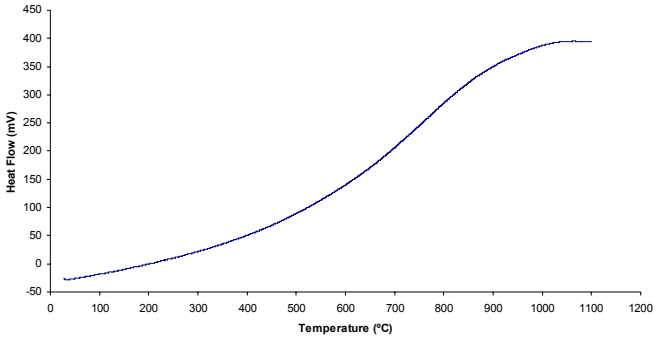

Figure 4 - DTA thermogram of CTP powder.

Zeta potential measurements

Zeta potential measurements of CTP powder as a function of pH are presented in Figure 5. The isoelectric point of CTP occurs at approximately pH=3. As a consequence, at physiological pH, CTP is negatively charged.

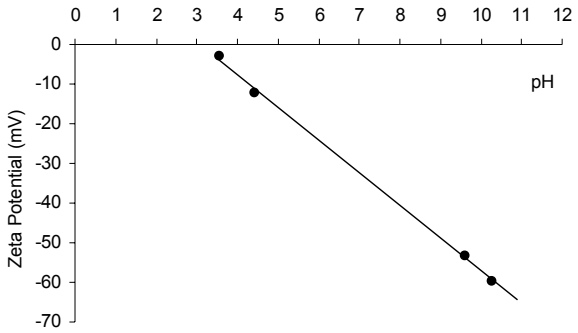

Figure 5 - Zeta potential of CTP as a function of pH.

Granulometric analysis and evaluation of the specific surface area

The results of the granulometric analysis of CTP powders are presented in Table III. Results showed that 90% (in volume) of the particles are smaller than 25.32 μm and have a volume average diameter of 11.00 μm. The specific surface area obtained using the BET method was 9.84 cm^2/mg.

Table III - Volume percentage particle size distribution.

%<	10	25	50	75	90
Size (μm)	0.343	2.428	8.608	17.92	25.24

Dissolution tests

After 24h of incubation of CTP in Tris/HCl no calcium, phosphorous or titanium ions could be found in solution in concentrations higher than 1 ppm. For a time of incubation of 120 h, the concentration of Ca in the supernatant was 44.6 ppm ($90.7x10^{-6}$ mg Ca/cm^2 CTP) and the concentration of P was of 18.5 ppm ($37.5x10^{-6}$ mg P/cm^2 CTP). The concentration of Ti was less than 1.1 ppm, which is the sensitivity of the method used for the determination. It is observed that CTP dissolution is not stoichiometric, as more calcium goes into the solution than phosphorous. The dissolution behaviour of CTP can be explained in terms of the different role of the two structural parts of the compound: the skeleton, $[Ti_4(PO_4)_6]^{2-}$, held together by strong covalent bonds, and the counter ions (Ca^{2+}) held in the

structure by weaker bonds [1]. Due to the nature of calcium chemical bonds, Ca^{2+} can leave the crystal lattice of CTP more easily than the other ions in the structure.

In vitro mineralisation studies

Surface characterisation

EDS analysis

EDS analysis of CTP after immersion for 15 days in SBF showed an increase of the peak intensity of Ca and a decrease in the peak of Ti, when compared to the EDS spectrum of the original material (Figure 6). These results support the possibility of formation of a calcium phosphate on the surface of CTP. As EDS is a bulk technique, the Ca, P and Ti from the substrate are also accounted for in the analysis. The Ca/P ratio of the calcium phosphate film formed after 15 days of immersion was 1.58. This value was calculated assuming that Ti exists only in the substrate and using its atomic percentage as a reference to estimate the contribution of the substrate to the total Ca and P concentration. The Ca/P ratio of the film increased with time of incubation (1.33 for 6 days), indicating the presence of a precursor phase in the formation of the calcium phosphate film. Although EDS is only a semi-quantitative technique, the Ca/P ratios obtained suggest an apatitic nature for the calcium phosphate formed. Sodium, magnesium and chloride are probably contaminants from the solution, although samples were rinsed in deionised water after immersion. It is also possible that the ions are incorporated in the film formed, but this aspect was not considered central in the present investigation.

Figure 7 shows SEM micrographs of the calcium phosphates formed over the surface of sintered CTP pellets, after immersion in SBF for 15 days. After 48 hours of incubation, aggregates of calcium phosphate particles are observed dispersed on the surface of the pellets. For a time of immersion of 6 days, a calcium phosphate film is covering the all surface of the ceramic, becoming thicker after 15 days of immersion (Figures 7 a), b), c) and d)).

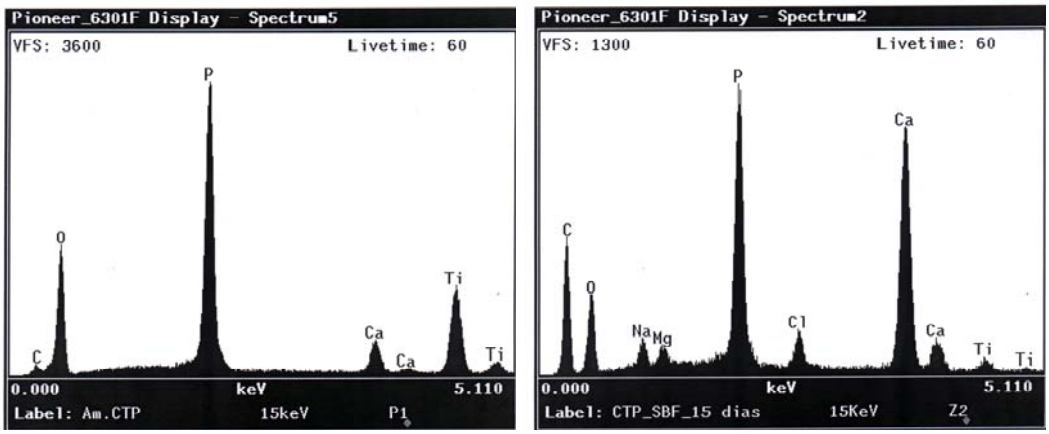

a) b)

Figure 6 - EDS spectra of a) CTP and b) CTP after immersion in SBF for 15 days.

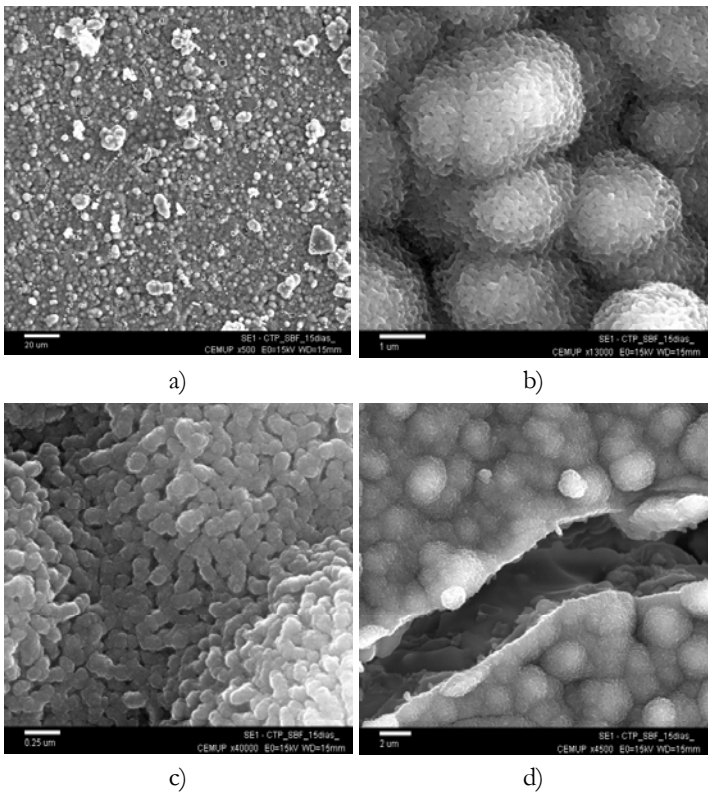

a) b)

c) d)

Figure 7 - SEM micrographs of the calcium phosphate film formed on CTP after immersion in SBF for 15 days: a) calcium-phosphate film covering the all surface, b) characteristic spherullites formed, c) detail of the microstructure of the spherullites, d) detail of disrupted film showing its thickness.

FT-IR (ATR) analysis

In order to further characterise the calcium phosphate film formed after immersion in SBF, FT-IR (ATR) analysis was performed. Figure 8 shows the spectrum of CTP after immersion in SBF for 6 and 15 days, as well as the spectrum of a commercial hydroxyapatite used as a reference. Since CTP FT-IR spectrum has some bands due to the vibration of PO_4^{3-} group that are common to the hydroxyapatite spectrum, analysis of the data will be focused on the new bands that arise after immersion of CTP in SBF. In the ν_4PO_4 region a new band at 561 cm^{-1} is observed after 48h of immersion and its intensity significantly increases after 15 days. This band corresponds to the triply degenerated bending mode ν_4, of the O-P-O bonds of the phosphate group [24-26]. Significant changes are also observed in the $\nu_3PO_4^{3-}$ (900-1200 cm^{-1}) region of the spectrum of CTP after immersion in SBF. CTP presents four bands in this region namely at 951, 1003, 1039 and 1200 cm^{-1}. After immersion, a very intense band at 1023 cm^{-1} is observed together with two other much less intense bands at 952 (ν_1 symmetric stretching vibration of phosphate group) and 1200 cm^{-1}. The band at 1023 cm^{-1} can be assigned to the $\nu_3PO_4^{3-}$ vibration from nonstoichiometric apatites [27, 28] but can also be attributed to the presence of OCP [28, 29]. A weak band at 488 cm^{-1} corresponding to the ν_2 bending vibration of PO_4^{3-} groups arises after immersion (small shoulder in CTP spectrum). Furthermore, peaks at 872, 1416 and 1450 cm^{-1} could also be observed, which can be attributed to the ν_2CO_3 vibration of carbonate groups, usually found in carbonated and biological apatites [30-34]. Carbonated apatite yields the ν_3 vibrations of C-O in the high-energy region between 1410 and 1470 cm^{-1} and ν_2 vibrations in the low-energy region between 850 and 890 cm^{-1}. The peak position of the carbonate ν_2 mode depends upon whether the CO_3^{2-} ion substitutes for OH^- (type A band) or PO_4^{3-} (type B band) in the HAp lattice [33, 34]. The 872 cm^{-1} band indicates the presence of type B carbonate apatite [32, 34]. LeGeros *et al* [30] presented experimental evidence that in apatites precipitated from aqueous solutions, carbonate substitutes some phosphate groups.

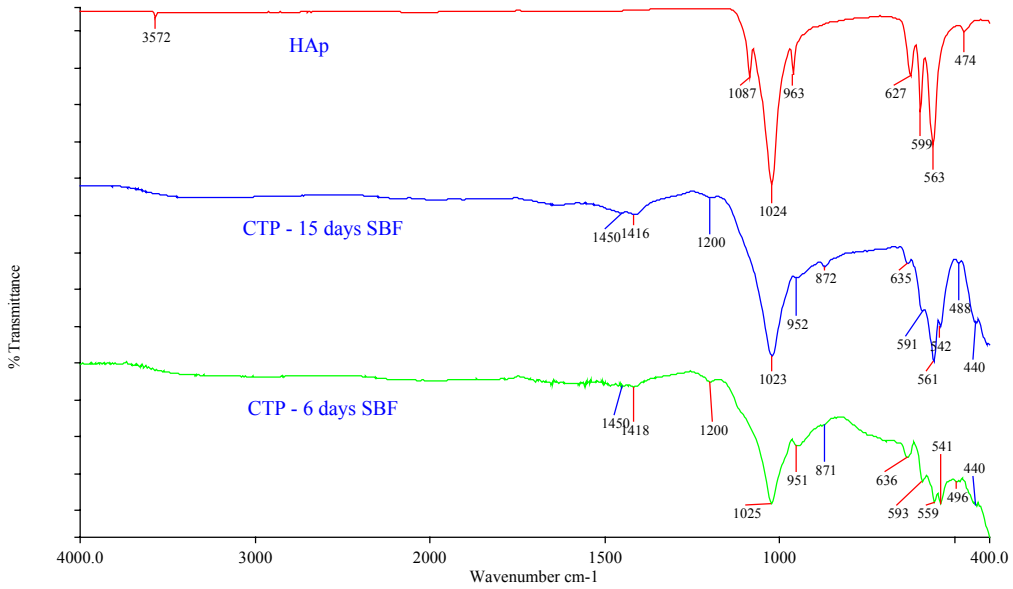

Figure 8 - FT-IR spectra of calcium phosphate film formed on CTP surface after immersion in SBF for 6 and 15 days.

Crystalline hydroxyapatite generates two characteristic OH bands at c.a. 3570 cm^{-1} (OH stretching mode) and 630 cm^{-1} (librational mode). A band at 635 cm^{-1} appears in the spectrum of immersed CTP that could be attributed to the OH librational mode. However, since its intensity decreases as the time of incubation increases, it is more likely that this band arises from the substrate (corresponds to the 638 cm^{-1} intense band characteristic of CTP). The OH stretching vibration is unique for crystalline hydroxyapatite and its intensity is considerably weaker compared to the strong P-O stretching vibration because of the hydroxyapatite stoichiometry. This band is absent in the FT-IR spectrum of CTP after immersion in SBF suggesting that the apatitic film formed is not completely crystalline. However, it should be noticed that when using a reflectance accessory (split pea), the bands at high wavenumber become less intense. The depth of penetration of the infrared radiation is dependent on wavenumber, decreasing as wavenumber increases [35]. Thus, low wavenumber light penetrates further into a sample than high wavenumber light. As a result, ATR spectra show peaks that are more intense at low wavenumber than at high wavenumber. Some authors attribute the missing OH modes to a perturbation of hydroxyl stretching and bending modes on the apatite surface by the hydrogen bonding of water molecules to the surface OH ions [36].

During the immersion period in SBF there were changes of absorption in the ν_1, ν_3 and ν_4PO_4 regions with time, indicating the evolution of the structure of the film formed to a structure similar to HAp. The doublets found in the ν_4PO_4 region indicate that the precursor of the calcium phosphate formed was octacalcium phosphate (OCP) and not amorphous calcium phosphate (ACP) [17, 37-39]. When HAp is formed from ACP these bands are broad singlets, whereas in the case of OCP band splitting usually occurs, indicating that minerals formed were poorly crystalline but not amorphous. ATR-FTIR results suggest that the calcium phosphates formed have an apatitic nature, similar to HAp [17, 28, 37, 38, 40-44].

Biocompatibility testing

Cytotoxicity evaluation (MTT assay)

The results shown in Figure 9 represent the viability of MG63 cells, exposed to extracts of CTP powders for 1, 3 and 5 days, which was assessed using the MTT assay. The results obtained using extracted culture medium (negative control) are also depicted. Changes in absorbance are related to changes in cell number, which enables cell proliferation to be estimated. Both control and extract-treated cells were able to proliferate along the 5 days in culture, and none of the CTP extracts induced significant changes in cell viability nor inhibit cell growth.

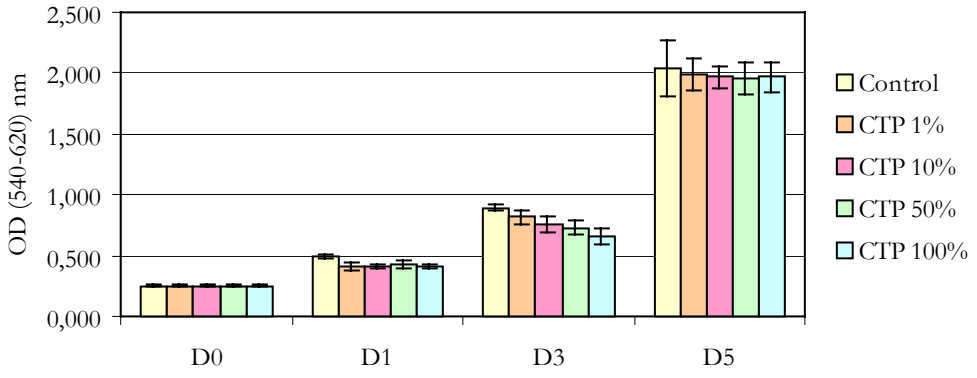

Figure 9 - Viability of MG63 cells exposed for 1, 3, and 5 days to CTP powder extracts or dilutions thereof, as determined by the MTT assay.

Adhesion tests

The percentage of adherent cells on the materials surface, with respect to those on the TCPS (control), was estimated 24h after seeding using the MTT assay. Approximately 60% of the cells were able to adhere to the CTP discs. The fact that this percentage was not extremely high could be related to the experimental conditions used. The adhesion tests were performed on sintered pellets the size of which was adequate to fit into the well but did not completely cover it. As a result, it was difficult to guarantee that no cells migrated to the bottom of the well when plating the cells on the surface of the discs.

SEM analysis of the samples revealed that seeded cells were able to attach and spread on the surface of CTP discs (Figure 10). After 4h (Figure 10 a) and b)), adherent cells exhibit a typical round morphology with the cytoplasm extending away from the central body and adhering to the adjacent surface. After 24h (Figure 10 c) and d)), cells are well spread exhibiting a flattened morphology with filopodial-like extensions adapted to the surface, and some of them are well conformed to the interstices of the surface.

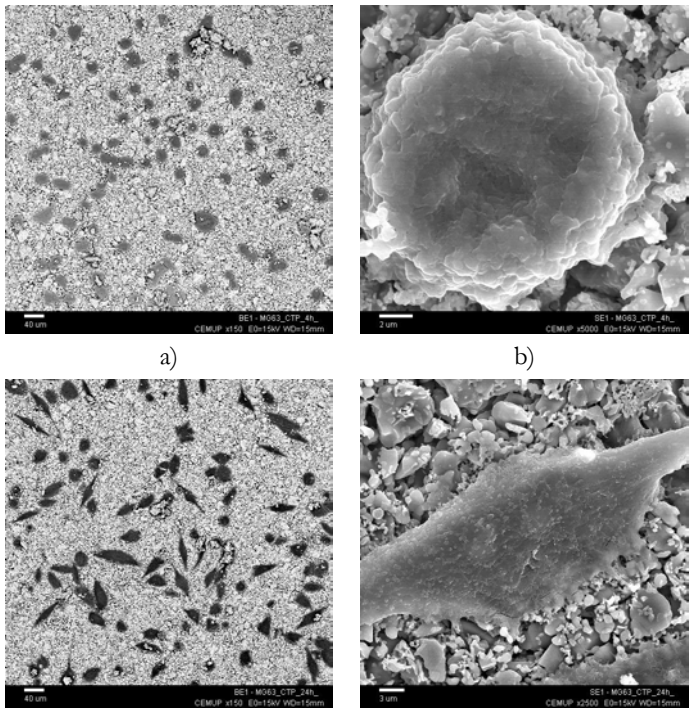

a) b)

c) d)

Figure 10 - SEM micrographs of the adhesion of MG63 cells after 4 hours (***a***) and (***b***) and 24 hours (***c***) and (***d***) on CTP. (***a***) and (***c***) are backscattered electron images.

Discussion

Calcium phosphate materials are widely used for biomedical applications, namely bone defect filling, bone replacement and reconstruction, as drug carriers and coatings of metal prostheses. The aim of the present study was to synthesise and characterise calcium titanium phosphate, a material that could act as an alternative to traditional calcium phosphates for some particular situations. For instance, in a previous work [7] the authors have shown that CTP could act as a carrier for glucocerebrosidase (GCR), an enzyme used in the treatment of Gaucher disease (type I). Gaucher disease is characterised by a number of disabling symptoms including bone pathologies [8]. Concerning the GCR loading capabilities of the ceramic, results showed that CTP adsorbs a much higher amount of enzyme per unit surface area than HAp [7].

Several requirements should be fulfilled by a material used in bone regeneration. For instance, it is generally accepted that the existence of a calcium phosphate on the surface of an implant can improve bone bonding. The results obtained in this study show that CTP mineralises when immersed in SBF. The surface negative charge of CTP at pH=7.4, as indicated by zeta potential measurements, certainly favours the nucleation of apatite, since several studies have shown that negatively charged surfaces are always favourable for the heterogeneous nucleation of apatite in a simulated body fluid [45, 46] whereas nucleation is inhibited on positive surfaces. This is a consequence of the fact that the accumulation of Ca^{2+} ions, due to the electrostatic attraction, increases the supersaturation near negative surfaces the initial nucleation being therefore preferentially triggered. The results of CTP dissolution tests indicated that Ca goes into solution more easily than PO_4 or Ti ions possibly contributing to a local surface saturation in Ca, favouring calcium phosphate film formation.

The detailed chemical composition and microstructure of freshly deposited bone mineral crystals is a subject that still remains controversial, with different theories being proposed to explain how bone mineral is formed and how its chemical composition changes with maturation [47-52]. This is a complex issue not only because of the numerous solid phases that may be involved but also because of the presence of multiple components in the solution media. A key question is whether the formation of the mineral phase of bone results

from the continuous transformation of a poorly crystalline calcium phosphate into a crystalline hydroxyapatite or if a precursor mineral phase such as octacalcium phosphate (OCP), amorphous calcium phosphate (ACP) or dicalcium phosphate dihydrate (DCPD) exists. The FT-IR analysis of the calcium phosphate formed on CTP, as a result of the *in vitro* mineralisation tests, suggests the existence of a precursor phase, possibly OCP, for the formation of the apatitic phase. The apatite structure that is formed is carbonated. It is generally believed that the formation of biologically active bone-like apatite containing carbonate on the implant surface is an important condition for obtaining direct, strong chemical bonding between the implant to living bone [53, 54].

A preliminary study on the effect of calcium-titanium-phosphate on bone cells behaviour was carried out using the human osteosarcoma cell line MG63. MG63 cells were used, since they express a number of features characteristics of relatively immature osteoblasts, and are a well-characterised model for examining the early stages of osteoblasts differentiation [55]. The ability of a material to cause toxic effects at the cellular level, is the first aspect to be taken in consideration when performing *in vitro* testing. In a typical cytotoxicity evaluation, cells are exposed to the materials or their extracts, and the presence and extent of an eventual cytotoxic effect is evaluated [56]. The toxic response may be measured through changes in cell survival or metabolism, and the percentage of cells which have died or undergone regressive phenomena after being exposed to the material, can be detected and quantified providing an indication about the cytotoxic potential of the material under study [56]. The cytotoxicity of CTP towards osteoblast-like MG63 cells was evaluated by analysing the effect of extracts obtained from CTP powders on cell viability/proliferation using the MTT assay. This assay is based in the reduction of the yellow tetrazolium salt 3-(4,5-dymethylthiazol-2-yl)-2,5-diphenyltetrazolium bromide to purple formazan crystals. The intracellular deposits will only appear in viable cells that still express the activity of succinnic dehydrogenase, a mitochondrial enzyme that catalyses the reaction. The intensity of the coloration obtained after dissolving the purple crystals in a suitable solvent will thus be proportional to the number of viable cells in the sample, and inversely proportional to the toxicity of the extract. Changes in absorbance are thereby directly related to changes in cell number, enabling cell proliferation to be estimated. Results from the cytotoxicity tests show

that CTP extracts did not induce significant toxic effects, since they did not reduce cell viability nor inhibit cell proliferation, when compared to the control.

The biocompatibility of implant materials towards anchorage-dependent cells is also closely related to cell behaviour in contact with them. The early events of cells-materials interactions that include attachment, adhesion and spreading are of crucial importance, as they will ultimately influence the capacity of cells to proliferate and differentiate [57, 58]. Results from the adhesion tests show MG63 cells were able to adhere and spread to CTP. The surface charge of CTP may also have a strong effect on cell adhesion. Several works show that ceramics with more negative surface charges appeared to result in surface structures with better characteristics for cell growth and differentiation [59, 60]. Nishizawa *et al* [60] showed that the affinity and adhesiveness of the cells to calcium-phosphate ceramics modified chemically by means of various silane-coupling agents were found to be dominantly regulated by the surface potential. A negative potential was effective in increasing the adhesiveness, even though living cells have negative charges. A possible explanation for this fact may be the difference in the selectivity of serum protein adsorption, or a difference in the adsorption of Mg^{2+} or Ca^{2+}, which is reported to be effective in accelerating cell adhesiveness [61].

Conclusions

The synthesis methodology followed in this investigation enabled the preparation of a very pure ceramic phase. It has been demonstrated that a carbonated apatite film was formed on the surface of CTP, indicating its ability to mineralise. The cell culture tests indicated that CTP is not cytotoxic and promotes MG63 cell adhesion. These results, together with those reported in a previously published paper [7], confirm that the properties of CTP are worth further research in its applicability in orthopaedic surgery.

Acknowledgements

The authors gratefully acknowledge Doctor Carlos Sá (CEMUP) for the assistance in the XPS investigation and Dr. Daniela Silva (CEMUP) for the assistance in the SEM studies.

References

[1] Alamo J. Chemistry and properties of solids with NZP skeleton. Solid State Ionics 1993; 63-65: 547-561.

[2] Roy R, Agrawal DK, Alamo J, Roy RA. [CTP]: A new structural family of near-zero expansion ceramics. Mat Res Bull 1984; 19: 471-477.

[3] Szmukler-Moncler S, Daculsi G, Delécrin J, Passuti N, Deudon C. Calcium-Metallic-Phosphates: a new coating biomaterial? In: Doherty PJ *et al*, editors. Biomaterial-Tissue Interfaces. Advances in Biomaterials, vol.10. Elsevier Science Publishers BV; 1992. p.377-383.

[4] Gross U, Muller Mai C, Voigt C, Mesgaran M, Berger G, Ploska U. Tissue response in the femur of rabbits after implantation of a new calcium titanium phosphate composition. Key Eng Mat 2001; 192-195: 383-386.

[5] Hosono H, Abe Y. Porous glass-ceramics composed of a titanium phosphate crystal skeleton: a review. J Non-Cryst Solids 1995; 190: 185-197.

[6] Suzuki T, Toriyama M, Hosono H, Abe Y. Application of a microporous glass-ceramic with a skeleton of $CaTi_4(PO_4)_6$ to carriers for immobilization of enzymes. J Ferment Bioeng 1991; 72: 384-391.

[7] Ribeiro CC, Barrias CC, Barbosa MA. Calcium phosphate-alginate microspheres as enzyme delivery matrices. Biomaterials 2004; 25: 4363-4373.

[8] Grabowski GA, Leslie N, Wenstrup R. Enzyme therapy for Gaucher disease: the first 5 years. Blood Rev 1998; 12: 115-133.

[9] Xu YH, Ponce E, Sun Y, Leonova T, Bove K, Witte D, Grabowski GA. Turnover and distribution of intravenously administered mannose-terminated human acid beta glucosidase in murine and human tissues. Pediatr Res 1996; 39: 313-322.

[10] Biological evaluation of medical devices - Part 14: Identification and quantification of degradation products from ceramics, ISO/FDIS 10993-14 : 2001(E). International Organisation of Standardisation, 2001.

[11] Kokubo T, Kushitani H., Sakka S, Kitsugi T, Yamamuro T. Solutions able to reproduce *in vitro* surface structure changes in bioactive glass-ceramic A-W. J Biomed Mater Res 1990; 24, 721-734.

[12] Biological evaluation of medical devices – Part 5: Tests for cytotoxicity: *in vitro* methods, ISO/DIS 10993-5 (EN 30993-5). International Organisation of Standardisation, Geneva, 1991.

[13] Mosmann T. Rapid colorimetric assay for cellular growth and survival: application to proliferation and cytotoxicity assays. J Immunol Methods 1983; 65: 55-63.

[14] Rao KJ, Sobha KC, Kumar S. Infrared and Raman spectroscopic studies of glasses with Nasicon-type chemistry. Proc Indian Acad Sci (Chem Sci) 2001; 113: 497-514.

[15] Ross SD. Phosphates and other Oxy-anions of group V. In: Farmer VC, editor. The infrared spectra of minerals. London, Great Britain: Adlard & Sons Ltd, 1974. p.383-422.

[16] EL Jazouli A, Krimi S, Manoun B, Chaminade JP, Gravereau P, De Waal D. Preparation and structural characterization of two new titanium phosphates $NaCa_{0.5}Ti(PO_4)_3$ and $Ni_{0.5}TiOPO_4$. Ann Chim Sci Mat 1998; 23: 7-10.

[17] Elliot JC. In: Elliot JC, editor. Structure and chemistry of the apatites and other calcium orthophosphates. Amsterdam, Holland: Elsevier, 1994.

[18] Chusuei CC, Goodman DW, Van Stipdonk MJ, Justes DR, Schweikert EA. Calcium phosphate phase identification using XPS and time-of-flight cluster SIMS. Anal Chem 1999; 71: 149-153.

[19] Santos JD, Jha LJ, Monteiro FJ. *In vitro* calcium phosphate formation on SiO_2-Na_2O-CaO-P_2O_5 glass reinforced hydroxyapatite composite: a study by XPS analysis. J Mater Sci: Mater Med 1996, 7: 181-185.

[20] Hanawa T, Ota M. Calcium phosphate naturally formed on titanium in electrolyte solution. Biomaterials 1991; 12: 767-772.

[21] Combes C, Rey C, Freche M. XPS and IR study of dihydrate nucleation on titanium surfaces. Col Surf B: Bioint 1998; 11: 15-27.

[22] Ferraz MP, Monteiro FJ, Santos JD. $CaO-P_2O_5$ glass hydroxyapatite double layer plasma sprayed coating: *in vitro* bioactivity evaluation. J Biomed Mater Res 1999, 45; 376-383.

[23] Nagai M. Three-dimensional network phosphates. In: Kanazawa T, editor. Inorganic Phosphate Materials. Tokyo, Japan: Kodansha, 1989. p.165-197.

[24] Fowler BO. Infrared studies of apatites I. Vibrational assignements for calcium, strontium and barium hydroxyapatites utilizing isotopic substitution. Inorg Chem 1974; 13: 194-207.

[25] Klee WE, Engel G. Infrared spectra of the phosphate ions in various apatites. J Inorg Nucl Chem 1970; 32: 1837-1843.

[26] Joris SJ, Amberg CH. Nature of deficiency in nonstoichiometric hydroxyapatites II Spectroscopic studies of calcium and strontium hydroxyapatites. J Phys Chem 1971; 75: 3172-3178.

[27] Gadaleta SJ, Paschalis EP, Betts F, Mendelsohn R, Boskey AL. Fourier transform infrared spectroscopy of the solution-mediated conversion of amorphous calcium phosphate to hydroxyapatite: new correlations between X-ray diffraction and infrared data. Calcif Tissue Int 1996; 58: 9-16.

[28] Rey C, Shimizu M, Collins B, Glimcher MJ (1991) Resolution Enhanced Fourier Transform Infrared Spectroscopy study of the environment of phosphate ion in the early deposits of a solid phase calcium phosphate in bone and enamel and their evolution with age: 2. Investigations in the ν_3PO_4 domain. Calcif Tissue Int. 49: 383-388.

[29] Fowler BO, Moreno EC, Brown WE. Infra-red spectra of hydroxyapatite, octacalcium phosphate and pyrolised calcium phosphate. Arch Oral Biol 1966; 11: 477-492.

[30] LeGeros RZ, Trautz OR, LeGeros JP, Klein E. Carbonate substitution in the apatite structure (1). Extrait du bulletin de la societé chimique de France 1968; special number: 1712-1718.

[31] Rehman I, Bonfield W. Characterization of hydroxyapatite and carbonated apatite by photo acustic FTIR spectroscopy. J Mater Sci: Mater Med 1997; 8: 1-4.

[32] Morgan H, Wilson RM, Elliot JC, Dowker SEP, Anderson P. Preparation and characterisation of monoclinic hydroxyapatite and its precipitated carbonate apatite intermediate. Biomaterials 2000; 21: 617-627.

[33] Bonel G, Montel G. Sur une nouvelle apatite carbonatée synthétique. Compt Rend 1964; 258: 923-926.

[34] Rey C, Collins B, Gohel T, Dickson RI, Glimcher MJ. The carbonate environment in bone mineral. A resolution enhanced Fourier transform infrared spectroscopy study. Calc Tissue Int 1989; 45: 157-164.

[35] Smith BC. In Smith BC, editor. Fundamentals of Fourier Transform Infrared Spectroscopy. CRC press, 1996. p.119-120.

[36] Blumenthal NC, Posner AS. Hydroxyapatite: mechanism of formation and properties. Calcif Tissue Int 1973; 13: 235-238.

[37] Sauer GR, Wuthier RE. Fourier transform infrared characterization of mineral phases formed during induction of mineralisation by collagenase-released matrix vesicles *in vitro*. J Biol Chem 1988; 263: 13718-13724.

[38] Rey C, Shimizu M, Collins B, Glimcher MJ. Resolution enhanced Fourier transform infrared spectroscopy study of the environment of phosphate ion in the early deposits of a solid phase calcium phosphate in bone and enamel and their evolution with age: investigations in the $\nu_4 PO_4^{3-}$ domain. Calcif Tissue Int 1990; 46: 384-394.

[39] Nancollas GH. *In vitro* studies of calcium phosphate crystallization. In: Mann S, Webb J, Williams RJP, editors. Biomineralisation. Chemical and Biochemical Perspectives. Weinheim, Germany: VCH, 1989. p.157-188.

[40] Li P, Ohtsuki T, Kokubo T, Nakanishi K, Soga N, Nakamura T, Yamamuro T. Process of formation of bone-like apatite layer on silica gel. J Mater Sci: Mater Med 1993; 4: 127-131.

[41] Tanahashi M, Hata K, Kokubo T, Minoda M, Miyamuto T, Nakamura T, Yamamuro T. Effect of substrate on apatite formation by a biomimetic process. In: Yamamuro T,

Kokubo T, Nakamura T, editors. Bioceramics, Vol. 5, Kyoto, Japan: Kobunshi-Kankokai, 1992. p.57-64.

[42] Rhee S-H, Tanaka J. Effect of citric acid on the nuclation of hydroxyapatite in a simulated body fluid. Biomaterials 1999; 20: 2155-2160.

[43] Radin SR, Ducheyne P. The effect of calcium phosphate ceramic composition and structure on *in vitro* behavior- II Precipitation. J Biomed Mater Res 1993; 27: 35-45.

[44] Hanawa T, Ota M. Calcium phosphate naturally formed on titanium in electrolyte solution. Biomaterials 1991; 12: 767-774.

[45] Calvert P, Mann S. The negative side of crystal growth. Nature 1997; 386: 127-128.

[46] Li P, Kangasniemi I, de Groot K, Kokubo T. Bonelike hydroxyapatite induction by a gel-derived titania on a titanium substrate. J Am Ceram Soc 1994; 77: 1307-1312.

[47] Wu Y, Glimcher MJ, Rey C, Ackerman JL. A unique protonated phosphate group in bone mineral not present in synthetic calcium phosphates- identification by phosphorous-31 solid state NMR spectroscopy. J Mol Biol 1994; 244: 423-435.

[48] Termine JD, Posner AS. Amorphous/crystalline interrelationships in bone mineral. Calcif Tissue Res 1967; 1: 8-23.

[49] Eanes ED, Termine JD, Posner AS. Amorphous calcium phosphate in skeletal tissues. Clin Orthoped 1967; 53: 223-235.

[50] Siew C, Gruninger SE, Chow LC, Brown WE. Procedure for the study of acidic calcium and phosphate precursor phases in enamel mineral formation. Calcif Tissue Int 1992; 50: 144-148.

[51] Brown WE, Smith JP, Lehr JR, Frasier AW. Crystallographic and chemical relations between octacalcium phosphate and hydroxyapatite. Nature 1962; 196: 1050-1055.

[52] Termine JD, Posner AS. Infrared analysis of rat bone: age dependency of amorphous and crystalline mineral fractions. Science 1966; 153: 1523-1525.

[53] Yubao L, Klein CPAT, Xingdong Z, de Groot K. Formation of a bone like apatite layer on the surface of porous hydroxyapatite ceramics. Biomaterials 1994; 15: 835-841.

[54] LeGeros RZ, Orly I, Gregoire M, Daculsi G. Substrate surface dissolution and interfacial biological mineralization. In: Davies JE, editor. The bone biomaterial interface. Toronto, Canada: University of Toronto Press; 1991. p.76-88.

[55] Ciapetti G, Cenni E, Pratelli L, Pizzoferrato A. *In vitro* evaluation of cell/biomaterial interaction by MTT assay. Biomaterials 1993; 14: 359-364.

[56] Pizzoferrato A, Ciapetti G, Stea S, Cenni E, Arciola CR, Granchi D, Savarino L. Cell culture methods for testing biocompatibility - review paper. Clin Mater 1994; 15: 173-190.

[57] Anselme K. Osteoblast adhesion on biomaterials - review. Biomaterials 2000; 21: 667-681.

[58] Hunter A, Ascher CW, Walker PS, Blunn GW. Attachment and proliferation of osteoblasts and fibroblasts on biomaterials for orthopaedic use. Biomaterials 1995; 16: 287-295.

[59] Suzuki T, Toriyama M, Kawamoto Y, Yokogawa Y, Kawamura S. The adhesiveness and growth of anchorage-dependent animal cells on biocompatible ceramic culture carriers. J Ferm Bioeng 1991; 72: 450-456.

[60] Nishizawa K, Toriyama M, Suzuki T, Kawamoto Y, Yokogawa Y, Nagae H. Effects of the surface wettability and zeta potential of bioceramics on the adhesiveness of anchorage-dependent animal cells. J Ferm Bioeng 1993; 75: 435-437.

[61] Takeichi M, Okada ST. Roles of magnesium and calcium ions in cell-to-substrate adhesion. Exp Cell Res 1972; 74: 51-60.

Chapter 6

CALCIUM PHOSPHATE-ALGINATE MICROSPHERES AS ENZYME DELIVERY MATRICES

Cristina C. Ribeiro[1,2,3], Cristina C. Barrias[1,2] and Mário A. Barbosa[1,2]

1 - INEB - Instituto de Engenharia Biomédica, Laboratório de Biomateriais, Rua do Campo Alegre 823, Porto 4150-180, Portugal
2 - FEUP - Faculdade de Engenharia da Universidade do Porto, Dep. de Eng. Metalúrgica e de Materiais, Porto, Portugal
3 - ISEP - Instituto Superior de Engenharia do Porto, Dep. de Física, Porto, Portugal

Abstract

The present study concerns the preparation and initial characterisation of novel calcium titanium phosphate-alginate (CTP-alginate) and hydroxyapatite-alginate (HAp-alginate) microspheres, which are intended to be used as enzyme delivery matrices and bone regeneration templates. Microspheres were prepared using different concentrations of polymer solution (1% and 3% w/v) and different ceramic-to-polymer solution ratios (0.1, 0.2 and 0.4 w/w). Ceramic powders were characterised using X-ray diffraction, laser granulometry, Brunauer, Emmel and Teller (BET) method for the determination of surface area, zeta potential and Fourier transform infrared spectroscopy (FT-IR). Alginate was characterised using high performance size exclusion chromatography. The methodology followed in this investigation enabled the preparation of homogeneous microspheres with a uniform size. Studies on the immobilisation and release of the therapeutic enzyme glucocerebrosidase, employed in the treatment of Gaucher disease, were also performed. The enzyme was incorporated into the ceramic-alginate matrix before gel formation in two different ways: pre-adsorbed onto the ceramic particles or dispersed in the polymeric matrix.

The two strategies resulted in distinct release profiles. Slow release was obtained after adsorption of the enzyme to the ceramic powders, prior to preparation of the microspheres. An initial fast release was achieved when the enzyme and the ceramic particles were dispersed in the alginate solution before producing the microspheres. The latter profile is very similar to that of alginate microspheres. The different patterns of enzyme release increase the range of possible applications of the system investigated in this work.

Keywords: microspheres, enzyme-delivery, alginate, hydroxyapatite, calcium titanium phosphate.

Introduction

Osseous tumours, trauma and other debilitating diseases can create a need to fill defects in the skeleton. Most bone tissue engineering strategies rely on the use of temporary scaffolds that can be seeded with cells prior to implantation, or designed to induce the formation of bone from the surrounding tissue after implantation [1, 2]. The effectiveness of such materials can be highly improved if they can simultaneously act as drug delivery systems. Depending on the specificity of the illness, bioactive agents (e.g. growth factors or other protein-drugs) can be locally released and potentially accelerate the process of bone regeneration.

In the past few years, increasing efforts have been devoted to the development of improved injectable materials aimed at providing an alternative for the filling of bone defects with less patient discomfort, as they can be applied through minimally invasive surgical procedures. Most injectable materials described in the literature consist of pastes, gels or liquid precursors that solidify *in situ* in response to some stimulus [3]. Micro- or nano-particles have also been described, but they must be suspended in either autologous blood or other appropriate vehicle prior to injection.

A variety of injectable materials, both ceramic- and polymer-based, have been developed for use in multiple orthopaedic applications [4-20]. The combination of ceramic particles with polymeric matrices has also been extensively investigated, in an attempt to mimic bone tissue, which may itself be seen as a complex composite material made of organic and inorganic components. Different ceramic phases have been used, hydroxyapatite and tricalcium phosphate being the most common [4-9], as well as several polymeric matrices, both from synthetic [10-14] or natural origin, the latter including collagen, chitosan, gelatine and alginate, among others [15-20].

This investigation describes the preparation and initial characterisation of novel calcium titanium phosphate-alginate (CTP-alginate) and hydroxyapatite-alginate (HAp-alginate) microspheres intended to be used as injectable enzyme delivery matrices and bone filling materials.

CTP is a bioactive ceramic currently under investigation in our laboratory [21]. Its properties, namely the capacity of ion exchange and chemical adsorption [22], and the ability to act as an immobilisation matrix for several enzymes [23], suggest that it can successfully be used in the biomedical field. Furthermore, recent *in vivo* studies showed direct bone contact of implanted cylinders containing calcium titanium phosphate as the main phase [24]. HAp, which has long been recognised for its bioactivity and osteoconductive properties and has been extensively tested as matrix in drug delivery applications [25, 26], was also used in the present investigation.

Alginate was chosen as the polymeric vehicle due to its useful properties and versatility. Ultra-pure grade alginates are considered biocompatible and biodegradable and have been widely used in many biomedical applications, not only as vehicles for biologically active molecules [27] or cells, but also as scaffolds for tissue engineering, either as porous structures [28] or modified with RGD-containing peptide sequences [29]. Sodium alginate and most other alginates from monovalent metals are soluble in water, forming solutions of considerable viscosity. Due to their suitable rheological properties, alginates have long been used in the pharmaceutical industry as thickening or gelling agents, as colloidal stabilisers and as blood expanders [30].

CTP-alginate and HAp-alginate microspheres were prepared using the droplet extrusion method. The ceramic granules were mixed with alginate enabling the preparation of spherical particles through instantaneous crosslinking in the presence of Ca^{2+} [30]. Compared to other methods of preparation of ceramic-polymer microspheres [31-33], this process presents the advantage of being simple and of being carried out at room temperature and in the absence of organic solvents, which makes it suitable for enzyme entrapment purposes. Moreover, the spherical particles can be easily recovered, without the need for fastidious washing processes, and present a regular size distribution even without subsequent fractionation by sieving.

Analysis of the ability of these matrices to act as carriers for the enzyme glucocerebrosidase (GCR) was also undertaken. This enzyme is used in the treatment of Gaucher disease (type I), which is characterised by a number of severe disabling symptoms,

including bone pathologies [34]. GCR is highly unstable in solution under physiological conditions [35]. Its immobilisation is currently under investigation in our group to overcome this problem.

Materials and Methods

Materials

Calcium titanium phosphate (CTP) was synthesised by solid state reaction as described elsewhere [21]. Commercial hydroxyapatite (HAp) powder (CAM Implants) pre-heated at 1000ºC was used as a reference. Pharmaceutical-grade sodium alginate (Protanal 10/60 LS) with a high α-L-guluronic acid content (65-75%, as specified by the manufacturer) was kindly donated by Pronova Biopolymers and used without further purification. Na-alginate solutions were prepared fresh as needed, using bi-distilled deionised water. Purified recombinant human glucocerebrosidase (GCR) was purchased from Genzyme Corporation as a lyophilised powder. $Na^{125}I$ and Sephadex columns were purchased from Amersham Pharmacia Biotech. Additional chemicals were purchased from Sigma.

Characterisation of CTP and HAp powders: X-ray diffraction, specific surface area, granulometry and zeta potential determination

The ceramic powders were analysed by X-ray diffraction (XRD, Philips PW 1710 diffractometer) and their specific surface area was measured by gas adsorption according to the Brunauer, Emmel and Teller (BET) method. Granulometric analysis was performed using a laser scanner particle size analyser (Coulter Electronics Incorporation). Zeta potential (ZP) of CTP and HAp powders was measured with a Coulter Delsa 440 instrument. ZP was calculated automatically by the instrument based on the Smoluchowski formula:

$$\zeta = 4\pi \frac{\mu\eta}{E}$$

where ζ is the ZP (mV), μ the electrophoretic mobility (μmcm/Vs), η the viscosity of the fluid, and E the dielectric constant of the fluid. The principle of electrophoresis is that a

particle will move in a liquid under the influence of an applied electric field provided its ZP is different from zero. The electrophoretic mobility is proportional to the ZP as shown in the equation above.

The ZP of CTP and HAp powders were determined at several pH values. The powders were dispersed in 10 mM KCl and the pH was adjusted with 0.1M HCl and 0.1M KOH.

Characterisation of alginate by HP-SEC

High performance size exclusion chromatography (HP-SEC) was performed at room temperature using a modular system, composed of an isocratic pump (K-1001 Knaeur), a vacuum degasser (K-5002 Knaeur), a viscometer/right angle laser light scattering (RALLS) dual detector (T60 Viscotek), and a refractive index detector (K-5002 Knaeur) operating at the same wavelength as the RALLS detector (670 nm). Separations were performed in a set of PL aquagel-OH mixed columns. The mobile phase consisted of 0.1M $NaNO_3$ with 0.02% w/v NaN_3 and the flow-rate was maintained at 1.0 ml/min. Samples were dissolved in the mobile phase, filtered and injected through a manual injection valve equipped with a 116 μl loop.

Preparation of CTP-alginate and HAp-alginate microspheres

CTP or HAp powders were dispersed in a pre-filtered (0.8 μm) Na-alginate solution under gentle stirring until a homogeneous paste was obtained. Different concentrations of the polymer solution (1% and 3% w/v), and different ceramic-to-polymer solution ratios (0.1, 0.2 and 0.4 w/w) were tested. These will be designated as 10/1, 20/1, 40/1 (ceramic-to-polymer solution ratios, using the 1% w/v Na-alginate solution) and 10/3, 20/3, 40/3 (ceramic-to-polymer solution ratios, using the 3% w/v Na-alginate solution). The pastes were extruded drop-wise into a 0.1 M $CaCl_2$ crosslinking solution, where spherical-shaped particles instantaneously formed and were allowed to harden for 30 min. The size was controlled by regulating the extrusion flow rate using a syringe pump (Cole-Parmer), and by applying a coaxial air stream (Encapsulation Unit Var J1– Nisco). At completion of the gelling period the microspheres were recovered and rinsed in water in order to remove the excess $CaCl_2$.

Finally, they were dried overnight in a vacuum oven at 30ºC. The diameter of the microspheres was measured using an inverted plate microscope (Olympus) equipped with an ocular micrometer with an accuracy of 10 μm.

Characterisation of CTP-alginate and HAp-alginate microspheres: SEM and FT-IR analysis

Morphological characterisation of the microspheres (surface and transversal sections obtained by criofracture in liquid nitrogen) was carried out using scanning electron microscopy (SEM). Samples were sputter coated with gold using a JEOL JFC-100 fine coat ion sputter device, and observed using a JEOL JSM-6301F scanning microscope.

Physical chemical characterisation of the microspheres and their components (CTP, HAp and Ca-alginate) were analysed by Fourier transform infrared spectroscopy (FT-IR) using a Perkin Elmer system 2000 spectrometer. The FT-IR spectrum of Na-alginate was also obtained and used as a reference. Microspheres were reduced to powder and were analysed as KBr pellets.

Enzyme immobilisation in CTP-alginate and HAp-alginate microspheres

The enzyme was incorporated into the ceramic-alginate microspheres (formulation 20/3) before gel formation in two different ways: pre-adsorbed onto the ceramic particles before mixing with the alginate solution, or dispersed in the polymeric-ceramic paste. Microspheres were subsequently prepared as previously described, without drying. In Figure 1 a schematic representation of the matrices tested is presented. The matrices A and B were used as controls.

Pre-adsorption of the enzyme onto CTP and HAp powders

A solution containing glucocerebrosidase (GCR) was obtained by dissolving the enzyme in phosphate buffered saline (PBS, pH 7.4) at a final concentration of 0.2 mg/ml and in the presence of 0.5 mg/ml of bovine serum albumin (BSA) as a stabiliser. The solution also contained radiolabeled (^{125}I) enzyme (Iodogen method) as a tracer and 0.01 M NaI to

competitively reduce binding by any free ^{125}I species present. The specific radioactivity of the solution was 6.5×10^7 cpm/mg GCR.

For the adsorption tests, CTP and HAp powders (50 mg) were incubated with 500 μl of the enzyme solution. Samples were maintained at 4ºC in an orbital shaker at 250 rpm. At predefined time intervals, samples were centrifuged (14,000 rpm, 5 min) and the supernatants collected for analysis. The powders were washed twice with PBS and separated by centrifugation. The powders and all the supernatants were counted for radioactivity. The counts of each sample were averaged and the surface concentration was calculated by the equation:

$$GCR(ng/cm^2) = \frac{Counts(cpm)}{A_{solution}(cpm/ng)\times SA(cm^2)}$$

where the Counts represent the radioactivity of the powders, the $A_{solution}$ is the specific activity of the protein solution and SA is the surface area of the powders, which was calculated as described previously.

Enzyme release studies

Enzyme release studies were performed in PBS. Samples (n=3) were maintained at 37±0.2ºC in an orbital shaker at 120 rpm. At predefined time intervals, the supernatants were collected and counted for radioactivity and fresh PBS was added. In the case of the powder matrices (Figure 1, matrix A) samples were centrifuged (14,000 rpm, 5 min) prior to collecting the supernatants. At the end, the matrices were recovered, washed twice with PBS and counted for residual radioactivity.

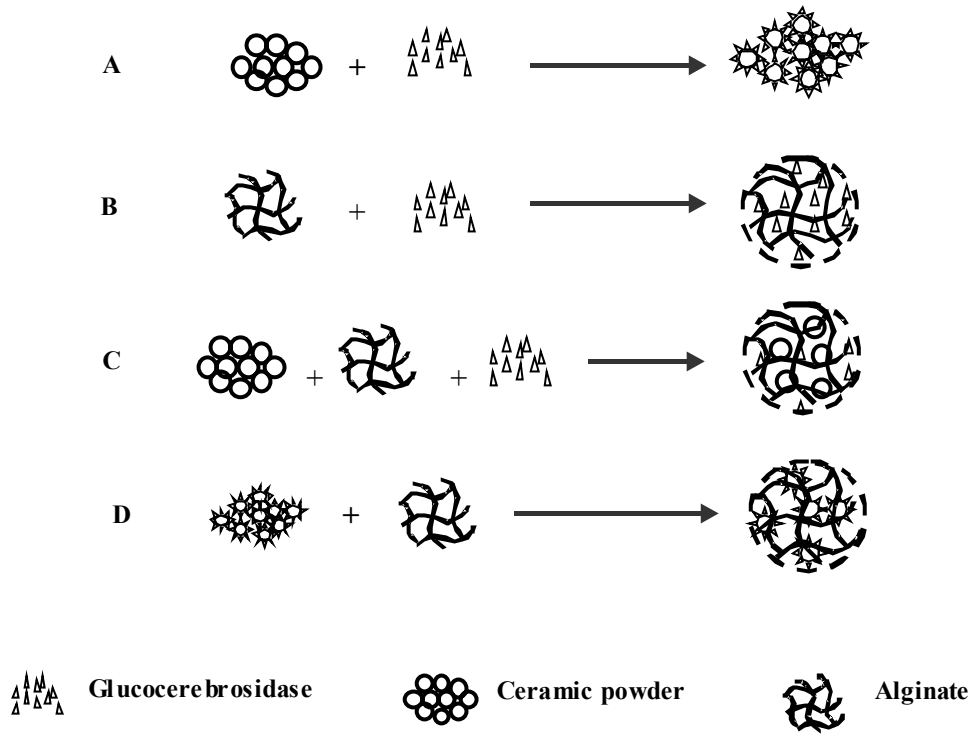

Figure 1 - Different enzyme immobilisation matrices tested: (A) enzyme adsorbed onto the ceramic powders, (B) enzyme dispersed in a pure alginate matrix, (C) enzyme and ceramic powders individually dispersed in the alginate matrix and (D) ceramic powders with pre-adsorbed enzyme dispersed in the alginate matrix. The matrices A and B were used as controls.

Results

Characterisation of CTP and HAp powders

X-ray diffraction and specific surface area

X-ray diffraction analysis of the ceramics indicated the presence of mono phase crystalline compounds. The specific surface areas obtained using the BET method were 9.84 cm^2/mg for the CTP powder and 76.00 cm^2/mg for the HAp.

Granulometric analysis

The granulometric analysis of HAp and CTP powders is presented in Figures 2a and 2b, respectively. The particle size distribution curves of both ceramics are narrow. In the case of the CTP powder 90% (in volume) of the particles are smaller than 25.32 μm and have a

volume average diameter of 11.00 μm. In the HAp powder 90% of the particles are smaller than 20.51 μm and the volume average diameter is 7.96 μm.

a)

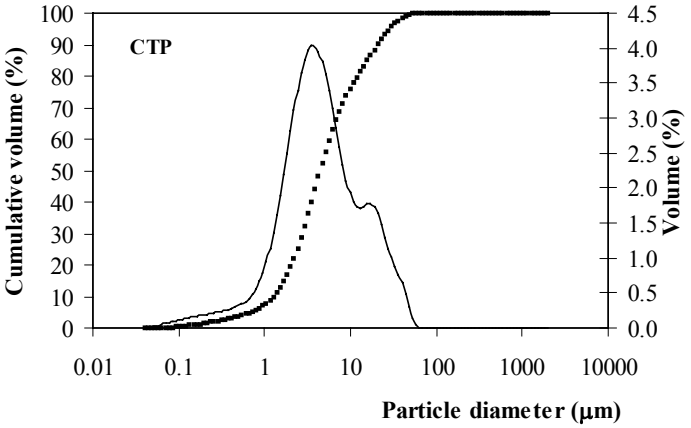

b)

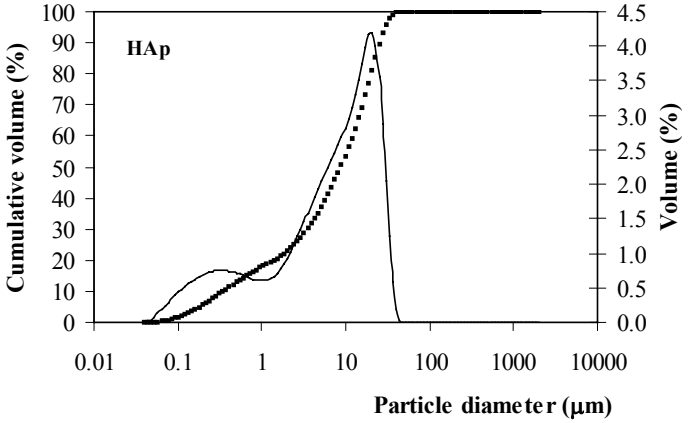

Figure 2 - Granulometric analysis of (a) CTP and (b) HAp powders. Cumulative (dashed line) and non-cumulative (solid line) volume percentage particle size distributions are plotted on the left and right axis, respectively.

Zeta potential measurements

ZP measurements of CTP and HAp powders as a function of pH are presented in Figure 3. As can be observed, the isoelectric point of CTP occurs approximately at pH 3 whereas the isoelectric point of HAp occurs approximately at pH 6. To the best of our

knowledge, the isoelectric point of CTP has not been reported in the literature before. As far as the HAp is concerned, the results obtained are in agreement with those reported by other authors [36, 37]. At physiological pH both ceramics are negatively charged, the CTP potential being more negative than that of HAp.

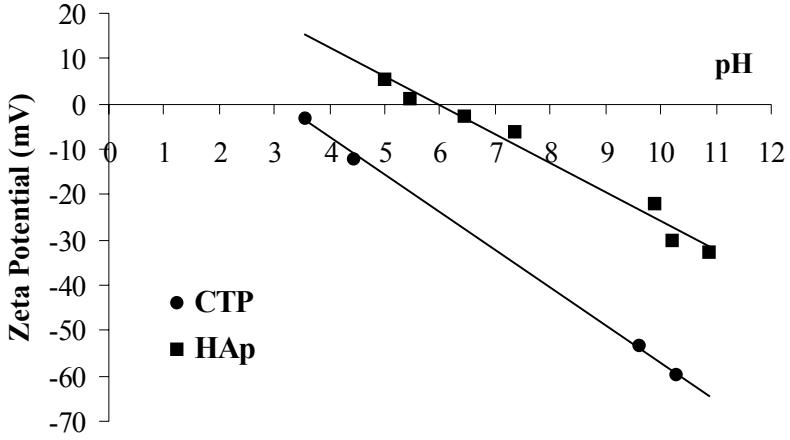

Figure 3 - Zeta Potential of CTP and HAp powders as a function of pH.

Characterisation of alginate by HP-SEC

The Na-alginate used in this study was characterised by an average molecular weight (Mw) of 1.3×10^5, a polidispersity index of 1.9 and an intrinsic viscosity of 6.4 dl/g, as determined by HP-SEC.

Characterisation of CTP-alginate and HAp-alginate microspheres

CTP-alginate and HAp-alginate microspheres were prepared using different concentrations of the polymer solution (1% and 3% w/v), and different ceramic-to-polymer solution ratios (0.1, 0.2 and 0.4 w/w). As soon as the ceramic-polymer droplets contacted with the crosslinking solution, spherical-shaped particles were instantaneously formed when using the 3% w/v alginate solution. An exception was observed for the HAp-alginate 40/3 paste, which was too viscous to be extruded in a reproducible manner. Particles obtained using the 1% w/v alginate solution presented a disc-shaped morphology and for that reason were not used in the subsequent experiments.

The diameters of the microspheres obtained (before and after drying) using the 3% w/v polymer solution and the different ceramic-to-polymer ratios are presented in Figure 4. Before drying, microspheres of approximately 1000 μm were obtained when using pure alginate, CTP with alginate, and HAp with alginate. Upon drying, microspheres have undergone a volume contraction, which was more significant for the lower ceramic-to-polymer solution ratio (0.1 w/w). Microspheres with diameters of 541±32, 606±21, and 796±39 μm were obtained for the CTP 10/3, 20/3 and 40/3 formulations, respectively. When using HAp, microspheres with diameters of 512±44 μm and 749±22 μm were obtained for the 10/3 and 20/3 formulations.

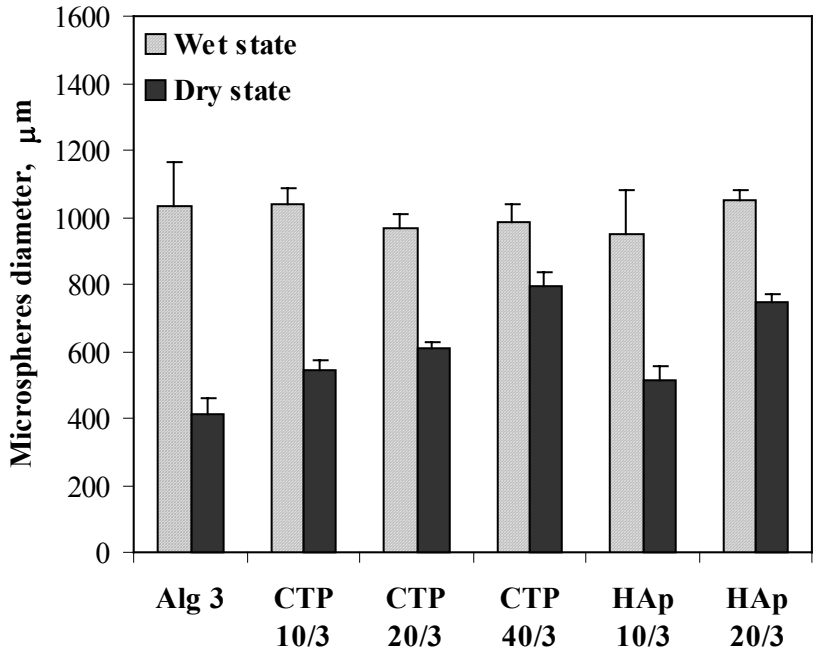

Figure 4 - Diameters of alginate, CTP-alginate and HAp-alginate microspheres prepared using the 3% w/v alginate solution, before (wet state) and after drying (dry state).

SEM analysis

SEM images of the microspheres (20/3 formulations) are presented in Figures 5 and 6. Upon drying, and contrary to alginate microspheres that shrank to a great extent and even collapsed (Figure 5a), CTP-alginate (Figure 5b) and HAp-alginate (Figure 5c) microspheres maintained their original shape, with no evidence of cracks. This suggests that both fillers

provided additional control of shrinkage and avoided structural collapse. Different surface roughnesses were obtained, those of the HAp-alginate microspheres being smoother than those of CTP-alginate.

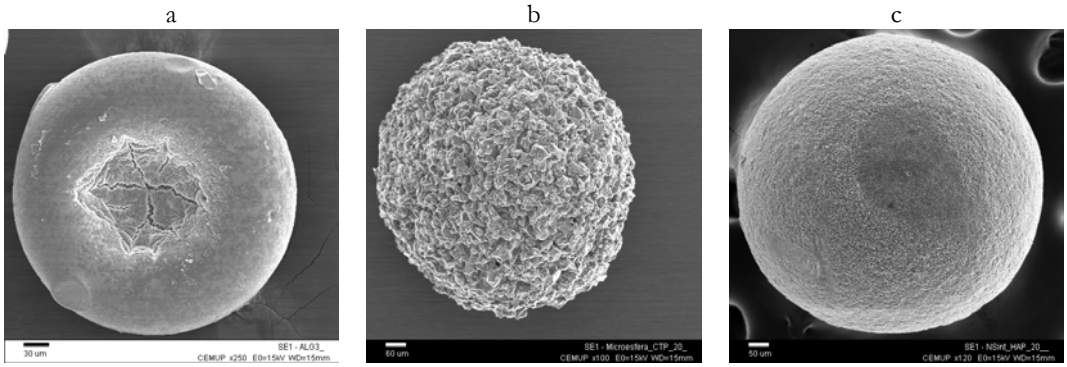

Figure 5 - SEM image of (a) Ca-alginate, (b) CTP-alginate and (c) HAp-alginate microspheres.

The ceramic powders are homogeneously distributed in the alginate matrix (Figure 6) with the granules densely packed and well embedded in the polymer.

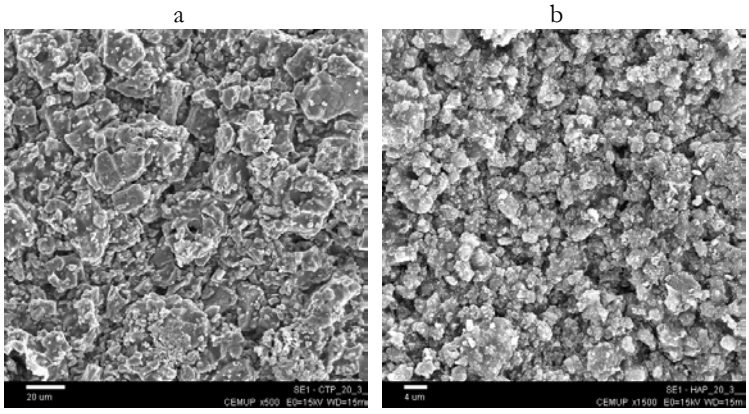

Figure 6 - Detail of a transversal section of CTP-alginate (a) and HAp-alginate (b) microspheres, showing that the ceramic particles are well embedded in the polymer matrix.

FT-IR analysis

FT-IR spectra of calcium and sodium alginate are represented in Figure 7. Table I shows the possible assignments for the FT-IR bands of the alginate salts [38]. Both spectra

are very similar and only slight differences can be observed in the width and height of the COO- bands.

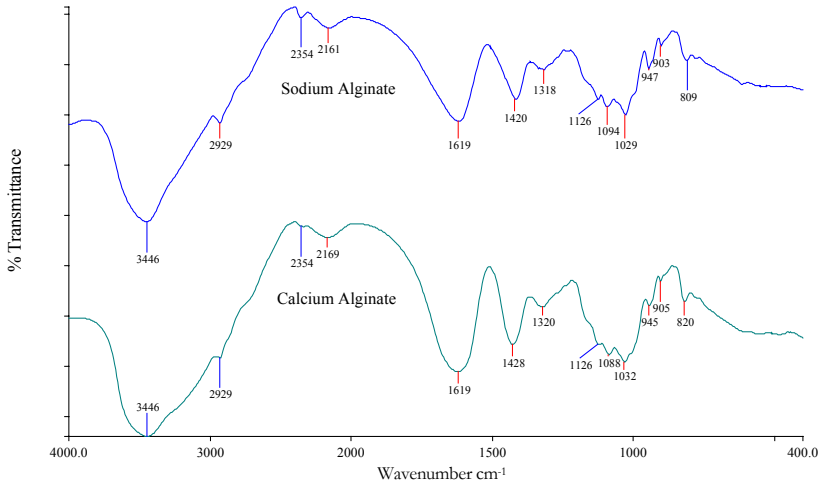

Figure 7 - FT-IR spectra of sodium and calcium alginate.

Table I - Peak assignment of transmittance bands of Na-alginate and Ca-alginate spectra obtained by FT-IR.

Na/Ca-alginate bands (cm^{-1})	Peak Assignment [36]	Na/Ca-alginate bands (cm^{-1})	Peak Assignment [36]
3446	ν (OH) hydrogen bonded	1126	ν (CC), ν (CO)
2929	ν (CH)	1088/1094	τ (CO), δ (CCO), δ (CC)
2354	-	1029/1032	τ (CO), δ (CCO), δ (CC)
2161/2169	-	947/945	ν (CO), δ (CCH)
1619	ν (COO-)	903/905	ν (CO), δ (CCH)
1420/1428	ν (COO-)	809/820	τ (CO), δ (CCO), δ (CCH)
1318/1320	ν (COO-)		

Figure 8 shows the FT-IR spectra of CTP powder, Ca-alginate and CTP-alginate microspheres (formulations 10/3 and 40/3). The FT-IR spectra of HAp powder, Ca-alginate and HAp-alginate microspheres (formulations 10/3 and 40/3) are presented in Figure 9. The characteristic bands of both ceramics are maintained in the microspheres indicating that the alginate did not induce subsequent modifications in the ceramics structure. Additional bands can be observed, corresponding to the presence of calcium alginate, namely at 3446 cm^{-1} (νOH), 1619 and 1428 cm^{-1} (νCOO-), and 820 cm^{-1}, identified in the literature as the

combination of three possible vibrational modes (τCO+δCCO+δCCH) [38]. The intensity of these bands increases as the ceramic-to-polymer solution ratio decreases. Also, the ν_3PO_4 region (900-1200 cm^{-1}) becomes broader in the spectra of the microspheres, denoting the presence of the polymer.

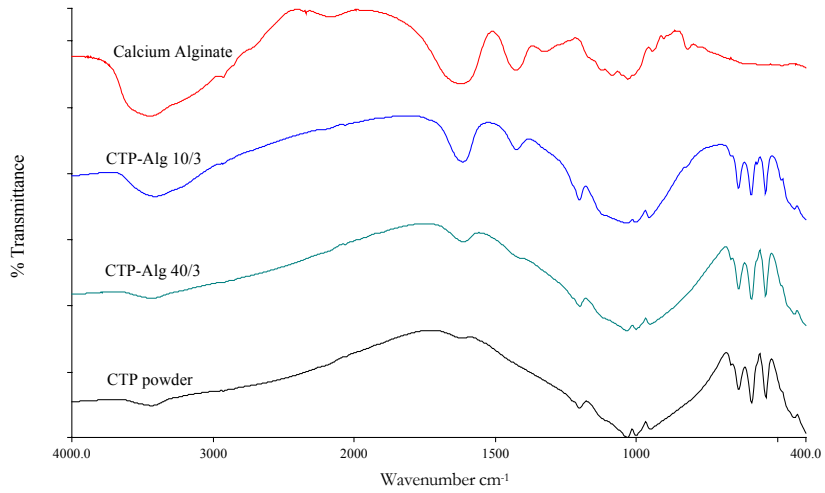

Figure 8 - FT-IR spectra of Ca-alginate, CTP-alginate 10/3 and 40/3 microspheres, and CTP powder.

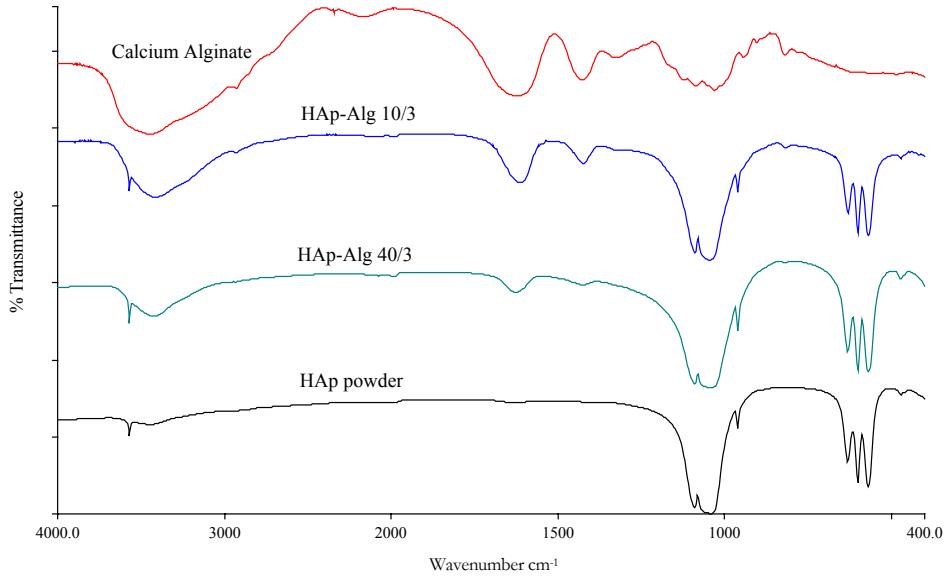

Figure 9 - FT-IR spectra of Ca-alginate, HAp-alginate 10/3 and 40/3 microspheres, and HAp powder.

Enzyme immobilisation in CTP-alginate and HAp-alginate microspheres

Pre-adsorption of the enzyme onto CTP and HAp powders

Figure 10 shows typical adsorption time profiles of GCR onto CTP and HAp powders. The adsorption process was carried out at 4°C for different periods of time (10, 120 and 1440 min). For both ceramics there is an initial period of rapid adsorption followed by a slower approach to a limiting value. After 1440 min, CTP adsorbed 41.28 ng GCR/cm^2, a much higher amount of enzyme per unit surface are than HAp (1.94 ng GCR/cm^2).

Figure 11 represents the percentage of enzyme, with respect to the total amount used, which becomes adsorbed to the ceramic powders (21% in the case of CTP and 10% in the case of HAp), as well as the percentage of enzyme that remains in solution after incubation. The percentage of enzyme removed from the solids during washing (first and second washes) is also represented. The percentages of 21% and 10% were measured after washing, indicating that the enzyme remained well adsorbed onto the powders.

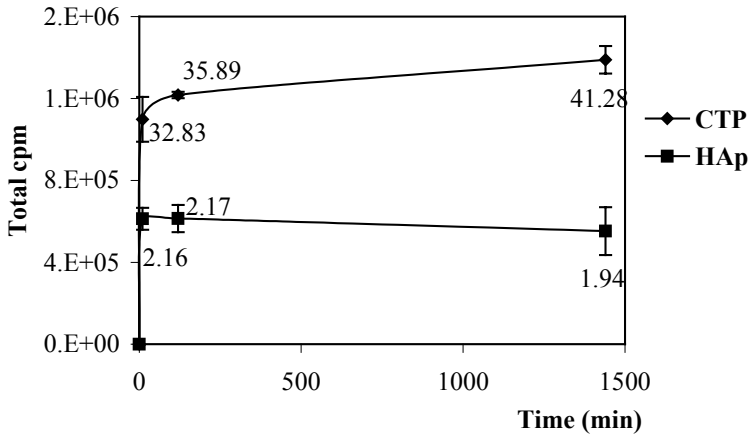

Figure 10 - Time profiles of glucocerebrosidase adsorption onto CTP and HAp powders. The adsorption process was carried out at 4°C for different periods of time (10, 120 and 1440 min). Data labels represent the amount of adsorbed protein per unit surface area (ng/cm^2) of the powders.

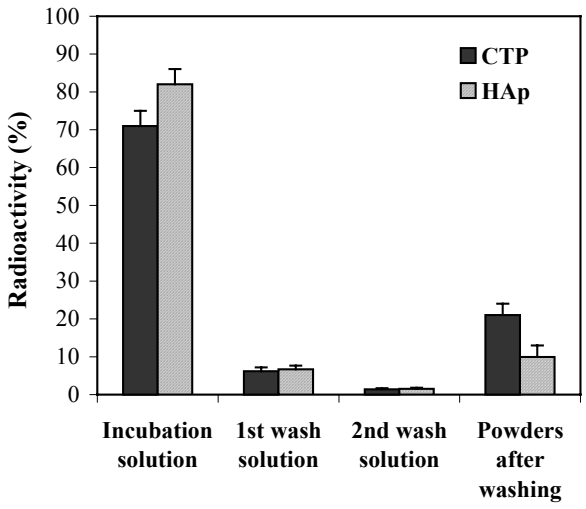

Figure 11 - Adsorption of glucocerebrosidase onto CTP and HAp powders: percentage of radioactivity that becomes associated to the powders after an incubation period of 10 min (4°C). The percentages of radioactivity that remain in the supernatant and are washed out from the powders are also depicted.

Enzyme release studies

Figure 12 shows the release profiles obtained for the different matrices previously described using CTP as the ceramic phase. The release profiles using HAp were similar (results not shown). When the enzyme was dispersed in the ceramic-alginate mixture before gel formation (matrix C), the release profile seems to be initially controlled by the diffusion of GCR from the surface of the beads, with a burst of 33.6±3.3% of total loading, followed by diffusion through the pores of the gel matrix until reaching a plateau at 55.4±4.6%. The overall release profile was not significantly different from what was obtained using a pure alginate matrix (matrix B). When the enzyme was pre-adsorbed onto the ceramic powders prior to the preparation of the microspheres (matrix D), the initial burst was significantly reduced (9.4±1.4%) and a slower release profile was obtained. The results obtained when using matrix A were similar to those reported for matrix D.

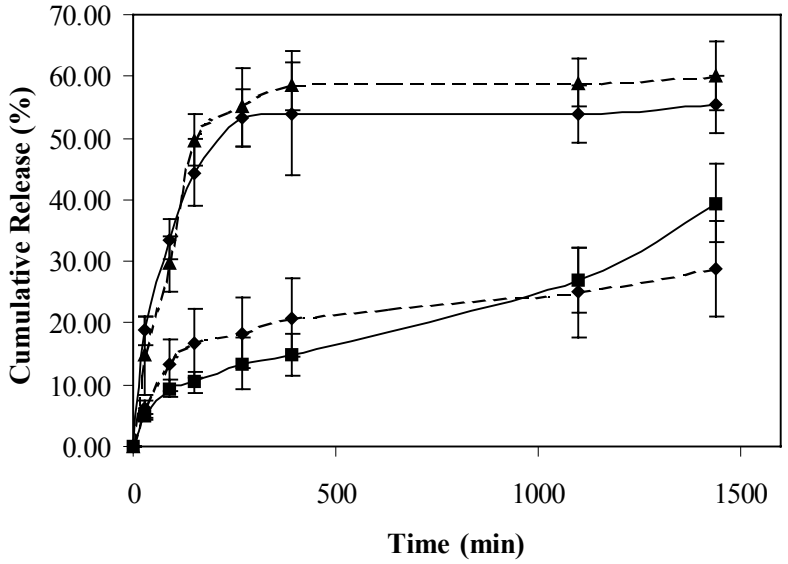

Figure 12 - Enzyme release profiles from the matrices tested using CTP: (A) enzyme adsorbed onto the ceramic powders; (B) enzyme dispersed in a pure alginate matrix; (C) enzyme and ceramic powders individually dispersed in the alginate matrix; and (D) ceramic powders with pre-adsorbed enzyme dispersed in the alginate matrix. The matrices A and B were used as controls.

Discussion

CTP-alginate and HAp-alginate microspheres were prepared using the droplet extrusion method combined with ionotropic gel formation in the presence of Ca^{2+} [27]. Polymer-ceramic mixtures of different compositions were prepared and drop-wise extruded into a crosslinking solution containing Ca^{2+}. As soon as the droplets contacted with the solution, spherical particles were instantaneously formed, due to the rapid establishment of calcium-mediated associations between poly-guluronic acid sequences on the polymer backbone [27]. This resulted in the formation of an alginate hydrogel network with entrapped ceramic particles.

The process was carried out at room temperature and in the absence of organic solvents, which is ideal for the envisaged applications of these materials as enzyme carriers.

The described methodology enabled the preparation of homogeneous microspheres presenting a regular size distribution, even without being fractioned by sieving. During the

drying process and depending on their composition, microspheres underwent volume contractions at different extents. Shrinkage is related to water loss from the polymeric hydrogel phase, explaining why formulations with high ceramic-to-polymer contents underwent less contraction.

SEM observation of the microspheres showed that the ceramic particles were well embedded and homogeneously distributed in the alginate matrix, suggesting a good wettability of the ceramics by the polymer solution. The surface morphology of the microspheres was dependent on the type of ceramic used, the HAp-alginate microspheres being smoother than the CTP-alginate ones. Differences were essentially attributed to the different mean particle sizes of the two ceramic powders. Although the granulometric analysis revealed that the particles of both powders were similar in size (90% of CTP particles are smaller than 25.32 μm and have an average diameter of 11.00 μm, while 90% of the HAp particles are smaller than 20.51 μm and the average diameter is 7.96), the surface area measurements indicated that HAp particles have a much higher surface area (76 cm^2/mg) than CTP (9.8 cm^2/mg).

Physico-chemical characterisation of CTP-alginate and HAp-alginate was carried out by FT-IR spectroscopy. The spectra showed that the characteristic bands of both ceramics are maintained in the microspheres, indicating that the alginate did not induce subsequent modifications in the structure of the ceramics.

A preliminary analysis of the ability of CTP-alginate and HAp-alginate microspheres to act as carriers for the enzyme glucocerebrosidase (GCR), a therapeutic enzyme used in the treatment of Gaucher disease, was carried out.

The possibility of exploiting the capacity of both components to act as enzyme delivery systems was investigated, since both may immobilise proteins [23-27]. For this reason, the enzyme was incorporated into the ceramic-alginate matrix before gel formation in two different ways, as described before. Concerning GCR loading capabilities of the ceramics used in this study, results showed that CTP adsorbs 41.28 ng/cm^2, a much higher amount of enzyme per unit surface than HAp (1.94 ng/ cm^2). This may be attributed to the presence of

BSA, used to stabilise the enzyme, as explained below. At physiological pH, both ceramics are negatively charged, the zeta potential of CTP being more negative than that of HAp. At pH 7.4, the enzyme is in the vicinity of its isoelectric point exhibiting a neutral net charge. Under the conditions used, BSA presents a net negative charge [39] and will probably bind to a lesser extent to CTP than to HAp, due to increased repulsive charge, thus leaving the surface more available for GCR adsorption. Decreased adsorption of HSA (human serum albumin) onto CTP than onto HAp powders was observed by the authors (unpublished data), supporting this hypothesis. Despite being a very complex process, protein adsorption generally reflects hydrophobic/ hydrophilic or electrostatic interactions between the protein and the surface. It seems that under the conditions used, the electrostatic characteristics of CTP favours the immobilisation of GCR.

Other authors, in studies concerning applications in the biotechnology industry [23], demonstrated the capacity of CTP to immobilise several enzymes. To the best of our knowledge this is the first time that this ceramic is used for the immobilisation of glucocerebrosidase.

Release studies were performed with different matrices. When the enzyme was dispersed in the ceramic-alginate mixture before gel formation (matrix C), the release profile seemed to be initially controlled by the diffusion of GCR from the surface of the beads, with a significant burst, followed by diffusion through the pores of the gel matrix until reaching a plateau. The overall release profile was not significantly different from what was obtained using a pure alginate matrix (matrix B), suggesting that the enzyme does not interact, to a great extent, with the embedded ceramic particles. When the enzyme was pre-adsorbed onto the ceramic powders prior to the preparation of the microspheres (matrix D) the initial burst was significantly reduced and a slower release rate was achieved. For matrix A (powders) the results were similar, suggesting that the alginate does not offer an additional resistance to enzyme diffusion.

With the different matrices proposed, distinct release kinetics can be obtained and suitable strategies can be selected depending on the final application. Some aspects remain, however, to be investigated, namely the activity of the enzyme when released from the

matrices used in this work (ongoing studies). Although protein immobilisation, either by entrapment or adsorption, often results in conformational alterations that may render the protein inactive, several authors have reported improved enzyme activity and/or stability in immobilised preparations when compared to their free forms [40].

Conclusions

This study describes the preparation and initial characterisation of CTP-alginate and HAp-alginate microspheres, which are intended to be used as enzyme delivery matrices and bone regeneration templates. The proposed methodology enabled the preparation of homogeneous microspheres with a uniform size, where the bulk properties of the ceramics were maintained, indicating that the alginate did not induce any modifications in the structure of the ceramics. Preliminary studies on the immobilisation and release of the therapeutic protein glucocerebrosidase were also performed. The enzyme was incorporated into the ceramic-alginate matrix before gel formation in two different ways: pre-adsorbed onto the ceramic particles or dispersed in the matrix. The two strategies resulted in distinct release profiles, suggesting that, depending on the application, the more suitable one can be selected.

Acknowledgements

The authors would like to acknowledge Dr. Clara Sá Miranda for the GCR samples, Eng. Alexandra Lemos for the zeta potential determinations, and programme Praxis XXI from the Portuguese Foundation of Science and Technology (FCT) for awarding Cristina Barrias a scholarship. This work was carried out under contract POCTI/FCB/41523/2001.

References

[1] Griffith LG, Naughton G. Tissue engineering: Current challenges and expanding opportunities. Science 2002; 295: 1009-1014.

[2] Hench LL, Polak JM. Third-generation biomedical materials. Science 2002; 295: 1014-1017.

[3] Temenoff JS, Mikos AG. Injectable biodegradable materials for orthopedic tissue engineering. Biomaterials 2000; 21: 2405-2412.

[4] Laurencin CT, Lu HH. Polymer-ceramic composites for bone tissue engineering. In: Davies JE, editor. Bone engineering. Toronto, Canada: EM Squared Inc, 2000. p.463-472.

[5] Gauthier O, Bouler J-M, Weiss P, Bosco J, Daculsi G, Aguado E. Kinetic study of bone ingrowth and ceramic resorption associated with the implantation of different injectable calcium-phosphate bone substitutes. J Biomed Mater Res 1999; 47: 28-35.

[6] Dupraz A, Delecrin J, Moreau A, Pilet P, Passut N. Long term bone response to particulate injectable ceramic. J Biomed Mater Res 1998; 42: 368-375.

[7] Grimandi G, Weiss P, Millot F, Daculsi G. *In vitro* evaluation of a new injectable calcium phosphate material. J Biomed Mater Res 1998; 39: 660-666.

[8] Gauthier O, Boix D, Grimandi G, Aguado E, Bouler JM, Weiss P, Daculsi G. A new injectable phosphate biomaterial for immediate bone filling of extraction sockets: a preliminary study in dogs. J Periodontol 1999; 70: 375-383.

[9] Peter SJ, Nolley JA, Widmer MS, Mervin JE, Yaszemski MJ, Yasko AW, Engel PS, Mikos AG. *In vitro* degradation of a poly (propylene fumarate)/β-tricalcium phosphate composite orthopedic scaffold. Tissue Eng 1997; 3: 207-215.

[10] Sims CD, Butler PEM, Casanova R, Lee BT, Randolph MA, Lee WPA, Vacant CA, Yamremchuk MJ. Injectable cartilage using polyethylene oxide polymer substrates. Plast Reconstr Surg 1996; 98: 843-850.

[11] Suggs LJ, Shive MS, Garcia CA, Anderson JM, Mikos AG. *In vitro* cytotoxicity and *in vivo* biocompatibility of poly (propylene fumarate-co-ethylene glycol) hydrogels. J Biomed Mater Res 1999; 46: 22-32.

[12] Suggs LJ, Krishnan RS, Garcia CA, Peter SJ, Anderson JM, Mikos AG. *In vitro* and *in vivo* degradation of poly(propylene fumarate-co-ethylene glycol) hydrogels. J Biomed Mater Res 1998; 42: 312-320.

[13] Frazier DD, Lathi VK, Gerhart TN, Hayes WC. Ex vivo degradation of a poly (propylene glycol-fumarate) biodegradable particulate bone cement. J Biomed Mater Res 1997; 35: 383-389.

[14] Kharas GB, Kamanetsky M, Simantirakis J, Beinlich KC, Rizzo A-MT, Caywood GA, Watson K. Synthesis and characterization of fumarate-based polyesters for use in bioresorbable bone cement composites. J Appl Polym Sci 1997; 66: 1123-1137.

[15] Paige KT, Cima LG, Yaremchuck MJ, Vacant JP, Vacant CA. Injectable cartilage. Plast Reconstr Surg 1995; 96: 1390-1400.

[16] Paige KT, Cima LG, Yaremchuck MJ, Vacant JP, Vacant CA. De novo cartilage generation using calcium-alginate-chondrocyte constructs. Plast Reconstr Surg 1996; 97: 168-180.

[17] Kulseng B, Skjak-Braek G, Ryan L, Andersson A, King A, Faxvaag A, Espevik T. Transplantation of alginate microcapsules. Transplantation 1999; 67: 978-984.

[18] Martinetti R, Dolcini L, Ravaglioli A, Krajewski A, Mangano C. Experimental study on hydroxyapatite/N-carboxymethyl chitosan fillers. In: Sedel L, Rey C, editors. Bioceramics, vol. 10. Oxford, UK: Elsevier, 1997. p.503-506.

[19] Maruyama M, Ito M. *In vitro* properties of a chitosan-bonded self hardening paste with hydroxyapatite granules. J Biomed Mat Res 1996; 32: 527-532.

[20] Dupraz A, Nguyen TP, Richard M, Daculsi G, Passuti N. Influence of a cellulosic ether carrier on the structure of biphasic calcium phosphate ceramic particles in an injectable composite material. Biomaterials 1999; 20: 663-673.

[21] Ribeiro CC, Barbosa MA. Calcium-Titanium-Phosphate; properties of an alternative biomaterial. Submitted for publication.

[22] Alamo J. Chemistry and properties of solids with NZP skeleton. Solid State Ionics 1993; 63: 547-561.

[23] Suzuki T, Toriyama M, Hosono H, Abe Y. Application of a microporous glass-ceramic with a skeleton of $CaTi_4(PO_4)_6$ to carriers for immobilization of enzymes. J Ferment Bioeng 1991; 72: 384-391.

[24] Gross U, Muller-Mai C, Voigt C, Mesgarian M, Berger G, Ploska U. Tissue response in femur of rabbits after implantation of a new calcium titanium phosphate composition. Key Eng Mat 2001; 192-195: 383-386.

[25] Otsuka M, Matsuda Y, Fox JL, Higuchi WI, Yu D, Wong J. A novel skeletal drug delivery system for anti bacterial drugs using self-setting hydroxyapatite cement. Chem Pharm Bull (Tokyo) 1990; 38: 3500-3502.

[26] Guicheux J, Grimandi G, Trecant M, Faivre A, Takahashi S. Apatite as a carrier for growth hormone: *in vitro* characterization of loading and release. J Biomed Mater Res 1997; 34: 165-170.

[27] Gombotz WR, Wee SF. Protein release from alginate matrices. Adv Drug Deliv Rev 1998; 31: 267-285.

[28] Eiselt P, Yeh J, Latvala RK, Shea LD, Mooney DJ. Porous carriers for biomedical applications based on alginate hydrogels. Biomaterials 2000; 21: 1921-1927.

[29] Alsberg V, Anderson K, Albeiruti A, Franceshi RT, Mooney DJ. Cell interactive alginate hydrogels for bone tissue engineering. J Dent Res 2001; 80: 2025-2029.

[30] Smidsrod O, Draget KI. Chemistry and physical properties of alginates. Carbohyd Europe 1996; 14: 6-13.

[31] Sivakumar M, Manjubala I, Panduranga Rao K. Preparation, characterization and in-vitro release of gentamicin from coralline hydroxyapatite-chitosan composite microspheres. Carbohyd Pol 2002; 49: 281-288.

[32] Qiu QQ, Ducheyne P, Ayyaswamy PS. New bioactive, degradable composite microspheres as tissue engineering substrates. J Biomed Mater Res 2000; 52: 66-76.

[33] Hsu FY, Chueh S-C, Wang YJ. Microspheres of hydroxyapatite/reconstituted collagen as supports for osteoblast cell growth. Biomaterials 1999; 20: 1931-1936.

[34] Grabowski GA, Leslie N, Wenstrup R. Enzyme therapy for Gaucher disease: the first 5 years. Blood Rev 1998; 12: 115-133.

[35] Xu YH, Ponce E, Sun Y, Leonova T, Bove K, Witte D, Grabowski GA. Turnover and distribution of intravenously administered mannose-terminated human acid beta glucosidase in murine and human tissues. Pediatr Res 1996; 39: 313-322.

[36] Ferraz MP, Monteiro FJ, Serro AP, Saramago B, Gibson IR, Santos JD. Effect of chemical composition on hydrophobicity and zeta-potential of plasma spayed HA/CaO-P_2O_5 glass coatings. Biomaterials 2001; 22: 3105-3112.

[37] Lopes MA, Monteiro FL, Santos JD, Serro AP, Saramago B. Hydrophobicity, surface tension, and zeta potential measurements of glass reinforced hydroxyapatite composites. J Biomed Mater Res 1999; 45: 370-375.

[38] Dupuy B, Arien A, Minnot AP. FT-IR membranes made with alginate/polylysine complexes. Variations with mannuronic or guluronic content of the polysaccharides. Art Cells, Blood Subs. Immob Biotech 1994; 20: 71-82.

[39] Peters T. All about albumin: biochemistry, genetics and medical applications. San Diego, CA: Academic Press Inc.; 1996.

[40] Nakanishi K, Sakiyama T, Imamura K. On the adsorption of proteins on solid surfaces, a common but very complicated phenomenon. J Biosci Bioeng 2001; 91: 233-244.

Chapter 7

PREPARATION AND CHARACTERISATION OF CALCIUM-PHOSPHATE POROUS MICROSPHERES WITH A UNIFORM SIZE FOR BIOMEDICAL APPLICATIONS

Cristina C. Ribeiro[1,2,3], Cristina C. Barrias[1,2] and Mário A. Barbosa[1,2]

1 - INEB - Instituto de Engenharia Biomédica, Laboratório de Biomateriais, Rua do Campo Alegre 823, Porto 4150-180, Portugal
2 - FEUP - Faculdade de Engenharia da Universidade do Porto, Dep. de Eng. Metalúrgica e de Materiais, Porto, Portugal
3 - ISEP - Instituto Superior de Engenharia do Porto, Dep. de Física, Porto, Portugal

Abstract

In the present work, a novel route for the preparation of porous ceramic microspheres is described. Two ceramic powders, calcium-titanium phosphate (CTP) and hydroxyapatite (HAp), were mixed with a sodium alginate solution that enabled the preparation of spherical particles, using the droplet extrusion method combined with ionotropic gelation in the presence of Ca^{2+}. The spherical particles were subsequently sintered, to burn-off the polymer and obtain calcium-phosphate microspheres with a uniform size and an interconnected porous network. CTP microspheres with diameters ranging from 513±24 μm to 792±35 μm and with pores of approximately 40 μm were obtained. HAp microspheres presented diameters of 429±46 μm and 632±40 μm and pores of c.a. 2 μm. Depending on the formulations tested, the structure of both calcium phosphates may become altered during the sintering process, suggesting that the ratio between the ceramic phase and the polymer solution is a critical parameter. Porous microspheres prepared using the described

methodology are promising candidates as bone defect fillers and scaffolds for bone tissue regeneration.

Keywords: injectable microspheres, bone tissue engineering, drug-delivery, alginate, hydroxyapatite, calcium-titanium-phosphate.

Introduction

Due to the large number of orthopaedic surgical interventions performed each year, bone repair has become a subject of intensive investigation. The use of calcium phosphate ceramics in bone regeneration, either alone or in combination with a polymeric phase, has become a common practice, since these materials generally provide good biological responses and adequate mechanical properties. Although calcium phosphate ceramics have traditionally been used as dense or porous three-dimensional scaffolds, increasing efforts have been devoted to the development of injectable formulations for bone defects filling applications, since they can be applied through minimally invasive techniques [1]. Most injectable ceramic materials described in the literature consist of micro or nanoparticles suspended in appropriate vehicles [2-7]. In such systems, the shape of the microparticles determines their packaging characteristics, spherical particles being more suitable for implantation than non-homogeneous granules, since they conform better to irregular implant sites. Moreover, uniform particles present more predictable flowing properties during injection [8-11].

In certain applications, the effectiveness of these microparticulate materials can be highly improved if they can act simultaneously as carriers for biologically active molecules. In this sense, porous materials are advantageous, since they present additional surface area, an important parameter that strongly influences the loading capacity and release rates that can be obtained.

In the present work, novel ceramic porous microspheres are proposed, which could find applicability in the field of bone regeneration, both as injectable bone-filling materials and drug delivery matrices. Two ceramic powders, calcium-titanium-phosphate (CTP) and hydroxyapatite (HAp), were tested. CTP, a bioactive ceramic currently under investigation in our laboratory [12], is a potential material to be used in the biomedical field as it presents interesting properties, namely the ability to act as an immobilisation matrix for several enzymes [13-16]. HAp, which possesses a chemical structure similar to bone mineral, has long been recognised in the biomedical field for its osteoconductivity and capacity to act as matrix for drug delivery [17-18] and was used as a reference material. Alginate was chosen

due to its suitable rheology and ability to form relatively stable hydrogels under mild conditions [19].

CTP-alginate and HAp-alginate microspheres were first prepared using the droplet extrusion method as described in a previous work [16]. The ceramic powders were mixed with alginate, which enables the preparation of spherical particles through instantaneous crosslinking in the presence of Ca^{2+} [16]. The obtained microspheres were then dried and subsequently sintered to burn-off the polymer and aggregate the ceramic granules, allowing the preparation of ceramic microspheres with a uniform size and interconnected porous network.

Compared to other methods of preparing ceramic microspheres described in the literature [8-11], this novel process presents the advantage of simplicity and of being carried out in the absence of organic solvents or oils, thus enabling the recovery of the spherical particles without the need of fastidious washing processes. Moreover, the obtained microspheres present a regular size distribution, even without a subsequent fractionation by sieving.

In this study, the preparation and physical-chemical characterisation of CTP and HAp microspheres prepared according to the described methodology are presented.

Materials and Methods

Characterisation of the ceramic powders

CTP was synthesised by solid-state reaction as described elsewhere [12]. HAp was kindly donated by CAM Implants. Both ceramics were analysed by X-ray diffraction (XRD, Philips PW 1710 diffractometer), and their granulometry characterised using a laser scanner particle size analyser (Coulter Electronics Incorporation). The specific surface area of each powder was measured by gas adsorption according to the BET (Brunauer, Emmel and Teller) method. Both powders were observed by scanning electron microscopy (SEM). Samples were sputter coated with gold using a JEOL JFC-100 fine coat ion sputter device,

and observed using a JEOL JSM-6301F scanning microscope, an accelerating voltage of 10 keV and an working distance of 15 mm.

Preparation of CTP and HAp microspheres

Ceramic powders were dispersed in a pre-filtered (0.8 μm) 3% w/v sodium alginate solution (Pronova Biopolymers) under gentle stirring until a homogeneous paste was obtained. Different ceramic-to-polymer solution ratios (0.1, 0.2 and 0.4) were tested. These will be designated as 10/3, 20/3 and 40/3 (different ceramic-to-polymer solution ratios, using a 3% w/v sodium alginate solution). Preliminary assays were conducted to determine the maximum ceramic-to-polymer solution ratio and it was observed that for ratios higher than 0.4 the pastes obtained became too viscous to be handled and extruded. The pastes were extruded drop-wise into a 0.1 M $CaCl_2$ crosslinking solution, where spherical-shaped particles instantaneously formed and were allowed to harden for 30 min. The size of the microspheres was controlled by regulating the extrusion flow rate using a syringe pump (Cole Parmer) and by applying a coaxial air stream (Encapsulation Unit Var J1–Nisco). At completion of the gelling period, microspheres were recovered and rinsed in water in order to remove the excess $CaCl_2$. Finally, they were dried overnight in a vacuum-oven at 30ºC, and then sintered at 1100ºC with a uniform heating rate of 5ºC/min, and a 1h stage at the maximum temperature.

Characterisation of the microspheres

The diameter of the microspheres (n=20) was measured using an inverted plate microscope (Olympus) equipped with an ocular micrometer with an accuracy of 10 μm.

Morphological and physico-chemical characterisation was carried out using SEM and Fourier transform infrared spectroscopy (FT-IR). For FT-IR analysis, microspheres were reduced to powder and analysed as KBr pellets using a Perkin Elmer System 2000 spectrometer.

In order to identify the composition of the residue that results from burning the polymer during sintering, calcium alginate microspheres, produced as described, were

submitted to the same heating cycle used for preparing CTP and HAp microspheres. The obtained residue was analysed by XRD and FT-IR.

Results

Characterisation of the ceramic powders

XRD of the ceramics indicated the presence of monophase crystalline compounds. Granulometric analysis of the powders revealed that 90% of the CTP particles are smaller than 25.32 μm, with a volume average diameter of 11.0 μm, and that 90% of the HAp particles are smaller than 20.51 μm, with a volume average diameter of 7.96 μm. However, surface area measurements indicated that HAp particles have a much higher surface area (76 cm^2/mg) than CTP (9.8 cm^2/mg) suggesting that the results obtained in the HAp granulometric analysis are overestimated, probably due to particle aggregation. Both powders were observed by SEM, which confirmed that CTP particles are in fact much larger than the HAp particles (data not shown).

Characterisation of CTP and HAp microspheres

To produce CTP and HAp microspheres, CTP-alginate and HAp-alginate mixtures of different compositions were prepared and drop-wise extruded into a 0.1M $CaCl_2$ solution. As soon as the ceramic-polymer droplets contacted with the crosslinking bath, spherical particles of approximately 1000 μm were instantaneously formed, due to the rapid establishment of calcium-mediated junctions between poly-guluronate chains on the polymer backbone [18]. An exception was observed for the 40/3 HAp formulation, with which it was not possible to obtain spherical particles due to the high viscosity of the ceramic-polymer mixture.

During drying, the volume contractions varied with the formulation as shown in Figure 1 which presents the diameters of dried CTP and HAp microspheres, that were obtained before (ceramic-polymer microspheres) and after sintering (ceramic microspheres).

a)

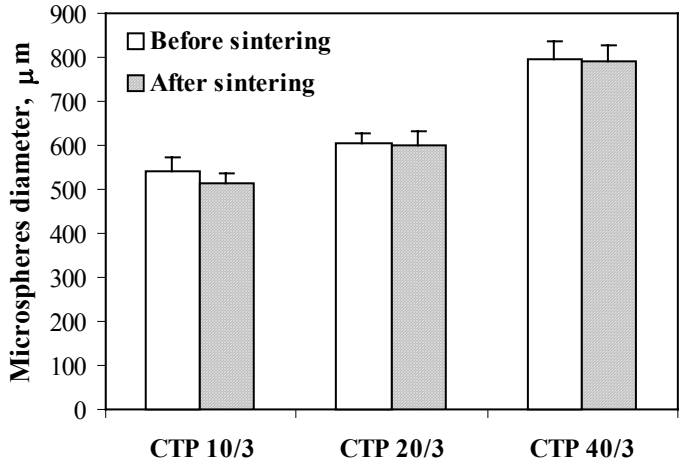

b)

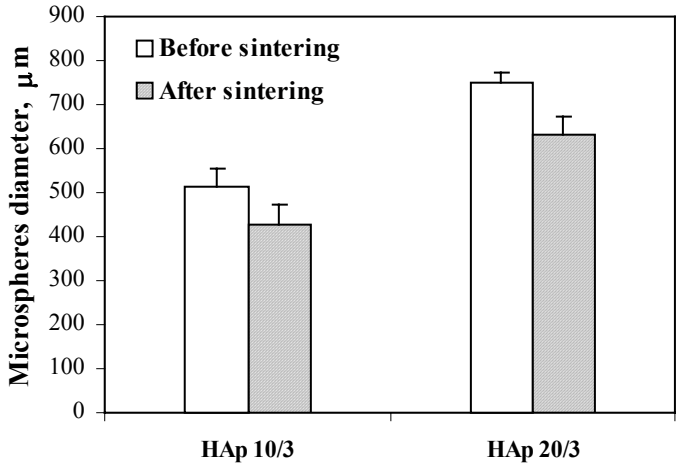

Figure 1 - Diameters of CTP (a) and HAp (b) microspheres before and after sintering.

It can be concluded that the higher the ceramic-to-polymer solution ratio used, the lower the particles contraction during drying. Upon sintering, microspheres maintained their original spherical shape. In the case of the HAp microspheres their diameter further decreased approximately 20%, while CTP microspheres practically maintained their original dimensions. Such differences are probably related to the different particle size distributions and, in particular, to the higher percentage of fine particles in HAp that results in a more

effective packaging during sintering. With the described methodology, microspheres with a regular size distribution were obtained without a subsequent fractioning by sieving being necessary.

Microspheres with average final diameters of 513±24 μm, 602±28 μm, and 792±35 μm were obtained for the CTP 10/3, 20/3 and 40/3 formulations, respectively; while with HAp microspheres diameters of 429±46 μm and 632±40 μm were obtained for the 10/3 and 20/3 formulations, respectively.

SEM analysis

SEM pictures of CTP and HAp microspheres, before and after sintering, are presented in Figure 2. Only the results obtained with the 20/3 formulation are given, as similar results were obtained for the other formulations tested. The analysis revealed that in both cases microspheres were homogeneous, in terms of size and shape. No evidence of cracks was found.

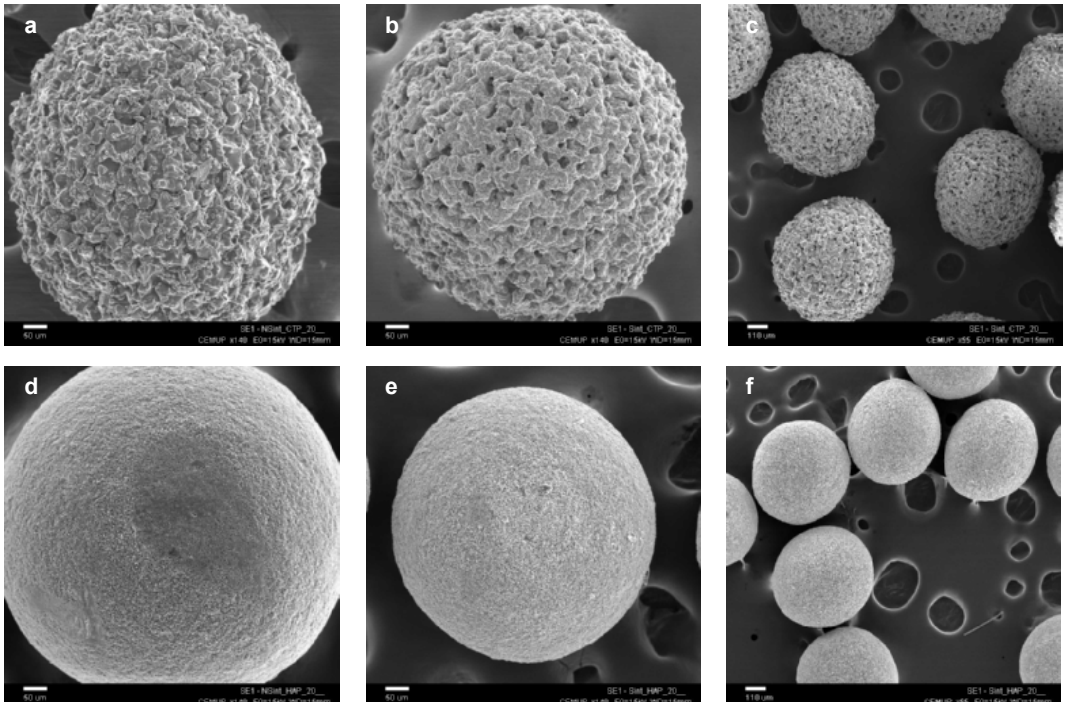

Figure 2 - SEM images of CTP and HAp microspheres before and after sintering: (a) Non-sintered CTP microsphere, (b, c) sintered CTP microspheres; (d) non-sintered HAp microsphere, (e, f) sintered HAp microspheres.

CTP microspheres (Figure 2 a, b, c) present a rather rough surface, while HAp microspheres (Figure 2 d, e, f) are smoother. Such differences are mainly attributable to the differences in granulometry of the two ceramics, since the CTP particles are much larger than those of HAp. The volume contraction that occurred upon sintering in the case of HAp microspheres is evident (Figure 2 a, b).

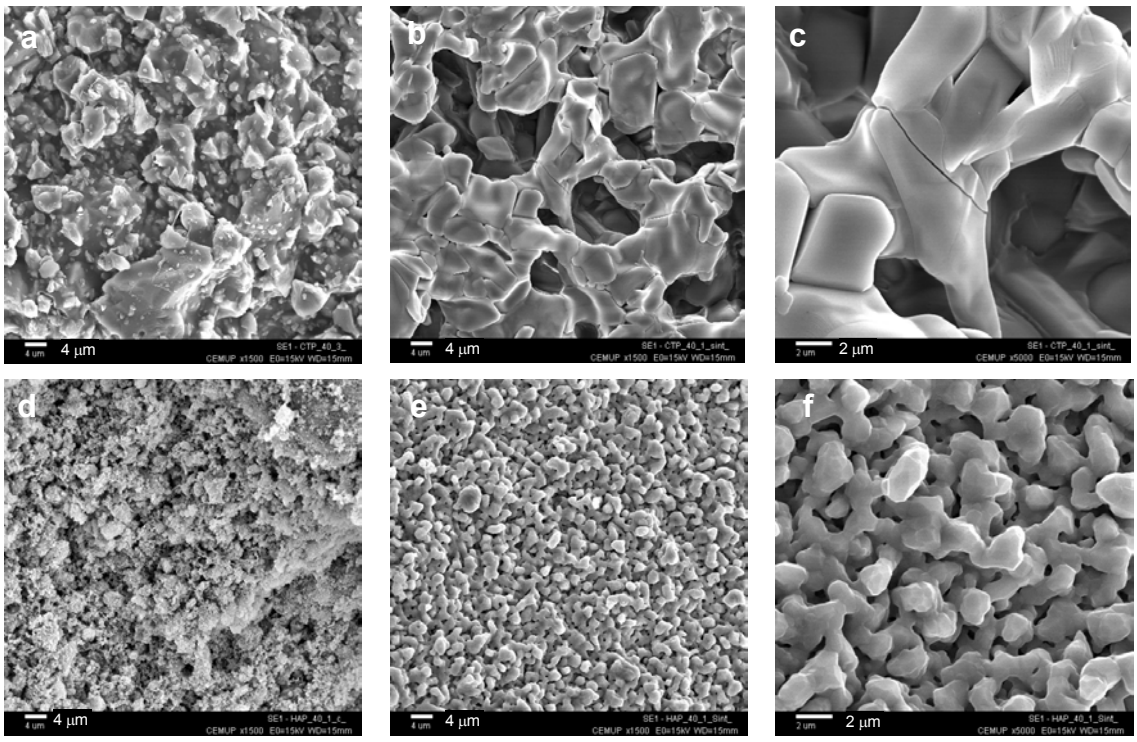

Figure 3 - Higher magnification SEM images of CTP and HAp microspheres before and after sintering: (a) Non-sintered CTP microsphere, (b, c) sintered CTP microspheres; (d) non-sintered HAp microsphere, (e, f) sintered HAp microspheres.

Non-sintered microspheres revealed, at higher magnifications, a homogeneous distribution of the ceramic phase in the alginate matrix (Figure 3 a, d). It should be noted, however, that since the particles of HAp powder are much smaller than those of CTP, the former appear to be more densely packed. Upon sintering the polymer phase is substituted by a porous network (Figure 3 a, b, e, f). The interconnectivity of the pores and their homogeneous distribution are clearly observed in Figure 3b, 3c and 3f, respectively. Pores of approximately 40 µm were obtained when using CTP as the ceramic phase, while HAp

resulted in pores of approximately 2 μm. Results were similar for all the formulations tested. Differences in porosity may be attributed to the different granulometries of the two compounds, which result in different packaging of the ceramic particles during drying and sintering, as suggested already.

FT-IR and XRD analysis

The FT-IR spectrum of the residue powder obtained after subjecting the calcium-alginate microspheres to sintering of the ceramic-alginate microspheres (Figure 4), showed the presence of bands characteristic of carbonates, namely the ones in the intervals 1409-1483 cm^{-1}, 1020-1100 cm^{-1} and 800-890 cm^{-1} [20, 21]. The band at 3642 cm^{-1} is assigned to O-H vibrations, suggesting the presence of a hydroxide compound [20, 22]. XRD analysis of the residue (Figure 5) identified it as a mixture of $Ca(OH)_2$ (portlandite) and $CaCO_3$ (calcite), confirming the results obtained by FT-IR.

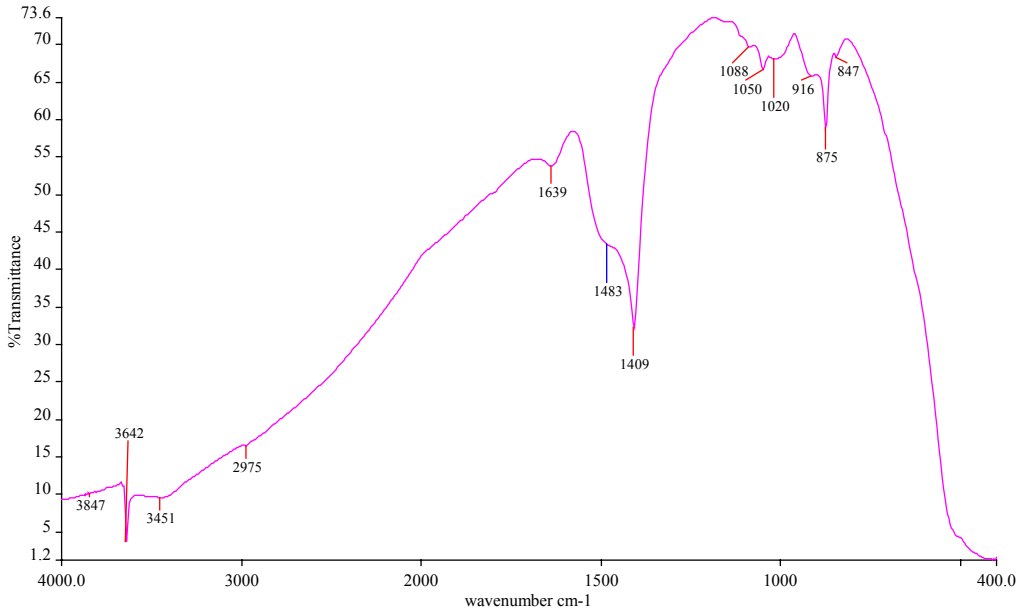

Figure 4 - FT-IR spectrum of the alginate-burning residue.

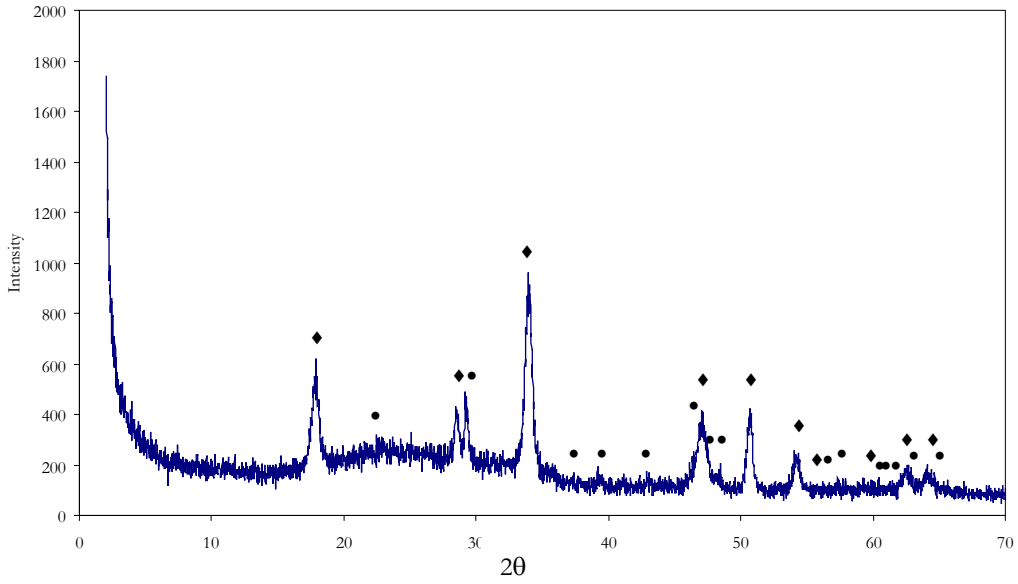

Figure 5 - XRD spectrum of the alginate-burning residue, ♦- Portlandite $Ca(OH)_2$, ●- Calcite $CaCO_3$.

FT-IR spectra of CTP powder and CTP microspheres are presented in Figure 6. The changes that are observed in the spectra of CTP microspheres when compared to those of the CTP powder, suggest that a reaction between CTP and calcium alginate must have occurred during sintering, leading to structural modifications that resulted in the appearance of new bands in the ν_3PO_4 and ν_2PO_4 phosphate zone, as well as a band at 726 cm^{-1}. These bands are more evident in the spectrum of the sample with the lowest ceramic-to-polymer solution ratio (10/3), and becomes less defined as the ceramic-to-polymer solution ratio increases, being the FT-IR spectrum of the 40/3 formulation very similar to the one of CTP powder. Figure 7 shows the FT-IR spectrum of (a) 10/3 CTP microspheres, (b) commercial calcium pyrophosphate ($Ca_2P_2O_7$ - Sigma Aldrich) and (c) titanium pyrophosphate synthesised in our laboratory. Several bands which are characteristic of pyrophosphate groups, namely the ones in the ranges: 900-1200 cm^{-1}, 700-770 cm^{-1} and 500-600 cm^{-1}, are common to spectra (a) and (b), suggesting the formation of a calcium pyrophosphate phase in the CTP microspheres as a consequence of the sintering process. However, the existence of that phase could not be detected by XRD analysis (Figure 8) leading to the assumption that the phase is either amorphous or present in residual concentrations. In addition, XRD analysis showed the presence of small quantities of titanium oxide (rutile) in the sintered CTP

microspheres, its concentration being higher in the formulation 10/3. This was not unexpected considering the hypothesis described above. If a calcium pyrophosphate is formed, probably some titanium will become available to form an oxide.

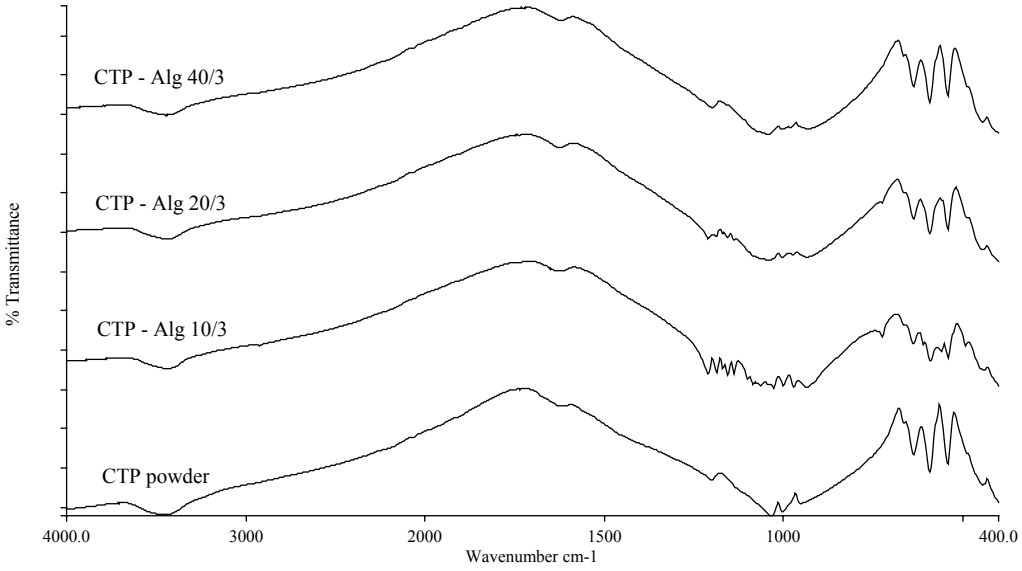

Figure 6 - FTIR spectra of CTP powder and of different formulations of CTP microspheres.

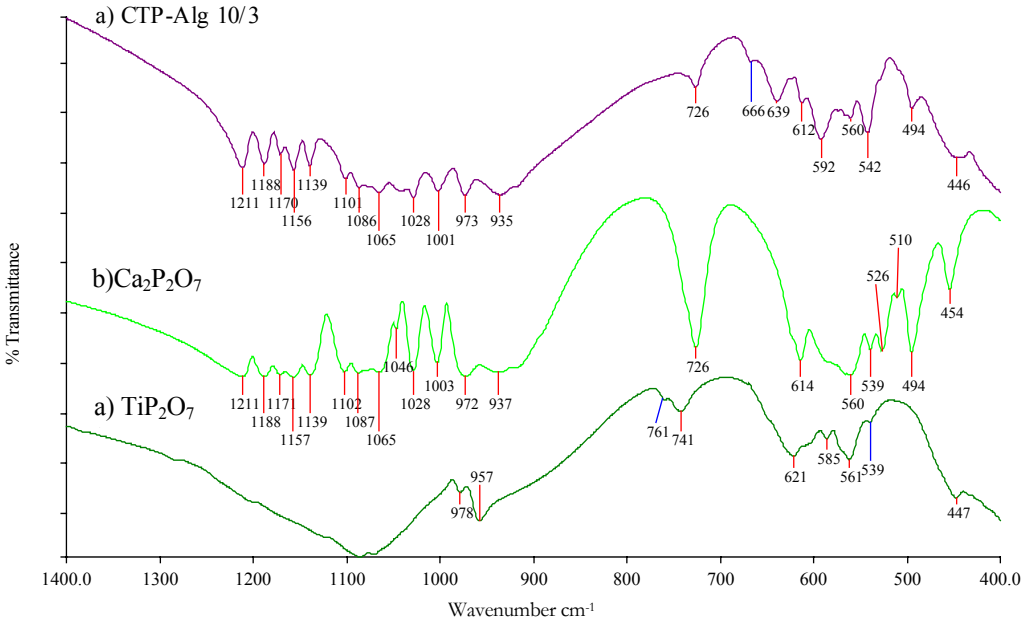

Figure 7 - FTIR spectra of CTP-Alg 10/3 microspheres, calcium pyrophosphate and titanium pyrophosphate.

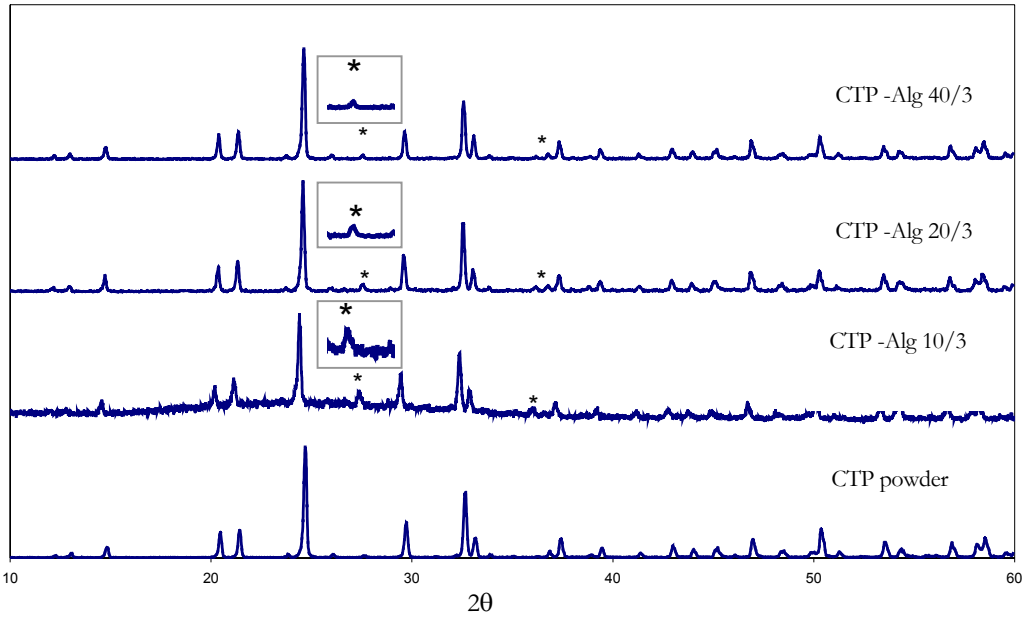

Figure 8 - XRD of CTP powder and of different formulations of CTP microspheres.

In what concerns HAp microspheres, XRD analysis of the HAp powder and HAp microspheres revealed that after sintering no decomposition of the ceramic occurred, since no extraneous phases could be identified. Figure 9 shows the FT-IR spectra of HAp powder and 10/3 HAp microspheres. It is worth noting the appearance of carbonate bands at 1440 cm^{-1} and 876 cm^{-1} in the samples with the 10/3 ceramic-to-polymer solution ratio, suggesting the presence of a carbonated hydroxyapatite. This may have practical implications, since it is well established that the presence of carbonates in calcium phosphate materials is an important factor contributing to the *in vivo* integration of the implant. For the 20/3 and 40/3 formulations, the FT-IR spectra of the microspheres are practically identical to the one of HAp, but the presence of carbonate bands is less evident. No signs of calcium hydroxide were observed in the sintered CTP-alginate and HAp-alginate microspheres.

In order to clarify if a carbonated apatite has been obtained, or if the carbonate bands were due to formation of a calcium carbonate residue, resultant from the burning of alginate, 10/3 HAp microspheres were subjected to a second sintering cycle at 1100ºC for 1h. When heated to this high temperature, any free calcium carbonate would disappear since calcium carbonate (calcite) decomposes at approximately 825ºC into CaO and CO_2 [23]. The FT-IR

spectra of the re-heated HAp microspheres still presented the carbonate bands, confirming the presence of a carbonated apatite.

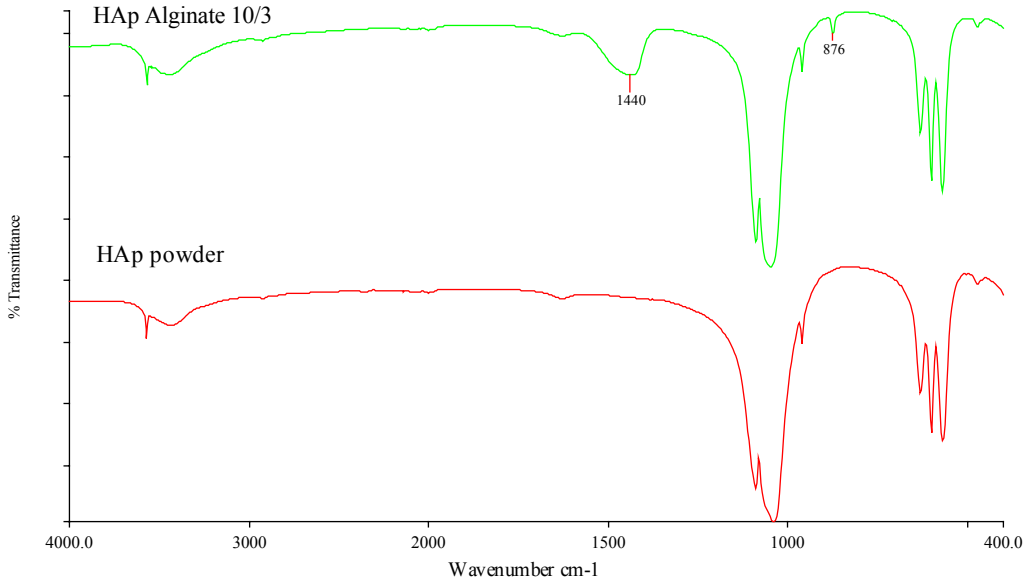

Figure 9 - FTIR spectra of HAp powder and of HAp-Alg 10/3 microspheres.

Discussion

There are several reports described in the literature concerning the development of HAp or HAp-polymer granulates with spherical geometry [8-11, 24-28]. Most of the methods used to produce microspheres have the disadvantage of using organic solvents or oils thus needing several washing stages to eliminate them. For instance, Sunny *et al* [10] produced HAp/chitosan microspheres by the dispersion of HAp/chitosan slurry in liquid parafin, with the addition of gluteraldehyde to harden the spheres. Sivakumar *et al* [11, 28] developed a method to produce coralline HAp/chitosan and coralline HAp/gelatin composite microspheres using a PMMA dispersion solution containing toluene as a crosslinking agent. The experimental method proposed in this study has the advantage of not using such reactants, thus allowing the recovery of the microspheres without the need of fastidious washing processes.

Another advantage of the present methodology is the possibility of producing spherically shaped particles with uniform sizes. Irregularly or densely packed granules have been described in the literature as being the cause of inflammatory reactions and slower bone formation [29]. Uniformly packed spherical particles would lead to a regular inter-particle porosity, thus contributing to easier migration of bone cells. Moreover, since our aim is to use the microspheres in an injectable form, their flowing properties during injection will be more predictable if their shape and size are more regular.

Since these microspheres may also be used to deliver growth factors and other proteins, their porosity is a critical parameter since it may strongly influence their loading capacity. The increase in porosity that occurs upon sintering will significantly increase the surface area and allow higher delivery efficiency.

This investigation has shown that the ratio between the ceramic phase and the polymer solution is of critical importance in the composition of the sintered microspheres. In the case of the CTP-alginate microspheres, a calcium pyrophosphate was formed after sintering, and its concentration increases as the ceramic to polymer ratio decreases. When subjected to the same heating cycle used for sintering the microspheres, CTP powder does not suffer any change in composition. These observations suggest that the formation of the pyrophosphate phase is related to the presence of alginate. Sodium alginate forms a relatively stable hydrogel of calcium alginate through ionotropic gelation in the presence of Ca^{2+}. A possible mechanism to explain the formation of the pyrophosphate phase after sintering is the interaction between calcium ions from the alginate and phosphate groups from the ceramic, possibly forming an acid salt. When a solid orthophosphate, which contains hydrogen bonds (e.g. $CaHPO_4$) is heated to an appropriate temperature, there is a loss of water accompanied by pyrophosphate formation [30, 31]. The amount of pyrophosphate formed is related to the number of hydrogen bonds present in the system. Pyrophosphate ion is a well-known inhibitor of apatite formation [31-33]. LeGeros *et al* [33] have demonstrated that the presence of pyrophosphate ions are efficient in promoting the formation of amorphous calcium phosphates. With the microspheres prepared in this investigation promotion of mineralization is an objective. Therefore, a formulation with a high ceramic to polymer ratio will be more adequate.

With HAp-alginate microspheres it was observed that the sintering process leads to the formation of carbonated hydroxyapatite. The carbonate ions were probably incorporated in the HAp structure according to the following reaction [34]:

$$2OH^- \text{ (apatite)} + CO_2 \rightarrow CO_3^{2-} \text{ (apatite)} + H_2O$$

that was probably favored by an increase of the local concentration of CO_2 resulting from the burning of alginate. This is in agreement with the fact that carbonate bands are more intense in the low ceramic to polymer ratio formulations. The substitution of carbonate in well and poorly crystallized hydroxyapatite is well documented in the literature. It has been suggested that planar CO_3 ion substitutes for tetrahedral PO_4 groups in hydroxyapatite prepared at room (or body) temperature while in high temperature preparations (about 1000ºC), CO_3 substitutes for OH [31].

Conclusions

Porous ceramic microspheres with an uniform size were prepared using a novel methodology consisting of sintering spherical particles, obtained by droplet extruding a mixture of ceramic powders and sodium alginate followed by ionotropic gelation in the presence of Ca^{2+}. Microspheres with different porosities may be produced by this method, by varying the granulometry of the ceramic powders. It was also found that the ratio between the ceramic phases and the polymer solution is a critical parameter in the composition of the sintered microspheres and must be carefully selected. These materials could find applicability in the field of bone regeneration, both as injectable bone-filling materials and drug delivery matrices.

References

[1] Temenoff JS, Mikos AG. Injectable biodegradable materials for orthopedic tissue engineering. Biomaterials 2000; 21: 2405-2412.

[2] Grimandi G, Weiss P, Millot F, Daculsi G. *In vitro* evaluation of a new injectable calcium phosphate material. J Biomed Mater Res 1998; 39: 660-666.

[3] Iooss P, Le Ray AM, Grimandi G, Daculsi G, Merle C. A new injectable bone substitute combining poly(epsilon-caprolactone) microparticles with biphasic calcium phosphate granules. Biomaterials 2001; 22: 2785-2794.

[4] Peter SJ, Nolley JA, Widmer MS, Mervin JE, Yaszemski MJ, Yasko AW, Engel PS, Mikos AG. *In vitro* degradation of a poly (propylene fumarate)/β-tricalcium phosphate composite orthopedic scaffold. Tissue Eng 1997; 3: 207-215.

[5] Martinetti R, Dolcini L, Ravaglioli A, Krajewski A, Mangano C. Experimental study on hydroxyapatite /N-carboxymethyl chitosan fillers. In: Sedel L, Rey C, editors. Bioceramics, vol.10. Oxford, UK: Elsevier, 1997. p.503-506.

[6] Maruyama M, Ito M. *In vitro* properties of a chitosan-bonded self-hardening paste with hydroxyapatite granules. J Biomed Mater Res 1996; 32: 527-532.

[7] Dupraz A, Nguyen TP, Richard M, Daculsi G, Passuti N. Influence of a cellulosic ether carrier on the structure of biphasic calcium phosphate ceramic particles in an injectable composite material. Biomaterials 1999; 20: 663-673.

[8] Qiu QQ, Ducheyne P, Ayyaswamy PS. New bioactive, degradable composite microspheres as tissue engineering substrates. J Biomed Mater Res 2000; 52: 66-76.

[9] Hsu FY, Chueh SC, Wang YJ. Microspheres of hydroxyapatite/ reconstituted collagen as supports for osteoblast cell growth. Biomaterials 1999; 20: 1931-1936.

[10] Sunny MC, Ramesh P, Varma HK. Microstructured microspheres of hydroxyapatite bioceramic. J Mater Sci: Mater Med 2002; 13: 623-632.

[11] Sivakumar M, Manjubala I, Rao KP. Preparation, characterisation and in-vitro release of gentamicin from coralline hydroxyapatite-chitosan composite microspheres. Carbohyd Polym 2002; 49: 281-288.

[12] Ribeiro CC, Barrias CC, Barbosa MA. Calcium-titanium-phosphate; properties of an alternative biomaterial. Submitted for publication.

[13] Alamo J. Chemistry and properties of solids with NZP skeleton. Solid State Ionics 1993; 63: 547-561.

[14] Suzuki T, Toriyama M, Hosono H, Abe Y. Application of a microporous glass-ceramic with a skeleton of $CaTi_4(PO_4)_6$ to carriers for immobilization of enzymes. J Ferment Bioeng 1991; 72: 384-391.

[15] Gross U, Muller-Mai C, Voigt C, Mesgarian M, Berger G, Ploska U. Tissue response in femur of rabbits after implantation of a new calcium titanium phosphate composition. Key Eng Mat 2001; 192-195: 383-386.

[16] Ribeiro CC, Barrias CC, Barbosa MA. Calcium phosphate-alginate microspheres as enzyme delivery matrices. Biomaterials 2004; 25: 4363-4373.

[17] Otsuka M, Matsuda Y, Fox JL, Higuchi WI, Yu D, Wong J. A novel skeletal drug delivery system for anti bacterial drugs using self-setting hydroxyapatite cement. Chem Pharm Bull 1990; 38: 3500-3502.

[18] Guicheux J, Grimandi G, Trecant M, Faivre A, Takahashi S, Daculsi G. Apatite as a carrier for growth hormone: *in vitro* characterization of loading and release. J Biomed Mater Res 1997; 34: 165-170.

[19] Smidsrod O, Draget KI. Chemistry and physical properties of alginates. Carbohyd Europe 1996; 14: 6-13.

[20] Socrates L. In: Socrates L, editor. Infrared and Raman Characteristic Group Frequencies - Tables and Charts. Chichester, England: John Wiley & Sons, Ltd, 2001. p.277.

[21] Rehman I, Bonfield W. Characterisation of hydroxyapatite and carbonated apatite by photo acustic FTIR spectroscopy. J Mater Sci: Mater Med 1997; 8: 1-4.

[22] Baumer A, Genteaume M, Klee WE. Determination of OH ions in hydroxyfluorapatites by infrared spectroscopy. Bulletin de Mineralogie 1985; 108: 145-152.

[23] The Merck Index - An Encyclopedia of Chemicals, Drugs and Biologicals (Merck &Co. Inc., Whitehouse Station, N I, 1996). p.271-272.

[24] Komlev VS, Barinov SM, Koplik EV. A method to fabricate porous spherical hydroxyapatite granules intended for time-controlled drug release. Biomaterials 2002; 23: 3449-3454.

[25] Krylova E, Ivanov A, Orlovski V, El-Registan G, Barinov S. Hydroxyapatite-polysaccharide granules for drug delivery. J Mater Sci: Mater Med 2002; 13: 87-90.

[26] Paul W, Sharma CP. Infection resistant hydroxyapatite/ alginate plastic composite. J Mater Sci Let 1997; 16: 2050-2051.

[27] Borden M, Attawia M, Khan Y, Laurencin CT. Tissue engineered microsphere-based matrices for bone repair: design and evaluation. Biomaterials 2002; 23: 551-559.

[28] Sivakumar M, Rao KP. Preparation, characterization and *in vitro* release of gentamicin from coralline hydroxyapatite-gelatin composite microspheres. Biomaterials 2002; 23: 3175-3181.

[29] Misiek DJ, Kent JN, Carr RF. Soft tissue response to hydroxylapatite particles of different shapes. J Oral Maxillof Surg 1984; 42: 150-160.

[30] Elliot JC. PhD Thesis, University of London, London, England, 1964.

[31] Posner AS. The mineral of bone. Clinical Orthopaedics 1985; 200: 87-99.

[32] Williams G, Sallis JD. Structural factors influencing the ability of compounds to inhibit hydroxyapatite formation. Calcif Tissue Int 1982; 34: 169-174.

[33] LeGeros RZ, Shirra WP, Miravite MA, LeGeros JP. Amorphous calcium phosphates: synthetic and biological. Colloques Internationaux C.N.R.S. - Physico-chimie et cristallographie d'intérêt biologique 1973; 230: 105-115.

[34] Elliot JC. In: Elliot JC, editor. Structure and chemistry of the apatites and other calcium orthophosphates. Amsterdam, Holland: Elsevier, 1994. p.213.

Chapter 8

GENERAL DISCUSSION AND MAIN CONCLUSIONS

Most orthopaedic applications of implants require materials with good mechanical performance. Metals are still, and will probably remain for a long time, the main constituents of load bearing prosthetic devices. Efforts have been made to improve the biological activity of metallic surfaces by coating them with calcium compounds. Plasma sprayed hydroxyapatite (HAp) coatings on titanium and titanium alloy implants have been used in an attempt to obtain reliable implant-to-bone fixation. The successful clinical performance of these materials will depend on a low rate of dissolution of HAp and on the integrity of the metal/coating interface. Although metallic prostheses coated with hydroxyapatite are extensively used clinically, both dissolution of the calcium phosphate and adhesion failure at the coating/substrate interface have been reported [1, 2]. It is also established that metal ion release occurs from metallic implants [3-18] but its effect on the degradation of HAp (as a coating and as a bone mineral constituent) is not well clarified. Due to the ability of HAp to incorporate metal ions in its lattice the coating could act as a barrier to elemental transfers from the underlying substrate to the surrounding tissues. Alternatively, as a consequence of the interaction of metal ions with HAp, new compounds could be formed, the chemical and structural properties of which would be determinant for the stability of the coating.

One of the main objectives of the present work was to investigate the effect of Ti ions on the molecular structure of HAp. For that purpose, dissolution studies of HAp were carried out in the presence of different concentrations of Ti in solution. It was observed that the mechanism of interaction of Ti ions with HAp is dependent on the metal ion concentration. Chapter 2 describes the results obtained for Ti concentrations ranging from 200 to 2000 ppm. The effects of HAp crystallinity, Ti concentration, incubation media and

time and temperature of incubation were investigated. The solids were analysed by X-ray diffraction techniques and Fourier transform infrared spectroscopy. It was demonstrated that for concentrations in Ti higher than 400 ppm, a dissolution-precipitation process occurs, leading to the formation of a new compound, a titanium protonated phosphate with a layered structure ($Ti(HPO_4)_2.nH_2O$; n=1-3). The model that is proposed to describe the structure of the titanium phosphate formed is the stratification of two layered structural phases (α-$Ti(HPO_4)_2.H_2O$ and γ-$Ti(H_2PO_4)PO_4.2H_2O$) stacked 1:1 along the c axis with a layer spacing of approximately 19.2 Å. The compound crystallinity slightly increases with time and temperature of incubation and is not influenced by the crystallinity of the HAp used in its preparation. Although this kind of phosphate may form at the metal/ HAp interface, as it is suggested by the results obtained in this work, its presence in retrieved prostheses has not been demonstrated probably because it exists as very thin layers in reduced areas (pores or cracks). The process of formation of the titanium phosphate could take place at pores or cracks in the coating, which would be saturated in calcium and phosphate ions as a result of the dissolution of HAp. Also, the identification by surface analysis techniques of any interfacial compounds is very difficult in coated prostheses due to the large surface roughness caused by grit blasting of the substrate prior to HAp deposition. The chemical affinity of titanium to protonated phosphate ions is also evidenciated in the process of formation of calcium phosphate films on titanium substrates. Studies on the characterisation of the surface film formed on titanium when immersed in a calcium phosphate rich electrolyte [19, 20] showed a tendency of hydrated phosphate ions to be adsorbed on titanium rather than calcium ions.

For a Ti concentration of 400 ppm in the incubation solution, a non-crystalline solid was formed. For concentrations in Ti lower than 400 ppm, it was observed that Ti ions were uptaken by HAp but the results obtained with the analytical techniques used were not sufficiently clear to describe a mechanism of interaction of the metal ions with the ceramic. Other studies were then performed with concentrations of Ti ranging from 50 to 350 ppm, using several analytical techniques, namely X-ray diffraction with Rietveld analysis, FT-IR, XPS and DTA analysis (chapter 3). The complementarity of information given by techniques of short, medium and long-range order was explored and very good correlation between the

data was attained. The mechanism that better explains the changes that were observed for concentrations in Ti lower than 200 ppm is the substitution of Ca for Ti in the HAp lattice, although, to the best of our knowledge, this substitution has not been reported before. The only references that were found in the literature concerning the possibility of substitution of Ca by a tetravalent ion in the HAp lattice refers to uranium [21, 22]. According to Altschuler *et al* [22] uranium may be as abundant as 0.1% in certain phosphorites and these authors indicate that tetravalent uranium probably enters the HAp structure as a replacement for calcium because of the similarity of the ionic sizes. Further evidence of the uranium association with apatite is the fact that isolated fossil bones or phosphate nodules may contain as much as 1% of uranium [19], an amount greatly in excess of that of the enclosing strata. Several results described in this thesis support the possibility of substitution of Ca for Ti, namely the X-ray diffraction analysis using Rietveld refinement. No additional phases were observed for the Ti-HAp samples and the diffraction pattern was identical to that obtained for stoichiometric HAp. Nevertheless, with increasing Ti concentration, changes were observed in the a and c parameters, as well as a shift in the peak position that corresponds to basal planes, indicating that alterations occurred in the HAp lattice. The surface analysis results were in agreement with the ones obtained for the bulk structure. The changes observed in the atomic percentages of the elements suggest a possible substitution of Ca by Ti when small concentrations of Ti are in solution (100 ppm), the Ca+Ti/P ratio obtained being practically the same as the Ca/P ratio of HAp. Also, several infrared parameters were consistent with the hypothesis of substitution, showing that there is a change of the orthophosphate environment in the presence of Ti. The ν_3 domain in IR deconvoluted spectra became more complex as the Ti concentration in solution increased. Moreover, the area of the OH librational band (632 cm^{-1}), which is especially sensitive to substitutions in the apatite structure, decreased, suggesting a decrease in the HAp crystallinity. The intensity of the OH stretching band varied in the same way, also indicating a change in the HAp structure. The DTA results, together with the IR data of the analysis of the powders obtained after DTA, indicated that the substitution of Ca for Ti in the HAp lattice results in the formation of a non-stoichiometric HAp which, after being submitted to heating until 1200ºC, dehydrates, forming β-$Ca_3(PO_4)_2$ plus HAp.

Ti-6Al-4V is the titanium alloy more widely used in the biomedical field. The effect of aluminium ions on the HAp structure, as well as the possibility of existence of a synergistic effect between Ti and Al ions was also investigated in this thesis (chapter 4). For that purpose, HAp was incubated in solutions containing different concentrations of Al, Ti and a mixture of Al and Ti ions. In the experiments with the two cations, the Ti/Al ratio was 15, corresponding to that in Ti-6Al-4V. After incubation, the supernatant liquid was analysed for Ca, Ti, Al and P ions. The solids were analysed using X-ray diffraction techniques, FTIR, FT-Raman and EDS. It was demonstrated that the presence of Al in solution significantly influences the dissolution of HAp. A linear relationship between the Al concentration and Ca concentration in solution was observed, which could not be simply attributed to pH changes, as shown by the results of the separate experiments with addition of HCl free of aluminium. These data suggest the substitution of Ca for Al in HAp. Aluminium has been associated with several bone disorders [23-31]. It is known to inhibit HAp formation, leading to hypocalcemia and hyperphosphatemia in patients submitted to hemodialysis for long periods of time [23-31]. According to several authors, trivalent ions, including Al^{3+} [32-34] and Y^{3+} [34, 35], can substitute calcium in the HAp lattice. Instead, other authors, consider that metal ions like Al^{3+} and Ga^{3+}, the ionic radius of which differ considerably from the calcium radius, tend to adsorb onto the calcium phosphate crystal surface [29, 36]. The ion exchange reaction of HAp with Fe^{3+}, Al^{3+} and La^{3+} have been investigated in relation to their dental applications [37, 38] and it has been reported that, in acidic solutions, those ions disrupt the HAp crystals to form orthophosphate compounds by removing Ca from the lattice. In the present study the formation of an hydrated aluminium phosphate compound was only detected for high concentrations of Al (2000 ppm) in solution.

FT-Raman analysis confirmed the formation of a titanium phosphate for high concentrations of Ti in solution, as indicated in chapters 2 and 3. It was also demonstrated that when Al was present together with Ti in the incubation media, the Ca concentration in the supernatant liquid was lower than when only Ti was present, although the Al was added in the form of an acid solution. These observations were in agreement with the EDS data for the powders of HAp incubated in the previously mentioned solutions. The wt% of Ca in the HAp powders incubated in solutions with Al was higher than the wt% of Ca in the powders

incubated without Al. These results suggest that Al and Ti jointly inhibit HAp dissolution and/or lead to formation of a calcium-containing compound. In what concerns the FT-IR and FT-Raman data, it was shown that for most metal ion concentrations tested Ti has an effect on the spectra that masks any possible influence of Al. Nevertheless, for the concentrations of 375ppmTi/ 25ppmAl, the formation of an hydrated phosphate compound, different from the one formed in the presence of the same concentration of Ti and in the absence of Al, was observed. The results obtained seem to be indicative of a synergistic effect between the two cations but further research on this aspect should be pursued.

The results described in chapters 2, 3 and 4 suggest that when HAp is used as a coating material it may prevent the release of Ti and Al ions from a metallic substrate to the surrounding tissues, either by precipitating the ions in the form of a phosphate compound or by incorporating them in the crystal lattice. These observations are of relevance when these cations are released from orthopaedic implants, since the type of compound formed is bound to interfere with the normal processes of bone formation. Although being the less soluble calcium phosphate of those traditionally used in implantology, it is expected that HAp coatings will partially dissolve *in vivo*. The resorbability of HAp can be as much as 15-30 μm per year [39] depending on its crystallinity. The fate of metal ion-containing compounds present within HAp coatings, particularly during the process of phagocytosis, should be further investigated. In what concerns bone, significant accumulation of a given metal can be expected to alter the characteristics of its constituent mineral phase. If, in addition, the metal interacts with bone cells, their metabolism and function may be affected. Fluoride and biphosphonates are examples of compounds that become part of the mineral phase of bone but also have an inhibitory effect on osteoclasts [40]. Furthermore, once a metal becomes incorporated in bone, it will eventually go into the circulation when the bone mineral is resorbed, a process that could have biological consequences.

The aim of the work described in chapter 5 was to synthesise and characterise calcium titanium phosphate (CTP, $CaTi_4(PO_4)_6$), a material that could act as an alternative to traditional calcium phosphates for some specific situations. The CTP synthesis methodology followed in this work enabled the preparation of a very pure ceramic phase. The material was

studied using different techniques, namely XRD, FT-IR, FT-Raman, EDS, XPS and DTA. The solubility of CTP in Tris-HCl solution was determined, as well as the zeta potential at different pH values. The capacity of the material to mineralise in simulated physiological conditions was also investigated. The *in vitro* biocompatibility of CTP was evaluated in cultured MG63 cells, in terms of cytoxicity and cell adhesion. The dissolution tests indicated that CTP dissolution is not stoichiometric as more calcium goes into solution than phosphorous. This is possibly due to the fact that Ca ions are held in the structure of the compound by weaker bonds than the $[Ti_4(PO_4)_6]^{2-}$ skeleton [41]. Zeta potential measurements showed that at physiological pH CTP is negatively charged. It was also demonstrated that CTP induces the formation of an apatitic carbonate layer on its surface when immersed in a simulated body fluid, indicating its ability to mineralise. The cell culture tests showed that CTP is not cytotoxic and promotes MG63 cell adhesion.

A possible application of CTP could be as a coating of titanium-based metallic prostheses, because it may have some chemical affinity to the implant surface. Moreover, since the thermal expansion coefficient of CTP is similar to that of titanium-based alloys [42], the possible failure of the coating due to mismatch of thermal expansion coefficients will probably be minimised. Lugscheider *et al* [42] were able to produce plasma spraying coatings of CTP, although it was observed that decomposition of the ceramic into other phases occurred for some of the granulometries tested. The potential advantages of using CTP as a coating were not investigated in this thesis. Instead, the idea was to explore the possibility of using this particular phosphate as a bone filling material and scaffold for bone tissue regeneration. In studies concerning applications in the biotechnology industry the capacity of CTP to immobilise several enzymes has been demonstrated [43]. The possibility of CTP acting simultaneously as delivery matrix for biologically active molecules was also explored in the present work. Two different injectable systems based on CTP microspheres were developed, which were described in chapters 6 and 7.

There is an increasing interest in the development of injectable materials for bone regeneration via minimally invasive surgery, thus providing less discomfort to the patients and lower costs. A variety of injectable materials, both ceramic- and polymer-based, have been developed for regeneration of bone [44-60]. Different types of injectable ceramic-based

materials are described in the literature, consisting essentially of pastes, granules and nano or micro particles suspended in an appropriate vehicle. The geometry of the particles that are injected is relevant in the *in vivo* response. Irregularly or densely packed granules often cause inflammatory reactions [61] and the bone formation may be slower. Spherical particles are more suitable for implantation because of their unique packing characteristics with uniform pores between particles [62]. This configuration is claimed to promote efficient osteoconduction with no inflammatory reaction [63]. Moreover, microspheres combined with a vehicle can be administered using a narrow gauge needle, thus enabling the filling of defects of different shapes and sizes. From all the above mentioned reasons microspheres are therefore one of the most advantageous types of injectable delivery systems.

One of the injectable systems developed in this thesis consisted of microspheres of a natural polymer and a ceramic phase. The polymer chosen was ultra-pure alginate, which is widely used in the biomedical field [64-68] and, according to its characteristics, is expected to be biocompatible and biodegradable. In what concerns the ceramic phases, CTP was used as well as HAp but as a reference material, since it is a bioactive and osteoconductive ceramic which has been extensively tested as a matrix in drug delivery applications [69-71]. The CTP-alginate and HAp-alginate microspheres were prepared using the droplet extrusion method combined with ionotropic gel formation in the presence of Ca ions. Polymer ceramic mixtures of different compositions were prepared and drop-wise extruded into a $CaCl_2$ solution. Spherical particles were instantaneously formed due to the rapid establishment of calcium-mediated association between polyguluronic acid sequences. This method of preparation of the microspheres is simple and presents some advantages when compared to other processes. It is carried out at room temperature and in the absence of organic solvents, which makes it ideal for enzyme or protein entrapment purposes. Using the methodology described, homogeneous microspheres were produced, presenting a regular size distribution without the need of additional sieving. The bulk characteristics of the ceramics were maintained, indicating that the alginate did not induce any modifications in the structure of the ceramics. The results obtained also indicate that it is possible to produce microspheres with different morphologies by changing the mean particle size of the ceramic powder.

Besides inducing bone regeneration, the ceramic-alginate microspheres developed in this work are intended to be used as a drug delivery system, capable of immobilising an enzyme or protein and releasing it *in vivo*. Consequently, studies were performed on the ability of CTP-alginate and HAP-alginate microspheres to act as carriers for glucocerebrosidase (GCR). This specific enzyme was chosen due to the fact that our research group is involved in a research project aiming at developing an enzyme delivery system to be used in patients suffering from bone lesions associated to Gaucher disease. Gaucher disease is an autosomal recessive disorder due to the deficient glucocerebrosidase activity, and is characterised by a number of severe disabling symptoms including skeletal deterioration [72]. To promote bone regeneration in Gaucher patients, besides the clinically used intravenous administration of exogeneous enzyme, alternative therapies are necessary to assure sustained enzyme release rates over prolonged periods of time. GCR is very unstable in solution under physiological conditions and, to overcome this problem, its immobilisation is being investigated in our group. In order to study the immobilisation and release of GCR using CTP-alginate and HAp-alginate microspheres, the enzyme was radiolabelled and incorporated into the ceramic-alginate matrix in two different ways: pre-adsorbed onto the ceramic particles or dispersed in the polymeric matrix. One of the common problems when using drug carrier materials is the possibility of a burst in drug release, especially during the first few hours after injection into the body. The two strategies used for the immobilisation of the enzyme resulted in distinct release profiles. When the enzyme was adsorbed to the ceramic prior to the preparation of the microspheres, a slow release was obtained. An initial fast release was obtained when the enzyme and the ceramic particles were dispersed in the alginate solution before producing the microspheres. The different patterns of enzyme release increase the range of possible applications of the system investigated in this work, so that, depending on the application, the most suitable can be selected. An important observation is that the electrostatic characteristics of CTP favour the immobilisation of GCR, when compared to HAp. It is the first time that this ceramic is used for the immobilisation of this particular enzyme. The works described in the literature concern the immobilisation on CTP of enzymes that are not used in biomedical applications (invertase, β- galactosidase and alkalophilic proteinase) [43]. In the present investigation CTP adsorbs 41.28 ng/cm^2 of GCR, a much higher amount of enzyme per unit surface than HAp (1.94 ng/cm^2). In a recent study [73] from our team (see

annex), it was shown that, while in the presence of HAp there is some degree of inactivation, in the presence of CTP a higher catalytic efficiency was observed.

The results obtained on the immobilisation of GCR, together with the ones described in chapter 5, support the interest in the use of CTP as an alternative ceramic to the traditional calcium phosphates for orthopedic surgery. The fact that CTP presents a low degradibility, as indicated by the dissolution tests described in chapter 5, can be advantageous in situations where a low bone turnover is observed, as is the case of Gaucher patients, since the ceramic may act as a reinforcement of the bone. The possibility of using pure ceramic CTP (without alginate) in an injectable form was also explored in this work and a novel methodology to prepare porous ceramic microspheres, to be used both as injectable bone-filling materials and drug delivery matrices, was successfully developed.

The efficiency of bone-biomaterial bonding is dependent on the interlocking of bone tissue with the implant, which is favoured by the existence of irregularities on the biomaterial surface, including porosity. Porous materials are typically defined as microporous (pore diameter < 0.002 μm), mesaporous (0.002 μm < diameter < 0.050 μm) or macroporous (diameter > 0.05 μm) [74]. Only small molecules (e.g. gases) are capable of penetrating microporous materials. Mesaporous materials allow transport of larger molecules such as small proteins, but transport of large proteins and cells is prevented [74]. Macroporous materials allow free transport of large molecules and if the pores are large enough (d> 100 μm), cells are capable of migrating through the pores of the device [74]. It is generally accepted that a uniform size of 100-200 μm in diameter is suitable for bone in-growth [75, 76] although there is a wide disagreement about the ideal pore size for it. Different methods to produce porous ceramics are described in the literature, namely those based on additives like starch, paraffin, wax or hydrogen peroxide, which release gases at elevated temperatures [77-83]. Ceramics like HAp can also be mixed with $CaCO_3$, NaCl and sugars which, after dissolution, result in a porous network [83-86]. Alternatively, calibrated foams impregnated with an HAp suspension, and then dried and sintered, are also in use [70, 87, 88]. In this study the porosity was produced by sintering, which resulted in the burning off of the alginate used in the microspheres preparation. Microspheres of CTP-alginate and HAp-

alginate were prepared according to the methodology previously described, and were sintered at 1100ºC for 1h. The microspheres obtained presented a uniform size and interconnected porous network. The porosity of the particles varied from 2 μm to 40 μm, depending on the ceramic used in its preparation. The size of the pores is not sufficiently large to allow bone in-growth. However, it is expected that the interstices between the particles will provide the necessary space for vascularisation and bone in-growth, leading to effective bone regeneration. In terms of delivery system the porosity observed allows a significant increase in the loading capacity of the matrix. Another advantage of the ceramic microspheres is the possibility of sterilisation without chemical degradation.

It was also demonstrated in this study that the ratio between the ceramic and the polymer solution influences the composition of the sintered microspheres. In the case of the CTP-alginate microspheres a calcium pyrophosphate was formed after sintering and its concentration increases as the ceramic to polymer ratio decreases. Since pyrophosphate is a well-known inhibitor of apatite formation [89-91] and promotion of mineralisation is one of the objectives of the use of the microspheres, a formulation with high ceramic to polymer ratio will be more adequate. For HAp-alginate microspheres it was observed that the sintering process leads to the formation of a carbonated hydroxyapatite. This may have beneficial implications since it is well established that the presence of carbonate in calcium phosphate materials is an important factor contributing to the *in vivo* integration of the implant.

Cell culture investigations of our team (see annex), using the CTP and HAp microspheres produced according to the methodology described in chapter 7, support the applicability of these materials as scaffolds for bone tissue regeneration and/or supports for the *in vitro* culture of bone cells [92, 93]. Studies on the proliferation, activity and osteogenic differentiation of bone marrow stromal cells cultured on CTP microspheres showed that cells were able to attach and spread on the surface of CTP microspheres, and gradually grow into nearly confluent monolayers [92]. Moreover, cells expressed ALP activity and secreted osteocalcin, which confirmed that differentiation along the osteoblastic lineage occurred. It

was also demonstrated that hydroxyapatite microspheres are able to support human osteoblastic cells adhesion and proliferation [93].

In conclusion, this work opens good perspectives for the application of ceramic-alginate and pure ceramic microspheres in the field of bone regeneration, both as injectable bone filling materials and drug delivery matrices.

References

[1] Albrektsson T. Hydroxyapatite coated implants: a case against their use. J Oral Maxillofac Surg 1998; 56: 1312-1326.

[2] Bloebaum RD, Beeks D, Loor LD, Savory LG, DuPont JA, Hoffmann AA. Complications with hydroxyapatite particulate separation in total hip arthroplasty. Clin Orthop 1994; 298: 19-26.

[3] Bauer Tw, Stulberg BN, Ming J, Geesink RGT. Uncemented acetabular components: histologic analysis of retrieved hydroxyapatite-coated and porous implants. J Arthroplasty 1993; 8: 167-177.

[4] Porter AE, Taak P, Hobbs LW. Coathup MJ, Blunn GW, Spector M. Bone bonding to hydroxyapatite and titanium surfaces on femoral stems retrieved from human subjects at autopsy. Biomaterials 2004; 25: 5199-5208.

[5] MacDonald DE, Betts F, Stranick M, Doty S, Boskey AL. Physicochemical study of plasma-sprayed hydroxyapatite-coated implants in humans. J Biomed Mater Res 2001; 54: 480-490.

[6] Michel R. Trace element analysis in biocompatibility testing. CRC Crit Rev Biocomp; 1987. p.235-317.

[7] Lewandowska-Szumielm M, Komender J. Aluminium release as a new factor in the estimation of alumina bioceramic implants. Clin Mater 1990; 5: 167-175.

[8] Jones LC, Hungerford DS. Urinary metal ion levels in patients implanted with porous coated total hip prostheses. Trans Orthop Res Soc 1987; 32: 317.

[9] Black J. Does corrosion matter? J Bone Joint Surg 1988; 70 B: 517-520.

[10] Ducheyne P, Healy K, Black J, Cuckler J. The effect of hydroxyapatite coatings on the metal ion release from porous titanium and cobalt chromium alloys. Trans Orthop Res Soc 1987; 12: 315.

[11] Woodman JL, Jacobs JJ, Galante JO, Urban RM. Metal ion release from titanium-based prosthetic segmental replacements of long bones in baboons: a long term study. J Orthop Res 1984; 1: 421-430.

[12] Sunderman FW Jr., Hopfer SM, Swift T, Rezuke WN, Ziebka L, Highman P, Edwards B, Folcik M, Gossling HR. Cobalt, Chromium and nickel concentrations in body fluids of patients with porous-coated knee or hip prostheses. J Orthop Res 1989; 7: 307-315.

[13] Black J, Skipor A, Jacobs J, Urban RM, Galante JO. Release of metal ions from titanium-based alloy total hip replacement prostheses. Trans Orthop Res Soc 1989; 14: 501.

[14] Ektessabi AM, Otsuka T, Tsuboi Y, Yokoyama K, Albrektsson T, Sennerby L, Johansson CB. Quantitative measurement of metal-ion release from biomedical implants- application of microbeam PIXE to detection of titanium ion release from dental and orthopaedic implants. Int J PIXE 4 1994; 2/3: 81-91.

[15] Ektessabi AM, Otsuka T, Tsuboi Y, Horino Y, Mokuno Y, Fujii K, Albrektsson T, Sennerby L, Johansson C. Preliminary experimental results on mapping of the elemental distribution of the organic tissues surrounding titanium-alloy implants. Nuc Inst Meth Phys Res B 1996; 109/110: 278-283.

[16] Niki Y, Matsumoto H, Otani T, Suda Y, Toyama Y. Metal ion concentrations in the joint fluid immediately after total knee arthroplasty. Mod Reum 2001; 11: 192-196.

[17] Tanaka N, Ichinose S, Kimijima Y, Mimura M. Investigation of titanium leak to bone tissue surrounding dental titanium implant: electron microscopic findings and analysis by electron diffraction. Med Elec Mic 2000; 33: 96-101.

[18] Lijian Z, Ti-Sheng C, Wei W, Lei C. Study of commercially pure titanium implants bone integration mechanisms. Eur J Plas Surg 2000; 23: 301-304.

[19] Ducheyne P, Healy K. Titanium: Immersion- induced surface chemistry changes and the relationship to passive dissolution and bioactivity. In: Davies JE, editor. The Bone-Biomaterials Interface. Toronto, Canada: University of Toronto Press, 1991. p.62-67.

[20] Hanawa T, Ota M. Characterization of surface film formed on titanium in electrolyte using XPS. App Surf Sci 1992; 55: 269-276.

[21] Baturin GN. Uranium and thorium in phosphatic bone debris from the ocean bottom. Lith Min Res 2001; 36: 115-125.

[22] Altschuler ZS, Cathcart JB, Young EL. Field guidebook geology and geochemistry of the bone valley formation and its phosphate deposits, west central Florida. Miami Geological Society, 1964.

[23] Posner AS, Blumenthal NC. *In vitro* model of aluminium- induced osteomalacia: inhibition of hydroxyapatite formation and growth. J Calcif Tissue Int 1984; 36: 439-441.

[24] Andress DL, Maloney NA, Endres DB, Sherrard DJ. Aluminum-associated bone disease in chronic renal failure: high prevalence in a long-term dialysis population. J Bone Min Res 1986; 1: 391-398.

[25] Andress DL, Maloney NA, Coburn JW, Endres DB, Sherrard DJ. Osteomalacia and aplastic bone disease in aluminum-related osteodystrophy. J Clin End & Metab 1987; 65: 11-16.

[26] Severson AR, Haut CF, Firling CE, Huntley TE. Influence of short-term aluminum exposure on demineralized bone matrix induced bone formation. Arch Toxicol 1992; 66: 706-712.

[27] Posner AS, Blumenthal NC, Boskey AL. Model of aluminum-induced osteomalacia: inhibition of apatite formation and growth. Kidney Int 1986; 29: 17-19.

[28] Christoffersen MR, Christoffersen J. The effect of aluminium on the rate of dissolution of calcium hydroxyapatite: a contribution to the understanding of aluminium- induced bone diseases. Calcif Tissue Int 1985; 37: 673-676.

[29] Christoffersen MR, Thyregod HC, Christoffersen J. Effects of aluminum(III), chromium(III), and iron(III) on the rate of dissolution of calcium hydroxyapatite crystals in the absence and presence of chelating agent desferrixamine. Calcif Tissue Int 1987; 41: 27-30.

[30] Goodman WG, Duarte MEL. Aluminum: effects on bone and role in the pathogenesis of renal osteodystrophy. Miner Electrolyte Met 1991; 17: 221-232.

[31] O´Brien Aaj, Moore DP, Keogh JAB. Aluminium osteomalacia in chronic renal failure patients neither on dialysis nor taking aluminium containing phosphate binders. Irish J Med Sci 1990; 150: 74-76.

[32] LeGeros RZ, Taheri MH, Quirolgico GB, LeGeros JP. Formation and stability of apatites: effects of some cationic substituents. In: Proceedings of 2nd International Congress on Phosphorous Compounds. Boston, USA, 1980. p.89-103.

[33] LeGeros RZ. Ultrastructural Properties of Human Enamel Apatite. In: Lazzari EP, editor. Handbook of Experimental Aspects of Oral Biochemistry. Florida, USA: CRC Press, 1983. p.159-179.

[34] Yamashita K, Kanazawa T. Hydroxyapatite. In: Kanazawa T, editor. Inorganic Phosphate Materials. Tokyo, Japan: Kodansha; 1989. p.15-54.

[35] Ergun C, Webster TJ, Bizios R, Doremus RH. Hydroxylapatite with substituted magnesium, zinc, cadmium, and yttrium. I. Structure and microstructure. J Biomed Mater Res 2002; 59: 305-311.

[36] Donnely R, Boskey A. The effect of gallium on seeded HAp growth. Calc Tissue Int 1989; 44: 138-142.

[37] Tanizawa Y, Sawamura K, Suzuki T. Reaction characteristics of dental and synthetic apatites with Fe^{2+} and Fe^{3+} ions. J Chem Soc Faraday Trans 1990; 86: 1071-1075.

[38] Tanizawa Y, Sawamura K, Suzuki T. Reaction Characteristics of dental and synthetic apatites with Al^{3+} and La^{3+} ions in acidic solutions. J Chem Soc Faraday Trans 1990; 86: 4025-4029.

[39] Groot de K. Hydroxyapatite coatings. Mater Technol 1993; 8: 12-18.

[40] Bronner F. Metals in bone: aluminium, boron, cadmium, chromium, lead, silicon, and strontium. In: Bilezikian JP, Lawrence GR, Gideon AR, editors. Principles of bone biology. San Diego, USA: Academic Press, 1996. p.295-303.

[41] Alamo J. Chemistry and properties of solids with NZP skeleton. Solid State Ionics 1993; 63-65: 547-561.

[42] Lugsheider E, Berger G, Knepper M, Sicking R, Nyland A. Plasma sprayed coatings of calcium titanium phosphate: a new generation of bioactive coatings. In: Wilson J, Hench LL, Greenspan DC, editors. Bioceramics, Vol. 8. Oxford, UK: Butterworth-Heinemann, 1995. p.317-322.

[43] Suzuki T, Toriyama M, Hosono H, Abe Y. Application of a microporous glass-ceramic with a skeleton of $CaTi_4(PO_4)_6$ to carriers for immobilization of enzymes. J Ferment Bioeng 1991; 72: 384-391.

[44] Laurencin CT, Lu HH. Polymer-ceramic composites for bone tissue engineering. In: Davies JE, editor. Bone engineering. Toronto, Canada: EM Squared Inc, 2000. p.463-472.

[45] Gauthier O, Bouler J-M, Weiss P, Bosco J, Daculsi G, Aguado E. Kinetic study of bone ingrowth and ceramic resorption associated with the implantation of different injectable calcium-phosphate bone substitutes. J Biomed Mater Res 1999; 47: 28-35.

[46] Dupraz A, Delecrin J, Moreau A, Pilet P, Passut N. Long term bone response to particulate injectable ceramic. J Biomed Mater Res 1998; 42: 368-375.

[47] Grimandi G, Weiss P, Millot F, Daculsi G. *In vitro* evaluation of a new injectable calcium phosphate material. J Biomed Mater Res 1998; 39: 660-666.

[48] Gauthier O, Boix D, Grimandi G, Aguado E, Bouler JM, Weiss P, Daculsi G. A new injectable phosphate biomaterial for immediate bone filling of extraction sockets: a preliminary study in dogs. J Periodontol 1999; 70: 375-383.

[49] Peter SJ, Nolley JA, Widmer MS, Mervin JE, Yaszemski MJ, Yasko AW, Engel PS, Mikos AG. *In vitro* degradation of a poly (propylene fumarate)/β-tricalcium phosphate composite orthopedic scaffold. Tissue Eng 1997; 3: 207-215.

[50] Sims CD, Butler PEM, Casanova R, Lee BT, Randolph MA, Lee WPA, Vacant CA, Yamremchuk MJ. Injectable cartilage using polyethylene oxide polymer substrates. Plast Reconstr Surg 1996; 98: 843-850.

[51] Suggs LJ, Shive MS, Garcia CA, Anderson JM, Mikos AG. *In vitro* cytotoxicity and *in vivo* biocompalibility of poly (propylene fumarate-co-ethylene glycol) hydrogels. J Biomed Mater Res 1999; 46: 22-32.

[52] Suggs LJ, Krishnan RS, Garcia CA, Peter SJ, Anderson JM, Mikos AG. *In vitro* and *in vivo* degradation of poly(propylene fumarate-co-ethylene glycol) hydrogels. J Biomed Mater Res 1998; 42: 312-320.

[53] Frazier DD, Lathi VK, Gerhart TN, Hayes WC. Ex vivo degradation of a poly (propylene glycol-fumarate) biodegradable particulate bone cement. J Biomed Mater Res 1997; 35: 383-389.

[54] Kharas GB, Kamanetsky M, Simantirakis J, Beinlich KC, Rizzo A-MT, Caywood GA, Watson K. Synthesis and characterization of fumarate-based polyesters for use in bioresorbable bone cement composites. J Appl Polym Sci 1997; 66: 1123-1137.

[55] Paige KT, Cima LG, Yaremchuck MJ, Vacant JP, Vacant CA. Injectable cartilage. Plast Reconstr Surg 1995; 96: 1390-1400.

[56] Paige KT, Cima LG, Yaremchuck MJ, Vacant JP, Vacant CA. De novo cartilage generation using calcium-alginate-chondrocyte constructs. Plast Reconstr Surg 1996; 97: 168-180.

[57] Kulseng B, Skjak-Braek G, Ryan L, Andersson A, King A, Faxvaag A, Espevik T. Transplantation of alginate microcapsules. Transplantation 1999; 67: 978-984.

[58] Martinetti R, Dolcini L, Ravaglioli A, Krajewski A, Mangano C. Experimental study on hydroxyapatite/N-carboxymethyl chitosan fillers. In: Sedel L, Rey C, editors. Bioceramics, vol. 10. Oxford, UK: Elsevier, 1997. p.503-506.

[59] Maruyama M, Ito M. *In vitro* properties of a chitosan-bonded self hardening paste with hydroxyapatite granules. J Biomed Mat Res 1996; 32: 527-532.

[60] Dupraz A, Nguyen TP, Richard M, Daculsi G, Passuti N. Influence of a cellulosic ether carrier on the structure of biphasic calcium phosphate ceramic particles in an injectable composite material. Biomaterials 1999; 20: 663-673.

[61] Misiek DJ, Kent JN, Karr RF. Soft tissue responses to hydroxylapatite particles of different shapes. J Oral Maxillofac Surg 1984; 42: 150-160.

[62] Paul W, Sharma CP, Infection resistant hydroxyapatite/alginate plastic composite, J Mat Sci Lett 1997; 16: 2050-2051.

[63] Parsons JR, Ricci JL, Alexander H, Bajpai PK. Osteoconductive grouts for orthopedic use. In: Ducheyne P, Lemons J, editors. Bioceramics: materials characteristics versus *in-vivo* behaviour, vol. 523. New York, USA:. The New York Academy of Sciences, 1988. p.190-207.

[64] Kuo CK, Ma PX. Ionically crosslinked alginate hydrogels as scaffolds for tissue engineering: Part I. Structure, gelation rate and mechanical properties. Biomaterials 2001; 22: 511-521.

[65] Rowley JA, Madlambayan G, Mooney DL. Alginate hydrogels as synthetic extracellular matrix materials. Biomaterials 1999; 20: 45-53.

[66] Alsberg V, Anderson K, Albeiruti A, Franceschi, Mooney DJ. Cell interactive alginate hydrogels for bone tissue engineering. J Dent Res 2001; 80: 2025-2029.

[67] Blandino A, Macias M, Cantero D. Glucose oxidase release from calcium alginate gel capsules. Enzyme and Microb Technol 2000; 27: 319-324.

[68] Gombotz WR, Wee SF. Protein release from alginate matrices. Adv Drug Deliv Rev 1998; 31: 267-285.

[69] Otsuka M, Matsuda Y, Fox JL, Higuchi WI, Yu D, Wong J. A novel skeletal drug delivery system for anti bacterial drugs using self-setting hydroxyapatite cement. Chem Pharm Bull (Tokyo) 1990; 38: 3500-3502.

[70] Queiroz AC, Santos JD, Monteiro FJ, Gibson IR, Knowles JC. Adsorption and release studies of ampicillin from hydroxyapatite and glass-reinforced hydroxyapatite composites. Biomaterials 2001; 22: 1393-1400.

[71] Guicheux J, Grimandi G, Trecant M, Faivre A, Takahashi S. Apatite as a carrier for growth hormone: *in vitro* characterization of loading and release. J Biomed Mater Res 1997; 34: 165-170.

[72] Grabowski GA, Leslie N, Wenstrup R. Enzyme therapy for Gaucher disease: the first 5 years. Blood Rev 1998; 12: 115-133.

[73] Barrias CC, Ribeiro CC, Rodrigues D, Sá Miranda MC, Barbosa MA. Effect of calcium phosphate addition to alginate microspheres: modulation of enzyme release kinetics and improvement of osteoblastic cell adhesion. Key Eng Mater 2005; 284-286: 689-692.

[74] Mooney DJ, Langer RS. Engineering biomaterials for tissue engineering: the 10-100 micron size scale. In: Bronzino JD, editor. The Biomedical Engineering Handbook. Connecticut, USA. CRC Press in cooperation with IEEE Press, 1995. p.1609-1618.

[75] Hing KA, Best SM, Bonfield W. Characterisation of porous hydroxyapatite. J Mater Sci: Mater Med 1999; 3: 135-160.

[76] Lu JX, Flautre B, Anselme K, Hardouin P, Gallur A, Descamps M, Thierry B.Role of interconnections in porous bioceramics on bone recolonization *in vitro* and *in vivo*. J Mater Sci: Mater Med 1999; 10: 111-120.

[77] Rodriguez-Lorenzo LM, Vallet-Regi M, Ferreira JMF. Fabrication of porous hydroxyapatite bodies by a new direct consolidation method: starch consolidation. J Biomed Mater Res 2002; 60: 236-240.

[78] Yuan H, Van Den Doel M, Li Shihong, Van Blitterswijk CA, De Groot K, De Bruijn JD. A comparison of the osteoinductive potential of two calcium phosphate ceramics implanted intramuscularly in goats. J Mater Sci: Mater Med 2002; 13: 1271-1275.

[79] Peon E, Fuentes G, Delgado JA, Morejon L, Almirall A, Garcia R. Preparation and characterization of porous blocks of synthetic hydroxyapatite. Latin Am Appl Res 2004; 34: 225-228.

[80] Oliveira JFD, Aguiar PFD, Rossi AM, Soares GA. Effect of process parameters on the characteristics of porous calcium phosphate ceramics for bone tissue scaffolds. Art Org 2003; 27: 406-411.

[81] Silva MP, Lemos AF, Ferreira JM, Santos JD. Porous glass reinforced hydroxyapatite materials produced with different organic additives. J Non-Cryst Sol 2002; 304: 286-292.

[82] Rejda BV, Peelen JGJ, de Groot K. Tricalciumphosphate as a bone substitute. J Bioeng 1977; 1: 93-97.

[83] Zhang R, Ma PX. Synthetic nano-fibrillar extracellular matrices with predesigned macroporous architectures. J Biomed Mater Res 2000; 52: 430-438.

[84] White E, Shors EC. Biomaterial aspects of Interpore-200 porous hydroxyapatite. Dental Clinics of North America 1986; 30(1): 49-67.

[85] Thomson RC, Yaszemski MJ, Powers JM, Mikos AG. Hydroxyapatite fiber reinforced poly (alpha-hydrogen ester) for bone regeneration. Biomaterials 1998; 19: 1935-1943.

[86] Tadic D, Beckmann F, Schwartz K, Epple M. A novel method to produce hydroxyapatite objects with interconnecting porosity that avoids sintering. Biomaterials 2004; 25: 3335-3340.

[87] Kwon S-H, Hong S-H, Lee I-S, Kim H-E. Calcium phosphate bioceramics with various porosities and dissolution rates. J Amer Cer Soc 2002; 85: 3129-3131.

[88] Fabbri M, Celotti GC, Ravaglioli A. Hydroxyapatite-based porous aggregates: physico-chemical nature, structure, texture and architecture. Biomaterials 1995; 16: 225-228.

[89] Posner AS. The mineral of bone. Clinical Orthopaedics 1985; 200: 87-99.

[90] Williams G, Sallis JD. Structural factors influencing the ability of compounds to inhibit hydroxyapatite formation. Calcif Tissue Int 1982; 34: 169-174.

[91] LeGeros RZ, Shirra WP, Miravite MA, LeGeros JP. Amorphous calcium phosphates: synthetic and biological. Colloques Internationaux C.N.R.S. - Physico-chimie et cristallographie d'intérêt biologique 1973; 230:105-115.

[92] Barrias CC, Ribeiro CC, Lamghari M, Sá Miranda MC, Barbosa MA. Proliferation, activity and osteogenic differentiation of bone marrow stromal cells cultured on calcium titanium phosphate microspheres. Journal of Biomedical Materials Research A 2005; 72 A: 57-66.

[93] Barrias CC, Ribeiro CC, Barbosa MA. Adhesion and proliferation of human osteoblastic cells seeded on injectable hydroxyapatite microspheres. Key Eng Mat 2004, 254-256: 877-880.

FUTURE WORK

- Compounds with a two-dimensional layered structure can be modified by insertion reactions of guest species with maintenance of the layer structure. Layered titanium phosphates are versatile materials amenable to structural design by modulation of both their ionic frameworks and organic constituents. Further research is needed in order to investigate the applicability of layered titanium phosphates in the biomedical field.

- Research should be pursued in order to better clarify the effect of titanium/aluminium on the molecular structure of hydroxyapatite and confirm the possibility of existence of a synergistic effect between the two cations. Solid state NMR studies could be performed, in order to determine if there are different types of phosphate phases in hydroxyapatite incubated in the presence of the above metals.

- Alginates form stable hydrogels through ionotropic gelation in the presence of Ca^{2+}, Ba^{2+} or Sr^{2+}. It would be of interest to prepare HAp-alginate microspheres using Sr^{2+} as the crosslinking agent instead of Ca^{2+} since it is well established that Sr stimulates bone formation. Regarding the sintered microspheres, the possibility of incorporation of Sr in the HAp lattice during sintering process is to be explored.

- Injectable materials must present adequate rheological characteristics. Their viscous properties must be balanced so that they can be easily manipulated and, at the same time, be malleable and adaptable to the irregular wound site where they must remain. The sintered and the non-sintered microspheres must be suspended in an

appropriate vehicle prior to injection. Rheological studies concerning the choice of the vehicle and the conditions for the injection are also of great importance.

- The possibility of using the microspheres developed in this work (the sintered and the non-sintered ones) for the immobilisation and release of growth factors and other proteins or enzymes that have crucial importance in bone remodelling is to be explored.

- In an enzyme delivery system, the retention of the activity of the enzyme is a very important criterion for the evaluation of the efficacy of the system. In a subsequent work, (see annex - paper 3), it was demonstrated that GCR activity is maintained when CTP powders are used as a matrix for the immobilisation of the enzyme. A higher catalytic efficiency is observed in this case in opposition to HAp powders matrix where some degree of inactivation occurs. Further studies should be carried out in order to evaluate the activity of the GCR enzyme after being released from the ceramic-alginate microspheres developed in this work.

- In a porous ceramic scaffold for bone regeneration, the size, morphology, volume content and connectivity of the pores are factors that have a direct influence on bone formation. The porosity of the ceramic microspheres described in chapter 7 was evaluated by SEM observation. Further analytical techniques, namely mercury porosimetry could also be used in order to better characterise the volume content and distribution of the pores in the microspheres, as well as to assess interconnectivity of the pore structure.

- The biological performance of the microspheres prepared in this study needs to be evaluated in a suitable animal model.

RELATED PAPERS TO WHICH THE AUTHOR HAS CONTRIBUTED

ADHESION AND PROLIFERATION OF HUMAN OSTEOBLASTIC CELLS SEEDED ON INJECTABLE HYDROXYAPATITE MICROSPHERES

Cristina C. Barrias[1,2] Cristina C. Ribeiro[1,3] and Mário A. Barbosa [1,2]

1 - INEB - Instituto de Engenharia Biomédica, Laboratório de Biomateriais, Rua do Campo Alegre 823, Porto 4150-180, Portugal
2 - FEUP - Faculdade de Engenharia da Universidade do Porto, Dep. de Eng. Metalúrgica e de Materiais, Porto, Portugal
3 - ISEP - Instituto Superior de Engenharia do Porto, Dep. de Física, Porto, Portugal

Abstract

In the present work, the interaction of human osteoblast-like MG63 cells with novel hydroxyapatite (HAp) microspheres was investigated. Cells were seeded on the microspheres and incubated for up to 7 days. The cell-material constructs were visualised by scanning electron microscopy and confocal laser scanning microscopy, and the rate of cell proliferation was estimated using the Neutral Red assay. The results showed that osteoblastic cells were able to adhere and proliferate on the HAp microspheres, which are intended to be used as injectable support-materials for bone regeneration.

Keywords: injectable microspheres, hydroxyapatite, bone regeneration, osteoblast-like MG63 cells

Published in: Key Engineering Materials 2004; 254-256: 877-880.

Introduction

The use of injectable biomaterials for bone regeneration purposes has received much attention recently.[1] The main advantage of such strategy relies on the possibility of filling defects of different shapes and sizes, while requiring only minimally invasive techniques for implantation, which provide less patient discomfort. Microparticles, suspended on appropriate vehicles, are among the most common forms of injectable materials. Once implanted, they are expected to conform to the irregular implant site, with more or less close packing, and to encourage host cell migration, attachment, proliferation and differentiation. The interstices between the particles, if presenting an appropriate size, may also provide a space for both tissue and vascular ingrowth.

In a previous work, a novel route for the preparation of calcium-phosphate microspheres was described.[2,3] The ceramic granules are first mixed with alginate, which enables the preparation of homogeneous spherical particles through ionotropic gelation in the presence of Ca^{2+}. The spherical particles are subsequently sintered to burn-off the polymer and fuse the ceramic granules, producing pure hydroxyapatite (HAp) microspheres.[2,3] In the present study, the ability of HAp microspheres to support the adhesion and growth of human osteoblastic cells was investigated using the MG63 cell line.

Materials and Methods

HAp microspheres were prepared as previously described.[2,3] Briefly, HAp powder (CAM Implants) pre-heated at 1000ºC was mixed with sodium alginate solution (3% w/v) at a ratio of 0.2 w/w and well homogenised. The paste was extruded drop-wise into a 0.1M $CaCl_2$ crosslinking solution, where spherical-shaped particles instantaneously formed and were allowed to harden for 30 min. The size of the microspheres was controlled by regulating the extrusion flow rate using a syringe pump and by applying a coaxial air stream (Encapsulation Unit Var J1, Nisco). At completion of the gelling period, microspheres were recovered and rinsed in water in order to remove the excess $CaCl_2$. Finally, they were dried overnight in a vacuum-oven at 30ºC, and then sintered at 1100ºC for 1 hr, with a uniform heating rate of 5ºC/min from room temperature.

The size of the microspheres was determined using a laser scanner particle size analyzer (Coulter Electronics), and their morphology was analyzed by optical microscopy.

Cell culture studies were performed using MG63 osteoblast-like cells, which express a number of features characteristic of relatively immature osteoblasts. Cells were routinely maintained in α-MEM supplemented with 10% v/v foetal calf serum, 2.5 μg/ml fungizone and 50 μg/ml gentamicine. Microspheres were steam-sterilised (120ºC, 20 min) and pre-incubated in culture medium over-night in non-tissue culture plates, to avoid cell adhesion on the bottom of the wells. MG63 cells were seeded on the microspheres at 500 cells/mg and incubated at 37ºC in a humidified atmosphere of 5% v/v CO_2 in air for 4 hrs, or 1, 3, 5 and 7 days with the medium being replaced every 2 days.

Cell proliferation was estimated using the Neutral Red (NR) assay. Cells seeded on tissue culture grade polystyrene (TCPS) plates were used as a control. Cell morphology was visualised at different time points by scanning electron microscopy (SEM) and confocal laser scanning microscopy (CLSM).

Results and Discussion

The granulometric analysis of the microspheres (Fig. 1a) revealed that the size distribution of the main population of particles is narrow and follows a normal distribution, with 90% (in volume) of the particles being smaller than 600 μm and having an average diameter around 550 μm. A second population of microspheres with an average diameter around 1000 μm and corresponding to approximately 4% of the particles was also identified. Sieving could easily eliminate these larger microspheres, which result from occasional particle-particle aggregation during the extrusion process. An optical micrograph of the microspheres is presented in Fig. 1b and illustrates their uniformity.

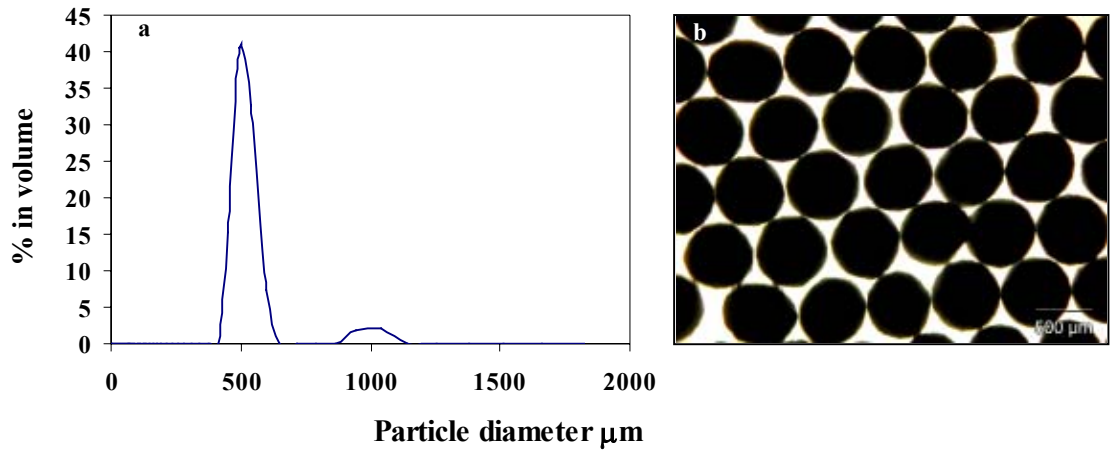

Figure 1. (a) Particle size distribution and (b) optical microscopy image of the HAp microspheres.

SEM analysis of the cell-microspheres constructs revealed that after an initial period of capacity to proliferate and differentiate in contact with the material, this initial phase is of critical importance.[4] After 1 day (Fig. 2b and 2c) several cells exhibiting a spindle-like 4 hrs (Fig 2a), some adherent cells could already be observed on the surface of the microspheres. Because the ability of cells to attach, adhere and spread will influence their morphology were dispersed on the surface of the microspheres. Some round cells (possibly mitotic cells) were also present.

At day 5 (Fig. 2d to 2f), cells were well flattened exhibiting numerous filopodial-like extensions and cell-cell contact points. Finally, at day 7 (Fig 2g to 2i) the microspheres were almost completely covered by cells that formed continuous layers in some regions.

The distribution of cells on HAp microspheres (day 5) was also visualised using CLSM. (Fig. 3a). Pictures constructed by superimposing images obtained using both the fluorescence and reflection channels showed numerous cells on the surface, a result similar to the one obtained by SEM.

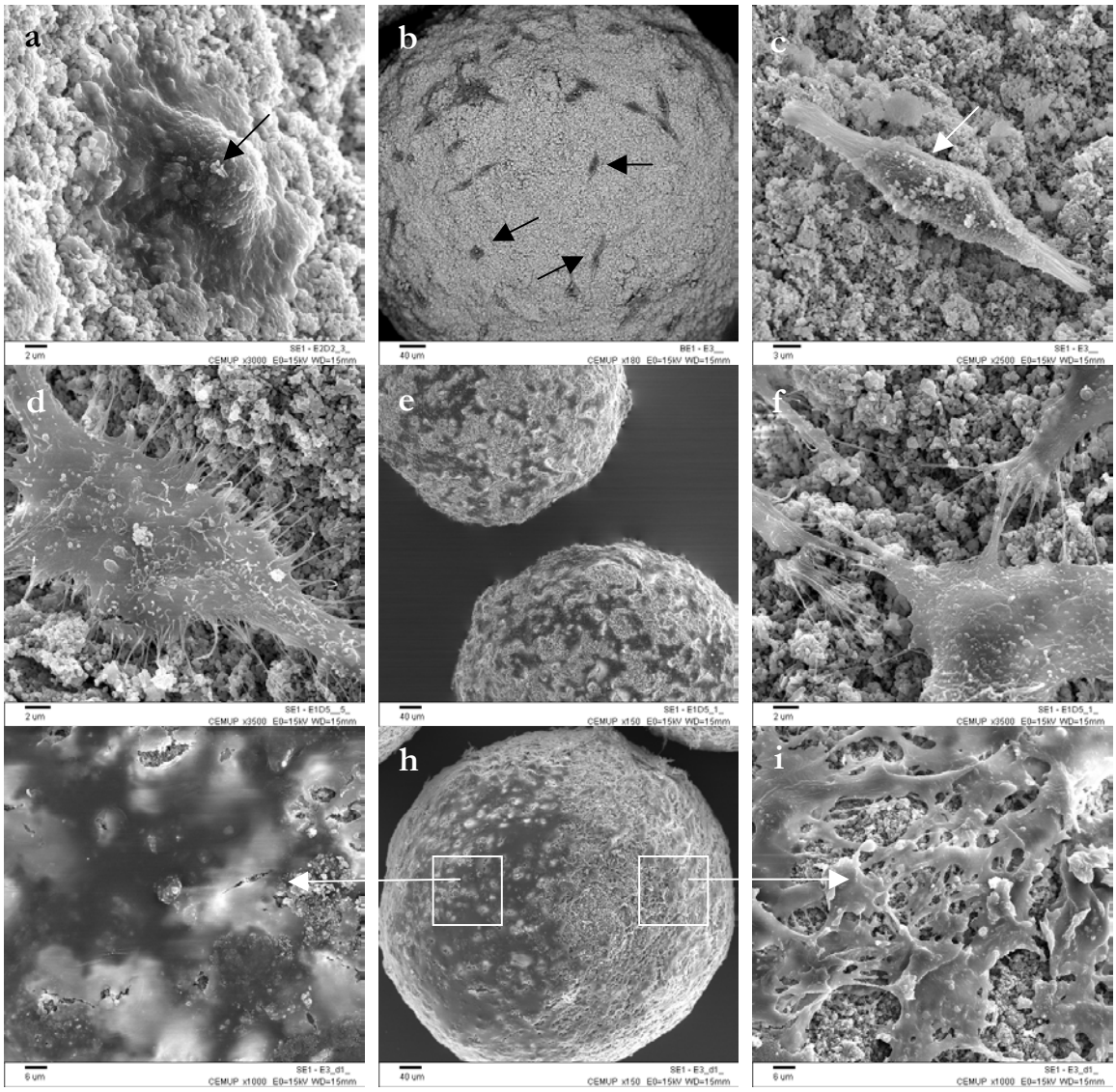

Figure 2. SEM images (several magnifications) showing MG63 human osteoblastic cells on the surface of hydroxyapatite microspheres after an incubation period of 4 h (a), 1 day (b- image obtained with the backscattered electrons mode and c), 5 days (d-f) and 7 days (g-i).

The number of viable cells on the surface of the microspheres was evaluated by performing the NR assay at different time points. This assay is based on the incorporation of a vital colorant by viable cells, and its subsequent fixation at anionic sites on the surface of lysosomal membranes. As any alteration of the membranes will result in a diminished fixation of the colorant, only viable cells will be stained, and so the intensity of the developed coloration allows the indirect quantification of the number of viable cells in the sample. Fig. 3b shows that the number of viable cells, both on the surface of the microspheres and on

control TCPS plates, gradually increased along the 7 days in culture, indicating that cells were actively proliferating.

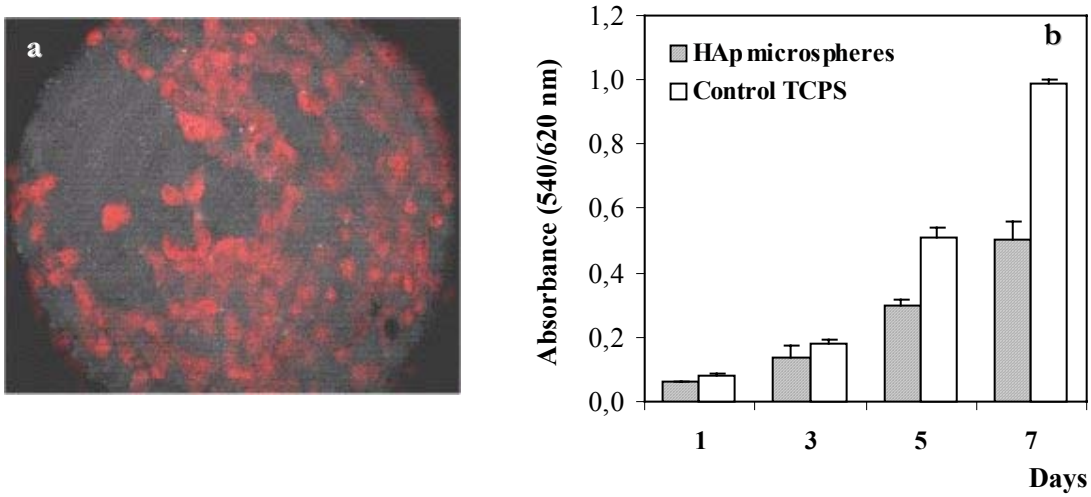

Figure 3. (a) CLSM image showing osteoblastic cells (light grey areas) on the surface of HAp microspheres (day 5), and (b) proliferation of cells on HAp microspheres estimated by the Neutral red assay.

Conclusions

In this study it was demonstrated that HAp microspheres are able to support human osteoblastic cells adhesion and proliferation. Further studies to evaluate the influence of these materials on the expression of the osteoblastic phenotype are in progress.

Acknowledgements

The authors are grateful to Dr. Paula Sampaio (IBMC) for her assistance with CLSM and to programme Praxis XXI from the Portuguese Foundation of Science and Technology (FCT) for awarding Cristina Barrias a scholarship. This work was carried out under contract POCTI/FCB/41523/2001.

References

[1] Temenoff JS and Mikos AG. Injectable biodegradable materials for orthopaedic tissue engineering. Biomaterials 2000; 21: 2405-2412.

[2] Ribeiro CC, Barrias CC and Barbosa MA. Calcium phosphate-alginate microspheres as protein delivery matrices for bone tissue regeneration. Biomaterials 2004; 25: 4363-4373.

[3] Ribeiro CC, Barrias CC and Barbosa MA. A novel route for the preparation of injectable ceramic porous microspheres for bone tissue engineering. In: Ravaglioli A and Krajewski A (ed). Ceramics, Cells and Tissues Annual Conferences: Bioceramic Surfaces Behavior *in vitro* and *in vivo*. Faenza: ISTEC-CNR Editions, 2003. p.228-232.

[4] Anselme K. Osteoblast adhesion on biomaterials. Biomaterials 2000; 21:667-681.

PROLIFERATION, ACTIVITY AND OSTEOGENIC DIFFERENTIATION OF BONE MARROW STROMAL CELLS CULTURED ON CALCIUM TITANIUM PHOSPHATE MICROSPHERES

Cristina C. Barrias[1,2], Cristina C. Ribeiro[1,2,3], Meriem Lamghari[1], Clara Sá Miranda[4] and Mário A. Barbosa[1,2]

1 - INEB - Instituto de Engenharia Biomédica, Laboratório de Biomateriais, Rua do Campo Alegre 823, Porto 4150-180, Portugal
2 - FEUP - Faculdade de Engenharia da Universidade do Porto, Dep. de Eng. Metalúrgica e de Materiais, Porto, Portugal
3 - ISEP - Instituto Superior de Engenharia do Porto, Dep. de Física, Porto, Portugal
4 - IBMC - Instituto de Biologia Molecular e Celular, Porto, Portugal
5 - Instituto de Genética Médica Jacinto de Magalhães, Porto, Portugal

Abstract

In this study, the behaviour of bone marrow stromal cells cultured on calcium titanium phosphate (CTP) microspheres was analysed. Cell adhesion and proliferation were estimated by the neutral red assay and by total DNA quantification. Morphology and deposition of extracellular matrix were assessed by confocal laser scanning microscopy and/or scanning electron microscopy. The expression of the osteoblastic phenotype was evaluated by monitoring alkaline phosphatase activity and osteocalcin secretion. Results revealed that cells were able to attach and spread on the surface of CTP microspheres, and gradually grow into

nearly confluent monolayers. Moreover, cells were able to bridge adjacent microspheres forming cell-microspheres clusters. Cells produced an abundant amount of fibrillar extracellular matrix that covered the substrate surface. Alkaline phosphatase activity peaked around days 7-14 and then decreased until day 21. Cells secreted osteocalcin, with higher levels being detected at day 14 than at day 21. Taken together, these results suggest that CTP microspheres are appropriate scaffolds for the growth and differentiation of cells along the osteoblastic lineage.

Keywords: calcium titanium phosphate, microspheres, bone marrow stromal cells, osteogenic differentiation.

Published in: Journal of Biomedical Materials Research 2005; 72 A: 57-66

Introduction

Microparticulate systems offer exciting possibilities across many fields of regenerative medicine and have been extensively studied for several applications. The most important ones include delivery vehicles for drugs, proteins or genes and matrices for immunoisolation of transplanted cells. Recently, attention has been drawn to the use of microparticles as injectable scaffolds for tissue regeneration.[1-5] Microparticles can be seeded with autologous cells before implantation, functioning as cell-carriers, or designed to encourage host cell migration, attachment, proliferation and differentiation once implanted. The main advantage of this approach, compared with the traditional block scaffolds, is that small particles can be combined with a vehicle and be administered by injection, thus giving the possibility of filling defects of different shapes and sizes through minimally invasive surgery. Upon implantation, the microspheres-vehicle system is expected to easily conform to the irregular implant site, whereas the interstices between the particles may provide a space for both tissue and vascular ingrowth, as required for effective healing.

In cell culture technology, microparticles have been used as an alternative culture-substrate to *in vitro* growth of anchorage-dependent cells, for large-scale cell expansion and/or production of numerous cell products including vaccines, enzymes, antibodies, etc. The concept of culturing cells as monolayers on the surface of small spheres, commonly referred as microcarriers, was first conceived by Van Wezel[6] and different types of microcarriers are currently available in the market. The large surface area-to-volume ratio provided by microcarriers allows easy propagation and high cell yields, and requires much less culture medium and space than traditional monolayer culture techniques. For the culture of some specific types of cells, a microcarrier culture may also present other advantages. For example, the phenotype of chondrocytes[7,8] is better retained in microcarriers than in flat surfaces. Although the exact reasons for this remain uncertain, it has been suggested that the three-dimensional structure provided by microcarriers may better mimic the environment found *in vivo*.[7]

In a previous work, a methodology for the preparation of calcium phosphate microspheres has been described.[9,10] Ceramic granules of hydroxyapatite (HAp) or calcium titanium phosphate (CTP) were mixed with sodium alginate, and microspheres were prepared by drop formation under coaxial air flow, followed by ionotropic gelation in the presence of Ca^{2+}. The particles were subsequently sintered to burn-off the polymer and aggregate the ceramic granules. Besides its simplicity and harmfulness, one of the most important advantages of this method is that it allows the preparation of spherical-shaped particles with an adequate and uniform size.

Calcium phosphate materials have long been recognized as adequate scaffolds for bone regeneration and some are already used in clinical practice. Moreover, they are amenable to sterilization, which is advantageous for both *in vitro* and *in vivo* applications. We have already reported that HAp microspheres promote the attachment and proliferation of human osteoblastic MG63 cells.[5] In the present work, the behavior of bone marrow stromal cells, recognized as osteogenic cells, cultured on CTP microspheres was investigated through analysis of cell attachment and morphology, cell proliferation, deposition of extracellular matrix and expression of osteogenic differentiation markers.

Materials and Methods

Preparation and characterisation of microspheres

Calcium titanium phosphate (CTP, $CaTi_4(PO_4)_6$) microspheres were prepared as reported previously.[9,10] Briefly, CTP was synthesised by solid-state reaction as described elsewhere[10] and mixed at a ratio of 0.4 with 2% w/v sodium alginate (Pronova Biopolymers) aqueous solution. After homogenisation the paste was extruded drop-wise into a 0.1 M $CaCl_2$ crosslinking solution, where spherical-shaped particles instantaneously formed and were allowed to harden for 30 min. The size of the microspheres was controlled by regulating the extrusion flow rate using a syringe pump and by applying a coaxial air stream (Encapsulation Unit Var J1, Nisco). At completion of the gelling period, microspheres were recovered and rinsed in water in order to remove the excess $CaCl_2$. Finally, they were dried overnight in a

vacuum oven at 30ºC, and then sintered at 1100ºC for 1 h, with a uniform heating rate of 5ºC/min from room temperature.

Physicochemical characterisation was performed using Fourier transform infrared (FTIR) spectroscopy. For analysis, microspheres were reduced to powder and analysed as KBr pellets using a Perkin Elmer System 2000 spectrometer. The size of the microspheres was estimated using an inverted platen microscope (Olympus PME3-ADL) equipped with an ocular micrometer with an accuracy of 10 μm, and their morphology was analysed by digital imaging and scanning electron microscopy (SEM). Tissue culture treated polystyrene (TCPS) microcarriers (Biosilon, Nunc™) were used as a control and were also characterised in terms of size and by SEM.

Cell isolation and culture

Rat bone marrow stromal cells were used under consent of the local ethic committee, and were isolated and cultured according to the method of Maniatopoulos *et al.*[11] Briefly, the femurs and tibias of Wistar rats (male, 4 weeks old) were aseptically excised from the hind limbs, the epiphyses were cut-off, and the medullary space was flushed with α-minimal essential medium (Gibco) supplemented with 10% v/v foetal bovine serum, 50 μg/ml gentamicin and 0.3 μg/ml fungizone (standard medium). Cells were plated in 75 cm^2 flasks and incubated at 37ºC in a humidified atmosphere of 5% v/v CO_2. Non adherent cells were removed after 24 h. Adherent cells were subsequently cultured for 1 week, with the medium renewed every 3 days. Cells from the first passage were used.

Cell seeding on microspheres

Microspheres were steam sterilised (120ºC, 20 min), placed in non treated 96-well plates (14 mg/well, c.a. 1-cm^2 surface area) to avoid cell adhesion to the bottom of the wells, and pre incubated in standard medium overnight. TCPS microcarriers (4.5 mg/well, c.a. 1-cm^2 surface area) were used as a control. Cells were seeded at 1.2×10^4 cells/cm^2 in half of the total volume to be used, and microsphere-cell constructs (n=5) were incubated (37ºC, 5% v/v CO_2 in air) in standard medium supplemented with 10^{-8} M dexamethasone, 50 μg/ml

ascorbic acid and 10 mM β-glycerophosphate. The remaining medium was added after 24 h. Medium was renewed every 3 days. Materials without cells processed and cultured under the same conditions were used as references.

Cell adhesion and morphology

The number of adherent cells on the microspheres was assessed by the neutral red (NR). Cell distribution and morphology were analyzed by SEM and by confocal laser scanning microscopy (CLSM). All assays are described in detail below.

NR assay

The culture medium was discarded and replaced by fresh medium containing 50 μg/ml NR (Sigma). Plates were incubated at 37ºC for 3 h. At the end, the supernatant was discarded and microsphere-cell constructs were washed twice with phosphate-buffered saline (PBS). The NR absorbed by the cells was extracted with 1% v/v acetic acid in 50% v/v aqueous ethanol. After being well homogenized on a shaker platform, the supernatants were transferred to another 96-well plate, and the optical density was read at 540 nm with reference to 620 nm ($OD_{540/620}$) in a microplate spectrophotometer. Cell number was determined using the linear region of a standard curve where absorbance was plotted against known numbers of cells counted using a Neubauer chamber.

SEM

Microsphere-cell constructs were washed twice with PBS and fixed in 1.5 % v/v glutaraldehyde in 0.14 M sodium cacodylate (pH 7.4) for 30 min at room temperature. Dehydration was performed by sequential immersion in serial diluted ethanol solutions of 50, 60, 70, 80, 90 and 100% v/v. Samples were then transferred to hexamethyldisilazane and air-dried at room temperature overnight. Finally, the microsphere-cell constructs were sputter-coated with gold using a JEOL JFC-100 Fine Coat Ion Sputter device, and observed using a JEOL JSM-6301F scanning microscope.

CLSM

Microsphere-cell constructs were washed twice with PBS, fixed in 4% v/v formaldehyde (methanol-free; Polyscience) for 15 min, permeabilised with 0.1% v/v Triton X-100 for 5 min and incubated in 10 mg/ml bovine serum albumin and 100 μg/ml RNAse for 45 min at room temperature. F-actin filaments were stained with Alexafluor-conjugated phalloidin (Molecular Probes) for 20 min and nuclei were counterstained with 10 μg/ml propidium iodide (Sigma) for 10 min. Finally, samples were washed with PBS and mounted in Vectashield®. CLSM images were acquired on a BioRad MRC 600 microscope.

Cell proliferation and differentiation

Cell proliferation was assessed by the NR assay (described above) and by total DNA quantification. Levels of alkaline phosphatase (ALP) activity and osteocalcin (OC) secretion, markers of osteoblastic differentiation, were determined.

Microsphere-cell constructs were rinsed twice with PBS and cell lysates were obtained by brief sonication in 1% v/v Triton X-100. The homogenates were centrifuged to remove ceramic particles and used in ALP and total DNA assays. The supernatant culture media were reserved for OC analysis. All assays are described in detail below.

Total DNA quantification

DNA content was determined by the method of Labarca and Paigen[12] using calf thymus DNA as a standard. Briefly, cell lysates were mixed with 0.1 μg/ml bisbenzimide (Hoechst 33258-Sigma) in 10mM Tris-HCl, 1mM ethylenediaminetetraacetic acid and 0.2M NaCl (pH 7.4) and fluorescence was read with excitation at 356 nm and emission at 458 nm.

ALP colorimetric analysis and histochemical staining

ALP was assayed as the hydrolysis of the artificial substrate p-nitrophenol phosphate. Cell lysates were incubated in 2 mM p-nitrophenol phosphate, 0.2 M bicarbonate buffer (pH 10), 0.05% v/v Triton X-100, and 4 mM $MgCl_2$ for 60 min at 37°C. The reaction was stopped by adding 1 M NaOH, and the product was quantified at 405 nm, using a set of p-

nitrophenol standards. For histochemical staining, microsphere-cell constructs were washed twice with PBS, fixed in 4% v/v formaldehyde for 15 min, washed in water and incubated for 30 min in Naphtol AS-MX phosphate/ Fast Violet B salt (Sigma) at room temperature and in the dark. Finally, cells were washed in water, air dried and observed under a stereo microscope (Olympus SZX9).

OC

For analysis of OC, supernatant media were centrifuged for 2 min at 10,000 rpm to remove cell debris, stored at -20ºC and then thawed before analysis. OC was assayed using the Rat-MID Osteocalcin ELISA kit (Osteometer BioTech A/S, Denmark) according to the manufacturer's instructions.

Statistical Analysis

Data are presented as mean±standard deviation (n=5) and were analyzed using the Mann-Whitney U test. Differences between groups were considered statistically different when $p<0.05$.

Results

Preparation and characterisation of CTP microspheres

The CTP-alginate suspension dropped into $CaCl_2$ solution formed gel beads instantaneously. During sintering, the polymer was burned-off and the CTP granules became associated, while the original spherical-shape of the particles was maintained. The average diameter of CTP microspheres was 607±30 μm (n=20), as assessed by optical microscopy. TCPS microcarriers have an average diameter of 205±120 μm. Figure 1 illustrates the spherical-shape of CTP particles [Fig. 1(a)] as well as their uniform size [Fig. 1(b)]. CTP microspheres present a rougher surface than TCPS microcarriers [Fig. 1(c)].

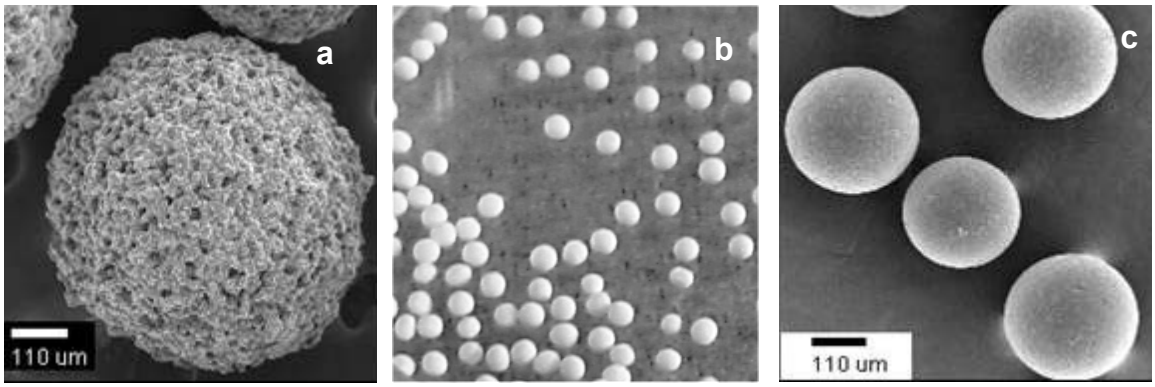

Figure 1. (a) SEM micrograph and (b) photograph (digital camera) of CTP microspheres illustrating their spherical shape and uniform size; (c) SEM micrograph of TCPS microcarriers.

Physico-chemical characterisation was performed by FTIR. The FTIR spectra of CTP powder and CTP microspheres were identical, showing that the ceramic kept its integrity, and for that reason were not included here. In a previous work[10], it was demonstrated that, depending on the ceramic-to-polymer ratio used in the preparation of the microspheres, the structure of CTP may become altered during the subsequent sintering process. In the present study, a high ceramic-to-polymer ratio was selected in order to guarantee the absence of extraneous phases, namely of calcium pyrophosphates, in the sintered microspheres. Further details on the characterisation of CTP microspheres are provided elsewhere.[9,10]

Culture of bone marrow stromal cells on CTP microspheres

Cell attachment, adhesion and spreading

Cells were seeded at approximately the same density per surface area on both materials (1.2×10^4 cells/cm^2). The number of adherent cells after 24 h of incubation was estimated using the NR assay [Fig. 2(a)]. Approximately 16% of the seeded cells attached to CTP microspheres, whereas 46% attached to TCPS microcarriers. After 24 h of culture, both spindle-shaped and well flattened cells were observed by SEM [Fig. 2(b)] on the surface of CTP microspheres.

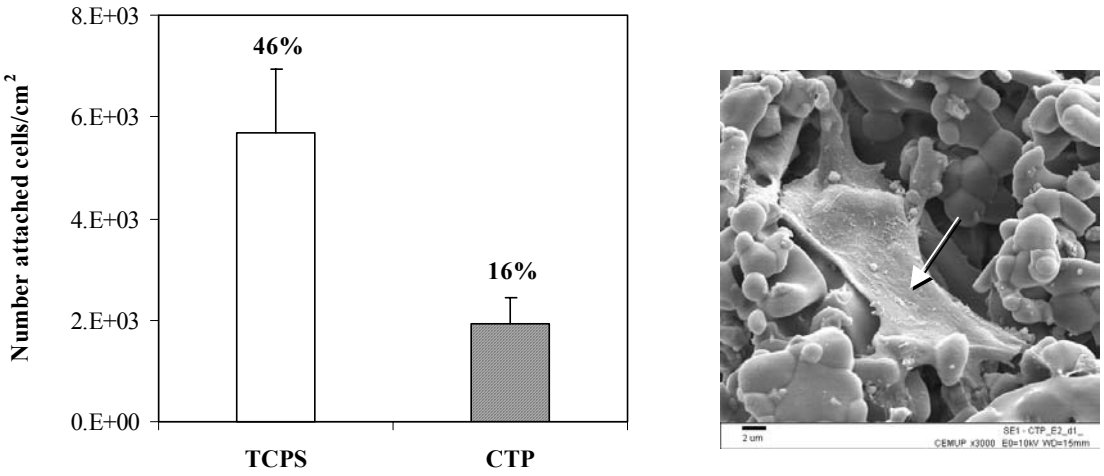

Figure 2. (a) Number of cells per cm^2 attached to CTP and TCPS microspheres following 24 h of incubation. Data labels represent the percentage of attached cells in relation to the amount of cells initially used (1.2×10^4 cells/cm^2); (b) SEM image of a flattened cell on the surface of a CTP-microsphere at 24 h.

CLSM images of bone marrow stromal cells after 5 days of culture on CTP microspheres are presented in Figure 3. Cells were found to be reasonably well distributed between microspheres [Fig. 3(a)]. Cells were able to spread throughout the substrate surface and adopt a typical osteoblast-like morphology [Fig. 3(b)]. Numerous cell-cell contact points were detected and, in some regions, cells started to form continuous cell layers. At higher magnification [Fig. 3(c)], filamentous actin organised in thick stress fibres could be visualised.

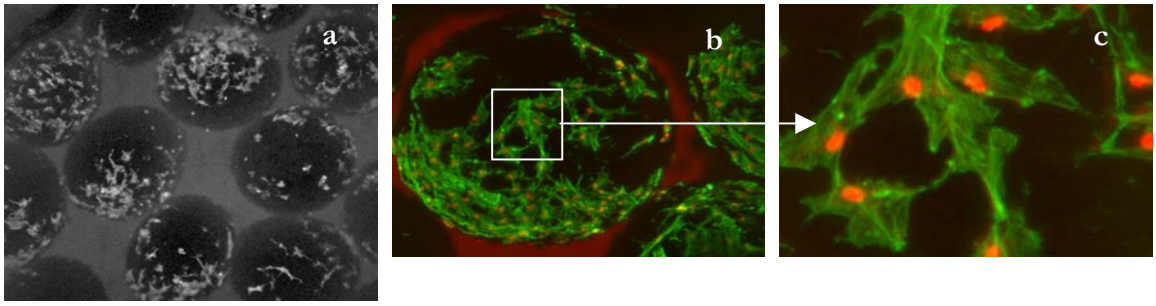

Figure 3. CLSM images of bone marrow stromal cells cultured for 5 days on the surface of CTP microspheres, showing: (a) a uniform distribution of cells between microspheres (original magnification, 50×); (b) cells with a typical osteoblast-like morphology throughout the surface (original magnification, 100×); and (c) filamentous actin organised in thick stress fibres (original magnification, 800×). Cells were stained with phalloidin (F-actin) and counterstained with propidium iodide (DNA).

Cell proliferation and production of extracellular matrix (ECM)

Cell proliferation, estimated by the NR assay and by total DNA quantification, is depicted in Fig. 4 (a, b). Cells proliferated during the first 2 weeks of culture as demonstrated by both assays. The number of cells increased approximately 12 fold in relation to day 1, both on CTP microspheres and on TCPS microcarriers. The gradual increase in DNA content during the same period followed a similar pattern [Fig. 4(b)].

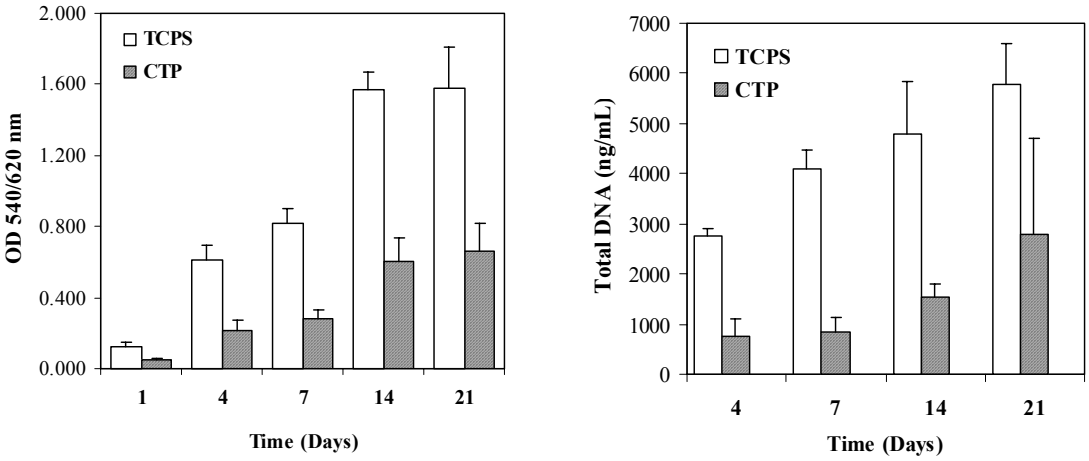

Figure 4. Cell proliferation on CTP microspheres as assessed by: (a) NR assay; (b) total DNA quantification. TCPS microcarriers were used as controls.

SEM images of bone marrow stromal cells cultured for 21 days on the surface of CTP and TCPS microspheres are presented in Figure 5. The surface of CTP microspheres is almost completely covered by dense layers of cuboidal cells [Fig. 5(a, b)] that deposited an abundant amount of ECM, forming a three-dimensional fibril network [Fig. 5 (b, c)]. The presence of ECM could already be detected at day 14 (data not shown). Cells grown on TCPS microcarriers [Fig. 5(d)] exhibit a flat, well-spread appearance and formed confluent monolayers. Cells were able to establish bridges between adjacent CTP microspheres, forming microsphere-cell clusters (Fig. 6).

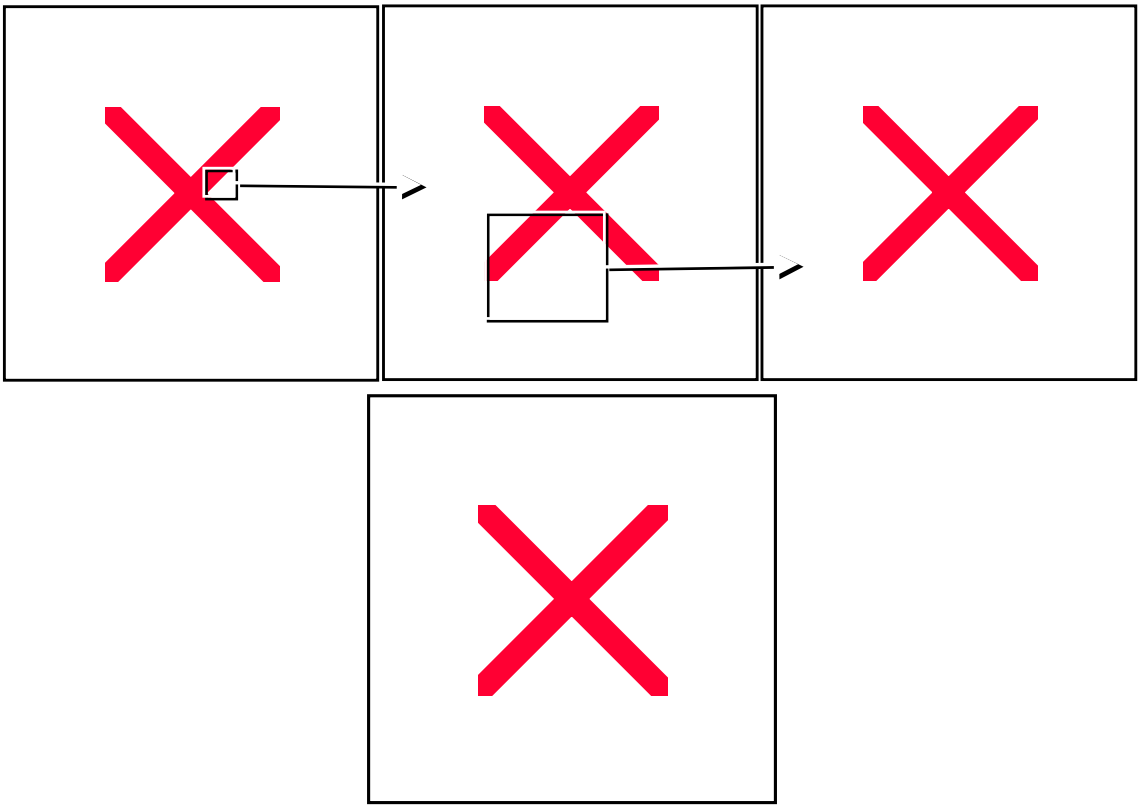

Figure 5. SEM images of bone marrow stromal cells cultured for 21 days on the surface of CTP microspheres, showing: (a, b) the substrate surface almost completely covered by dense layers of bone marrow cells; (b, c) a fibrillar ECM underlying cells; (d) SEM image of bone marrow stromal cells cultured for 21 days on the surface of a TCPS microsphere

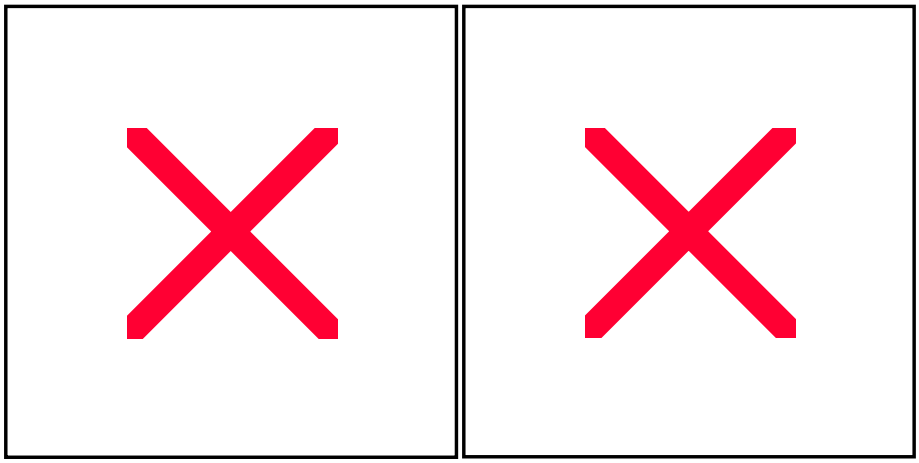

Figure 6. SEM images of bone marrow stromal cells cultured for 21 days on the surface of CTP microspheres, showing the establishment of cell bridges between adjacent microspheres.

Osteogenic differentiation

The expression of the osteoblastic phenotype was evaluated by monitoring ALP activity and OC secretion. Bone marrow stromal cells cultured on microspheres expressed ALP activity as assessed by histochemical staining and colorimetric analysis (Fig. 7). Temporal expression of ALP activity is depicted in Figure 7(a). As shown, ALP activity of cells cultured on CTP microspheres gradually increased along the first 2 weeks of culture, peaked around days 7-14 and then started to decrease. ALP levels were always significantly higher ($p<0.05$) than those of cells cultured on TCPS microcarriers. Histochemical ALP staining of microsphere-cell constructs after 7 days of culture [Fig. 7(b)] showed localised areas with intense staining for ALP (dark gray regions).

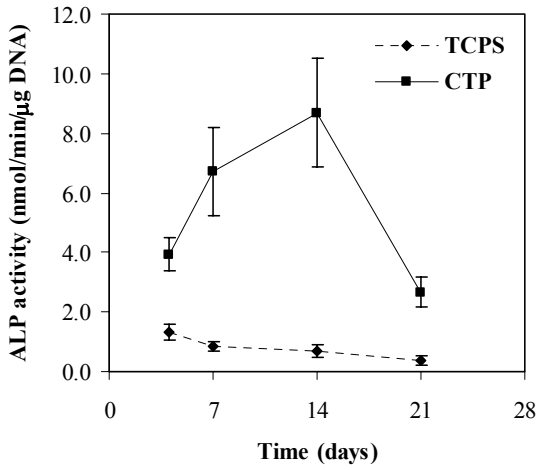

(a)

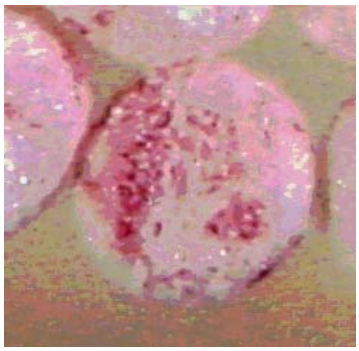

(b)

Figure 7. Expression of ALP activity by bone marrow stromal cells cultured on the surface of CTP microspheres as assessed by: (a) colorimetric analysis; (b) histochemical staining. TCPS microcarriers were used as controls. Differences between days 7 and 14 are not statistically significant, but differences between the two materials are always statistically significant ($p<0.05$).

OC secretion of cells cultured on CTP microspheres (Fig. 8) was higher at day 14 than at day 21 ($p=0.03$), and levels were significantly enhanced when compared with cells grown on TCPS microcarriers ($p=0.03$).

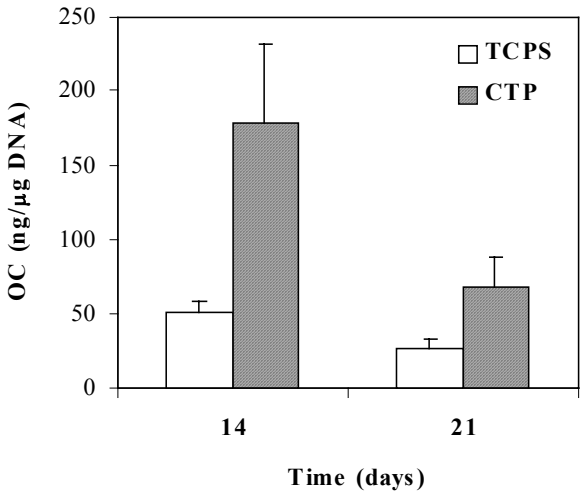

Figure 8. Osteocalcin secretion by bone marrow stromal cells cultured on the surface of CTP microspheres at days 14 and 21. TCPS microcarriers were used as controls. Differences between the two materials, and between days 14 and 21 for each material, are statistically significant ($p=0.03$).

Discussion

In this study, CTP microspheres were investigated for their ability to support adhesion, growth, and osteogenic differentiation of bone marrow stromal cells *in vitro*.

The methodology used to prepare CTP microspheres has been previously reported.[9,10] One of the most important advantages of this method is that it allows the preparation of spherical-shaped particles with an adequate and uniform size. It has been previously suggested[13] that the size and shape of microparticles for bone regeneration have a critical role in new bone formation by dictating the relative arrangement of particles within the implant site. Although some empty space is necessary to allow tissue and capillary ingrowth, excessive interstitial space, associated with the use of very large particles, may favor the development of fibrous tissue and compromise adequate healing. In addition, large particles are more difficult to inject, leading to a more invasive implantation. However, very small particles, as well as particles with broad size distributions, result in dense packing at the defect, which may impair tissue ingrowth and vascularization,[13] and some may be able to migrate from the implant site and cause injury elsewhere. Some authors found superior bone formation around particles

measuring 0.3–0.6 mm, and demonstrated that larger and smaller particles were associated with less bone formation.[13,14] The microparticles' shape is equally important. Irregularly shaped particles have sharp edges that are more susceptible to wear and may damage the surrounding tissue once implanted and/or induce strong inflammatory responses.[15] For all the above reason, it seams that spherical-shaped particles with a uniform and adequate size may present some advantages compared with other type of microparticles described in the literature.

Cell-material interaction studies were performed using rat bone marrow stromal cells. Bone marrow has long been recognized as a source of progenitor stromal cells that can be induced to differentiate along the osteoblastic lineage if cultured under appropriate conditions.[11,16-18] The development of osteoblastic cells from bone marrow stromal precursors is characterized by a sequence of events, involving cell adhesion, proliferation and expression of osteogenic differentiation markers, which are related to the synthesis, deposition and subsequent mineralisation of a collagenous ECM.

The initial phase of the culture is probably the most critical stage, because the ability of cells to attach, adhere and spread will influence their capacity to proliferate and differentiate in contact with the material.[19] In a microparticulate culture, the percentage of attached cells, in relation to the amount initially used, is generally lower than the one obtained using flat surfaces, and the number of cells per microsphere is likely to be distributed over a range. To increase the possibility of cell-microspheres effective collisions, microspheres were inoculated with cells suspended in the smallest possible volume, because often proliferation will only occur if there is a sufficient density of attached cells per microsphere. The percentage of adherent cells after 24 h of culture was lower on CTP microspheres (16%) that on TCPS microcarriers (46%). Despite the lower percent of adhesion, CLSM images of the microsphere-cell constructs after 5 days of culture revealed that CTP microspheres were uniformly colonised by cells, which underwent cytoskeleton reorganisation, spread on the surface and adopted a typical osteoblast-like morphology. Moreover, differences in cell adhesion apparently did not have an effect on growth and activity, because cells proliferated on both substrates at a similar rate, increasing approximately 12 fold in relation to day 1 in 2 weeks, and produced an abundant amount of fibrillar ECM. The results presented in this

study further demonstrated that cells cultured on CTP microspheres are able to differentiate, and that ALP activity and OC secretion levels are significantly enhanced when compared to cells cultured on TCPS microcarriers.

The two substrates differ in terms of size, chemical composition and surface roughness, all of which are likely to influence protein adsorption and ultimately cell behaviour in contact with the materials.[20,21] In particular, CTP microspheres present a rougher surface than TCPS microcarriers, which may partially explain our results, because it has long been known that cell attachment, proliferation and differentiation are sensitive to surface microtopography.[22,23] Several authors have reported altered attachment and enhanced differentiation of osteoblast-like cells on rough surfaces in comparison with smother ones, and suggested that structural features of the surface modulate the expression of phenotypic markers and influence the way cells respond to regulatory factors.[21,22,24] On smooth surfaces, osteoblasts-like cells are able to attach and proliferate but generally assume a more flattened fibroblastic appearance, and express relatively low levels of osteogenic markers.[22]

Regarding the chemical composition of the cell culture substrate, several reports on the positive effects of different types of calcium phosphates on osteogenic differentiation may be found in the literature, and it has already been reported that osteoblastic cells grown on these materials express increased alkaline phosphatase activity and/or OC levels compared with plastic surfaces.[25-27] For the particular case of CTP, Knabe *et al.* examined the effect of this calcium phosphate on the expression of bone-related genes and proteins by human bone-derived cells, and compare it to that of titanium and HAp-coated titanium.[28] They showed that CTP had a more pronounced effect on osteoblastic differentiation, because it induced a greater expression of an array of osteogenic markers than that recorded for cells cultured on the other materials.

Conclusions

Bone marrow stromal cells were cultured for up to 21 days on CTP microspheres. Cells were able to attach, adopt a typical osteoblast-like morphology and gradually proliferate along 2-3 weeks of culture. SEM images showed that the substrate surface becomes almost

completely covered by dense layers of bone cells and a fibrillar ECM. Cells expressed ALP activity and secreted OC, which confirmed that differentiation along the osteoblastic lineage occurred.

Acknowledgements

Cristina C. Barrias is grateful to the Portuguese Foundation for Science and Technology (FCT) for awarding her a scholarship under the programme PRAXIS XXI and to Dr. Paula Sampaio (IBMC) for her assistance with CLSM. This work was carried out under contract POCTI/FCB/41523/2001.

References

1. Senuma Y, Franceschin S, Hilborn JG, Tissieres P, Bisson I, Frey P. Bioresorbable microspheres by spinning disk atomization as injectable cell carrier: from preparation to *in vitro* evaluation. Biomaterials 2000;21(11):1135-44.
2. Hsu FY, Chueh SC, Wang YJ. Microspheres of hydroxyapatite/reconstituted collagen as supports for osteoblast cell growth. Biomaterials 1999;20(20):1931-6.
3. McGlohorn JB, Grimes LW, Webster SS, Burg KJ. Characterization of cellular carriers for use in injectable tissue-engineering composites. J Biomed Mater Res 2003;66A(3):441-9.
4. Wu TJ, Huang HH, Lan CW, Lin CH, Hsu FY, Wang YJ. Studies on the microspheres comprised of reconstituted collagen and hydroxyapatite. Biomaterials 2004;25(4):651-8.
5. Barrias CC, Ribeiro CC, Barbosa MA. Adhesion and proliferation of human osteoblastic cells seeded on injectable hydroxyapatite microspheres. Key Eng Mat 2004;254-256:877-880.
6. van Wezel AL. Microcarrier technology. Present status and prospects. Dev Biol Stand 1983;55:3-9.

7. Malda J, Kreijveld E, Temenoff JS, Blitterswijk CAv, Riesle J. Expansion of human nasal chondrocytes on macroporous microcarriers enhances redifferentiation. Biomaterials 2003;24(28):5153-5161.

8. Frondoza C, Sohrabi A, Hungerford D. Human chondrocytes proliferate and produce matrix components in microcarrier suspension culture. Biomaterials 1996;17(9):879-888.

9. Ribeiro CC, Barrias CC, Barbosa MA. A novel route for the preparation of injectable ceramic porous microspheres for bone tissue engineering. In: Ravaglioli A, Krajewski A, editors. Ceramics, cells and tissues annual conferences: bioceramic surfaces behavior *in vitro* and *in vivo*. Faenza: ISTEC-CNR Editions; 2003. p. 228-232.

10. Ribeiro CC, Barrias CC, Barbosa MA. Preparation and characterisation of calcium-phosphate microspheres for biomedical applications. Submitted to J Mat Sci Mat Med 2004.

11. Maniatopoulos C, Sodek J, Melcher AH. Bone formation *in vitro* by stromal cells obtained from bone marrow of young adult rats. Cell Tissue Res 1988;254(2):317-330.

12. Labarca C, Paigen K. Simple, rapid, and sensitive DNA assay procedure. Anal Biochem 1980;102(2):344-352.

13. Mankani MH, Kuznetsov SA, Fowler B, Kingman A, Robey PG. *In vivo* bone formation by human bone marrow stromal cells: Effect of carrier particle size and shape. Biotechnol Bioeng 2001;72(1):96-107.

14. Higashi T, Okamoto H. Influence of particle size of calcium phosphate ceramics as a capping agent on the formation of a hard tissue barrier in amputated dental pulp. J Endod 1996;22(6):281-3.

15. Misiek DJ, Kent JN, Carr RF. Soft tissue responses to hydroxylapatite particles of different shapes. J Oral Maxillofac Surg 1984;42(3):150-60.

16. Maniatopoulos C. Bone formation by young adult bone marrow stromal cells *in vitro*. J Dent Res 1987;66:104-104.

17. Pittenger MF, Mackay AM, Beck SC, Jaiswal RK, Douglas R, Mosca JD, *et al.* Multilineage potential of adult human mesenchymal stem cells. Science 1999;284(5411):143-7.

18. Ter Brugge PJ, Jansen JA. *In vitro* osteogenic differentiation of rat bone marrow cells subcultured with and without dexamethasone. Tissue Eng 2002;8(2):321-31.

19. Anselme K. Osteoblast adhesion on biomaterials. Biomaterials 2000;21(7):667-81.

20. Anselme K, Linez P, Bigerelle M, Le Maguer D, Le Maguer A, Hardouin P, *et al.* The relative influence of the topography and chemistry of TiAl6V4 surfaces on osteoblastic cell behaviour. Biomaterials 2000;21(15):1567-77.

21. Deligianni DD, Katsala ND, Koutsoukos PG, Missirlis YF. Effect of surface roughness of hydroxyapatite on human bone marrow cell adhesion, proliferation, differentiation and detachment strength. Biomaterials 2001;22(1):87-96.

22. Boyan BD, Lossdorfer S, Wang L, Zhao G, Lohmann CH, Cochran DL, *et al.* Osteoblasts generate an osteogenic microenvironment when grown on surfaces with rough microtopographies. Eur Cell Mater 2003;6:22-7.

23. Brunette DM. The effects of implant surface topography on the behavior of cells. Int J Oral Maxillofac Implants 1988;3(4):231-46.

24. Schwartz Z, Lohmann CH, Oefinger J, Bonewald LF, Dean DD, Boyan BD. Implant surface characteristics modulate differentiation behavior of cells in the osteoblastic lineage. Adv Dent Res 1999;13:38-48.

25. Shu R, McMullen R, Baumann MJ, McCabe LR. Hydroxyapatite accelerates differentiation and suppresses growth of MC3T3-E1 osteoblasts. J Biomed Mater Res 2003;67A(4):1196-1204.

26. Nordstrom E, Ohgushi H, Yoshikawa T, Yokobori AT, Yokobori T. Osteogenic differentiation of cultured marrow stromal stem cells on surface of microporous hydroxyapatite based mica composite and macroporous synthetic hydroxyapatite. Biomed Mater Eng 1999;9(1):21-26.

27. Oreffo ROC, Driessens FCM, Planell JA, Triffitt JT. Growth and differentiation of human bone marrow osteoprogenitors on novel calcium phosphate cements. Biomaterials 1998;19(20):1845-1854.

28. Knabe C, Berger G, Gildenhaar R, Klar F, Zreiqat H. The modulation of osteogenesis *in vitro* by calcium titanium phosphate coatings. Biomaterials 2004;25:4911-4919.

Annex C

EFFECT OF CALCIUM PHOSPHATE ADDITION TO ALGINATE MICROSPHERES: MODULATION OF ENZYME RELEASE KINETICS AND IMPROVEMENT OF CELL ADHESION

Cristina C. Barrias,[1,2] Cristina C. Ribeiro,[1,2,3] Daniel Rodrigues,[4] M. Clara Sá Miranda,[4] and Mário A. Barbosa[1,2]

1 - INEB - Instituto de Engenharia Biomédica, Laboratório de Biomateriais, Rua do Campo Alegre 823, Porto 4150-180, Portugal
2 - FEUP - Faculdade de Engenharia da Universidade do Porto, Dep. de Eng. Metalúrgica e de Materiais, Porto, Portugal
3 - ISEP - Instituto Superior de Engenharia do Porto, Dep. de Física, Porto, Portugal
4 - IBMC - Instituto de Biologia Molecular e Celular, Porto, Portugal

Abstract

In this study, the addition of calcium phosphate powders to an alginate matrix was evaluated as a strategy to modulate enzyme release-kinetics from alginate microspheres and, simultaneously, to improve cell adhesion to the polymer. Pre-adsorption of the enzyme to the ceramic powders resulted in a more adequate release pattern. The ratio of ceramic-to-polymer had a pronounced effect on osteoblast adhesion to microspheres. Cells were only able to spread on microspheres with the highest percentage of ceramic (0.4 w/w using a 1.5% w/v alginate solution).

Keywords: alginate, calcium titanium phosphate, cell adhesion, enzyme release, hydroxyapatite, microspheres

Published in: Key Engineering Materials 2005; 284-286: 689-692.

Introduction

The activity of the enzyme glucocerebrosidase (GCR) is deficient in type I Gaucher disease (GD), a genetic disturbance that characteristically results in severe haematological abnormalities, organomegaly and skeletal deterioration [1]. The currently available treatment is based on the intravenous administration of exogenous enzyme, and it seems to be efficient in reverting most of the symptoms [1]. However, in terms of bone pathology, which is among the most disabling manifestations of GD (type 1), a slow and incomplete response to the treatment is observed, even when high doses are used, indicating that adjuvant therapies are necessary in order to consistently restore enzyme activity in bone [1]. An injectable vehicle for local GCR-delivery to bone is currently under investigation. GCR was previously entrapped in alginate microspheres, retaining full activity and exhibiting improved stability at physiological pH. Studies using GCR-deficient cells from a GD patient showed that released GCR was internalised by cells, significantly enhancing their residual enzymatic activity, with only one half of the dose required using free-GCR. However, release profiles were inadequate, being characterised by a high burst effect followed by incomplete release. As a strategy to modulate GCR release-kinetics and at the same time improve osteoblastic cell adhesion to alginate microspheres, calcium phosphate powders of hydroxyapatite (HAp) or calcium titanium phosphate (CTP) were added to the polymeric matrix and ceramic-alginate microspheres were prepared by droplet extrusion followed by ionotropic gelation with Ca^{2+}. In this study, GCR release kinetics and osteoblast adhesion to ceramic-alginate microspheres of different compositions were analysed

Materials and Methods

Preparation and characterisation of HAp-alginate and CTP-alginate microspheres

HAp or CTP powders were mixed with Na-alginate solution (1.5 and 3% w/v) at different ratios (0.1, 0.2 and 0.4 w/w). The different formulations are designated in the text as 40/1.5 (0.4 w/w ceramic using 1.5% w/v Na-alginate) and 10/3, 20/3 and 40/3 (0.1 to 0.4 w/w ceramic, using 3% w/v Na-alginate). The paste was extruded drop-wise into a $CaCl_2$

bath, where microspheres were instantaneously formed. Size was controlled by applying a coaxial air stream. After 30 min, microspheres were recovered and rinsed in water. Characterisation was carried out by FTIR and SEM. Diameters were measured using an optical microscope with an ocular micrometer.

GCR entrapment in HAp-alginate and CTP-alginate microspheres and release studies

Radiolabeled enzyme (^{125}I-GCR, Iodogen method) was incorporated in the polymeric/ceramic paste prior to extrusion in two different ways: directly dispersed in the paste or pre-adsorbed onto the ceramic particles. Ceramic-alginate microspheres with entrapped GCR were then prepared as already described. Alginate microspheres with entrapped GCR were used as controls. For enzyme adsorption, the ceramic powders were immersed in 0.1 mg/ml GCR solution in phosphate buffered saline (PBS, pH 7.4) and incubated at room temperature for 30 min under agitation. A control GCR solution at 0.1 mg/ml was incubated under the same conditions (without powders) to account for eventual enzyme losses due to adsorption to the tubes walls. At the end, powders were washed in PBS and separated by centrifugation. To determine the amount of adsorbed GCR, the concentration of enzyme in the supernatants before and after adsorption was quantified by the bicinchoninic acid method. GCR activity in the supernatants and in the powders was assayed as the hydrolysis of the substrate 4-methylumbelliferyl-β-D-glucopyranoside (5 mM) in 50-100 mM citrate-phosphate buffer (pH 5.5) and in the absence of activators. GCR release studies from the different matrices were performed in PBS at 37ºC and 120 rpm. At predefined time intervals, aliquots from the supernatants were collected and counted for radioactivity and fresh PBS was added to maintain a constant volume.

Cell adhesion studies

Microspheres were pre-incubated in 70% v/v ethanol, equilibrated overnight in α-Minimal Essential Medium (α-MEM) supplemented with 10% v/v foetal bovine serum, and finally seeded with osteoblast-like MG63 cells. Alginate and HAp microspheres were used as controls. After 24 h, cells-microspheres constructs were visualised by SEM and by confocal

laser scanning microscopy (CLSM). For CLSM, f-actin filaments were stained with Alexafluor 488-conjugated phalloidin (Molecular Probes) and nuclei were counterstained with propidium iodide.

Results and Discussion

Preparation and characterisation of HAp-alginate and CTP-alginate microspheres

Spherical-shaped microparticles presenting a uniform size (Fig.1a) were prepared. The diameters of CTP-alginate microspheres ranged from 450±14 μm to 796±39 μm, while the diameters of HAp-alginate microspheres ranged from 412±23 μm to 749±22 μm, both depending on the formulation. SEM images of both types of microspheres revealed that the ceramic particles are well embedded and homogeneously distributed in the alginate matrix as illustrated in Fig.1b (20/3 HAp-alginate microspheres). FTIR analysis (data not shown) indicates that the characteristic spectral bands of both ceramics are maintained in the microspheres, in comparison with the starting powders, suggesting that the alginate did not induce subsequent modifications in the ceramics structure.

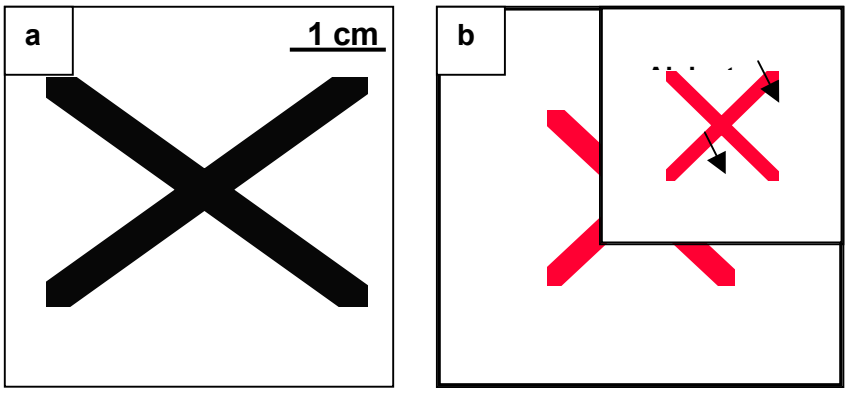

Fig 1. a) Photograph of 40/3 CTP-alginate microspheres illustrating their uniform size; b) SEM micrograph of the surface of a 20/3 HAp-alginate microsphere showing the ceramic particles embedded in the polymeric matrix

GCR entrapment in HAp-alginate and CTP-alginate microspheres and release studies

The enzyme was incorporated in the ceramic-alginate paste prior to the preparation of the microspheres in two different ways: directly dispersed in the paste or pre-adsorbed onto the ceramic particles. The ceramic powders used were characterised by a specific surface area of 9.8 cm^2/mg (CTP) and 76.0 cm^2/mg (HAp). Adsorption was performed at pH 7.4, which is near the enzyme isoelectric point (in the range 7 to 8) where the enzyme exhibits higher structure stability and therefore a smaller tendency to denaturate upon adsorption. The amount of adsorbed GCR was calculated by quantifying GCR depletion from the supernatant. Preliminary assays showed that the incubation time selected (30 min) was sufficiently long to attain steady-state adsorption values. GCR has higher affinity for CTP powder, which adsorbed 41.8±1.1 ng GCR/cm^2, than for HAp, which adsorbed 4.3±0.4 ng GCR/cm^2. The variation in plateau values for the two ceramics is probably related to differences in protein-surface electrostatic interactions. Fig. 2a depicts GCR activity in the initial solution (free enzyme only) and in the presence of the two ceramic powders after adsorption (free + adsorbed enzyme) as a function of the GCR amount in the assay. In all cases, GCR activity increases linearly with the amount of enzyme present, but while in the presence of HAp there is some degree of inactivation, in the presence of CTP a higher catalytic efficiency was observed. Differences probably result from GCR conformational alterations in the adsorbed state. The specific activity (activity per unit mass) of GCR adsorbed on CTP and HAp powders after washing and re-suspending in fresh PBS (adsorbed enzyme only) were c.a. 91.5±4.9% and 10.3±0.1% of the control (free enzyme), respectively. These values may however be underestimated due to enzyme losses by desorption during washing.

Release studies

The two strategies used for GCR entrapment in the alginate matrix resulted in distinct release kinetics, but similar results were obtained for both ceramics tested. Fig. 2 shows typical release profiles obtained with HAp-alginate and alginate microspheres. When GCR was pre-adsorbed onto the ceramic powders prior to microspheres formation the initial burst

was significantly reduced, from c.a. 50% to 11% (t=150 min) compared to the one of alginate microspheres, and a slower and more linear release profile was obtained, showing that release-kinetics modulation was achieved. The release profile of GCR directly dispersed in the ceramic/polymer matrix was not significantly different from the control (data not shown), suggesting that the GCR does not interact, at least to a great extent, with the embedded ceramic particles.

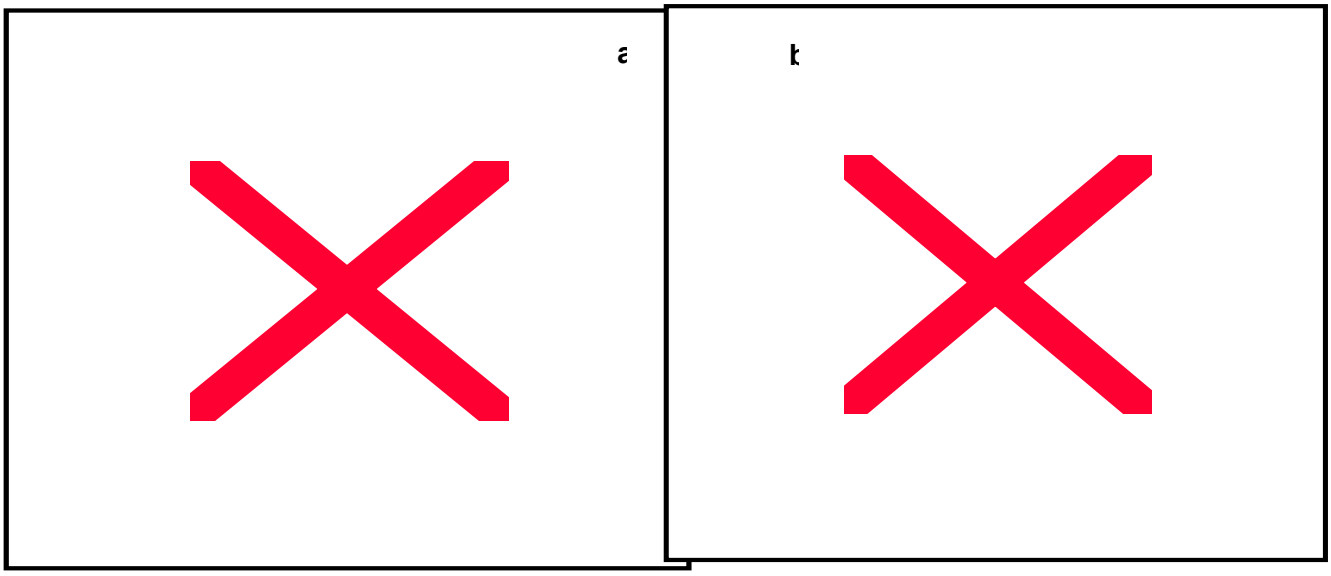

Fig 2. a) GCR activity in the absence and in the presence of the two ceramic powders after adsorption, as a function of the GCR amount in the assay; b) GCR release from alginate and HAp-alginate microspheres

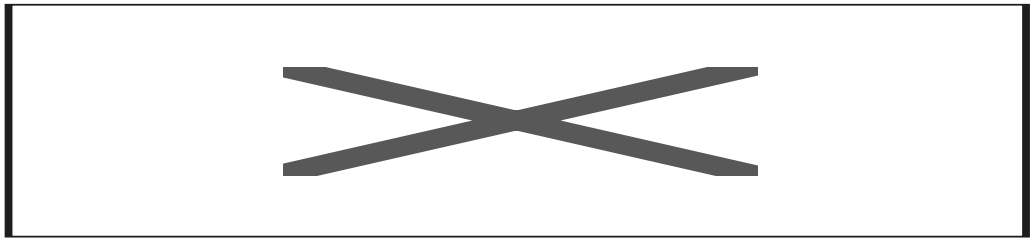

Fig.3 CLSM images of MG63 cells cultured on: a) 10/3, b) 20/3, c) 40/1.5 HAp-alginate microspheres and d) HAp microspheres

Cell adhesion studies

The ability of cells to adhere and spread on the surface of HAp-alginate and CTP-alginate microspheres of different compositions was assessed by CLSM (Fig. 3) and SEM

(Fig. 4). Figures are referred to HAp-alginate microspheres but similar results were obtained for both ceramics tested. No adherent cells could be found on the surface of control alginate microspheres (data not shown). This was not unexpected since it has been previously reported that attachment-dependent cells are unable to specifically interact with alginate hydrogels, which promote minimal protein adsorption presumably due to their high hydrophilic nature [2]. Upon addition of HAp or CTP particles to the alginate matrix a distinct cell behaviour was observed, depending on the ceramic-to-polymer ratio used. For the lower ceramic-to-polymer ratios (formulations 10/3, 20/3 and 40/3) only dispersed round cells and/or multicellular aggregates could be observed on the microspheres surface (Fig. 3a, 3b and 4a) However, on microspheres prepared with the higher ceramic-to-polymer ratio (formulation 40/1.5) cells were able to attach, spread and adopt a spindle-shaped morphology (Fig. 3c and 4b). Filopodial extensions could be observed both by CLSM and SEM. Cells on control HAp microspheres were well flattened exhibiting a typical osteoblastic-like morphology (Fig. 3d and 4c). Enhanced cell adhesion in polymer-ceramic composites in comparison with their polymeric counterparts has been previously demonstrated by other authors [3].

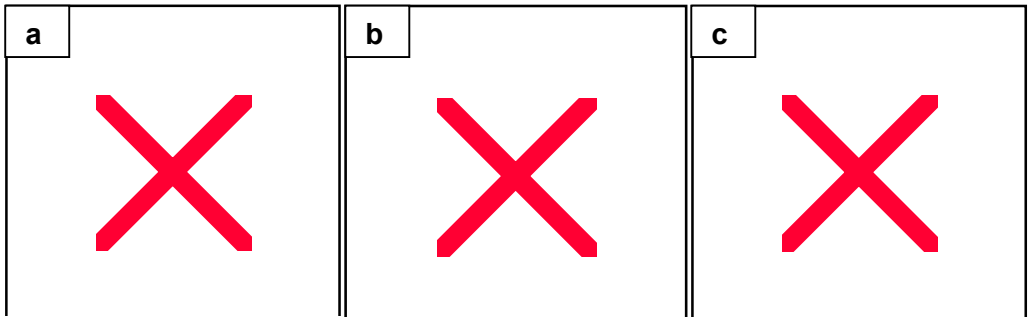

Fig. 4 SEM images of MG63 cells cultured on: a) 20/3, b) 40/1.5 HAp-alginate microspheres and c) HAp microspheres

Conclusions

The addition of calcium-phosphate particles to alginate allowed the modulation of GCR release kinetics. The ratio of ceramic-to-polymer had a pronounced effect on

osteoblasts adhesion to microspheres. Cells were only able to spread on microspheres with the higher percentage of ceramic.

Acknowledgements

The authors are grateful to Dr. Paula Sampaio (IBMC) for her assistance with CLSM and to programme Praxis XXI from the Portuguese Foundation of Science and Technology (FCT) for awarding Cristina Barrias a scholarship. This work was carried out under contract POCTI/FCB/41523/2001.

References

[1] G.A. Grabowski, N. Leslie and R. Wenstrup: Blood Rev. Vol. 12 (1998), p. 115

[2] J.A. Rowley, G. Madlambayan, D.J. Mooney: Biomaterials Vol. 20 (1999), p. 45

[3] M.J. Dalby, L. Di Silvio, E.J. Harper, W. Bonfield: Biomaterials. Vol. 23 (2002), p. 569